

**A New Ground Motion Intensity Measure,
Peak Filtered Acceleration (PFA),
to Estimate Collapse Vulnerability of Buildings in Earthquakes**

Thesis by
Shiyan Song

In Partial Fulfillment of the Requirements for the degree
of
Doctor of Philosophy



CALIFORNIA INSTITUTE OF TECHNOLOGY
Pasadena, California
2014
(Defended September 12, 2013)

UMI Number: 3603154

All rights reserved

INFORMATION TO ALL USERS

The quality of this reproduction is dependent upon the quality of the copy submitted.

In the unlikely event that the author did not send a complete manuscript and there are missing pages, these will be noted. Also, if material had to be removed, a note will indicate the deletion.



UMI 3603154

Published by ProQuest LLC (2013). Copyright in the Dissertation held by the Author.

Microform Edition © ProQuest LLC.

All rights reserved. This work is protected against unauthorized copying under Title 17, United States Code



ProQuest LLC.
789 East Eisenhower Parkway
P.O. Box 1346
Ann Arbor, MI 48106 - 1346

©2014
Shiyan Song
All Rights Reserved

ACKNOWLEDGEMENTS

This thesis exists because of the vision and guidance of my advisor, Professor Tom Heaton. I truly appreciate the way he advises me, providing me the freedom to find a challenging problem and the solution to it, as well as his ready advice and support based on his broad knowledge in earthquake engineering and seismology.

I would like to thank Swami Krishnan and Anna Olsen for providing me the building designs and models, as well as helping me interpret the results

Shijia (Wendy) Chen, Vanessa Heckman, and Grant Hollis reviewed early drafts of this thesis, and I appreciate their great feedback.

My fellow graduate students in the Civil Engineering Department, Michael Cheng, Ramses Mourhatch, Hemanth Siriki, and Stephen Wu. Life would be different without you guys.

This thesis also would not exist but for the love and support of my parents. They sent me to United States for my higher education, and I hope this thesis shows that that was the right decision.

ABSTRACT

In this thesis, we develop an efficient collapse prediction model, the PFA (Peak Filtered Acceleration) model, for buildings subjected to different types of ground motions.

For the structural system, the PFA model covers modern steel and reinforced concrete moment-resisting frame buildings (potentially reinforced concrete shear wall buildings). For ground motions, the PFA model covers ramp-pulse-like ground motions, long-period ground motions, and short-period ground motions.

To predict whether a building will collapse in response to a given ground motion, we first extract long-period components from the ground motion using a Butterworth low-pass filter with suggested order and cutoff frequency. The order depends on the type of ground motion, and the cutoff frequency depends on the building's natural frequency and ductility. We then compare the filtered acceleration time history with the capacity of the building. The capacity of the building is a constant for 2-dimentional buildings and a limit domain for 3-dimentional buildings. If the filtered acceleration exceeds the building's capacity, the building is predicted to collapse. Otherwise, it is expected to survive the ground motion.

The parameters used in PFA model, which include fundamental period, global ductility and lateral capacity, can be obtained either from numerical analysis or interpolation based on the reference building system proposed in this thesis.

The PFA collapse prediction model greatly reduces computational complexity while archiving good accuracy. It is verified by FEM simulations of 13 frame building models and 150 ground motion records.

Based on the developed collapse prediction model, we propose to use PFA (Peak Filtered Acceleration) as a new ground motion intensity measure for collapse prediction. We compare PFA with traditional intensity measures PGA, PGV, PGD, and S_a in collapse prediction and find that PFA has the best performance among all the intensity measures.

We also provide a close form in term of a vector intensity measure (PGV, PGD) of the PFA collapse prediction model for practical collapse risk assessment.

TABLE OF CONTENTS

Acknowledgement.....	iii
Abstract.....	iv
Table of Contents	v
List of Figures.....	viii
List of Tables	xi
Chapter 1	
INTRODUCTION	1
1.1 Motivation	1
1.2 Previous Work.....	3
1.2.1 Building Representations.....	3
1.2.2 Ground Motion Intensity Measures.....	6
1.2.3 Analysis Methods.....	10
1.3 Outline of Chapters	13
Chapter 2	
COLLAPSE PREDICTION FRAMEWORK.....	14
2.1 Computation-based Fast Prediction Method.....	14
2.2 Reference Building System	17
2.2.1 Data Structure of Reference Building System.....	18
2.2.2 The Reference Building System Used in this Thesis	19
2.3 Important Definitions in This Thesis	22
2.3.1 Global Ductility.....	23
2.3.2 Lateral Capacity	24
2.3.3 Collapse	24
Chapter 3	
PFA COLLAPSE PREDICTION MODEL FOR 2D BUILDINGS.....	26
3.1 Development of PFA Collapse Prediction Model	28
3.1.1 Building Models Used in the Development.....	28
3.1.2 Methodology of the PFA Model	30
3.1.3 Determining the Parameters Used in the PFA Model	33
3.1.4 Summary of the PFA Model for 2D Buildings.....	42

3.2 Fragility Curves Based on the PFA Model	43
3.2.1 Determining the Statistical Distribution Used for the Fragility Curves	43
3.2.2 Determining the Regression Models for the Standard Deviations of the Log-normal Fragility Curves	46
3.3 (PGV, PGD) Description of the PFA Collapse Prediction Model	49
3.3.1 Converting the PFA Model into (PGV, PGD) Model.....	50
3.3.2 Verification of the Developed Model	51
3.3.3 Comparison between the (PGV, PGD) Model and PFA Model.....	54
Chapter 4	
PFA COLLAPSE PREDICTION MODEL FOR 3D BUILDINGS	57
4.1 Building Models	58
4.2 2D Pushover Analysis and Limit Domain	62
4.2.1 Procedures of 2D Pushover Analysis.....	62
4.2.2 Result of 2D Pushover Analysis – Limit Domain	63
4.2.3 Comparison with the Results from Petti et al.	67
4.3 Extending PFA Collapse Model to 3D Frame Buildings.....	69
4.3.1 PFA Collapse Prediction Model for Regular 3D Buildings.....	70
4.3.2 Verification Using B1 Building.....	70
4.3.3 PFA Collapse Prediction Model for Irregular 3D Buildings	73
4.3.4 Verification Using B3 Building.....	74
4.3.5 Summary of PFA Collapse Prediction Model for 3D Frame Buildings	76
4.4 Discussion on the Effect of Torsion.....	77
4.4.1 Twistor Analysis.....	78
4.4.2 Effect of Torsion on Limit Domain.....	81
Chapter 5	
PREDICTING THE COLLASPE OF A BUILDING TESTED BY E-DEFENSE USING THE PFA MODEL	84
5.1 Brief Description of the Experiment	84
5.2 Collapse Prediction using the PFA Model.....	86
5.2.1 Pre-test Prediction	87
5.2.2 Post-test Prediction.....	92
Chapter 6	
DISCUSSION	94

6.1 Estimating the Fundamental Period, Global Ductility, and Lateral Capacity of an Actual Building.....	94
6.1.1 Fundamental Period	94
6.1.2 Lateral Capacity	95
6.1.3 Global Ductility.....	98
6.1.4 Transfer Functions between Direct Parameter and Indirect Parameters	99
6.2 Comparison of PFA with other Intensity Measures in Collapse Prediction	100
6.2.1 Comparison with Traditional Ground Motion Intensity Measures	100
6.2.2 Comparison with Modified Ground Motion Intensity Measures	106
6.3 Potential Application of PFA Collapse Prediction Model to other Structural Systems	110
Chapter 7	
CONCLUSIONS AND FUTURE WORK.....	114
7.1 Summary of PFA Collapse Prediction Model	114
7.2 Conclusions	116
7.3 Future Work.....	117
7.3.1 Full-range Intensity Measure.....	117
7.3.2 Updating Scheme Using Measured Data	117
7.3.3 3D Limit Domain and the Corresponding Collapse Prediction.....	118
BIBLIOGRAPHY	120
APPENDIX A: BUILDING MODELS USED IN THIS THESIS	126
APPENDIX B: GROUND MOTIONS USED IN THIS THESIS	161
APPENDIX C: EQUIVALENCY BETWEEN BUTTERWORTH FILTER AND DAMPED OSCILLATOR	170

LIST OF FIGURES

<i>Number</i>	<i>Page</i>
Chapter 1	
1.1 Example of building collapse in destructive earthquake	2
Chapter 2	
2.1 Framework of empirical collapse prediction methods.....	15
2.2 Framework of computational methods	16
2.3 Framework of computation-based fast prediction method	17
2.4 Buildings studied in this thesis.....	20
2.5 Definition of global ductility	23
2.6 Illustration of P- Δ effect	25
2.7 Pushover curve with and without P- Δ effect.....	25
Chapter 3	
3.1 Procedures for prediction of the PFA model.....	27
3.2 Steel frame building designs used to develop PFA collapse prediction model	29
3.3 Reinforced concrete frame building designs used to develop PFA collapse prediction model.....	30
3.4 Illustration of the procedures to obtain MinCPGA curves	31
3.5 Examples of minimum Collapse PGA in sinusoidal ground motions for three selected buildings.....	32
3.6 Regression model for cutoff period coefficient c	34
3.7 Response spectra and example of ramp-pulse-like ground motions	36
3.8 Response spectra and example of long-period ground motions.....	37
3.9 Response spectra and example of short-period ground motions	38
3.10 U6P building in long-period ground motion No. 4	40
3.11 Comparison of peak values of original records, filtered records at thresholds of collapse with maximum values of pushover curves	41
3.12 Collapse fragility curve of U6P building in long-period ground motions ...	45
3.13 Computed standard deviations in collapse prediction.....	47

3.14 Regression of standard deviations for ramp-pulse-like, long-period, and short-period ground motions	49
3.15 Example of minimum collapse PGA for U20B.	52
3.16 Example of collapse threshold in terms of PGV and PGD of the same building in Figure 3.15.....	52
3.17 Minimum collapse PGA spectra in sinusoidal ground motions for U6P, U6B, U20P and U20B	52
3.18 Comparison of predicted collapse thresholds and Olsen's computed result	54
3.19 Gain functions of 2 nd -order Butterworth filter and integration.....	55
Chapter 4	
4.1 Typical floor plans and isometric views of studied building models.....	61
4.2 Limit domain in term of base shear over seismic weight for B1	65
4.3 Limit domain in term of base shear over seismic weight for B2.....	65
4.4 Limit domain in term of base shear over seismic weight for B3	66
4.5 Roof position of original and deformed B3 building in 45° pushover.....	66
4.6 Plan views of two benchmark structures in the study of Petti et al. (2008)...	67
4.7 Limit domains in term of base shear of benchmark structure A and B.....	68
4.8 Example of collapse curvature domain for columns.....	68
4.9 Comparison of PFA collapse scales and Frame3D collapse scales (building B1)	72
4.10 Collapse prediction for an irregular 3D frame building.....	73
4.11 Comparison of PFA collapse scales and Frame3D collapse scales (building B3)	76
4.12 Force couple applied at each story of building B1	79
4.13 Twistor curve of building B1	80
4.14 Rotational angles along the height of building B1 at different deformation stages.....	80
4.15 Effect of torsion on the limit domain of building B1	82
4.16 Second floor plan of building B1	83
Chapter 5	
5.1 Photos of the specimen building	85
5.2 Plan and elevation views of the specimen building	85

5.3 EW, NS, and UD components of Takatori record in 1995 Kobe earthquake	86
5.4 Story shear versus story drift relationships obtained from pushover analyses	87
5.5 Estimating the ductility ratio of the tested structure using the J6P building designed by Hall (1997).....	88
5.6 Estimating the upper limit and lower limit of lateral capacity for the specimen building under the 1.0-scaled Takatori record.....	89
5.7 Estimating the lower limit of lateral capacity for the damaged building after being shaken by the 0.6-scaled Takatori record	90
5.8 Pre-test collapse prediction for the structure subjected to the 0.6-scaled Takatori record	91
5.9 Pre-test collapse prediction for the structure subjected to the 1.0-scaled Takatori record	91
5.10 Collapse of the specimen building after being shaken by the 1.0-scaled Takatori record	92
5.11 Calculating the cutoff period coefficient c using the measured data.....	92
5.12 Post-test collapse prediction for the structure subjected to the 1.0-scaled Takatori record	93
Chapter 6	
6.1 Over-strength factors versus fundamental periods for space and perimeter RC frame buildings in Haselton's study.....	97
6.2 Ductility ratios versus fundamental periods for frame buildings analyzed in Chapter 3	99
6.3 Procedures to obtain indirect parameters from direct parameters	100
6.4 Comparison of performance of PFA, PGA, PGV, PGD, and S_a in collapse prediction of buildings subjected to ramp-and-pulse ground motions.....	101
6.5 Comparison of performance of PFA, PGA, PGV, PGD, and S_a in collapse prediction of buildings subjected to long-period ground motions.....	102
6.6 Comparison of performance of PFA, PGA, PGV, PGD, and S_a in collapse prediction of buildings subjected to short-period ground motions.....	103
6.7 Examples of a record with a positive ε and a record with a negative ε scaled to the same $S_a(T_1)$	106

6.8 Calculation of R_{T_1, T_2} for a given response spectrum	107
6.9 Comparison of PFA, $S_a R_{T_1, T_2}^{0.5}$, and S_a in collapse prediction	101
6.10 Floor plan of building U6SW	111
6.11 Elevation view of building U6SW	111
6.12 Minimum Collapse PGA (left) and pushover curve (right) for U6 shear wall building.....	111
Chapter 7	
7.1 3D limit domain of building B1	118

LIST OF TABLES

<i>Number</i>	<i>Page</i>
Chapter 2	
2.1 Possible key parameters for dimensions in a reference building system	19
2.2 Archetypes in the reference building system used in this thesis	21
2.3 Two representations for the reference building system used in this thesis ...	22
Chapter 3	
3.1 Information of the building models.....	29
3.2 Calibrated order and intensity measure.....	39
3.3 Geometric mean values of collapse thresholds (g).....	42
3.4 Parameters of Butterworth filter.....	43
3.5 Chart of collapse prediction (g is gravity acceleration)	43
3.6 AIC values for log-normal and Weibull distribution	45
3.7 Standard deviation of ln(PFA)	46
3.8 Regression equations of standard deviations of collapse thresholds for three ground motion sets	49
Chapter 4	
4.1 Information on studied 3D frame building models	62
4.2 B1 building in long-period ground motion set	71
4.3 B3 building in long-period ground motion set	74
Chapter 6	
6.1 Performance of different ground motion intensity measures.....	104
Chapter 7	
7.1 Parameters of Butterworth Filter.....	114
7.2 Chart of collapse prediction (g is gravity acceleration)	114

INTRODUCTION

Collapse prevention is a fundamental requirement in seismic building codes. Even though seismic building codes are continuously updated in response to findings from destructive earthquakes and laboratory research, collapse still occurs in every large earthquake. The collapsed buildings in recent earthquakes, including 2008 Wenchuan, China, 2010 Maule, Chile, and 2011 Tohoku, Japan, serve as a reminder of the importance of seismic design and preparedness. Unfortunately, current technology is unable to predict when and where the next big earthquake will occur, and hence is unable to predict when and where building collapse will next occur. However, what is certain is that there is no guarantee for buildings to survive the next big earthquake without collapse.

1.1 Motivation

There have been numerous collapses of multi-story buildings in recent earthquakes. These include examples from near-source ground motions that are characterized by strong displacement pulses and ramps (1995 Kobe, 1999 Izmit, 1999 Chi-Chi), examples from long-duration harmonic motions that occurred at relatively large distance (1985 Mexico City in Michoacán earthquake), and examples from large broadband motions with large duration (2008 Wenchuan, 2010 Chile). Examples of buildings that collapsed in larger earthquakes from the past three decades are shown in Figure 1.1.

In addition to real earthquakes, simulations of the response of buildings in simulated ground motions from large earthquakes suggest that numerous buildings could collapse in future large earthquakes. These studies include simulations of a large earthquake on the San Andreas fault in southern California (Lynch et al., 2011; Muto & Krishnan, 2011) and simulations of long-duration motion in the Seattle region from a giant earthquake on the Cascadia subduction zone (Yang, 2009). These studies have demonstrated that ground motions of quite different characteristics can all pose a serious threat to multi-story buildings.



(a) The Nuevo Leon apartment building collapsed in 1985 Michoacán earthquake

(b) A precast concrete parking structure of California State University Northridge collapsed in 1994 Northridge earthquake



(c) Wenchuan Middle School building collapsed in 2008 Wenchuan earthquake



(d) The Alto Rio apartment building in Concepcion collapsed in 2010 Chile earthquake

Figure 1.1 Examples of building collapse in destructive earthquakes

A large loss could result from collapse, both directly and indirectly. Direct loss includes economic loss and casualty. Economic loss refers to the partial or total loss of a building and the damage caused to the equipment housed inside the building. Casualty refers to the deaths and injuries caused by collapse. In addition to direct loss, collapse also causes various indirect losses, such as the loss of insurers and reinsurers due to the insurance coverage and the loss of business owners due to the business downtime.

In order to mitigate loss, collapse risk assessment is needed by various sectors (building owner, insurance, and government) both pre- and post-earthquake. A building owner would like to know whether his or her building will survive the next large earthquake in order to determine if the building needs to be retrofitted. An insurance or reinsurance company would like to know the collapse risk of the buildings in its business region in order to determine the cost of the insurance. The government would like to know the collapse risk of a state or the whole country in order to create disaster-related policies. A quick post-earthquake collapse risk assessment would be useful for the government in order to mitigate casualties through an effective rescue plan.

In every case, an efficient collapse prediction model is needed. The model needs to be accurate to achieve the best assessment. It also needs to be easy to use, applicable to a large range of buildings, and require the least professionals and computational effort in order to be widely used by various sectors. However, such a collapse prediction model currently does not exist.

All of the above issues motivated us to develop a collapse prediction model that combines accuracy, speed, and simplicity.

1.2 Previous Work

A collapse prediction model consists of three parts: building representation, ground motion intensity measure, and analysis method. Building representation is the way a building is modeled in collapse prediction. Ground motion intensity measure is a parameter that measures the potential of ground motion to damage buildings. Analysis method is the process through which the collapse prediction is obtained. A collapse prediction model takes the building representation and ground motion intensity measure as input and gives the collapse prediction result (standing or collapsed) as output through its analysis method.

In the following section, previous work done by various researchers in the selection of building representation, ground motion intensity, and analysis method is briefly reviewed.

1.2.1 Building Representations

There are three commonly used building representations: direct use of real buildings, single-degree-of-freedom (SDOF) model, and multi-degree-of-freedom (MDOF) model.

Direct Use of Real Buildings

This kind of representation is usually used in statistical methods (see Section 1.2.3) and expert opinion methods (see Section 1.2.3). Since these two methods do not need numerical modeling and simulation, real buildings can be directly used as input. Usually, important parameters such as year built, structural type, number of stories, and floor area are documented to provide a detailed description of buildings.

Single-Degree-of-Freedom (SDOF) Model

In this model, a building is represented by a single-degree-of-freedom oscillator. In order to simulate the nonlinear collapse process, the oscillator needs to exhibit an elastoplastic force-displacement relationship.

Takizawa and Jennings (1980) examine the collapse capacity of ductile moment-resisting reinforced concrete frame buildings under extreme earthquake motions using the single-degree-of-freedom model. Their model has a tri-linear force-displacement relationship that accounts for the destabilizing action of gravity. They state that the model could provide a satisfactory description of the structural deformation at large deflections by approximately incorporating the effects of gravity, cracking, yielding, and degradation of stiffness.

Bernal (1987) also employs a single-degree-of-freedom model to study the collapse of buildings. In this study, Bernal proposes an amplification factor which accounts for P- Δ effect. Bernal calculates the amplification factor using an empirical formula in terms of ductility factor and stability coefficient.

More recently, in order to study the damage accumulation and P- Δ effect on the response of inelastic systems, Williamson (2003) explicitly considers the state of damage in a system to determine the response of a number of single-degree-of-freedom systems under various earthquake ground motions. The model is a rigid column with a concentrated mass at top and a rotational spring with a bilinear, damage-degrading moment-rotation relationship at the base.

Multi-Degree-of-Freedom (MDOF) model

In contrast to single-degree-of-freedom models, multi-degree-of-freedom models are designed to represent buildings in detail. Usually, this is done by modeling buildings in member level (beam, column, and slab) using a finite-element technique.

Hall (1995; 1997) investigates the nonlinear response and collapse of eight steel moment-resisting frame buildings under the effect of severe ground motions. Four of the eight buildings are designed according to the Japanese seismic building provisions of 1997, and the other four are designed according to 1994 Uniform Building Code seismic provisions. The buildings are modeled as planar frames with the displacement restricted in 2-dimensional space (vertical and horizontal). The building models use the fiber method, where each beam and column is subdivided along the length into eight segments, and each segment is divided into eight or ten fibers on the cross-section. Each fiber has a hysteretic, axial stress-strain relationship, and each segment has a linear shear stress-strain relationship. The panel zones are also modeled. Four of the building models are considered to have brittle welds. For these four models, an axial fracture strain is assigned to each fiber at the weld section according to a user-defined distribution. If the developed axial strain of a fiber in a weld exceeds the fracture strain, then the fiber no longer resists tension, but will still resist compression. The modeling software is a finite-element code written by Hall (1995).

A group of researchers (Haselton, 2006; Haselton et al., 2011; Liel et al., 2011) studied the seismic collapse safety of reinforced concrete moment frame buildings. 56 archetype buildings were designed specifically for the study. Among the 56 buildings, 30 buildings were ductile frames and the other 26 buildings were non-ductile frames. The buildings were modeled as planar frames in OpenSEES structural analysis platform. The gravity system was simplified into a leaning column to account for P- Δ effect. The frames were modeled with lumped plastic beam-column elements and finite joint shear panel springs. The beam-column elements were modeled using a nonlinear hinge model with degrading strength and stiffness developed by Ibarra et al. (2005). The joint shear panel springs were defined by a monotonic backbone and hysteretic rules which are similar to beam-column elements. The difference between ductile frame models and non-ductile frame models is the plastic hinge behavior. The backbone and hysteretic curves of non-ductile frames have smaller ultimate deformation and higher degradation, and hence exhibit more brittle behavior than those of

ductile frames. The collapse criterion is also different for ductile and non-ductile frame models (see Section 1.2.3 for details).

Krishnan et al. (Krishnan et al., 2006; Krishnan, 2007) investigate the behavior of 6 steel moment-resisting frame tall buildings subjected to strong ground motions. The buildings are modeled using fiber beam-column elements and panel zone elements, which is similar to Hall's approach. Krishnan's models differ from Hall's models in that Krishnan models buildings in 3-dimensional space instead of 2-dimensional space. The analysis platform used in the study is Frame3D developed by Krishnan (Krishnan 2003).

Lu et al. (2013) simulated the collapse of two reinforced concrete frame-core tube buildings subjected to extreme earthquakes. The frame part of the building was modeled using fiber beam-column elements. Unlike the steel frame buildings, the beam-column elements in RC frames have steel fibers and concrete fibers, and all fibers in the same section follow the assumption that "plane section remains plane". The confinement effect of the stirrups in columns is considered by using confined uniaxial constitutive relationship for the fibers in core concrete. Since concrete exhibits brittle shear failure, the strength and stiffness of the element drop to zero when the internal shear force exceeds the prescribed shear strength of the beam-column element. The shear-wall members (walls and coupling beams) were modeled using multi-layer shell elements. This type of element is based on the principles of composite material mechanics and is capable of simulating coupled in-plane/out-of-plane bending as well as in-plane direct shear and coupled bending-shear behavior of RC shear walls. A multi-layer element consists of layers with different thickness and materials. Rebars are smeared into one or more layers. For the boundary zones, the concentrated reinforcing bars were modeled using truss elements incorporated into the shell elements. The analysis platform is MSC.MARC.

1.2.2 Ground Motion Intensity Measures

Generally, there are two kinds of ground motion intensity measures: traditional intensity measures and modified intensity measures. Traditional intensity measures are already widely used in earthquake engineering (e.g. S_a and PGA). Modified intensity measures have been recently proposed by researchers to improve the accuracy of collapse prediction models.

Traditional Intensity Measures

In collapse prediction, the most commonly used traditional intensity measure is spectral acceleration (S_a). Spectral acceleration is the maximum acceleration a damped, elastic single-degree-of-freedom oscillator experiences in an earthquake. Spectral acceleration can be measured at different oscillation periods and with different degrees of damping. In practical earthquake engineering, spectral acceleration is usually measured at the fundamental period of the corresponding building, and with 2% or 5% of critical damping. Even though spectral acceleration is measured using an elastic oscillator, it still gives a relatively good estimation of building response, especially those buildings that are dominated by the fundamental mode. Since spectral acceleration is fairly easy to compute, it is selected by many researchers in developing collapse prediction models. Kirçil and Polat (2006), Krawinkler et al. (2009), Haselton et al. (2011), Liel et al. (2011), and Champion and Liel (2012) all chose spectral acceleration as the ground motion intensity measure in their collapse prediction models.

Peak ground acceleration (PGA) is also a commonly used traditional intensity measure. PGA is usually correlated with spectral acceleration at short periods, and hence is mostly used for the collapse prediction of buildings with short periods. Lee et al. (2002) collected data of totally and partially collapsed buildings in the Chi-Chi earthquake, and developed fragility curves in terms of PGA based on the collected data. Most of the surveyed buildings were masonry and concrete buildings with short periods. Kirçil and Polat (2006) designed three sample buildings (3, 5, and 7 stories, respectively) with fundamental periods ranging from 0.46s to 0.83s, according to the Turkish seismic design code and used them to develop the fragility curves for mid-rise reinforced concrete buildings in Istanbul. PGA was selected as one of the intensity measures for the fragility curves.

Besides S_a and PGA, another traditional intensity measure is the Modified Mercalli Intensity scale (MMI) that describes the effects of an earthquake on the earth's surface, humans, objects of nature, and man-made structures on a scale from I (not felt) to XII (total destruction). Since MMI could not be computed numerically like S_a and PGA, it is not the primary option for intensity measure when numerical simulation is employed in collapse prediction. However, in the collapse prediction models that lack adequate information from ground motions, MMI is still a reasonable option. U.S. Geological Survey's Prompt Assessment of Global Earthquake's Response (PAGER) Project and

the Earthquake Engineering Research Institute's World Housing Encyclopedia (WHE) developed a global database of building stocks and their earthquake vulnerability using MMI as the intensity measure (Porter et al., 2008).

Modified Intensity Measures

Among the aforementioned three traditional intensity measures, spectral acceleration (S_a) usually has the best performance in predicting building collapse since it is able to capture the difference between buildings with different periods. However, one limitation in S_a is that S_a is computed using an elastic single-degree-of-freedom oscillator. Hence, it only approximates the linear elastic response of the corresponding building, while collapse is a nonlinear plastic behavior that is quite different from the elastic approximation. Plastic deformation will elongate the period of a structure in dynamic response, which makes the structure vulnerable to a different frequency band. As a result, spectral acceleration is not the best intensity measure in collapse prediction.

Knowing the limitations of traditional intensity measures, researchers have been looking for new intensity measures to improve the performance of collapse prediction models. The new intensity measures they propose are referred to as modified intensity measures in this thesis.

Cordova et al. (2000) proposed a new two-parameter earthquake hazard intensity measure, $S_a R_{Sa}^{0.5}$. R_{Sa} is defined as $S_a(T_f) / S_a(T_1)$ where T_1 is the first mode period and T_f is a longer period (optimized value is approximately $1.65T_1$) that represents the inelastic (damaged) structure. Basically, the new intensity measure is a weighted average between $S_a(T_1)$ and $S_a(T_f)$, considering both spectral intensity and spectral shape, and thus accounting for inelastic strength and stiffness degradation (period elongation). The results of the study show that the new intensity measure significantly reduces the record-to-record variability in the predicted response obtained from inelastic time history analysis. Instead of combining S_a and R_{Sa} into one scalar, Vamvatsikos (2002) proposes a vector intensity measure (S_a, R_{Sa}). The optimized value of R_{Sa} is $S_a(1.5T_1) / S_a(T_1)$ in Vamvatsikos's research. In a similar study, Haselton and Baker (Haselton and Baker, 2006; Baker and Cornell, 2008) use the same vector intensity measure (S_a, R_{Sa}) and suggest $S_a(2T_1) / S_a(T_1)$ as the optimized value of R_{Sa} .

Baker and Cornell (2005, 2006) propose another spectral shape indicator, Epsilon (ϵ). Epsilon is defined by engineering seismologists studying ground motions as the number of standard deviations

by which an observed logarithmic spectral acceleration differs from the mean logarithmic spectral acceleration of a ground motion prediction (attenuation) equation (Baker and Cornell, 2005). They studied the response of a reinforced concrete moment-resisting frame building and conclude that epsilon has a significant effect on the nonlinear response of structures, because it tends to indicate whether S_a at a specified period is in a peak or a valley of the spectrum (Baker and Cornell, 2005). Based on the above result, they proposed to use Epsilon together with spectral acceleration as a vector intensity measure (S_a, ε) in collapse prediction.

Based on Baker and Cornell's research, Mousavi et al. (2011) proposed an improved spectral shape indicator, Eta (η), which is a linear combination of spectral acceleration Epsilon (ε_{Sa}) and peak ground velocity Epsilon (ε_{PGV}). They studied the influence of η -filtration in the collapse analysis of an 8-story reinforced concrete structure with special moment-resisting frames. The results show that the correlation between η and the nonlinear response is about 50% better than the correlation between ε_{Sa} and the response. Based on the above results, they concluded that η is remarkably more efficient than ε_{Sa} as a non-linear response predictor.

Instead of using the intensity measures related to spectral shape, Olsen and Heaton (2013) proposed a vector intensity measure (PGD, PGV) consisting of peak ground displacement and peak ground velocity. They collected 59,965 synthetic, seismic ground motions and applied them to eight models of steel, moment-resisting frames. They used regression method to develop collapse thresholds in PGV-PGD plane for the eight studied buildings and conclude that (PGD, PGV) works better than (S_a, ε) in collapse prediction.

It could be noticed that all of the aforementioned modified intensity measures have one similarity: they all put emphasis on the longer period component (usually longer than the first period) of ground motions. R_{Sa} explicitly uses the spectral acceleration at a period longer than the first period. Epsilon indirectly provides the information of the spectral acceleration at the periods longer than the first period by indicating whether $S_a(T_1)$ is in a peak or a valley of the spectrum. Although PGV and PGD are not directly related to any period of a building, they still provide information about the long period component of a ground motion. Velocity and displacement are obtained through integration(s) on acceleration. Since integration itself is a low-pass filter in frequency domain, PGV and PGD are actually indicators of the long period component in a ground motion. Usually, the

periods corresponding to PGV and PGD are longer than the first period of mid-rise buildings due to the inherent features of integration filters (see Chapter 3, Section 3.3.3 for details).

1.2.3 Analysis Methods

A variety of methods are used in developing collapse prediction models. In this section, we group them into statistical methods, expert opinion methods, nonlinear static methods, and dynamic step-by-step time history analyses.

Statistical Methods

Statistical methods are the most straightforward methods in developing collapse prediction models. In these methods, collapse fragility relationships are established using statistical methods based on the observed damage in past earthquakes.

After the 1994 Northridge earthquake, building damage inspection was carried out by United States Geological Survey (USGS) in collaboration with EQE International. The survey results and preliminary analyses are documented in ATC-38 (2000). Recently, Tan and Irfanoglu (2012) re-examined the database in order to find reliable building damage indicators that provide more accurate relations between ground motion intensity and damage levels. Regular statistical correlation analysis, as well as the random parameter ordered probit statistical model, are considered in their study.

Lee et al. (2002) used statistical methods to obtain the fragility curves for buildings in Taiwan based on the damage data of the 1999 Chi-Chi earthquake. In their study, Geographic Information Systems (GIS) is used as a spatial analysis tool to collect and quantify data, as well as to locate damaged buildings.

Yakut et al. (2006) used statistical procedures to develop the empirical fragility functions for low- to mid-rise reinforced concrete buildings in Turkey, based on a damage database of nearly 500 representative buildings that experienced the 1999 Kocaeli and Düzce earthquakes.

Expert Opinion Methods

Expert opinion methods obtain seismic vulnerability of buildings by consulting experts. ATC (Applied Technology Council) conducted one of the first systematic attempts in expert opinion methods and summarized the results in the report ATC-13 (1985). ATC-13 derived damage probability matrices for 78 different engineering facility classes, 40 of which refer to buildings, by having asked 58 experts to estimate the expected damage of a specific structural type subjected to a given ground motion intensity. Experts provided their opinions by filling a questionnaire based on their knowledge and experience. In some cases, however, only a few felt themselves sufficiently expert with respect to a particular structural type to venture an opinion (Lang, 2002).

More recently, the U.S. Geological Survey's Prompt Assessment of Global Earthquake's Response (PAGER) Project and the Earthquake Engineering Research Institute's World Housing Encyclopedia (WHE) conducted a survey that involved experts from more than 30 countries worldwide to assess the collapse fragility of different structure types. The uncertainty on collapse fragility and the median collapse probability estimates at each shaking intensity level were then developed from the estimations provided by experts.

It could be easily noticed that the primary drawback of expert opinion method is its subjectivity, as the vulnerability functions are based exclusively on the subjective opinion of experts.

Nonlinear Static Methods

The nonlinear static method, commonly known as “pushover analysis”, has become a standard method for estimating seismic deformation demands, as well as local and global capacities of building structures. Due to its simplicity, it is widely used by practicing engineers in evaluating the safety of buildings against earthquake-induced collapse. Nonlinear static method is introduced in FEMA 273 (1997) and updated in FEMA 356 (2000). It is recommended to use for structures in which higher mode effects are not significant.

In nonlinear static method, a nonlinear model of a buildings structure is constructed. Then the base shear versus lateral displacement (usually roof displacement) relationship is obtained by applying gradually increasing forces with a prescribed distribution (uniform or triangle) to the above-ground part of the model. The analysis is terminated when the control node (usually in the middle of the roof) reaches the target displacement or the building model collapses. The target displacement represents the maximum displacement a building could experience in a certain level of ground

motions. Collapse is assumed to occur when the base shear-lateral displacement reaches negative slope and the base shear becomes zero. The resultant demands are compared with the capacities of the corresponding building to determine whether the building satisfies the requirements.

The nonlinear static method lacks a solid theoretical foundation (Villaverde, 2007). It is based on an incorrect assumption that the cyclic behavior of a structure could be approximated by the mono-directional force-displacement relationship of the same structure. In addition, the deformation demands strongly depend on the characteristics of ground motions, and hence could not be easily obtained for pushover analysis. Researchers (Krawinkler and Seneviratna, 1998; Chi et al., 1998; Gupta and Kunnath, 2000; Chopra and Goel, 2004) have already shown that nonlinear static method does not provide an accurate estimation of building response in earthquakes. Although improved recently (Gupta and Kunnath, 2000; Chopra and Goel, 2002), nonlinear static method is still not proved to be universally applicable (Villaverde, 2007).

Dynamic Step-by-Step Time History Analysis

Dynamic step-by-step time history analysis could be applied to a variety of numerical models, ranging from single-degree-of-freedom oscillators to detailed 3D finite-element models. It is done by numerically solving the governing equation of motion step by step. Usually, since the models used in collapse simulation have elastoplastic behavior, Newton-Raphson iteration or its modified version is used to achieve convergence in each step.

An important criterion in collapse simulation using dynamic step-by-step time history analyses is the definition of collapse. Generally, there are two kinds of collapse considered in numerical simulation, vertical collapse and sidesway collapse. Vertical collapse, sometimes referred to as pancake collapse, is defined as the point where a building loses its primary gravity load bearing member, due to the inadequate requirements on shear design for old buildings (typically pre-1980 designs). Sidesway collapse, sometimes referred to as P- Δ collapse, is defined as the point of dynamic instability, where the lateral story drifts of the building increase without bounds. Sidesway collapse is the typical collapse mechanism for modern ductile buildings, in which capacity design requirements ensure no significant shear damage. Vertical collapse is considered in the study of Liel et al. (2011). It is done by comparing the joint shear deformation with the deformation capacity in each step. If the deformation exceeds the capacity, shear failure is assumed to happen and collapse

is achieved. Sidesway collapse is considered by Hall (1995; 1997), Haselton et al. (2011), Liel et al. (2011), Krishnan et al. (2006), and Lu et al. (2013) in their studies.

In order to obtain collapse threshold, incremental dynamic analysis (IDA) is usually applied to the numerical models. It is done by scaling up the ground motion in the analysis from zero to the point that the building model collapses.

1.3 Outline of Chapters

Chapter 2 briefly introduces the collapse prediction model developed in this thesis. It includes the framework of the developed prediction model and the difference between the developed model and other collapse prediction models. Chapter 2 also introduces a fundamental tool, a reference building system, upon which the collapse prediction model is developed.

The next two chapters, Chapter 3 and Chapter 4, describe the development of a collapse prediction model based on a new parameter, Peak Filtered Acceleration (PFA). Chapter 3 describes the development of the PFA model for 2D frame buildings. Chapter 4 describes how to extend the PFA model from 2D frame buildings to 3D frame buildings, and also discusses the effect of torsional irregularity on the capacity of buildings.

Chapter 5 demonstrates the efficiency and effectiveness of the PFA model by predicting the collapse of a frame building tested by E-defense and comparing the prediction to the result of the experiment.

Chapter 6 discusses several important topics, including how to obtain the parameters used in the PFA model from an actual building, the comparison between PFA and other intensity measures in collapse prediction, and the possibility of extending PFA model to other structural systems.

Chapter 7 concludes the thesis by summarizing the PFA collapse prediction model, identifying the significant conclusions and suggesting how to expand on this work.

COLLAPSE PREDICTION FRAMEWORK

This chapter introduces the framework and important concepts of the collapse prediction model developed in this thesis. The developed collapse prediction model differs from traditional prediction models in that it serves as a computation-based fast prediction model. It was developed based on the results of numerical simulations, but highly simplified to minimize the computational effort needed in collapse prediction. This chapter also introduces a useful tool, the reference building system, upon which we developed the collapse prediction model. The reference building system serves as a data structure to systematically document information from real buildings and numerical models, as well as an interpolation tool in collapse prediction.

2.1 Computation-based Fast Prediction Method

Traditional collapse prediction methods (as reviewed in Chapter 1, Section 1.2) can be generally divided into two categories: empirical methods and computational methods (see Figure 2.1 and 2.2). Empirical methods include statistical methods and expert opinion methods; computational methods include nonlinear static methods and dynamic step-by-step time history analyses.

The procedures to predict collapse using empirical models are straightforward: ground motion and building are taken as input, and prediction is provided through an empirical model.

The benefits of empirical methods are obvious. First, they are fast, since they do not require any modeling or simulation process in the prediction procedures. The prediction is done by matching the information of target ground motions and buildings with the information in the damage database. Ideally, the prediction could be done in real-time using proper computer-aided tools. Second, less professional skills are required in performing collapse prediction using empirical methods. Because of the simple procedures in these methods, only fundamental earthquake engineering and structural engineering knowledge is needed to perform the analysis.

The shortcomings of empirical methods are obvious as well. First, since these models are developed based on the existing damage data, the applicability of these models is limited by the availability of

data. For example, the newly built buildings that are not yet covered by the damage database could not be assessed using empirical methods. Second, empirical methods are developed under a statistical framework, and hence only have statistical meanings. In other words, the collapse fragility they provide is a mean value and a corresponding deviation for a group of buildings, not specifically for a single building.

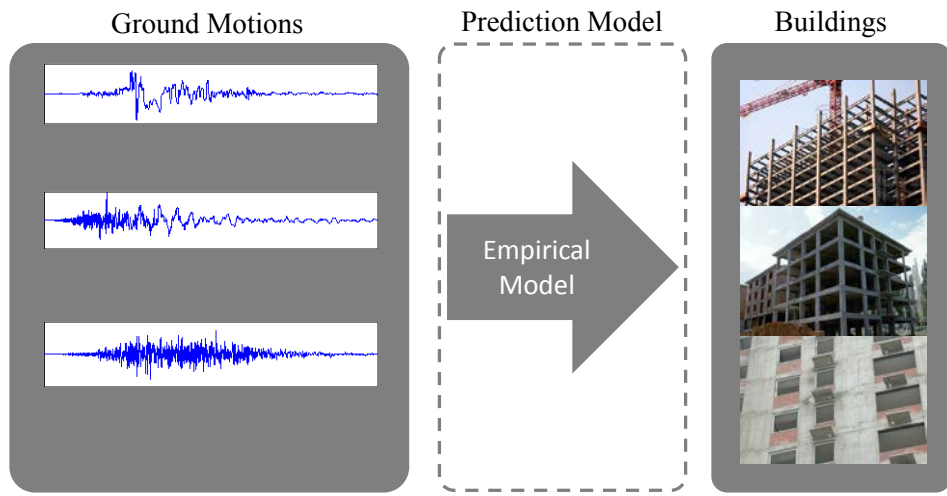


Figure 2.1 Framework of empirical collapse prediction methods

Compared with empirical methods, computational methods assess safety against earthquake-induced collapse under a different framework, by simulating the response of buildings subjected to ground motion excitations. In order to perform collapse prediction using these methods, a numerical model of the studied building is first constructed. The model could vary from a single-degree-of-freedom oscillator to a detailed multi-degree-of-freedom finite-element model. A ground motion record is then applied to the building model, by either equivalent static force (pushover analysis) or dynamic step-by-step time history analysis. Collapse is assessed based on the result of the simulation.

Compared with empirical methods, the computational methods are designed specifically for the collapse assessment of a single building, since the numerical model is constructed based only on the information of the studied building. Given significant time, however, the statistical result for a group of buildings can be calculated by repeating the simulation to a number of buildings or ground

motions. Since computational methods use detailed information about buildings in the modeling process, they could provide a very accurate prediction of building responses under ground motion excitations.

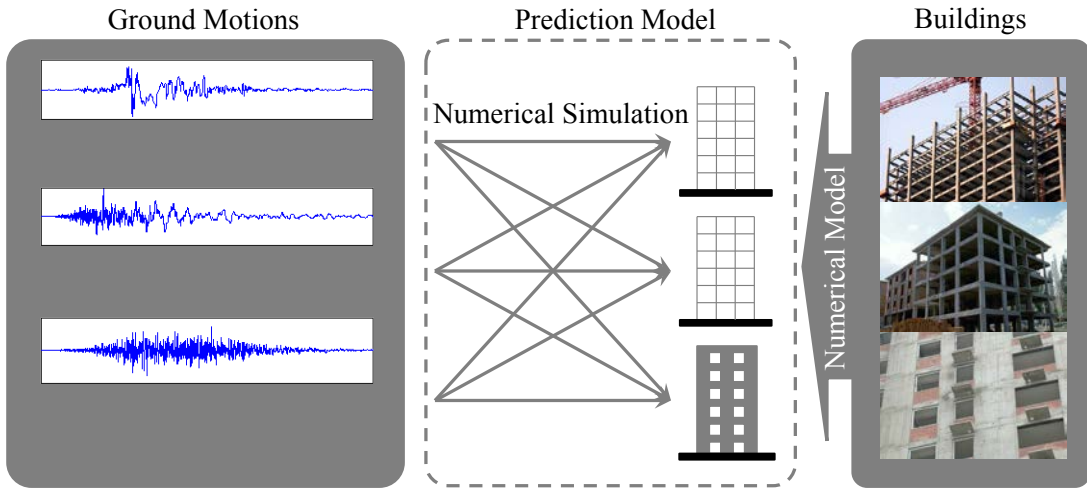


Figure 2.2 Framework of computational collapse prediction methods

The accuracy comes at the cost of analysis speed. The more detailed the model is, the more time-consuming the analysis is. For example, it usually takes hours to simulate the response of a mid-rise steel frame building under a strong ground motion. Because of the required computational effort, these methods are almost impossible to be achieved in real-time. Compared with empirical methods, a higher level of professional skills is required in conducting analysis using computational methods. Usually, knowledge of structural mechanics and finite-element analysis is the basic requirement.

From the above discussion, it could be concluded that traditional collapse prediction methods could not achieve speed and accuracy simultaneously, which makes collapse risk assessment in some cases very difficult. The building-by-building collapse assessment for the Los Angeles area in the ShakeOut scenario is one of the examples. First, there was no large earthquake in Los Angeles after the 1994 Northridge earthquake. As a result, the damage data is quite limited, especially for buildings designed according to later versions of building codes (e.g. UBC 97, IBC 2003, and ACI-318 2002), making empirical methods inapplicable. Furthermore, the large number of buildings in Los Angeles makes computational methods extremely time-consuming.

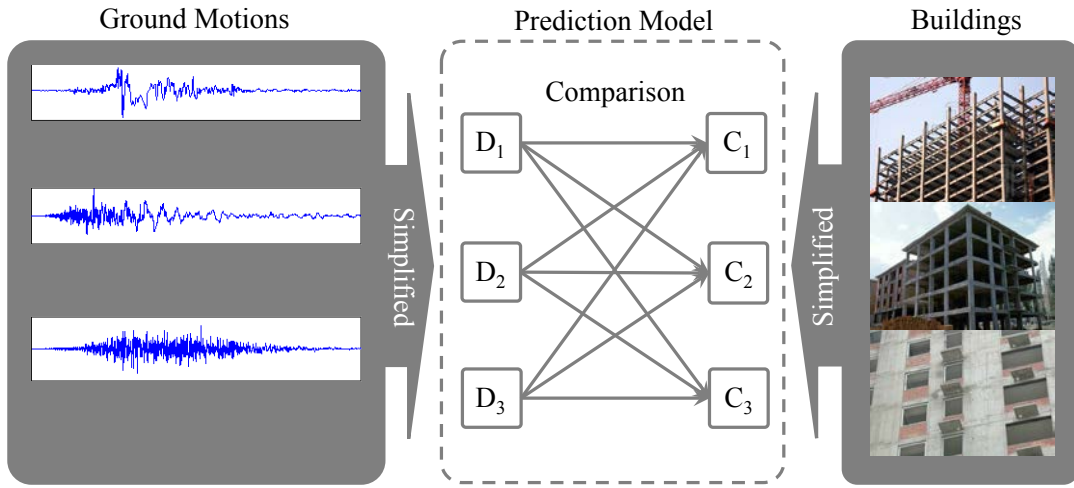


Figure 2.3 Framework of computation-based fast prediction method

In order to conduct building-by-building collapse risk assessment at a community scale efficiently, a computation-based fast collapse prediction method is developed in this thesis. It is real-time fast while achieving computational accuracy. In this model, capacities are obtained from buildings through pushover analysis, and demands are obtained from ground motions using low-pass Butterworth filters with recommended order and cutoff frequency. To predict whether a building will collapse when subjected to a ground motion, it only needs to compare building capacity with ground motion demand. If the capacity is larger, the building will survive the ground motion, otherwise, it will collapse. Building capacity is an inherent property that could be computed beforehand and documented for the future use. The low-pass Butterworth filter is a simple computation that could be achieved in real-time. As a result, this prediction model is real-time fast since no simulation is needed in the prediction process. In addition, the model is developed based on the detailed finite-element analyses and hence has accuracy comparable to the methods using step-by-step dynamic time history analysis.

2.2 Reference Building System

In this section, we introduce an important tool used in this thesis: the reference building system. The reference building system has two uses, serving as a database to systematically document information and behaviors of various buildings, as well as a powerful interpolation tool in collapse prediction.

A reference building system consists of various structural archetypes that are comprehensive enough to represent typical collapse behaviors under earthquake excitations of a real-world building inventory of interest. An archetype is a prototypical representation of a seismic-force-resisting system. It could be developed based on either a real-world or a hypothetical building design, as long as it could represent the behavior of a typical category of buildings. If we consider the whole building inventory of the studied region as a set, the reference building system of the whole building inventory is a much smaller set. However, it is not a necessary subset, since hypothetical designs are allowed in reference building system.

As for the selection of archetypes, since each archetype needs to be analyzed and the result needs to be documented, a smaller number of archetypes helps to reduce the computational effort and ensure the simplicity of the reference building system. However, due to the fact that the reference building system also serves as an interpolation tool to estimate parameters in collapse prediction, the distribution of archetypes needs to be dense enough to ensure the accuracy of interpolations, especially nonlinear interpolations. Thus, the selection of archetypes for a reference building system is always a trade-off between simplicity and accuracy.

2.2.1 Data Structure of Reference Building System

Considering that a reference building system serves as both a database and an interpolation tool, we choose to use a multidimensional array to describe the structure of a reference building system. In mathematics, a multidimensional array is an array having more than two dimensions. A two-dimensional array is often called a matrix. When the number of dimensions is less than or equal to three, we can virtualize the array in 3D space. However, if the number of dimensions is larger than three, it is difficult to virtualize the array.

In this thesis, we denote a multidimensional array with Building (d_1, d_2, \dots, d_n), where d_n is the n^{th} dimension of the array. Since this multidimensional array is designed to represent buildings, we choose each dimension to be a key parameter of a building. A parameter is a key parameter if its change results in a significant change in building behavior. For example, fundamental period is a key parameter, but temperature is not, because when the fundamental period changes, the building will respond to a different frequency band. However, if temperature changes (assume the temperature is in normal range), the property of the building material will remain approximately

constant, therefore the building will respond in nearly the same way. Several possible key parameters are listed in Table 2.1.

Table 2.1 Possible key parameters for dimensions in a reference building system

Group	Parameter	Example
Direct parameters	Structural system	Steel frame, RC frame
	No. of stories	1, 2, ..., 20, ...
	Year built	1960, 1980, 2000, ...
	Location	1200 E California Blvd
	Design building code	UBC94
	Design base shear	$0.1 \times \text{Weight}$
Indirect parameters	Fundamental period	1.54s, 3.47s
	Global ductility	5.6, 7.8
	Lateral capacity	0.1g, 0.2g

It could be noticed that some key parameters could be obtained directly from the document pertaining to a building. These parameters include structural system, number of stories, year built, location, design building code, etc. Other key parameters must be obtained from either measurement or analysis. For example, we can obtain the fundamental period of a building either by ambient noise vibration measurement or by numerical analysis using a finite-element model. We name those parameters that could be obtained directly from buildings “direct parameters” and all others as “indirect parameters”. Usually, indirect parameters are related to direct parameters. For example, fundamental period is related to number of stories since taller buildings generally have longer fundamental periods, and lateral capacity is related to year of built since later versions of building codes generally have higher requirements in seismic design, which results in higher lateral capacities. Hence, there exist transfer functions between direct parameters and indirect parameters. We will discuss these transfer functions in detail in Chapter 6.

2.2.2 The Reference Building System Used in this Thesis

In the previous section, we discussed the data structure of a reference building system. A reference building system consists of typical archetypes selected to study the collapse behaviors of the whole

building inventory. If we would like to understand the behaviors of the whole building inventory, we need to construct a reference building system that can represent the whole building inventory.

Buildings usually cover a large range of characteristics. Take Los Angeles County as an example, buildings have been built from 1900 to present, and the structural system could be unreinforced concrete frame, reinforced concrete frame, steel frame, reinforced concrete shear wall, or wooden structure. If there is a reference building system that can represent the whole building inventory, it will consist of a large number of archetypes, even if all of them are properly selected.

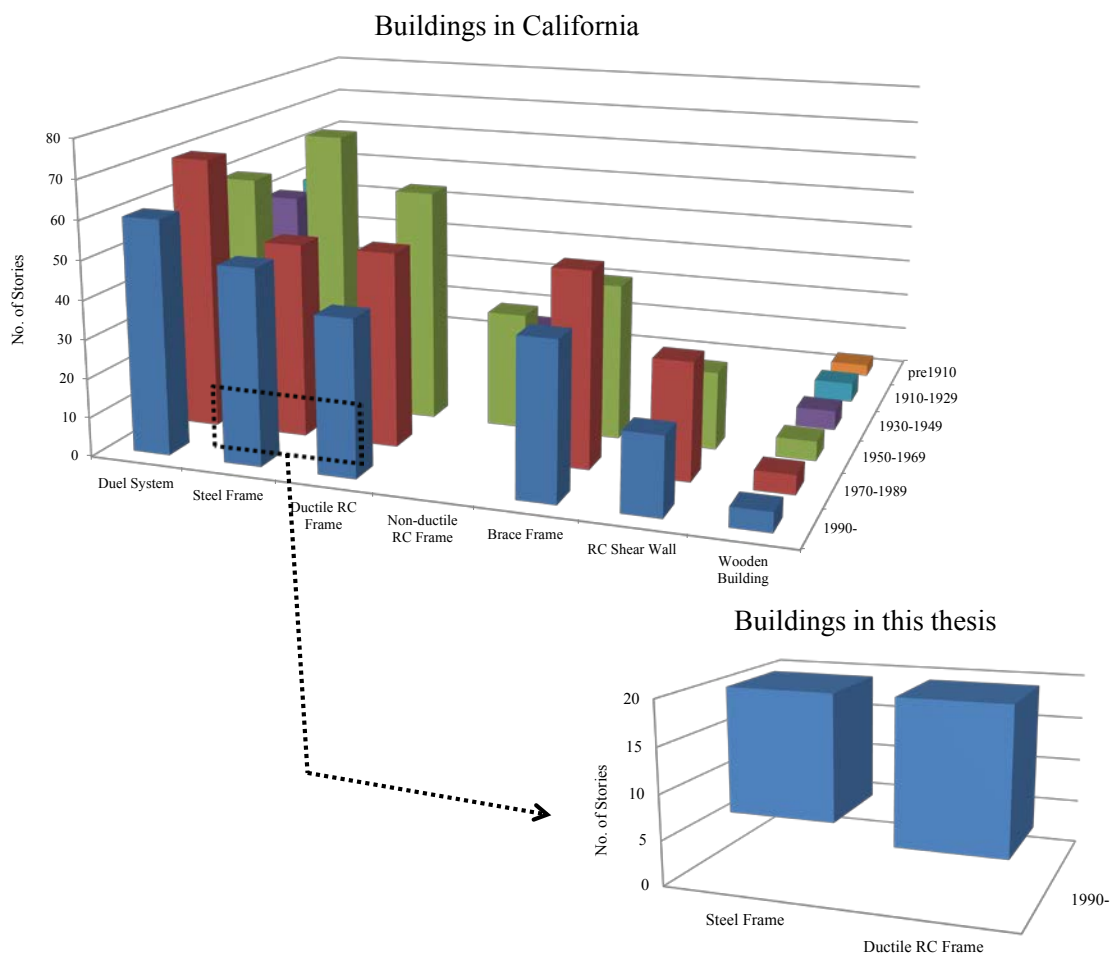


Figure 2.4 Buildings studied in this thesis

However, in this thesis, we are aiming to propose a new methodology and demonstrate its capability in building collapse predictions. We are not aiming to study the seismic behavior of every building

category. Hence, we only chose a small subset of the whole building inventory to develop and demonstrate our new collapse prediction model. The extension of the collapse prediction model to the whole building inventory is considered as future work and will not be covered in this thesis.

The subset of the building whole inventory studied in this thesis consists of buildings designed according to building codes no earlier than UBC94, with a height range from 4 to 20 stories (see Figure 2.4). We mainly focus on the structural system of steel and reinforced concrete moment-resisting frame buildings and briefly discuss the potential application of the collapse prediction model on reinforced concrete shear wall buildings. In order to study the collapse behaviors of this building inventory subset, we select thirteen archetypes for the reference building system. The archetypes consist of six planar steel frames, four planar reinforced concrete frames, and three 3D steel frames. The fundamental information of the archetypes is listed in Table 2.2.

Table 2.2 Archetypes in the reference building system used in this thesis

Structural system	Model dimensions	No. of stories	Number of archetypes	Design building code
Steel frame	2D	6	2	UBC94
		13	2	
		20	2	
	3D	18	1	
		19	2	
RC frame	2D	4	1	ASCE 7-02 ACI 318-02
		8	1	
		12	1	
		20	1	
Total			13	

Since there are two kinds of key parameters, direct parameters and indirect parameters (see Section 2.2.1), we propose two ways to represent a building in a reference building system, one using direct parameters (named as direct representation) and the other using indirect parameters (named as indirect representation).

Table 2.3 Two representations for the reference building system used in this thesis

Building representation	Parameter	Comments
Direct representation	Structural system	Could contain additional parameters
	No. of stories	
	Location	
	Design building code	
Indirect representation	Fundamental period	Generally no additional parameters are needed
	Global ductility	
	Lateral capacity	

For direct representation, we chose structural system, number of stories, location, and design building code as primary key parameters. The number of key parameters is not limited to four. Additional information could be provided for a more detailed description of buildings. For indirect representation we chose three parameters, fundamental period, global ductility, and lateral capacity, as key parameters. The number of dimensions is strictly three in the second representation. Thus, for example, a 20-story steel moment-resisting frame building, designed according to UBC 94, located in Downtown LA, could be represented by either Building {steel moment-resisting frame, 20, Downtown LA, UBC 94} or Building {3.47s, 4.25, 0.106W}, assuming that its fundamental period is 3.47s, its ductility ratio (see Section 2.3.1 for definition) is 4.25, and its lateral capacity is 0.106W (W is the seismic weight of the building).

Direct representation is designed to document the information of building designs, while indirect representation is used in the development of collapse prediction model, and also for the interpolation in collapse prediction. As discussed in section 2.2.1, the two building representations are related to each other. In Chapter 6, we will discuss how to obtain the values of key parameters in the indirect representation from the information provided by the direct representation.

2.3 Important Definitions in This Thesis

In this section, we introduce several important definitions used in this thesis, which may be different from other researchers' definitions.

2.3.1 Global Ductility

In this thesis, besides the traditional definition of ductility (material or structural element level), we introduce another ductility: global ductility. Global ductility is a parameter that can represent the deformation capacity of an entire structure. It combines the effects from material ductility, geometric nonlinearity, and P-Δ effect.

The global ductility is defined as

$$\mu = \frac{d_{0.5}}{d_y} \quad (2.1)$$

where d_y is the roof displacement at which a structure starts to yield globally, and $d_{0.5}$ is the roof displacement at which a structure losses half of its lateral capacity (see Figure 2.5). In this thesis, if not clarified, ductility refers to global ductility.

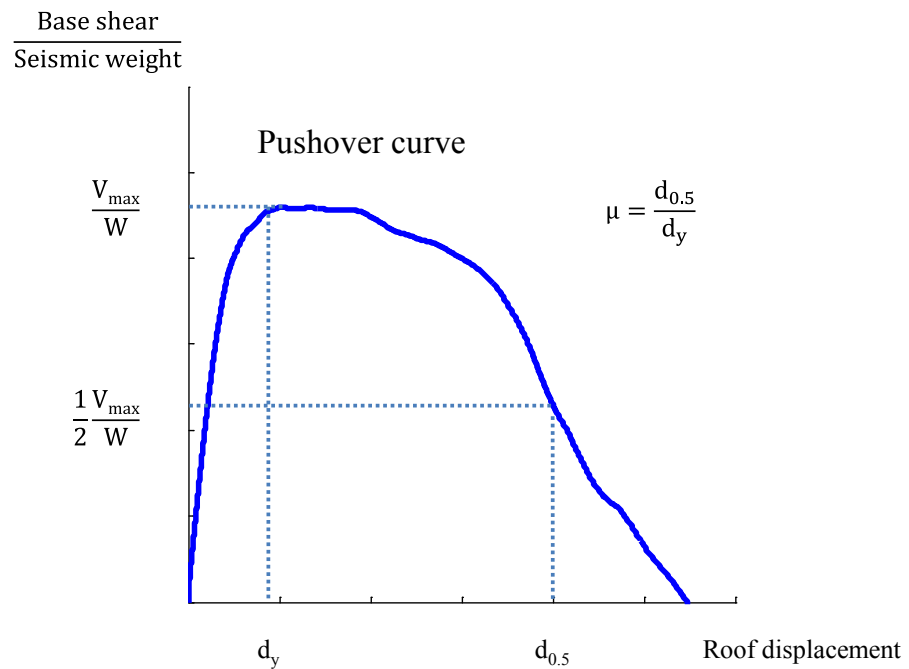


Figure 2.5 Definition of global ductility

2.3.2 Lateral Capacity

Lateral capacity is the maximum total lateral load a structure can resist. If pushover curve is available, lateral capacity is just the maximum base shear. Otherwise, we could approximate lateral capacity using the method discussed in Chapter 6. In the following chapters which introduce the development of the collapse prediction model, the lateral capacity needs to be compared with the peak filtered acceleration. In order to make this comparison, the same unit needs to be used for both parameters. Hence, in this thesis, lateral capacity is normalized by the seismic weight of the corresponding building and percentage of g (%g) is used as its unit.

2.3.3 Collapse

Collapse can be induced by different causes. For example, vertical collapse is caused by the loss of vertical load bearing members (e.g. shear failure in columns), and P- Δ collapse (also called sidesway collapse) is caused by P- Δ instability. In this thesis, we focus on the prediction model for P- Δ collapse.

P- Δ instability comes from the P- Δ effect. Lateral displacement of a structure induces arms for the gravity loads, which will result in an overturning moment proportional to lateral displacement (see Figure 2.6). This is called P- Δ effect. Since the overturning moment will make the structure deform further away from its equilibrium position, P- Δ effect will decrease the lateral resistance of a structure (see Figure 2.7). When the overturning moment is equal to or larger than the overall restoring moment, the displacement will predominately increase in only one direction. This is called P- Δ instability and the corresponding collapse is called P- Δ collapse.

P- Δ collapse is achieved only if the lateral global ductility of the structure is large enough. Otherwise, vertical collapse due to the shear failures will develop at smaller story drift while P- Δ instability is not reached yet. However, since all of the buildings used in this thesis are designed according to building codes no earlier than UBC94, we assume shear failure is prevented by the modern design requirements, and thus only P- Δ collapse is considered for all the building models used in this thesis. In the numerical simulations, P- Δ collapse is defined as the point of dynamic instability, where the lateral story drifts of a building increase without bound.

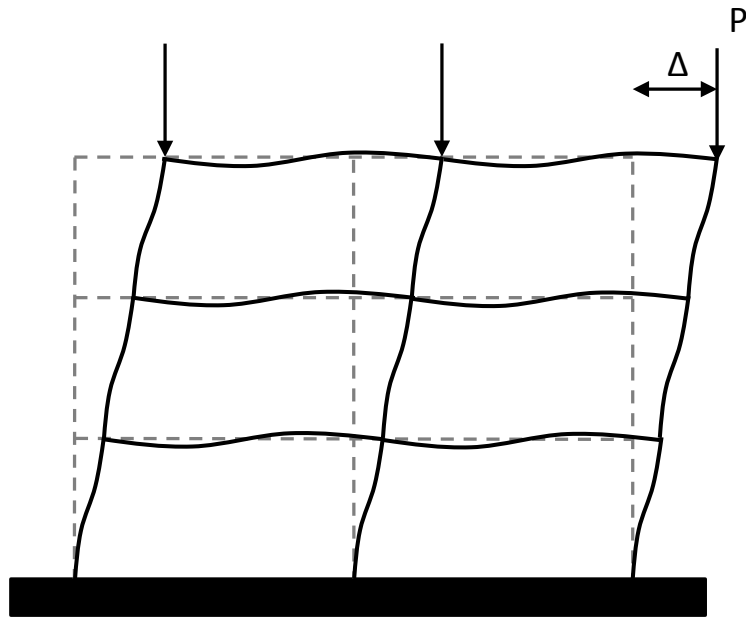


Figure 2.6 Illustration of P- Δ effect

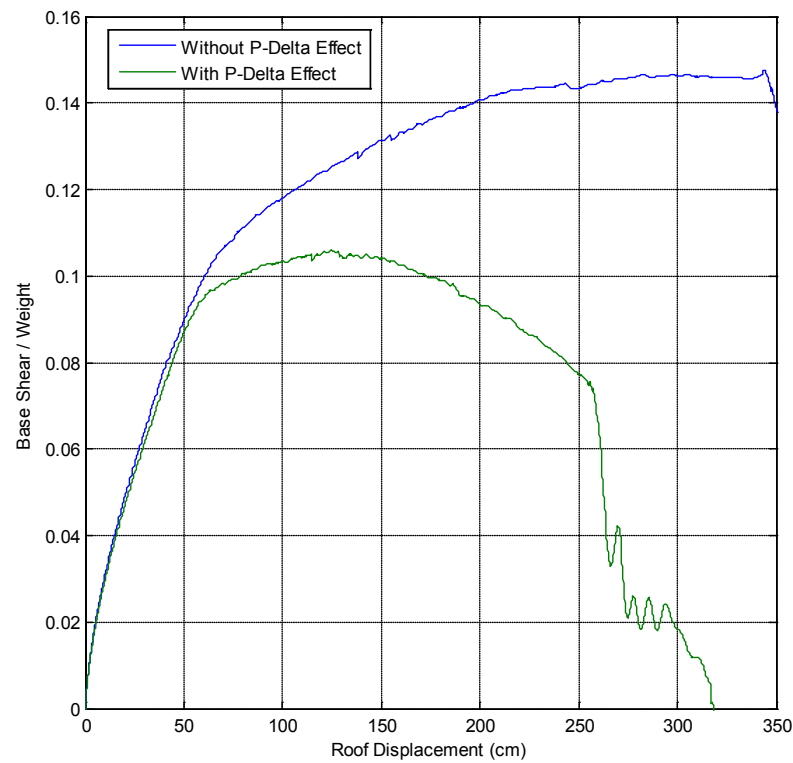


Figure 2.7 Pushover curve with and without P-Delta effect

PFA COLLAPSE PREDICTION MODEL FOR 2D BUILDINGS

In this chapter, we develop a new building collapse prediction model and this model is based on a new parameter: peak filtered acceleration, or PFA. Peak filtered acceleration (PFA) is the peak value (or half peak-to-peak value) of the Butterworth low-pass filtered ground acceleration time history.

The model developed in this chapter covers two types of buildings (steel and reinforced concrete moment-resisting frame buildings) and three types of ground motions (ramp-pulse-like, long-period, and short-period ground motions). All of the buildings we study in this chapter are 2D frame buildings. We will extend the model from 2D buildings to 3D buildings in Chapter 4, and discuss the potential of extending the method from frame buildings to other structural systems in Chapter 6.

The procedures of the PFA collapse prediction model for 2D frame buildings are surprisingly simple. To predict whether a building will collapse when subjected to a given ground motion, we first estimate the maximum lateral capacity of the building. We then filter the ground acceleration time history using a low-pass Butterworth filter with suggested parameters and compare the result to the building lateral capacity (see Figure 3.1).

It could be noticed that we chose a specific filter, the Butterworth filter, for the filtering process in the PFA model. There are two reasons why we chose the Butterworth filter: 1) compared with short-period ground accelerations, much smaller long-period ground accelerations cause buildings to collapse (see Section 3.1.2 for details). Thus to predict collapse, we neglect the unnecessary short-period component and extract the long-period component, which is dominant; 2) the peak acceleration from a 2nd-order Butterworth filtered record is equivalent to a 70.7% damped pseudo-acceleration response spectrum (see Appendix A.3 for proof). 70.7% is the smallest damping at which an oscillator loses resonance behavior. When a building collapses due to P-Δ instability, the drift predominantly increases in only one direction; it no longer oscillates about an equilibrium position and tends to lose its resonant behavior. Consequently, a collapsing building does not respond to a particular frequency and will not have a resonance peak as is assumed in a traditional response spectrum. These two reasons explain why Butterworth low-pass filtered ground

acceleration time history is a proper tool in collapse prediction.

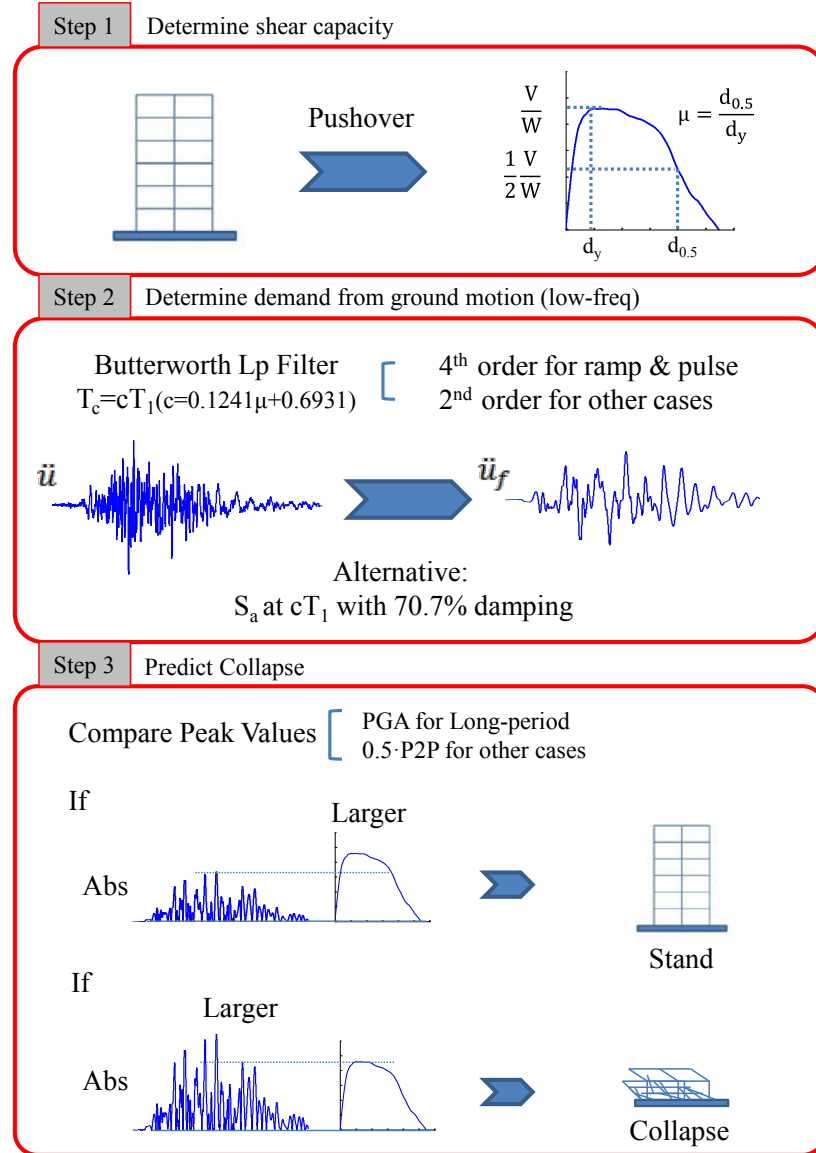


Figure 3.1 Procedures for prediction of the PFA model (T_1 -fundamental period, T_c -cutoff period of Butterworth filter, c -developed coefficient which depends on the global ductility and ranges between 0.9 and 2.0)

In this chapter, we first discuss the development of the PFA collapse prediction model. We then provide an alternative to the PFA model, a collapse prediction model based on a vector intensity measure (PGV, PGD). We also discuss the equivalency between the two collapse prediction models.

3.1 Development of the PFA Collapse Prediction Model

3.1.1 Building Models Used in the Development

Seven building designs are used to develop the PFA collapse prediction model in this chapter. They are denoted with U6, U13, U20, ID1003, ID1011, ID1013, and ID 1021, respectively.

U6 and U20 are 6-story and 20-story steel moment-resisting frame (MRF) buildings designed by Hall (1995; 1997). The design of the lateral force-resisting system conforms to 1994 Uniform Building Code (UBC) seismic provisions for zone IV and site class C. U13 is a 13-story steel MRF building designed by the author using the same seismic provisions (UBC 94). In this study, each steel frame building could have perfect welds (denoted with P) or brittle welds (denoted with B). A Fiber beam-column model is used to simulate the weld condition. Fibers in perfect welds will never fracture during the dynamic simulation, while fibers in brittle welds will fracture at a random strain generated from the statistical distribution given by Hall (1997).

ID1003, ID1011, ID1013, and ID1021 are reinforced concrete (RC) special moment frame (SMF) buildings designed by Haselton (2006) according to ASCE7-02 (2002) and ACI318-02 (2002). The numbers of stories are 4, 8, 12, and 20, respectively. The nonlinear hinge model with degrading strength and stiffness developed by Ibarra et al. (2005) is used in the element modeling.

Considering the variations of steel frame buildings with perfect welds and brittle welds, there are ten building models in total in this chapter. The basic information of the ten building models is listed in Table 3.1, and the details of the ten building models can be found in Appendix A.1 and A.2.

Table 3.1 Information of the building models

Model	No. of Stories	Material	T_1 (s) ⁽¹⁾	Max Strength ⁽²⁾	Ductility ⁽³⁾	Welds
U6P	6	Steel	1.54	0.2319	6.67	Perfect
U6B	6	Steel	1.54	0.1629	7.50	Brittle
U13P	13	Steel	2.63	0.1387	8.00	Perfect
U13B	13	Steel	2.63	0.0844	6.86	Brittle
U20P	20	Steel	3.47	0.1060	4.25	Perfect
U20B	20	Steel	3.47	0.0630	4.50	Brittle
ID1003	4	RC	1.12	0.1472	8.50	
ID1011	8	RC	1.71	0.0800	7.40	
ID1013	12	RC	2.01	0.0748	7.55	
ID1021	20	RC	2.36	0.0880	6.80	

(1) - Fundamental period

(2) - The maximum base shear in pushover analysis, normalized by seismic weight of the building

(3) - Ductility as defined in section 2.3.1

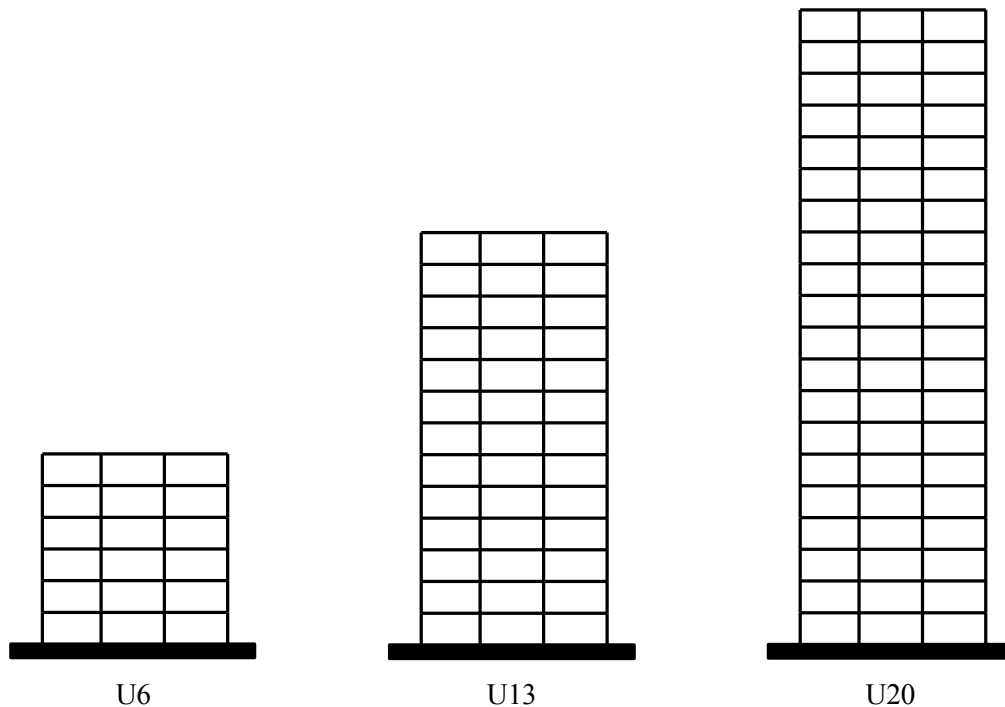


Figure 3.2 Steel frame building designs used to develop the PFA collapse prediction model

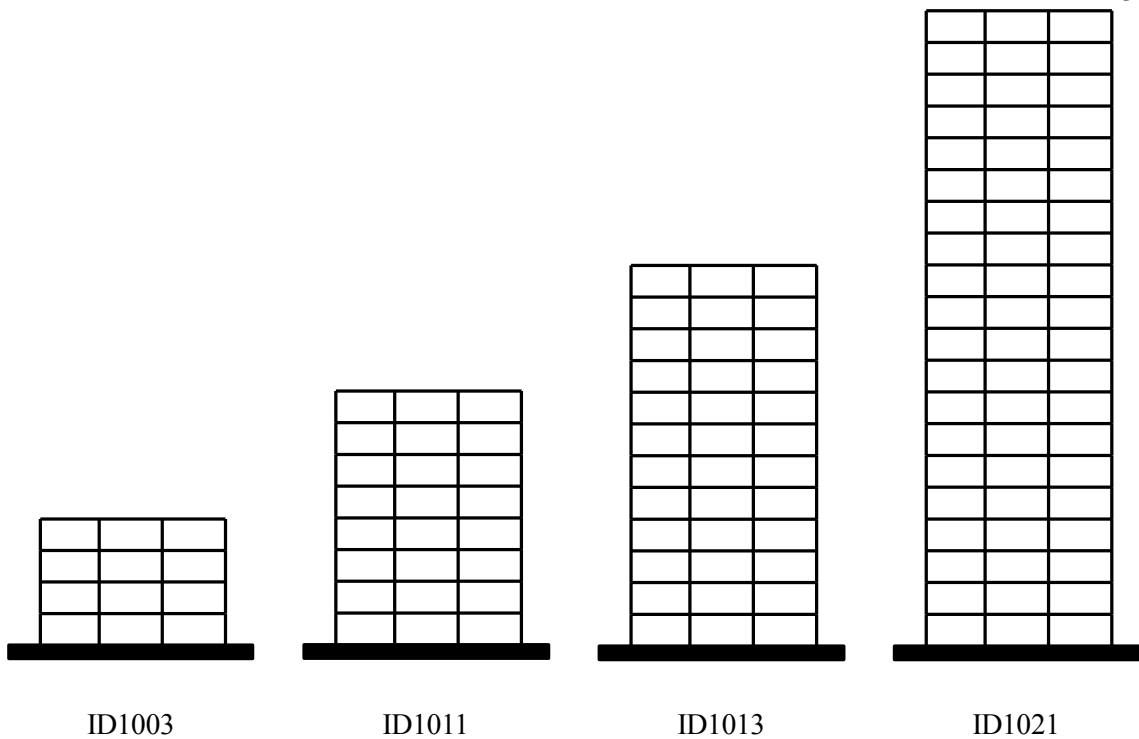


Figure 3.3 Reinforced concrete frame building designs used to develop the PFA collapse prediction model

3.1.2 Methodology of the PFA Collapse Prediction Model

Earthquake ground motions display great variety; some are best characterized as pulse-like, others appear to be more like random noise, and yet others seem to resonate at characteristic frequencies. When a building is close to collapse instability, its behavior is extremely nonlinear and it is not possible to decompose the solution into a linear sum of responses at a spectrum of frequencies. Nevertheless, it can be quite instructive to investigate a building's response to harmonic ground motion that is large enough to cause collapse. Towards this end, a series of sinusoidal ground motions of different periods and durations were generated. Incremental dynamic analysis (IDA) was applied to determine the threshold of collapse (see Figure 3.4). We denote this threshold with minimum collapse peak ground acceleration (MinCPGA). We conducted this analysis on all ten building models. The period of sinusoidal ground motion varies from 0.5 to 4 times the fundamental period of each building, and three ground motion durations (20s, 40s, and 100s) were chosen for the analysis. Examples of this analysis for a 6-story steel frame building with perfect welds (U6P), a 20-story steel frame building with brittle welds (U20B), and an 8-story RC frame building (ID1011)

are shown in Figure 3.5. MinCPGA is plotted versus T_s/T_1 (T_s is the period of sinusoidal ground motion and T_1 is the fundamental period of the building, 1.54s for U6P, 3.47s for U20B, and 1.71s for ID1011).

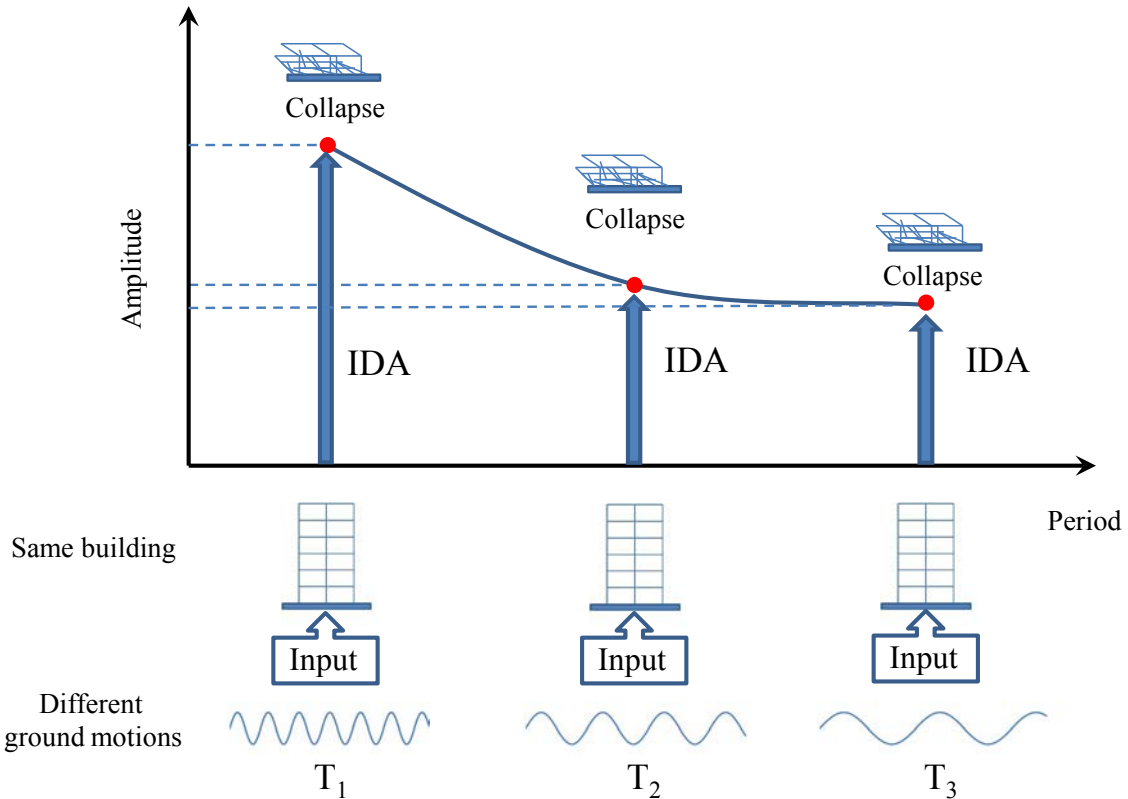
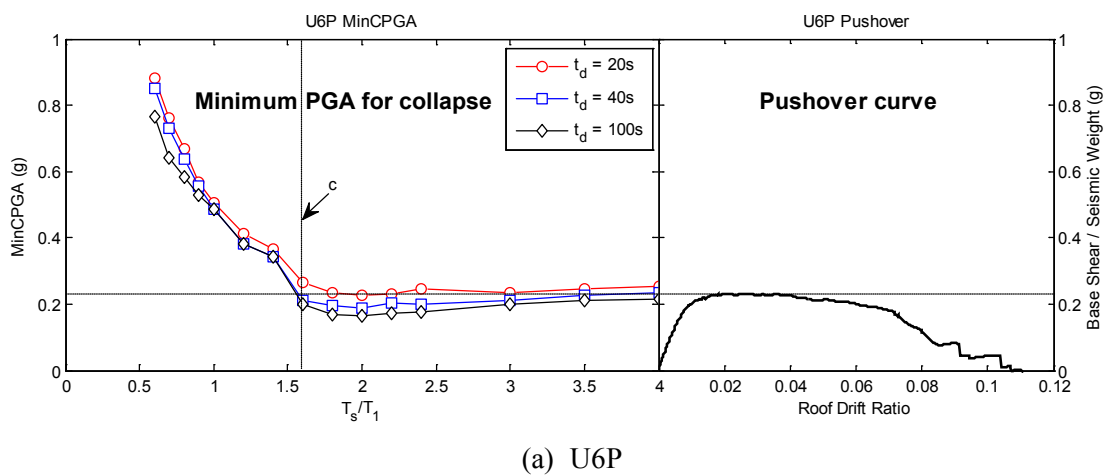


Figure 3.4 Illustration of the procedures to obtain MinCPGA curves



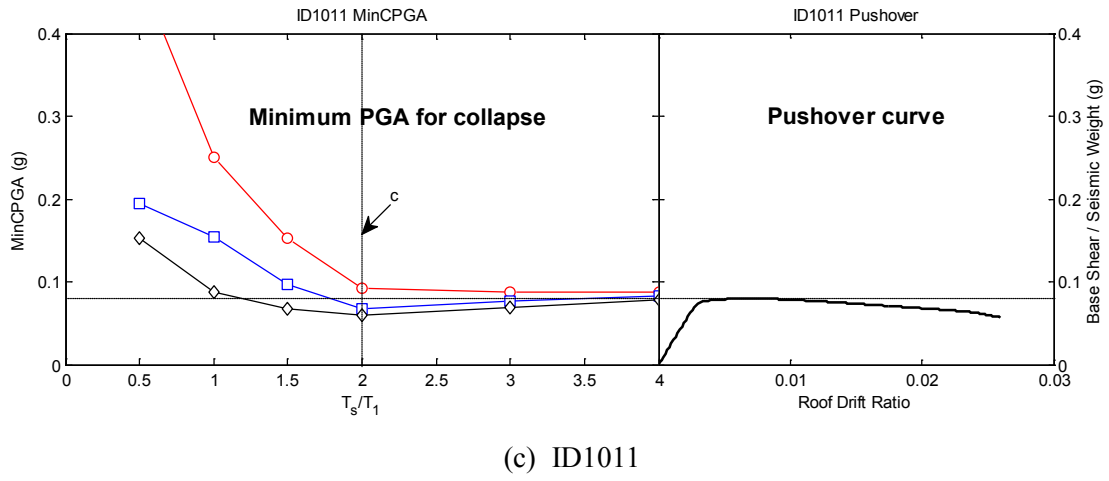
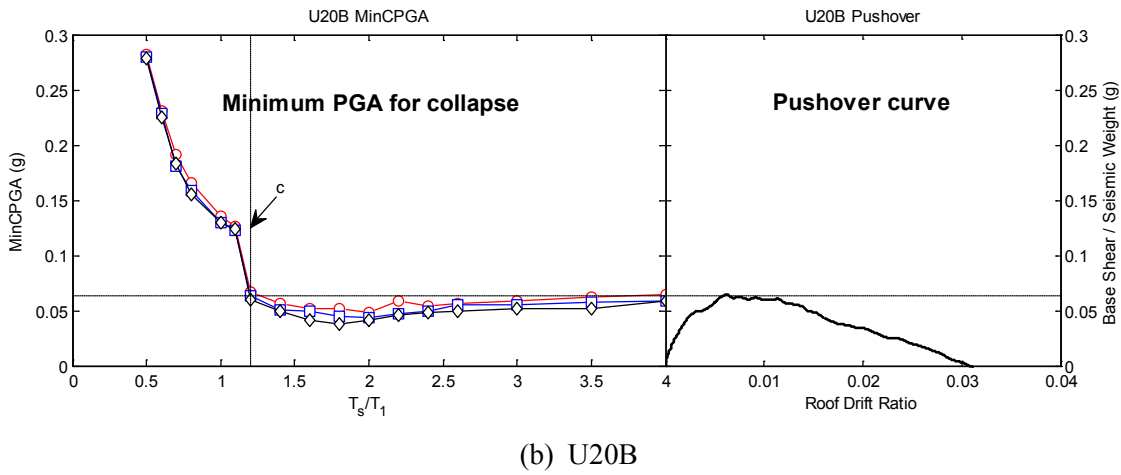


Figure 3.5 Examples of minimum collapse PGA in sinusoidal ground motions for three selected buildings. The MinCPGA curves are shown on the left. The pushover curves are shown on the right. A common vertical axis is used for both panels in each plot.

From Figure 3.5, it can be concluded that much smaller amplitudes are needed at long-period ground motions ($T_s/T_1 > c$) to cause collapse, and these long-period amplitudes are close to the maximum lateral strength calculated in the pushover analysis. This result implies that we should pay special attention to the long-period parts of the ground motion. Hence, we chose to use a low-pass Butterworth filter to remove the high-frequency parts of the record that seem to have little overall effect on collapse, and used the long-period parts to predict collapse.

3.1.3 Determining the Parameters Used in the PFA Model

A low-pass Butterworth filter is fully described by two parameters: cutoff frequency (or cutoff period) and filter order, n , where the response decays as f^n . We conducted a series of tests to determine these parameters. In addition, the measurement of the maximum size of the filtered acceleration can be determined by either the absolute maximum with respect to zero, or by measuring the peak-to-peak amplitude of the largest swing.

Regression Model for Cutoff Period Coefficient c

The cutoff period is determined from the MinCPGA spectrum for each of the different building models considered in this study. We chose it as the lowest period ($T_s/T_1 = c$ in Figure 3.5), where the MinCPGA spectrum approaches a constant. We found that the cutoff period is not necessarily the building's fundamental period (see Figure 3.5). Furthermore, it is related to building's ductility ratio. In this thesis, we define the ductility ratio μ to be $d_{0.5}/d_y$, where d_y denotes the roof displacement at which building starts to yield globally, and $d_{0.5}$ denotes the roof displacement at which the building loses 50% of the maximum strength. We used a linear equation to find the regression model between the cutoff period coefficient c and the ductility ratio. The result is shown in Figure 3.6 and Equation 3.1.

$$c = 0.1241 \frac{d_{0.5}}{d_y} + 0.6931 \quad (3.1)$$

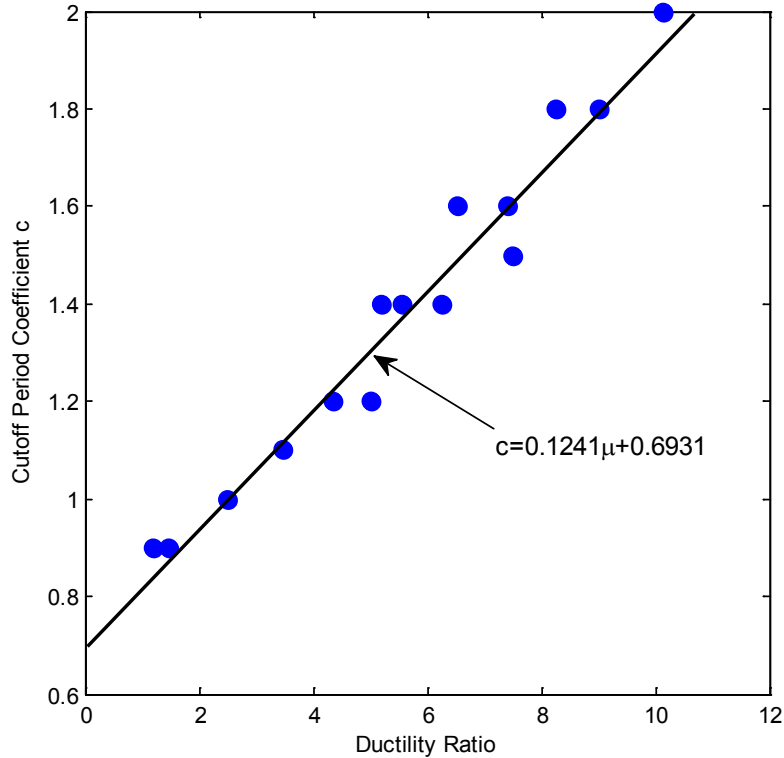


Figure 3.6 Regression model for cutoff period coefficient c

Adjusting Order of Butterworth Filters and Peak Values of Ground Motions

After obtaining the cutoff period, we still have to decide the order of the Butterworth filter, and also decide between methods to determine the peak motion (single peak or half of the peak-to-peak). To make our study more systematic, we 1) selected three ground motion sets of one hundred and fifty records, and 2) we used nonlinear finite element simulations for an incremental dynamic analysis to compute the collapse thresholds of ten building models for the three ground motion sets. We then determined which filter order and amplitude determination method best fit the finite-element predictions for each class of ground motion.

Ground Motions

Researchers have shown that different types of ground motions have different impacts on building response (Kalkan and Kunnath, 2006; Champion and Liel, 2012). To ensure the proposed model

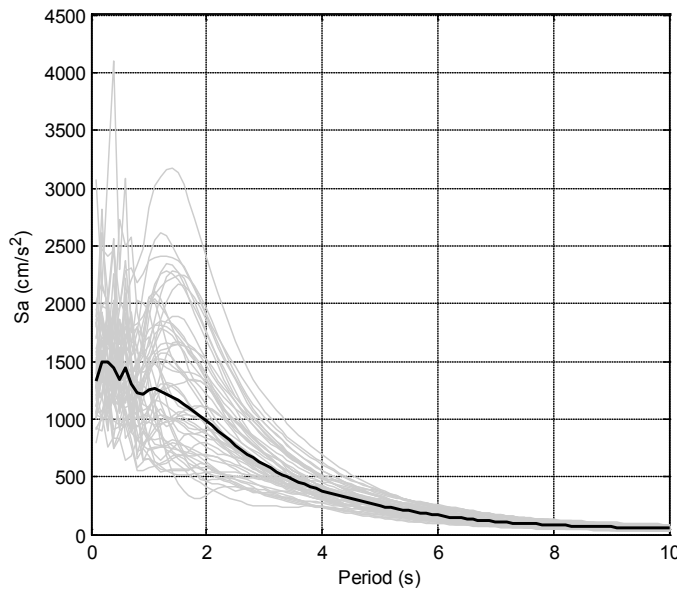
covered a wide range of ground motions, we divided them into three groups: 1. Ramp-pulse-like (RP) ground motions, 2. Long-period (LP) ground motions, and 3. Short-period (SP) ground motions.

Ramp-pulse-like ground motion is actually the name of two kinds of ground motions: ramp-like ground motions and pulse-like ground motions. Ramp-like ground motions, also known as fling steps, are the result of the evolution of residual ground displacement due to tectonic deformation associated with rupture mechanism, and is generally characterized by a unidirectional velocity pulse and a monotonic step in the displacement time history (Kalkan and Kunnath, 2006). Pulse-like ground motions, also known as directivities, are observed when the rupture propagates forward toward the site and the direction of slip on the fault is aligned with the site. Ground motions oriented in this forward-directivity path may follow certain radiation patterns and generate long-period, short-duration, and large-amplitude pulses (Somerville, 1998). In this thesis, we found that the two kinds of ground motions have a similar effect on building collapse, and hence are combined into one category.

Long-period ground motions are rich in long-period components and seem to resonate at characteristic frequencies. This kind of ground motion usually results from basin amplification, and the characteristic frequencies are the model frequencies of the basin. Long-period ground motions are found to be very destructive, especially in 1985 Michoacán earthquake.

Short-period ground motions are the most common ground motions. They do not exhibit ramps, pulses, or long-period components, and only have short-period vibrations. This kind of ground motion is widely observed as far-fault ground motions in every earthquake.

In this thesis, ramp-pulse-like records are selected from a study by Graves and Somerville (2006). Long-period and short-period records are selected from the 1999 M 7.6 Chi-Chi earthquake. The corresponding response spectra and examples are plotted in Figure 3.7 to 3.9. The details of the selected ground motion records can be found in Appendix B.



(a) Response spectra of ramp-pulse-like ground motions

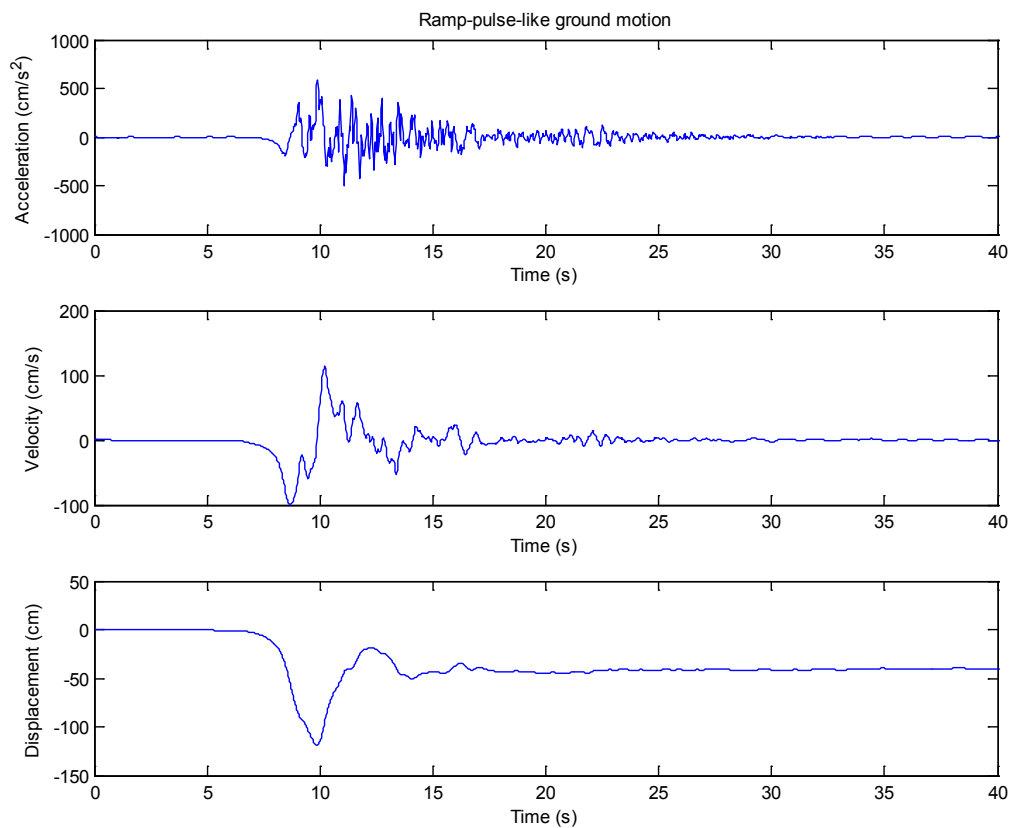
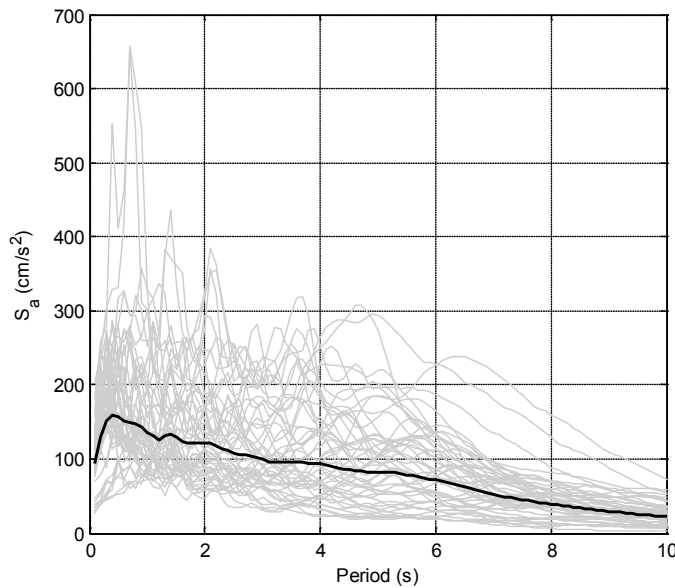
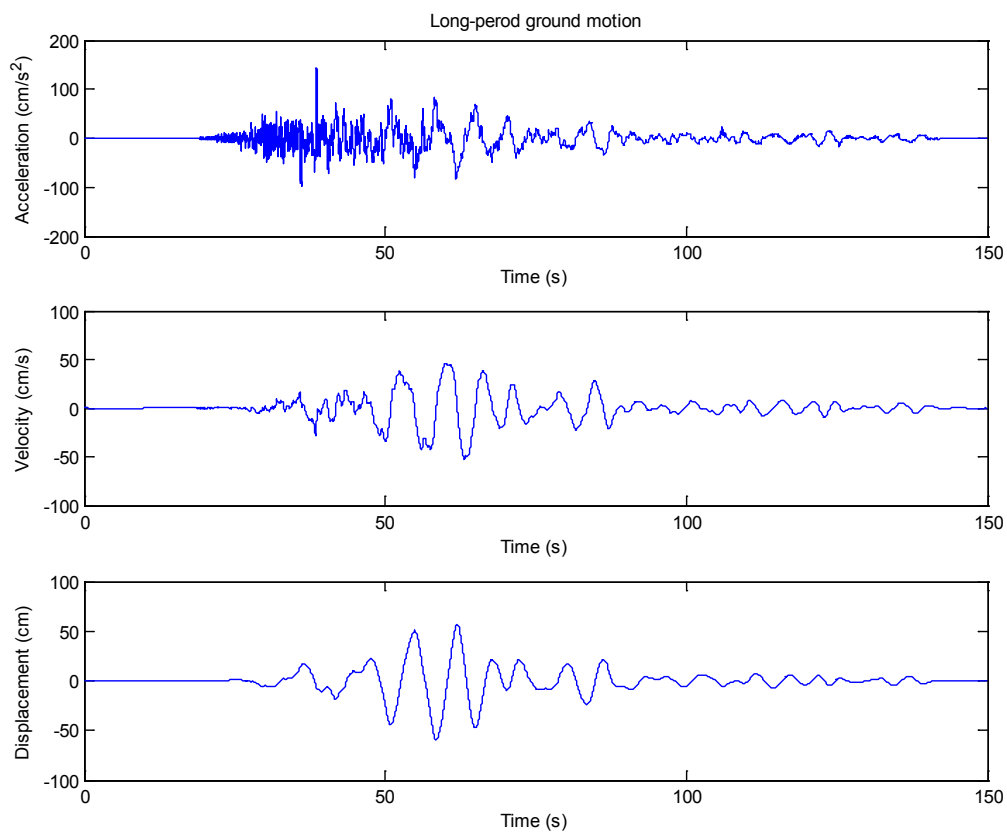
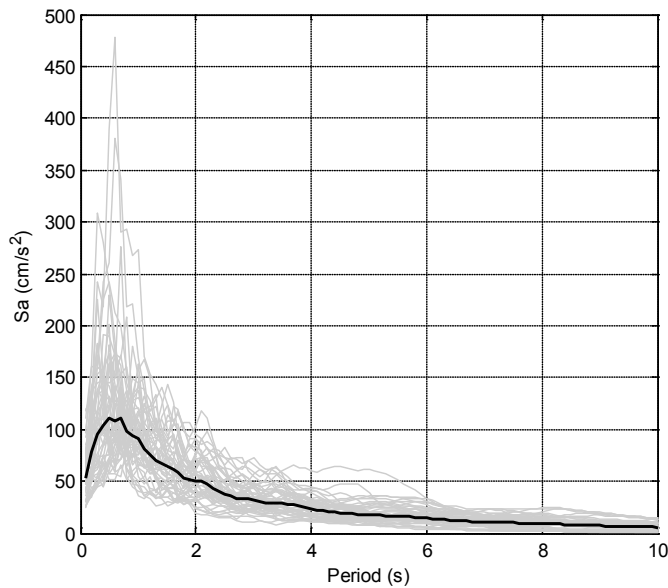


Figure 3.7 Response spectra and example of ramp-pulse-like ground motions

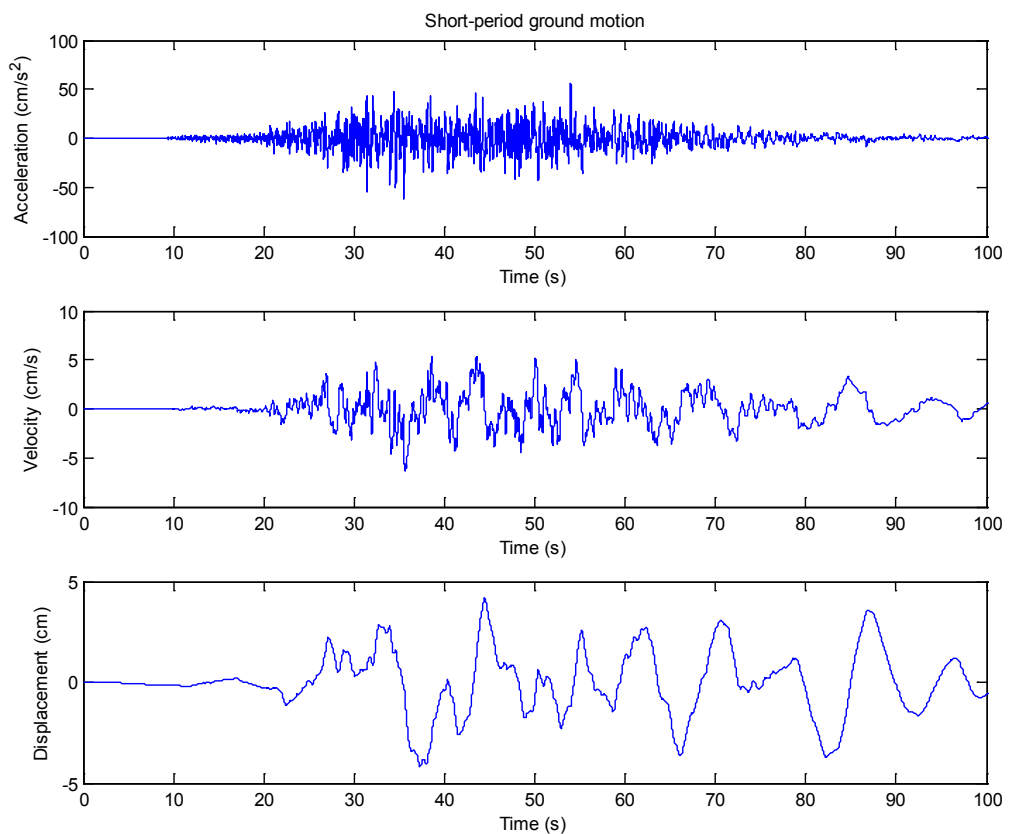


(a) Response spectra of long-period ground motions

(b) Example of long-period ground motions
Figure 3.8 Response spectra and example of long-period ground motions



(a) Response spectra of short-period ground motions

(b) Example of short-period ground motions
Figure 3.9 Response spectra and example of short-period ground motions

Result of Filter Order and Peak Representative Value

After linearly scaling all 150 records so that they were just large enough to induce collapse (IDA analysis), we Butterworth low-pass filtered the scaled records and then determined the maximum value of the filtered record. This filtering process was repeated several times, each time with a different order Butterworth filter. While a 2nd-order filter seemed to work best for most records, a 4th-order filter works better than 2nd-order for ramp-pulse-like ground motions. Furthermore, measuring half peak-to-peak filtered acceleration seems to provide more consistent results for ramp-pulse-like and short-period ground motions, while peak ground acceleration works better for long-period ground motions. Interestingly, determining the peak value of a 2nd-order Butterworth filter acceleration record is identical to obtaining the linear acceleration spectral value at the cutoff period and with 70.7% damping.

The results are shown in Table 3.2, Table 3.3, Figure 3.10, and Figure 3.11. In Figure 3.10, we plotted ground acceleration, spectral acceleration at fundamental period, base shear of elastic finite-element model, filtered acceleration, base shear of elastoplastic finite-element model, and roof displacement together. From Figure 3.10, it could be concluded that, in the plastic yielding region, filtered acceleration nearly capture the base shear of elastoplastic finite-element model, which is the indicator of damage state. Especially when the base shear is close to the lateral strength of the building, filtered acceleration almost exactly captures the shape of base shear, which explains why peak filtered acceleration is a good intensity measure for collapse prediction. In Figure 3.11, we plotted peak values of unfiltered acceleration and filtered acceleration at collapse threshold. It could be concluded that before filtering, the peak values are scattered, but approach a constant after filtering. Also it could be noticed that the constant is just the lateral capacity of the corresponding building.

Table 3.2 Calibrated order and intensity measure

Ground Motion Set	Order of Butterworth Filter	Intensity Measure
RP	4	Half peak-to-peak acceleration
LP	2	Peak ground acceleration
SP	2	Half peak-to-peak acceleration

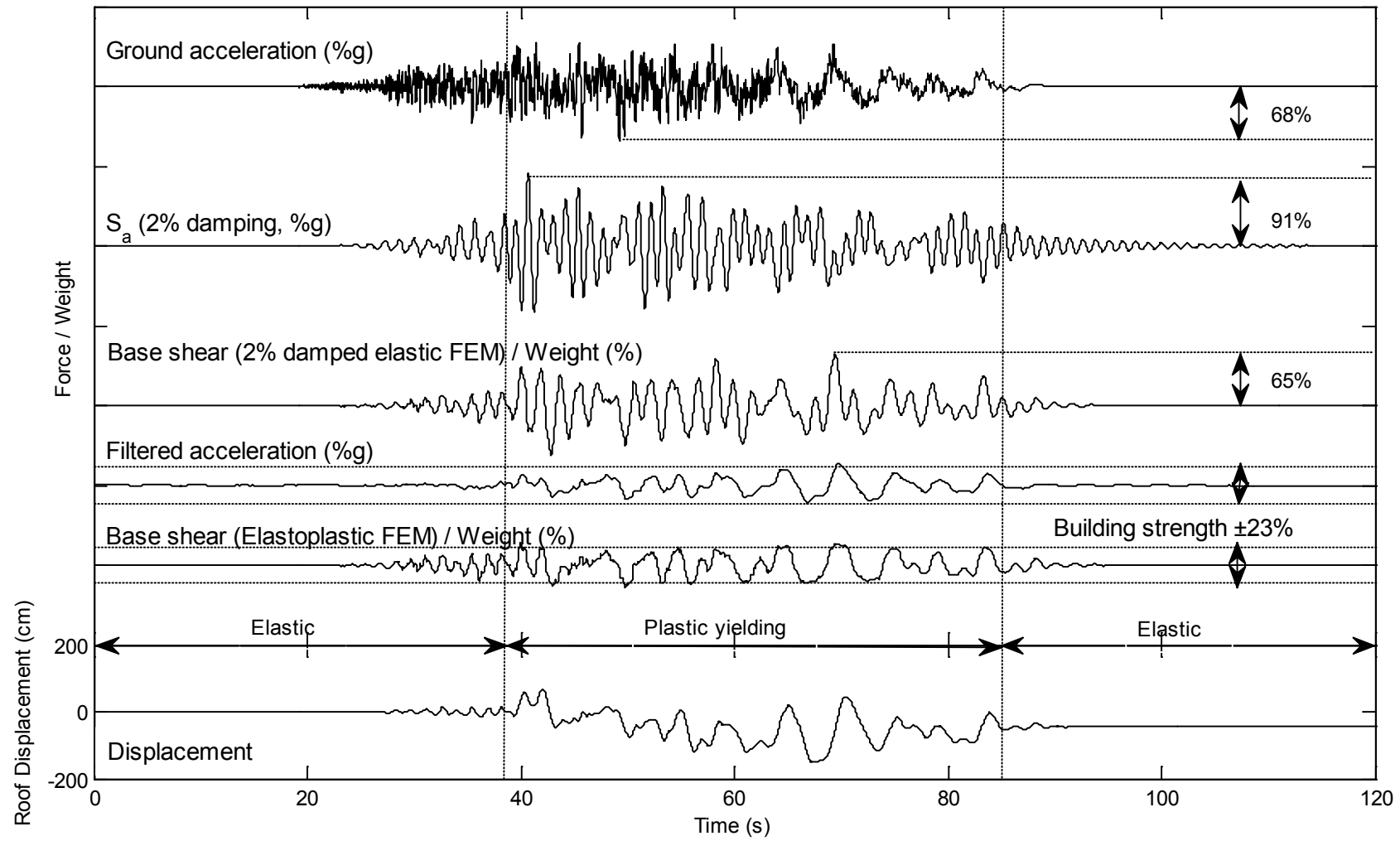


Figure 3.10 U6P building in long-period ground motion No. 4

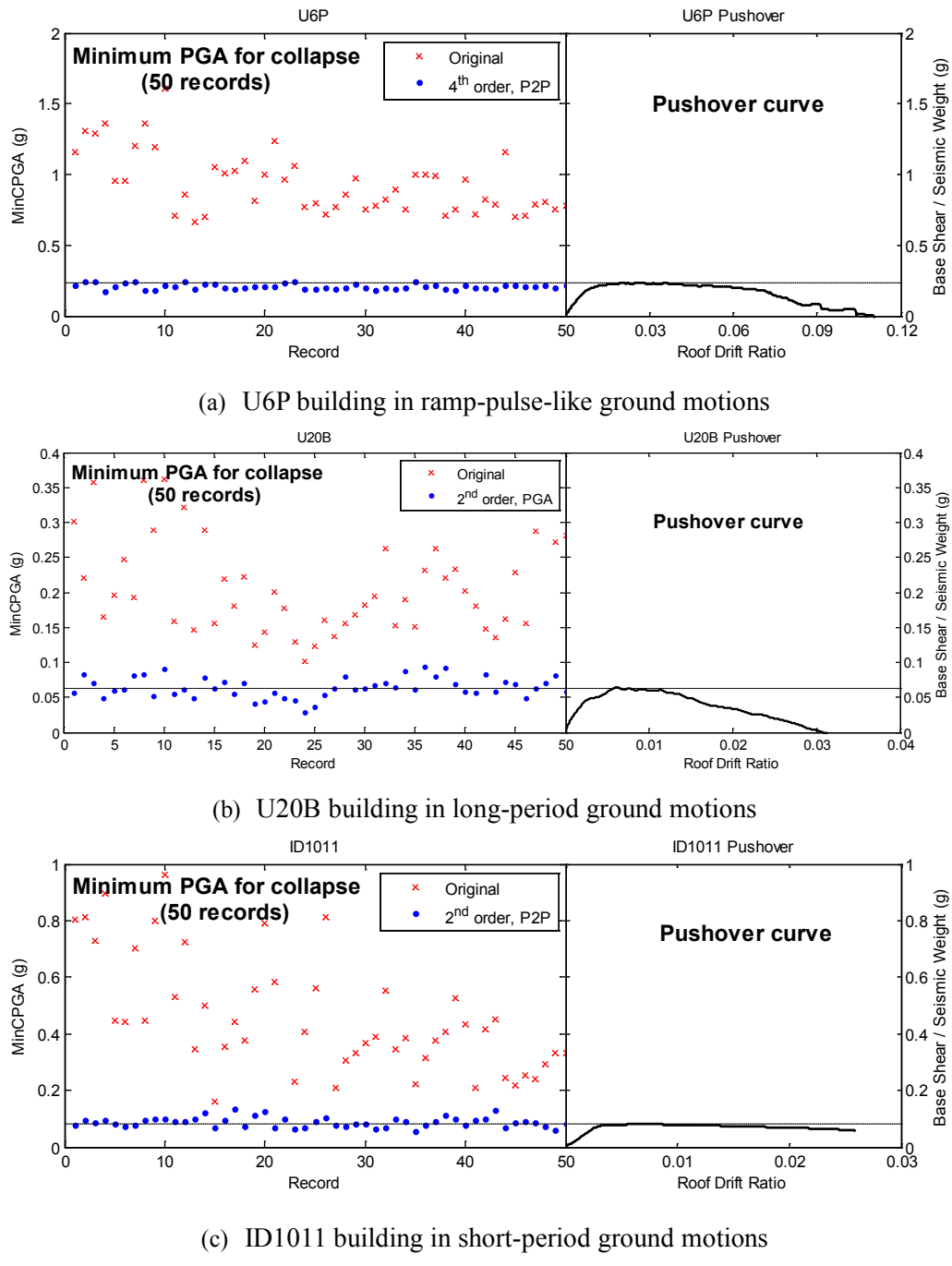


Figure 3.11 Comparison of peak values of original records, filtered records at thresholds of collapse with maximum values of pushover curves. In the left panels each record is represented by the PGA of the scaled motion that caused collapse (red) and the $\frac{1}{2}$ peak-to-peak amplitude of the filtered acceleration (blue). The right panel shows a pushover curve for the building where the vertical scale (acceleration) is common to both panels.

Table 3.3 Geometric mean values of collapse thresholds (g)

Building	Ramp-pulse-like	Long-period	Short-period	Pushover
U6P	0.207	0.230	0.212	0.232
U6B	0.173	0.162	0.164	0.163
U13P	0.123	0.139	0.139	0.139
U13B	0.072	0.086	0.081	0.084
U20P	0.119	0.106	0.110	0.106
U20B	0.062	0.063	0.062	0.063
ID1003	0.155	0.134	0.122	0.147
ID1011	0.072	0.081	0.086	0.080
ID1013	0.066	0.078	0.081	0.075
ID1021	0.091	0.088	0.087	0.088

3.1.4 Summary of the PFA Model for 2D Buildings

To make the method more practical, we summarized the result in this study into standard procedures to predict the collapse of steel and RC frame buildings.

Given a target building and a ground motion record, five steps should be followed to predict whether the building will collapse:

Step 1: Obtain the fundamental period T_1 , the maximum base shear force V_{max} , the seismic weight W , and the ductility of the building.

Step 2: Compute the cutoff period coefficient c for the building using Equation 3.1.

Step 3: Identify the type of the ground motion as one of the following:

- a. Ramp-pulse-like ground motion (RP).
- b. Long-period ground motion (LP).
- c. Short-period ground motion (SP).

Step 4: Filter the acceleration time history using a Butterworth filter with the order and the cutoff frequency given in Table 3.4.

Table 3.4 Parameters of Butterworth filter

Type of ground motion	Order	Cutoff frequency
Ramp-pulse-like	4	$1/cT_1$
Long-period & Short-period	2	$1/cT_1$

Step 5: Predict the building behavior with Table 3.5.

Table 3.5 Chart of collapse prediction (g is gravity acceleration)

Type of ground motion	Intensity measure	Condition	Prediction
Ramp-pulse-like	Half of peak-to-peak acceleration	$>V_{max}/W \cdot g$	Collapse
		$<V_{max}/W \cdot g$	Standing
Long-period	Peak ground acceleration	$>V_{max}/W \cdot g$	Collapse
		$<V_{max}/W \cdot g$	Standing
Short-period	Half of peak-to-peak acceleration	$>V_{max}/W \cdot g$	Collapse
		$<V_{max}/W \cdot g$	Standing

3.2 Fragility Curves Based on the PFA Model

The fragility curve, defined as a relationship between ground shaking intensity and the probability of reaching or exceeding a certain response level, is a powerful tool in the assessment of seismic losses, both for pre-earthquake disaster planning, and post-earthquake recovery and retrofitting programs (Jeong and Elnashai, 2007).

In this section, we develop the fragility curves for the analyzed building at collapse level and give the regression model for the parameters of the fragility curves.

3.2.1 Determining the Statistical Distribution Used for the Fragility Curves

We first need to find the continuous probability distribution which best describes the distribution of computed collapse thresholds. We propose two candidates for investigation: log-normal distribution and Weibull distribution.

A log-normal distribution is a continuous probability distribution of a random variable, the logarithm of which is normally distributed. The probability density function of a log-normal distribution is

$$f(x; \mu, \sigma) = \frac{1}{x\sigma\sqrt{2\pi}} e^{-\frac{(lnx-\mu)^2}{2\sigma^2}} \quad x > 0 \quad (3.2)$$

Named after Waloddi Weibull, Weibull distribution is a continuous probability distribution, for which the failure rate is proportional to a power of time. The probability density function of a Weibull distribution is

$$f(x; \lambda, k) = \begin{cases} \frac{k}{\lambda} \left(\frac{x}{\lambda}\right)^{k-1} e^{-(x/\lambda)^k} & x \geq 0 \\ 0 & x < 0 \end{cases} \quad (3.3)$$

where $k > 0$ is the shape parameter and $\lambda > 0$ is the scale parameter of the distribution. The reason why we chose log-normal distribution and Weibull distribution as two candidates is that the shapes of their probability density functions are quite close to the distribution of the computed collapse thresholds of the analyzed buildings.

We used Akaike information criterion (AIC) to select a better model from the two candidates. The Akaike information criterion (AIC) is defined as

$$AIC = 2k - 2\ln(L) \quad (3.4)$$

where k is the number of parameters in the statistical model and L is the maximized value of the likelihood function for the estimated model. Founded on information entropy, the Akaike information criterion is a measure of the relative quality of a statistical model for a given set of data. The smaller the AIC value is, the better the model is. Since both candidates have two parameters, evaluating the AIC values is then equivalent to evaluating the maximum likelihood. The AIC values of all the ten building models subjected to three ground motion sets are listed in Table 3.6 for log-normal and Weibull distribution.

Table 3.6 AIC values for log-normal and Weibull distribution

Building	Ramp-and-pulse		Long-period		Short-period	
	Log-normal	Weibull	Log-normal	Weibull	Log-normal	Weibull
U6P	-256	-247	-199	-181	-134	-125
U6B	-257	-249	-245	-237	-167	-156
U13P	-261	-250	-222	-214	-175	-163
U13B	-330	-325	-289	-281	-235	-230
U20P	-215	-208	-240	-228	-192	-176
U20B	-280	-251	-274	-277	-251	-242
ID1003	-234	-224	-269	-254	-252	-241
ID1011	-388	-377	-312	-306	-263	-254
ID1013	-347	-332	-292	-280	-272	-252
ID1021	-316	-308	-261	-252	-264	-255

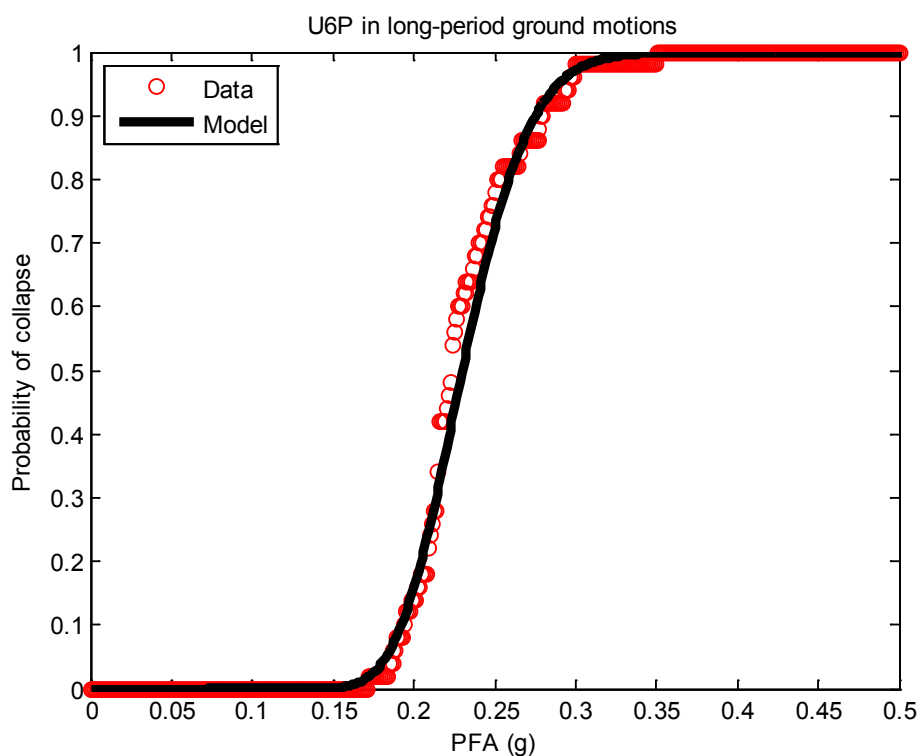


Figure 3.12 Collapse fragility curve of U6P building in long-period ground motions

From the AIC values in Table 3.6, it could be concluded that log-normal distribution is the ideal model for the collapse prediction. We then fit a log-normal distribution to the data to obtain the corresponding fragility curve. An example (U6P in long-period ground motions) of the resultant fragility curves is shown in Figure 3.12. The fragility curves for all the ten buildings subjected to three ground motion sets can be found in Appendix A.3.

3.2.2 Determining the Regression Models for the Standard Deviations of the Log-normal Fragility Curves

For the fragility curves described by log-normal distribution, there are two parameters: mean value and standard deviation of $\ln(PFA)$, respectively. In the previous sections, we have already shown that the mean value is just the maximum value (fraction of g) of the pushover curve computed from the corresponding building. In this section, we will give a regression model for the remaining parameter, the standard deviation. The standard deviations of $\ln(PFA)$ for ten building models in three ground motion sets (thirty standard deviations in total) are shown in Table 3.7 and Figure 3.13.

Table 3.7 Standard deviation of $\ln(PFA)$

Building	Ramp-pulse-like	Long-period	Short-period
U6P	0.0877	0.1398	0.2909
U6B	0.1037	0.1243	0.2694
U13P	0.1415	0.1834	0.2926
U13B	0.1204	0.1507	0.2774
U20P	0.2295	0.2018	0.3116
U20B	0.2295	0.2425	0.3073
ID1003	0.1451	0.1190	0.1544
ID1011	0.0675	0.1289	0.1968
ID1013	0.1101	0.1620	0.1901
ID1021	0.1089	0.1972	0.1930

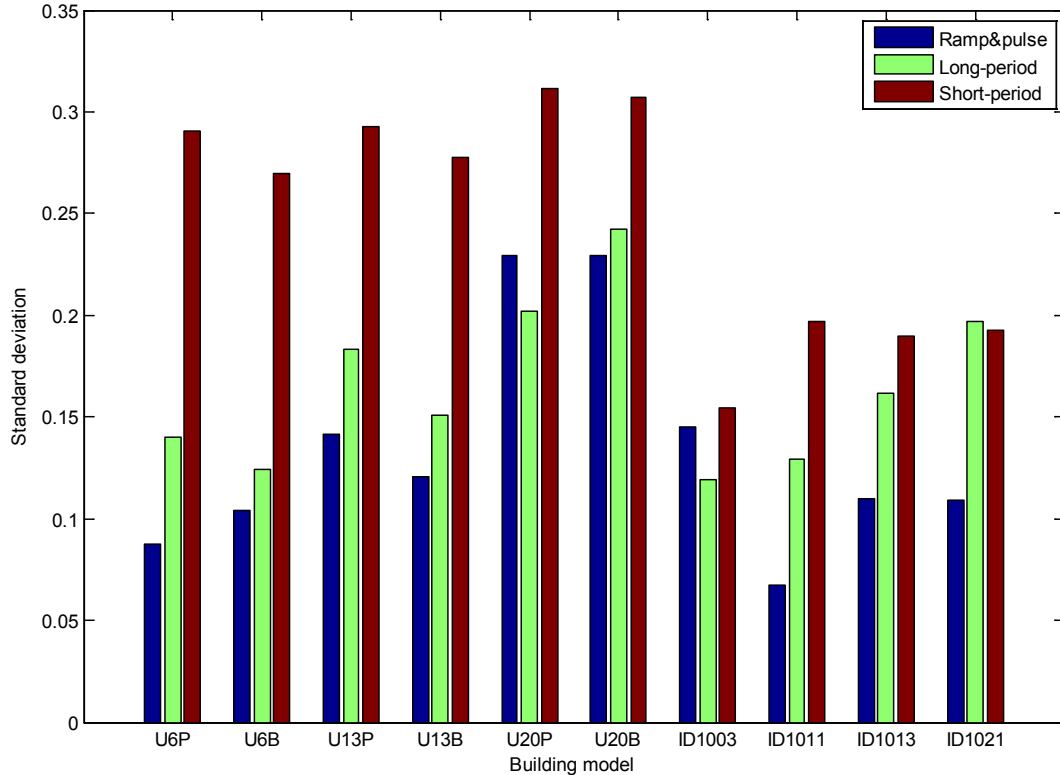
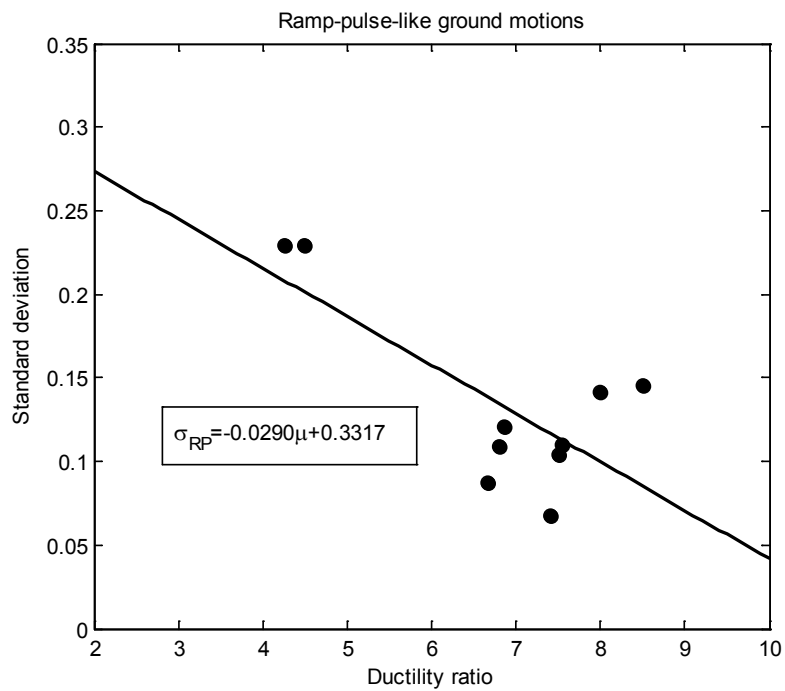


Figure 3.13 Computed standard deviations in collapse prediction

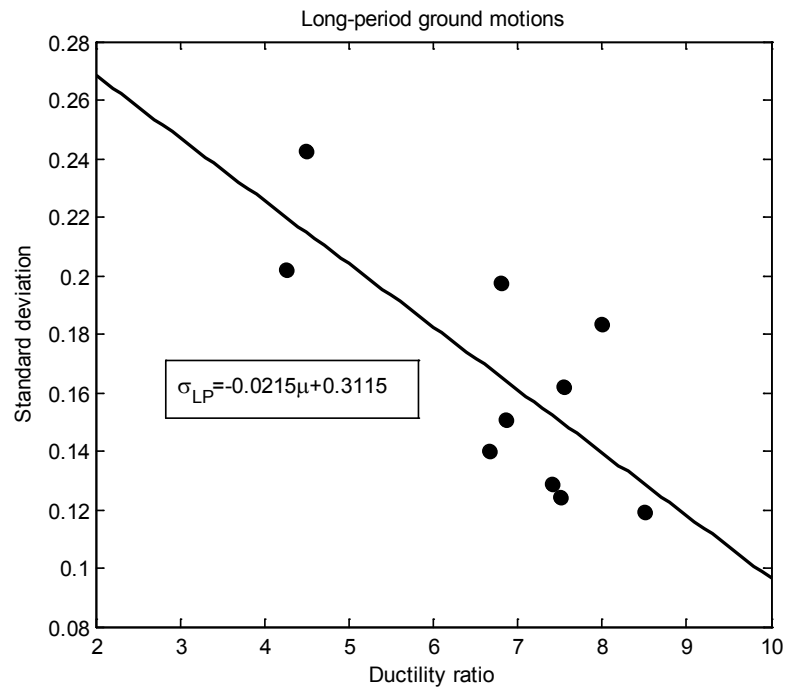
From Table 3.7 and Figure 3.13, it could be concluded that generally $\sigma_{RP} < \sigma_{LP} < \sigma_{SP}$. Short-period ground motions have more high-frequency components, which would not control the collapse according to PFA model. Hence, in the framework of the current PFA model, high-frequency components are just considered noise. When the noise level increases, the uncertainty of the prediction will also increase.

It is also found that the standard deviation is correlated with the ductility of the building. Generally, the standard deviation decreases when ductility increases.

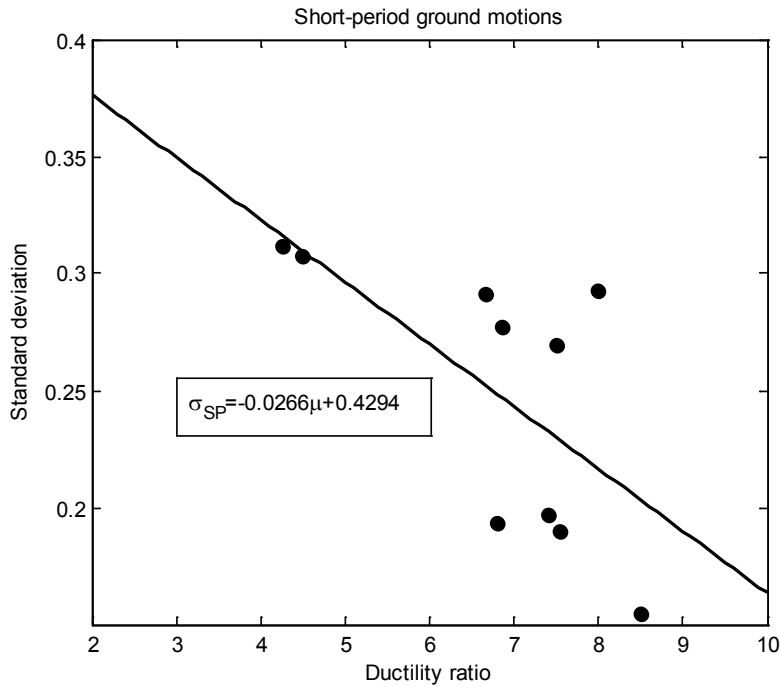
Based on the above conclusions, we developed the regression model for three ground motion sets separately. The results are shown in Figure 3.14 and Table 3.8.



(a) Regression of standard deviation for ramp and pulse ground motions



(b) Regression of standard deviation for long-period ground motions



(c) Regression of standard deviation for short-period ground motions

Figure 3.14 Regression of standard deviations for ramp-pulse-like, long-period, and short-period ground motions

Table 3.8 Regression equations of standard deviations of collapse thresholds
for three ground motion sets

Ground motions	Regression equations
Ramp-pulse-like	$\sigma_{RP} = -0.0290\mu + 0.3317$
Long-period	$\sigma_{LP} = -0.0215\mu + 0.3115$
Short-period	$\sigma_{SP} = -0.0266\mu + 0.4294$

3.3 (PGV, PGD) Description of the PFA Collapse Prediction Model

This section is a continuation of the PFA collapse prediction model. In the previous sections, we proposed a collapse prediction method based on a new parameter: peak filtered acceleration (PFA). To predict whether a building will collapse in response to a given ground motion, we first estimated the maximum lateral capacity of the building. We then filtered the ground acceleration time history

using a low-pass 2nd-order Butterworth filter (4th-order Butterworth filter for ramp-pulse-like ground motions) and with a cutoff frequency that is typically lower than the first mode frequency. If the amplitude of the filtered acceleration record (given as a fraction of g) exceeds the building's pushover maximum strength (given as a fraction of the building weight) then P-delta instability is expected.

While PFA is simple and effective for predicting collapse, it is a new parameter and thus unfamiliar. The purpose of this section is to demonstrate the relationship between the new unfamiliar PFA parameter and the vector parameter (PGV, PGD), which consists of two traditional ground motion intensity measures. In particular we show how to convert our PFA model for collapse into an equivalent (PGV, PGD) model for collapse. We also show a good agreement between our predicted results with Olsen and Heaton's (2013) computational results.

3.3.1 Converting PFA Model into (PGV, PGD) Model

Although the proposed prediction method in previous sections is straightforward in concept, peak filtered acceleration (PFA) is a brand new concept which might not be adopted by engineers easily. In this section, we describe the same method in alternative measures, PGV and PGD, which are more widely used in measuring ground motion intensities.

In order to obtain PGV and PGD, we first need to integrate ground acceleration time history with respect to time once and twice to get ground velocity and displacement time history. Since we use sinusoidal ground motion in computing MinCPGA, to obtain the corresponding PGV and PGD, simply multiply the amplitude by $T_s/2\pi$ once and twice (T_s denotes the period of sinusoidal ground motion).

However, in the PFA model we measured the size of a real ground motion record by the $\frac{1}{2}$ peak-to-peak value (except in the case of long-period motions when we use the peak value). Hence, to convert $\frac{1}{2}$ peak-to-peak values into peak values (PGV and PGD), we needed to multiply the PFAs by coefficients c_V and c_D , where c_V denotes the average ratio of peak ground velocity to $\frac{1}{2}$ peak-to-peak ground velocity and c_D denotes the average ratio of peak ground displacement to $\frac{1}{2}$ peak-to-peak ground displacement. From the statistical results of the ground motions used in the previous sections, c_V was chosen as 1.08 and c_D was chosen as 1.57. Then the collapse threshold in terms of PGV and PGD could be obtained as a function of period from Equation 3.5 and Equation 3.6.

$$PGV_{threshold} = c_V \cdot \frac{T_s}{2\pi} \cdot MinCPGA \quad (3.5)$$

$$PGD_{threshold} = c_D \cdot \left(\frac{T_s}{2\pi}\right)^2 \cdot MinCPGA \quad (3.6)$$

After obtaining $PGV_{threshold}(T_s)$ and $PGD_{threshold}(T_s)$, we eliminated the common variable, T_s , and plotted the collapse threshold in Log (PGV)-Log (PGD) space, where T_s is now a parameter along the collapse curve. An example is shown in Figure 3.16 for U20B, a 20-story steel building with brittle welds. To predict whether a building will collapse when subjected to a given ground motion, first compute PGV and PGD of the ground motion record, then plot the point (PGV, PGD) in the corresponding collapse prediction chart (e.g. Figure 3.16). If the point falls into region B, it is expected to collapse. Otherwise, it is expected to survive the ground motion if it is located in region A.

Using the simple relationship between velocity and displacement for a sinusoid, we used equations 3.7 and 3.8 to plot lines of constant period T_s in Figure 3.16. Generally, most real data that is classified as strong shaking has periods between $\frac{1}{2}$ and 5 seconds. Therefore most (PGV, PGD) points fall into a banded region.

$$PGV = 2\pi PGD/T_s \quad (3.7)$$

$$\log(PGV) = \log(PGD) - \log(T_s) + 0.8 \quad (3.8)$$

3.3.2 Verification of the Developed Model

Olsen (2008) collected 64,765 synthetic, seismic ground motions and applied them to eight finite element models of welded, steel moment-resisting frame buildings. Each ground motion is characterized with a vector intensity measure (PGV, PGD), and the building model response to each ground motion is characterized as “collapsed” or “standing”. Among the eight finite element models, four are identical with what we used in the previous sections. They are U6P, U6B, U20P, and U20B, respectively. In this section, we predict collapse thresholds of the four building models using the (PGV, PGD) prediction model derived from the PFA prediction model. We then compare the predicted collapse thresholds with the computational results Olsen has obtained.

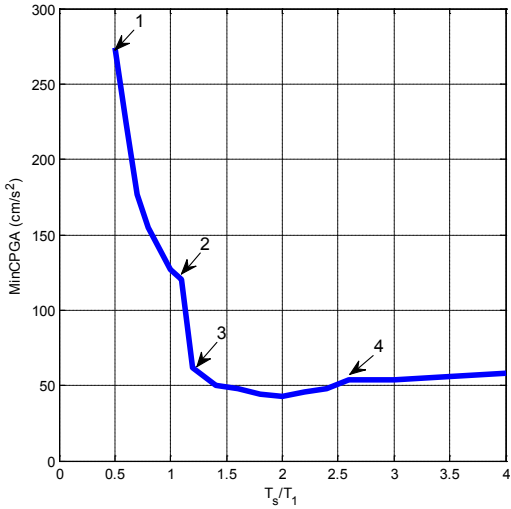


Figure 3.15 Example of minimum collapse PGA for U20B. The motion is sinusoidal, with duration of 40s and period T_s . T_1 is the period of the 1st mode, which is 3.47 s for this building.

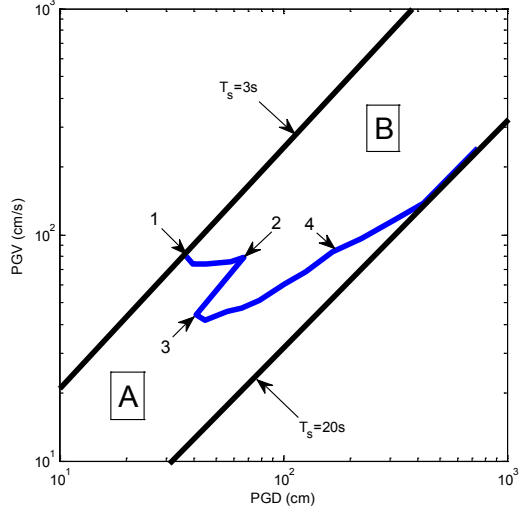


Figure 3.16 Example of collapse threshold in terms of PGV and PGD of the same building in Figure 3.15

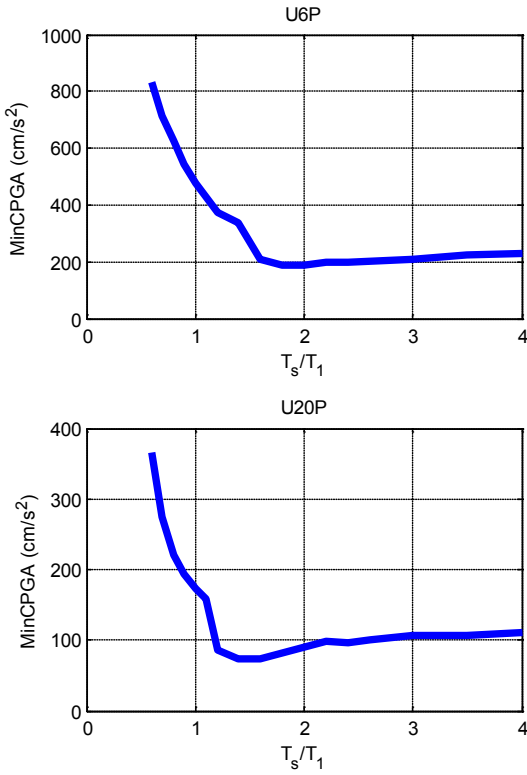


Figure 3.17 Minimum collapse PGA spectra in sinusoidal ground motions for U6P, U6B, U20P, and U20B

MinCPGA Spectra of the Studied Buildings

In section 3.1.2, we have discussed the procedures to generate the minimum collapse PGA (MinCPGA) spectrum. Figure 3.17 shows the computed MinCPGA spectra for U6P, U6B, U20P, and U20B; a 40s duration of sinusoidal ground motions is used in each case.

Comparison of the Predicted and Computational Results

After obtaining collapse thresholds in term of PGA, we converted them into collapse thresholds in terms of PGV and PGD using Equation 3.5 and Equation 3.6. The predicted collapse thresholds, based on our proposed model and the computational results obtained by Olsen, are plotted in Figure 3.18. The first mode of the U20P and U20B is 3.47s, and Olsen was able to use simulated records that had a 2s cutoff frequency dictated by the grid size in finite element models used to simulate ground motions. However, the first period of U6P and U6B is only 1.54s, and so Olsen was forced to use broad-band simulated motion records; unfortunately, there were far fewer of these available to study. To ensure enough data points, results for U6P and U6B from previous sections are also included in Figure 3.18. In Figure 3.18, black dots represent the ground motions that cause collapse of the corresponding building, while gray dots are those that do not. The predicted thresholds are plotted in red solid lines. Since our proposed model is developed based on the minimum ground motions that cause collapse of buildings, the threshold we predict is actually the lower boundary of collapse. In Figure 3.18, the predicted thresholds and lower boundaries of collapse show good agreement. Especially for U20P and U20B, the predictions captured the features of the collapse boundaries. However, the predictions work slightly worse for U6P and U6B, especially when they are subjected to high frequency ground motions (high PGV to PGD ratios). One possible explanation is that when computing collapse thresholds, we assumed the ground motions to be harmonic. However, high frequency ground motions are quite different from harmonic motions, which leads to poor performance in predicting collapse of buildings subjected to high frequency ground motions.

Olsen and Heaton (2013) proposed a collapse prediction model based on the regression from the computed results. However, it is difficult to capture the features of collapse threshold using this method, since it needs a complicated regression equation.

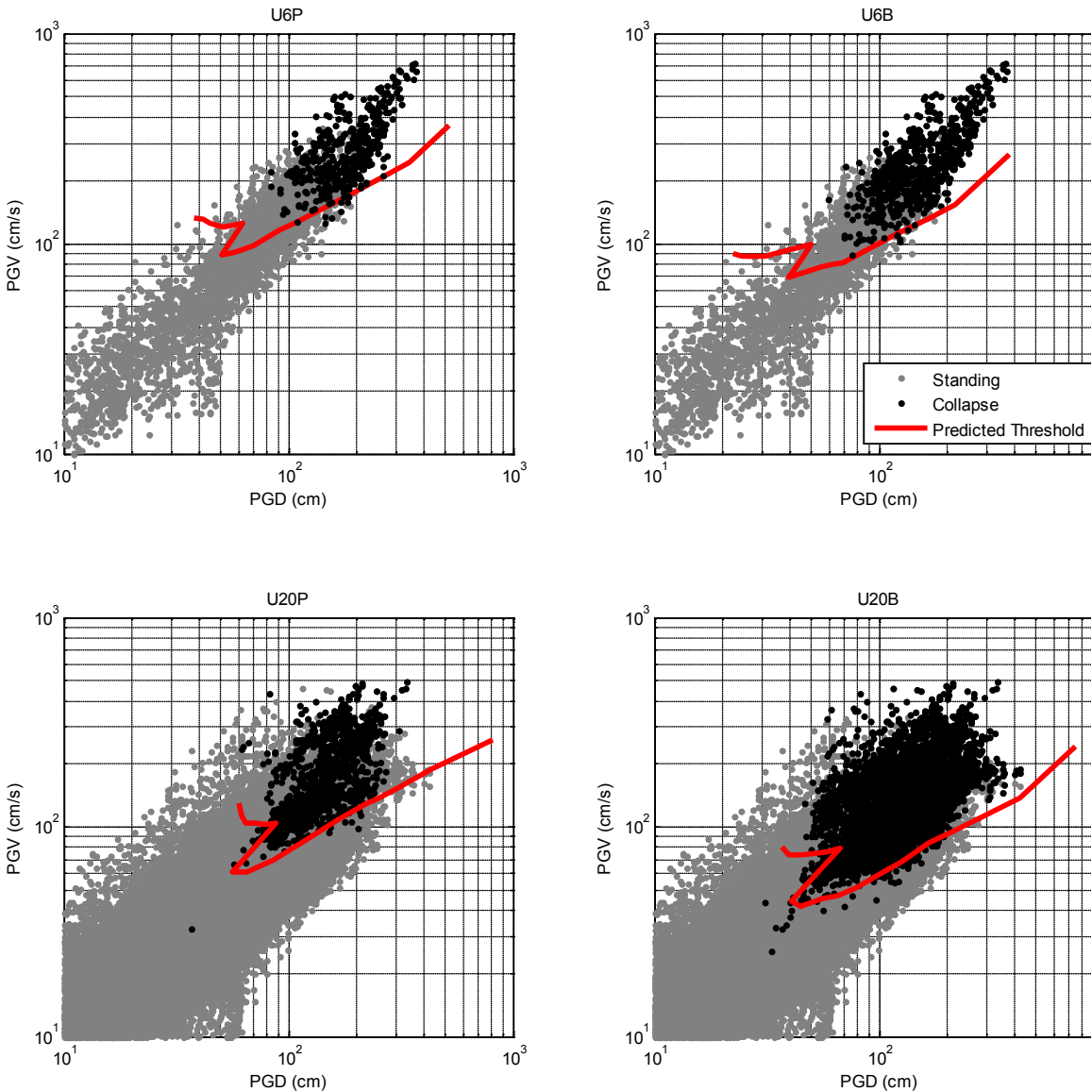


Figure 3.18 Comparison of predicted collapse thresholds and Olsen's computed result

3.3.3 Comparison between (PGV, PGD) Model and PFA Model

In this chapter, we developed two models to predict the collapse of moment-resisting frame buildings. One model predicts collapse with peak filtered acceleration (PFA), while the other does with PGV and PGD. Both models assume that the long-period component of a ground motion controls the collapse of buildings. Hence, to predict collapse of buildings, we neglected unnecessary short-period components and only considered the long-period components

The first model, the PFA, extracts long-period components from a ground motion record with a Butterworth filter, while the second (PGV, PHD) model does it with integration. The log-log gain functions of 2nd-order Butterworth filtering, time integration (acceleration to velocity), and double integration (acceleration to displacement) are plotted in Figure 3.19.

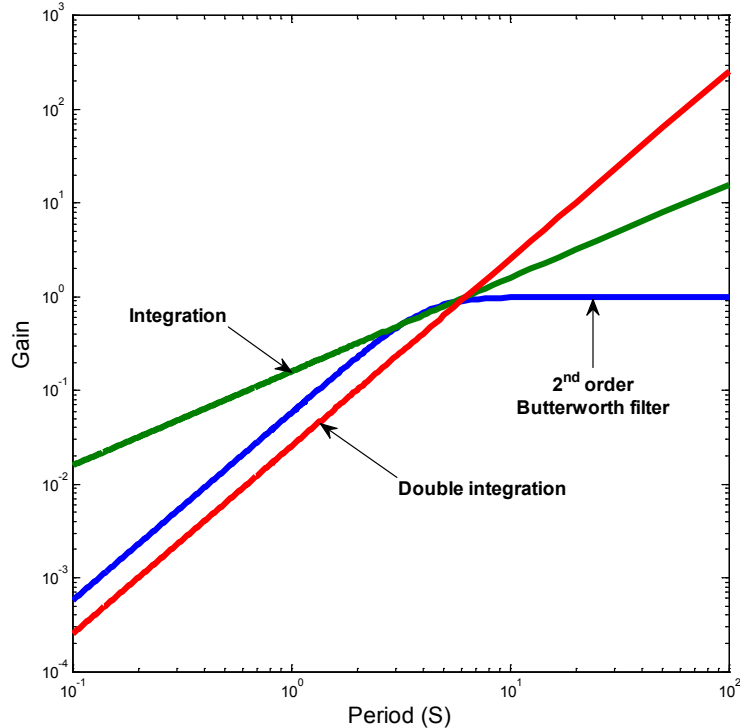


Figure 3.19 Gain functions of 2nd-order Butterworth filter and integration

Although integration can be viewed as a type of filter that enhances long periods linearly with period (or as period squared in the case of double integration), integration has no inherent scale. This is different from the Butterworth filter, where we used the natural period of the building in the formula to define the corner in the filter. That is, the PFA collapse methodology explicitly includes the building properties, whereas the (PGV, PGD) parameter cannot reflect the difference between buildings. The (PGV, PGD) model solves this problem by introducing a different 2D collapse threshold for each building. The PFA model only has a 1D collapse threshold (a constant derived from pushover analysis).

In summary, the PFA model and the (PGV, PGD) model represent the same physics, but they are stated in different ways. The PFA model filters out extraneous high-frequency motions using a

Butterworth filter, the parameters of which are determined by the dynamic characteristics of the building. Alternatively, the (PGV, PGD) model ignores the extraneous high frequencies by integration, and then considers the difference among buildings to be given by a threshold curve that is determined from nonlinear analysis of a broad range of ground motions.

PFA COLLAPSE PREDICTION MODEL FOR 3D BUILDINGS

This chapter is a continuation of Chapter 3. In Chapter 3, we proposed a collapse prediction model based on a new parameter: peak filtered acceleration (PFA). To predict whether a building will collapse in response to a given ground motion, we first estimated the maximum lateral capacity of the building. We then filtered the ground acceleration time history using a low-pass Butterworth filter with suggested order and cutoff frequency. If the amplitude of the filtered acceleration record (given as a fraction of g) exceeded the building's pushover maximum strength (given as a fraction of the building weight) then P- Δ instability was expected.

The result in Chapter 3 is verified only by 2D frame buildings. In this chapter, we extend the PFA collapse prediction model from 2D frame buildings to 3D frame buildings. In the PFA model, we obtain two important parameters, lateral capacity and global ductility, through pushover analysis. The pushover analysis, also known as non-linear static procedure, was developed by Saiidi and Sozen (1981), Fajfar and Gapersic (1996), and Chopra and Goel (2002) over the past thirty years, and recommended by FEMA 273 and ATC 40. However, pushover analysis is usually performed in principal directions. Thus, we could only obtain the properties of a building in principal directions through commonly used pushover analysis.

In this chapter, we apply pushover analysis to a 3D steel moment-resisting frame building in various horizontal directions (from 0 to 360 degree) and obtain its limit domain (maximum base shear versus angle in polar coordinates). The limit domain is either of square shape (regular stiffness distribution) or square shape with round corners (irregular stiffness distribution). Based on these results, we extend the PFA collapse prediction model developed in the previous chapter from 2D frame buildings to 3D frame buildings. We show that for a regular 3D frame building, we could decompose it into two 2D frame buildings and apply the PFA collapse prediction model to each of them. The performance of the 3D frame building could be predicted by combining the results from the two decomposed 2D frame buildings. For an irregular 3D frame building, we directly use the bi-directional filtered ground acceleration and the 2D limit domain to predict collapse. If the filtered bi-directional acceleration exceeds the 2D limit domain, the building will collapse, otherwise, the

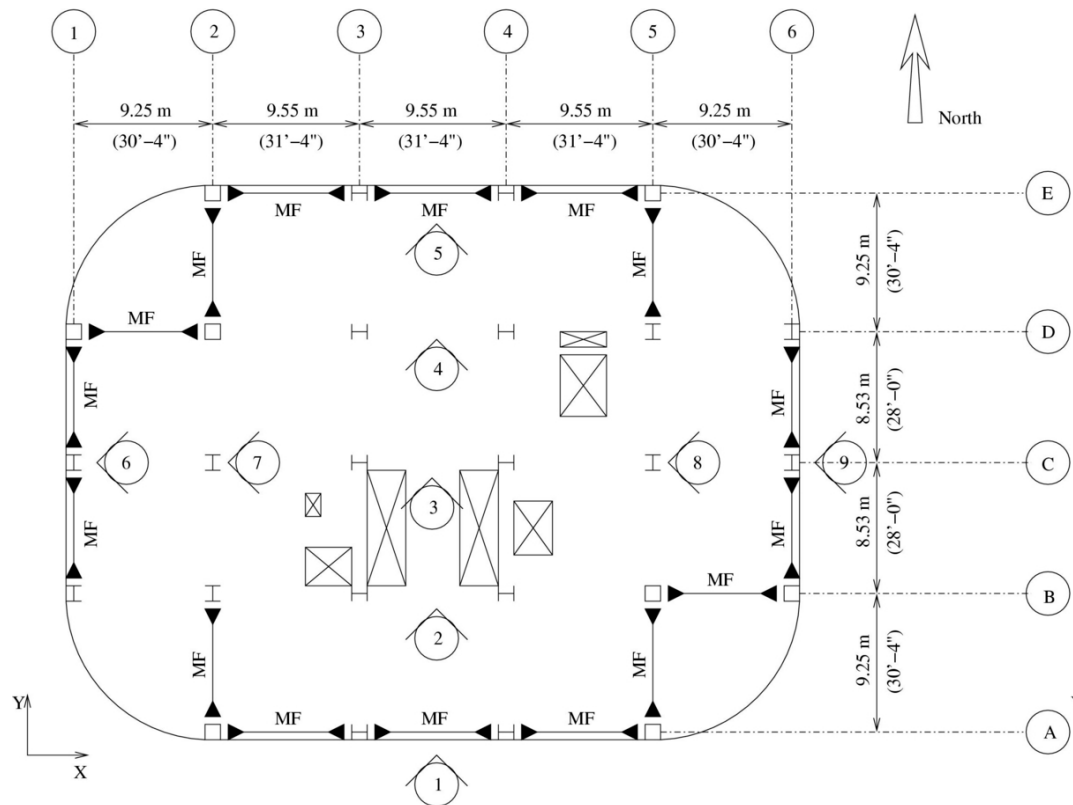
building will survive the ground motion. The results are compared with the FEM simulations in Frame3D and show good agreement in collapse prediction.

4.1 Building Models

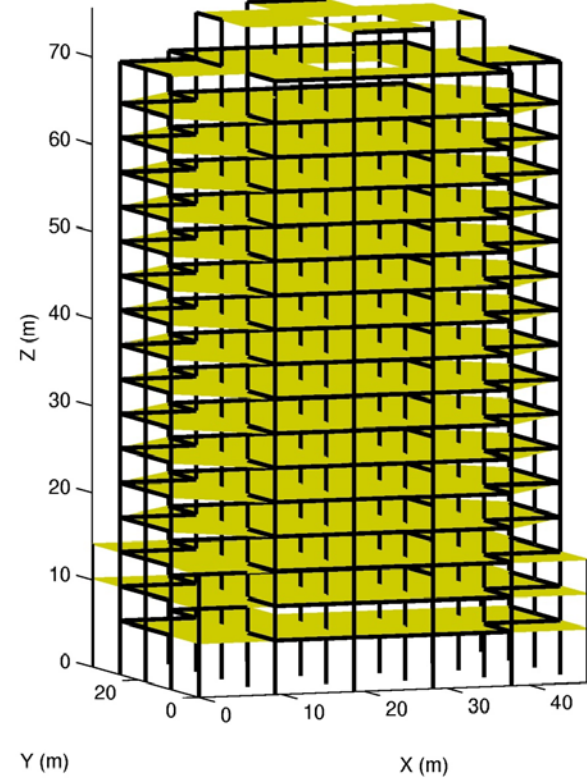
We use three building models in this chapter: an 18-story building (denoted with B1) (Krishnan et al., 2006), a 19-story L-shaped irregular building (denoted with B2), and a 19-story torsionally irregular building (denoted with B3) (Krishnan, 2007). All three buildings are steel moment-resisting frame buildings designed according to UBC 97 (ICBO 1997).

B1 is a redesigned version of an existing modern 18-story welded steel moment-resisting frame building located within five miles of the epicenter of the 1994 Northridge earthquake. The original design was done in 1984 according to the lateral force requirements of the 1982 Uniform Building Code (ICBO, 1982), and redesigned according to UBC 97 (ICBO, 1997). The new design gives a relatively symmetric plan view. B2 is L-shaped in plan, with one elevator core serving both wings of the building. The two wings are identical in design. B3 is rectangular-shaped in plan, with the elevators and stairs located along one face of the building to obtain a better ocean view.

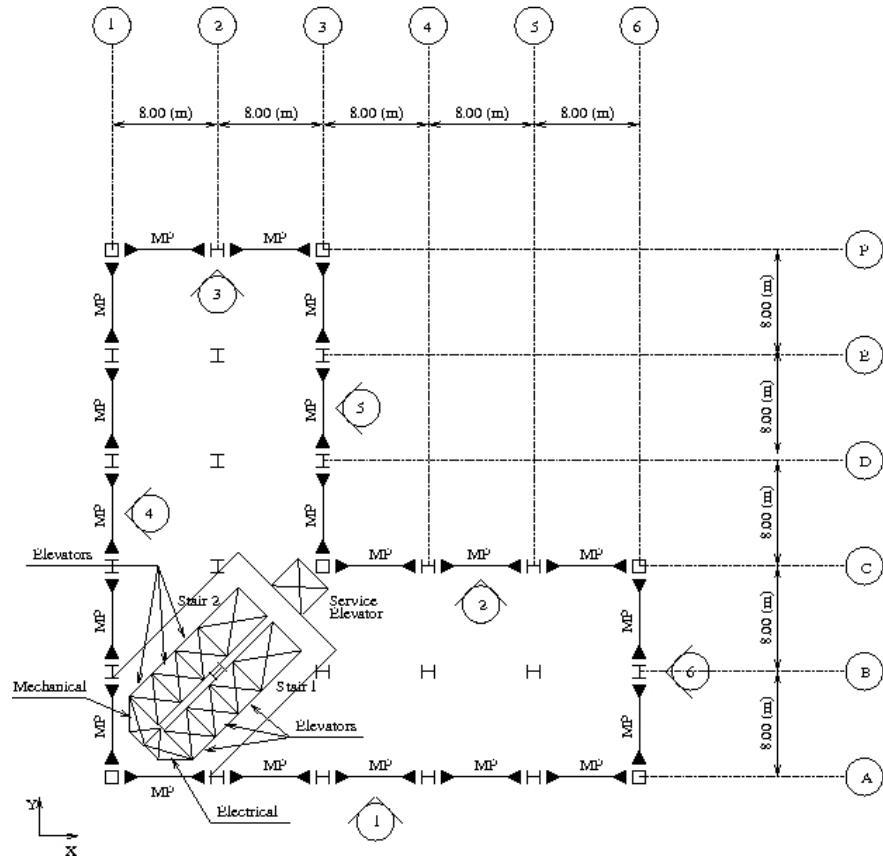
The three selected building models could represent a large range of existing buildings, since B1 is relatively symmetric both in plan and in stiffness, B2 has an asymmetric plan but regularly distributed frames that give regular stiffness distribution, and B3 is symmetric in plan but asymmetric in stiffness.



(a) Typical floor plan of B1

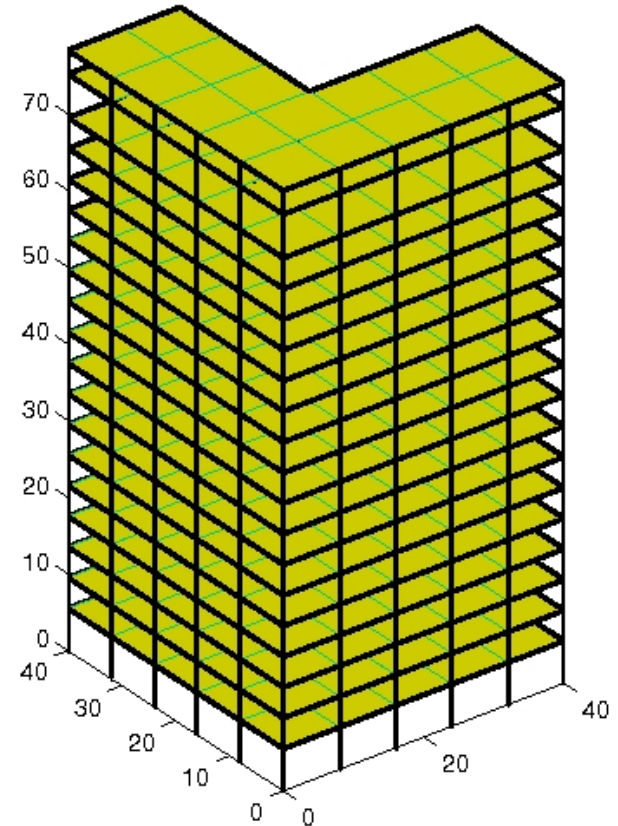


(b) Isometric view of B1

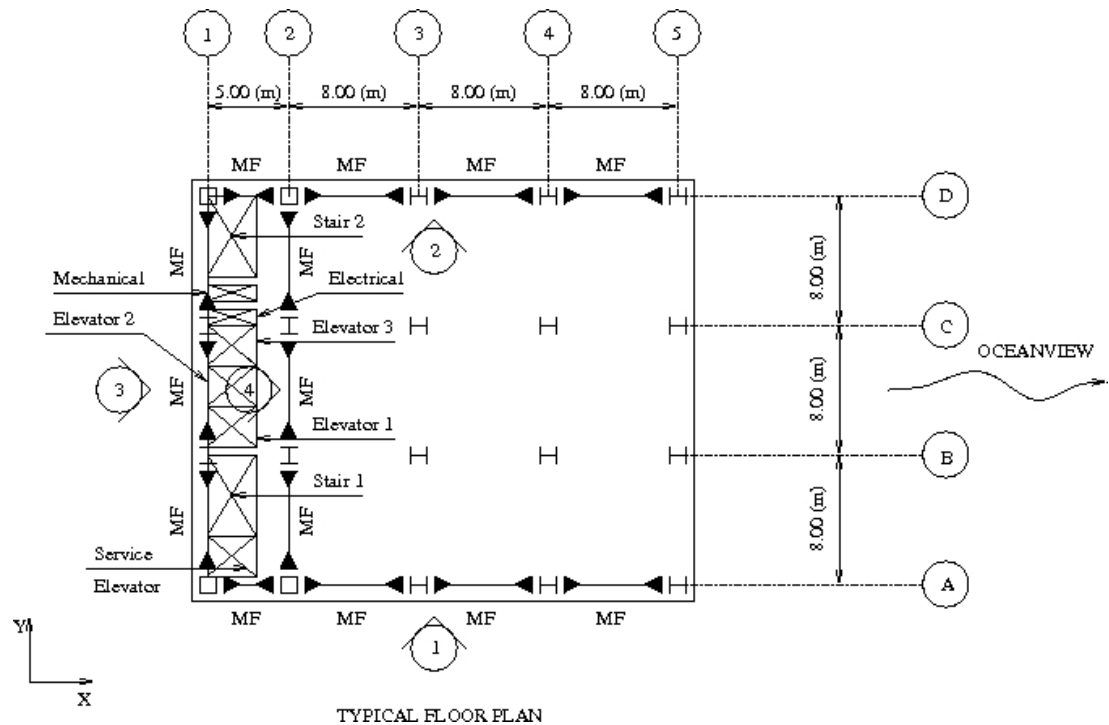


(c) Typical floor plan of B2

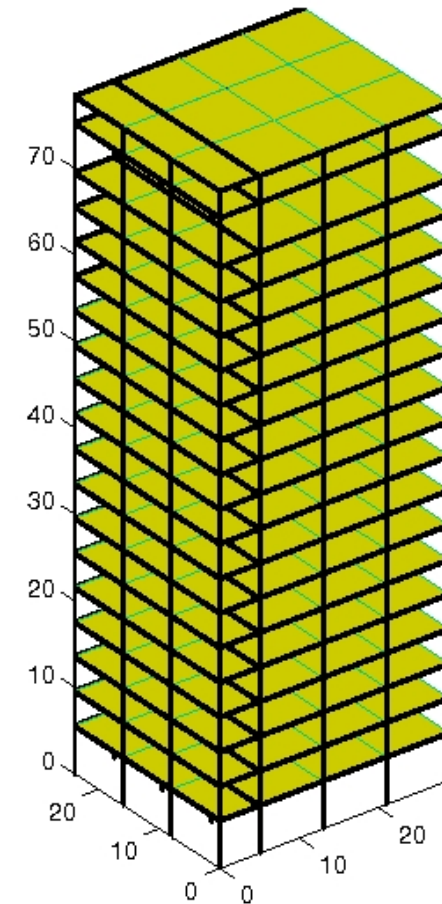
TYPICAL FLOOR PLAN



(d) Isometric view of B2



(e) Typical floor plan of B3



(f) Isometric view of B3

Figure 4.1 Typical floor plans and isometric views of studied building models

The periods and modal direction factors corresponding to the first three modes of the three buildings are listed in Table 4.1.

Table 4.1 Information on the studied 3D frame building models

Building Model	Mode	T (s)	Modal direction factor		
			X-translational	Y-translational	Z-rotational
B1	1	3.72	47.24	52.72	0.04
	2	3.51	52.71	47.27	0.02
	3	2.24	0.08	0.01	99.91
B2	1	3.39	50.00	50.00	0.00
	2	3.32	49.89	49.89	0.22
	3	2.33	0.12	0.12	99.76
B3	1	3.21	0.00	72.64	27.36
	2	2.03	100.00	0.00	0.00
	3	1.22	0.00	30.99	69.01

All three buildings are modeled and analyzed in Frame3D (Krishnan, 2003). Beams and columns are modeled using elasto-fiber elements, beam-column joints are modeled using panel zone elements, and floor slabs are modeled using elastic plane-stress elements. The elasto-fiber beam element is divided into three segments, with the interior segment being modeled as a cubic-interpolated displacement-based elastic beam, and nonlinearity being restricted to the two exterior segments (Krishnan, 2007).

4.2 2D Pushover Analysis and Limit Domain

In this section, we introduce 2D pushover analysis and its result, limit domain, which is different from commonly used pushover analysis and its result, pushover curve.

4.2.1 Procedures of 2D Pushover Analysis

We performed pushover analyses to all building models in the horizontal directions from 0° to 360° with a 15° interval. In these analyses, the building model was subjected to a slow, ramped, horizontal ground acceleration that increased by $0.001g/s$, and the building response was

computed dynamically. In order to produce the lateral forces, the mass in horizontal directions of each node was recalculated to match the UBC 97 force distribution.

4.2.2 Result of 2D Pushover Analysis – Limit Domain

We extracted the maximum base shear in the loading direction from each pushover analysis and computed its components in the principal directions X and Y. We repeated the process for all 24 pushover analyses and plotted the maximum base shear forces into one figure defined as limit domain. The limit domains (LD) in term of maximum base shear over seismic weight of all three building models are shown in Figure 4.2, Figure 4.3, and Figure 4.4.

From Figure 4.2 to 4.4, it could be noticed that LD1 and LD2 are close to square shapes, while LD3 has a square shape with round corners. Although not intuitive, these results are easy to understand. Moment-resisting frame buildings resist lateral force through moment-frames. A moment-frame resists the lateral force through a frame mechanism along the direction it is placed (the direction of beam axis). If the force is in a perpendicular direction, the frame mechanism does not deform, and the moment-frame resists it only through the bending of columns. The out-of-plane strength of a moment-frame is much lower compared with the in-plane strength. Therefore, when we applied a lateral force to a building, we could decompose the lateral force into the two principal directions of the building, and assign them directly to the moment-frames in the corresponding directions, neglecting the contribution from the out-of-plane strength of frames in the perpendicular direction. As a result, a regular moment-frame building without torsion should be strongest in a 45° direction approximately, since the moment-frames in both principal directions contribute their maximum strengths. This conclusion comes from the assumption that the building has similar strength and ductility in both principal directions, which prevents the frames in one direction from failing much earlier than the frames in the other direction. In design procedures, design requirements such as base shear and displacement limit are identical for both principal directions; hence a regularly designed building should have similar properties in two principal directions.

Building B1 is a regular building with a relatively symmetric floor plan and a regular frame distribution. Thus, it does not have torsional deformation when subjected to lateral force. It is therefore not surprising that the limit domain is close to a square. However, it should be noted that the limit domain is not a perfect square, since the values at the corners decrease slightly from

those along the edge. This is mainly caused by the corner columns that are shared by two frames in perpendicular directions. By decomposing the lateral force directly into the frames in two principal directions of the building, we applied force to a corner column twice each time in one principal direction. It is therefore equivalent to saying the corner column is subjected to biaxial loading. The limit domain in term of maximum base shear for a column under biaxial bending is close to an ellipse (not a square), which provides less strength than simply adding the strengths in two principal directions together. In other words, for a column under biaxial bending, the maximum strength in either of the principal directions is smaller than its maximum strength under uniaxial bending. Since the corner column could not contribute its maximum uniaxial strength in two principal directions simultaneously, the limit domain is reduced by a small amount at the 45° direction.

Building B2 has an irregular L-shape in plan. However, its limit domain is still very close to a square. A possible explanation is that even though the building is irregular in plan, the frames are still regularly distributed, which results in a regular stiffness distribution and does not cause significant torsional response. Hence, when the building is loaded at 45° direction, the frames in two principal directions will still contribute their maximum strengths, which results in a square-shaped limit domain. It could be concluded that the primary factor which controls the shape of limit domain is the irregularity in stiffness, not the irregularity in plan.

B3 is a torsionally irregular building. Since the lateral force is applied through inertial force in the analysis, it is equivalent to applying the total force at the center of mass. Because the building is symmetric in plan but asymmetric in stiffness, the center of mass and the center of stiffness are not located at the same position. Hence, when we apply the lateral force, it introduces a torque and the building deforms in both translation and torsion. For the loading in 45° , as the lateral force increases, the directions of frames will change due to the torsional effect (see Figure 4.5). As a result, frames in one direction take larger portion of load while frames in the other direction take smaller portion of load. Thus the load is no longer equally distributed along frames in two directions. The frames which take the larger portion of the load will fail before the frames in the perpendicular direction have reached their maximum strength, which significantly reduces the total strength of the building in 45° loading. This is the reason why LD3 shows four rounded corners, which is different from LD1 and LD2.

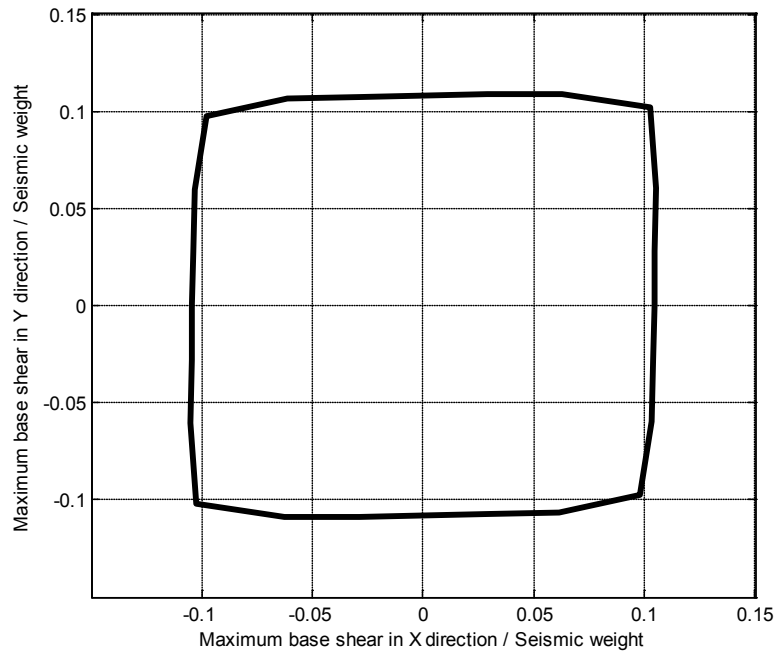


Figure 4.2 Limit domain in term of base shear over seismic weight for B1

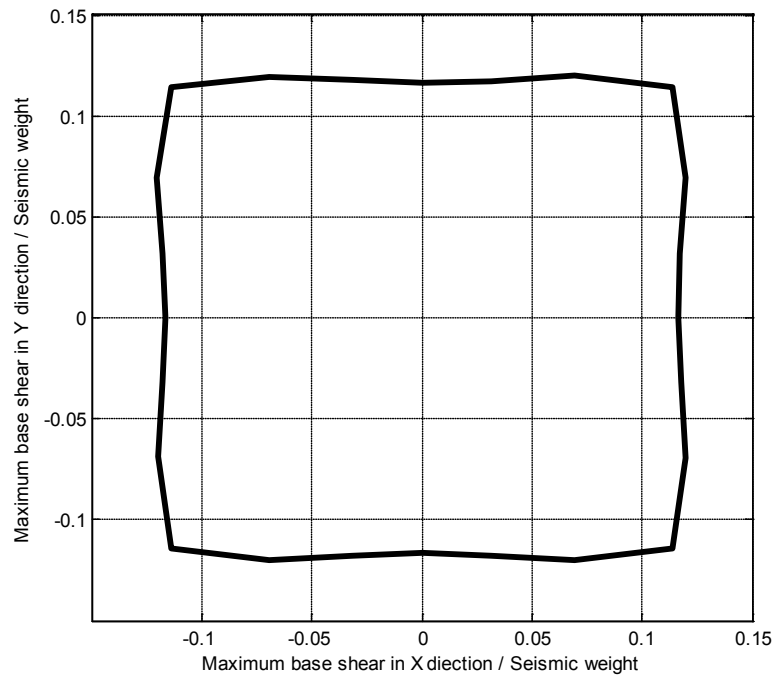


Figure 4.3 Limit domain in term of base shear over seismic weight for B2

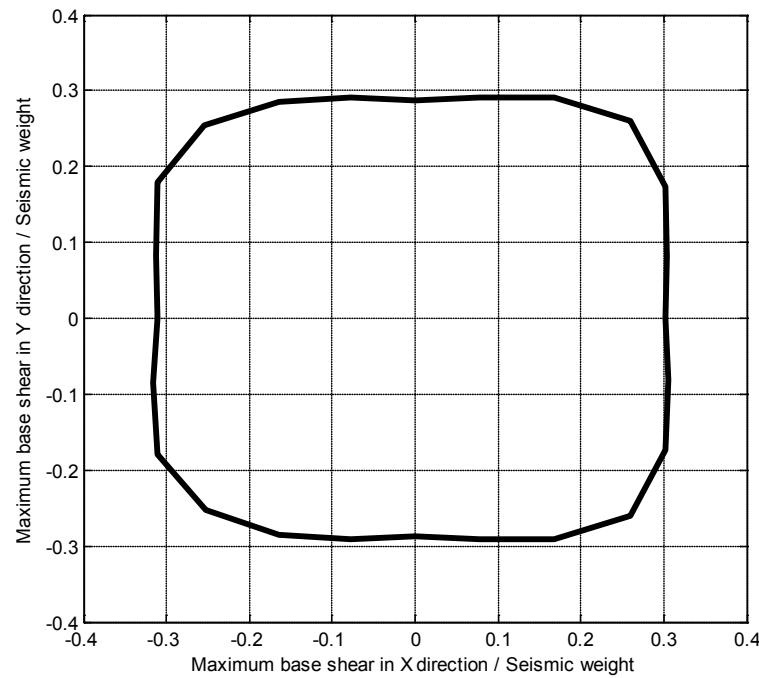


Figure 4.4 Limit domain in term of base shear over seismic weight for B3

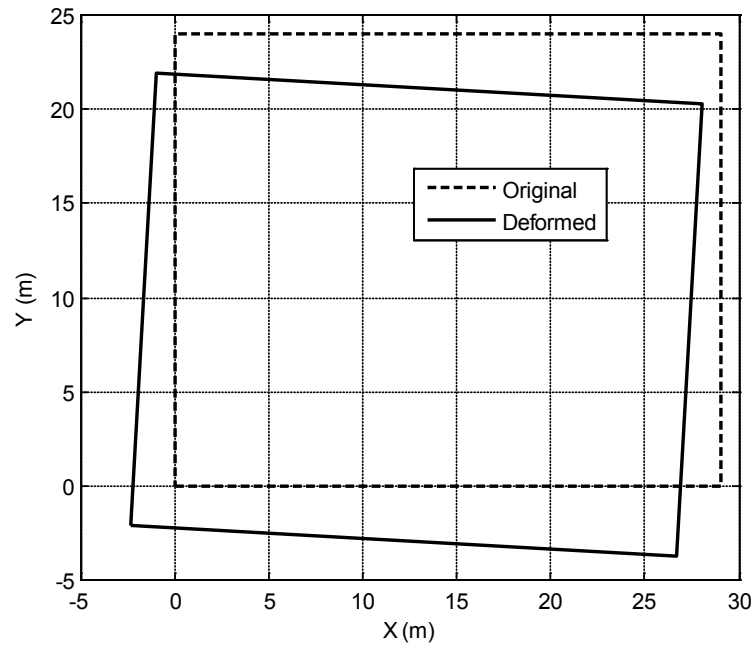


Figure 4.5 Roof position of original and deformed B3 building in 45° pushover

4.2.3 Comparison with the Results from Petti et al.

Petti et al. (2008) have analyzed two benchmark structures with a similar approach and obtained the limit domains of collapse. The first structure (Structure A) is a 5-story L-shaped building from the ReLUIS project, with RC frames in two orthogonal directions. The second structure (Structure B) is the 3-story building from the Spear Project. Both structures are modeled and analyzed in OpenSEES. Structure A uses spread plasticity non-linear elements with fiber sections for beams and columns, and elastic shells with appropriate thickness for floors. Structure B uses lumped plasticity with plastic hinges for beams and columns, and numeric constraints for floors.

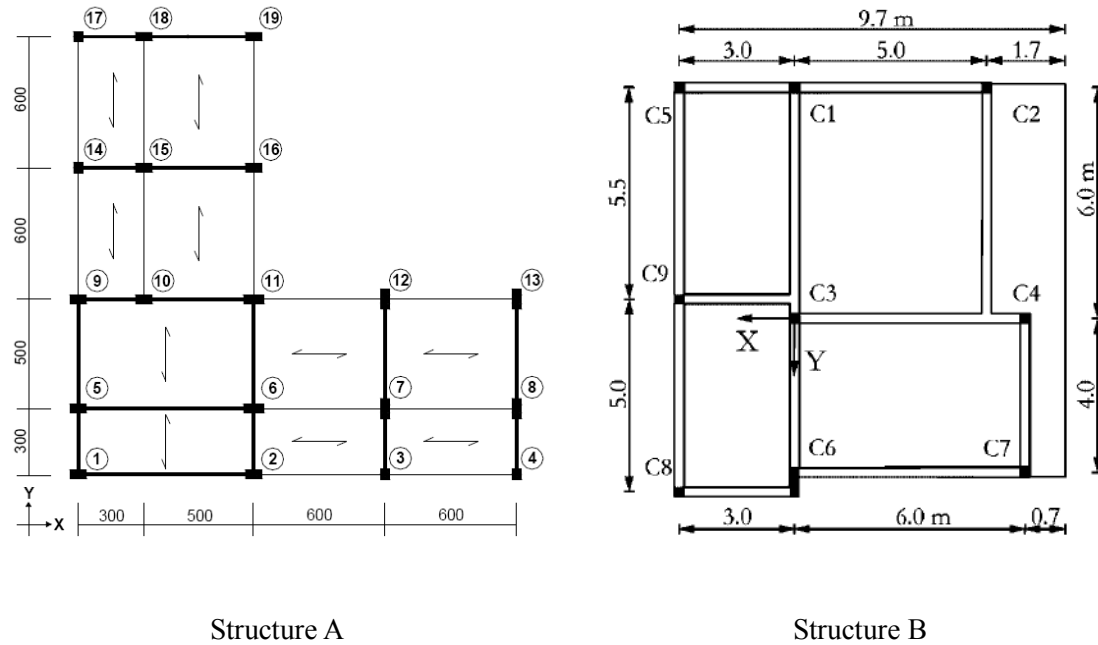


Figure 4.6 Plan views of two benchmark structures in the study of Petti et al. (2008)

The limit domains of structure A and B in term of base shear given by Petti et al. (2008) are shown in Figure 4.7. It could be noticed that the limit domain of structure A is close to a circle and the limit domain of structure B is close to a square.

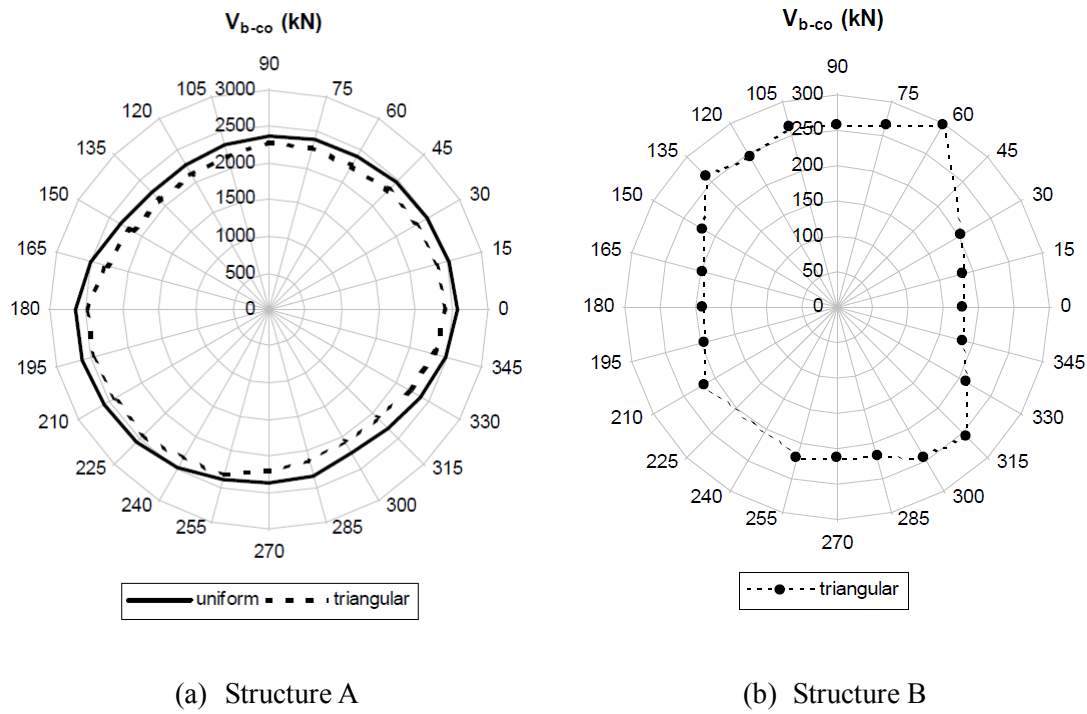


Figure 4.7 Limit domains in term of base shear of benchmark structure A and B

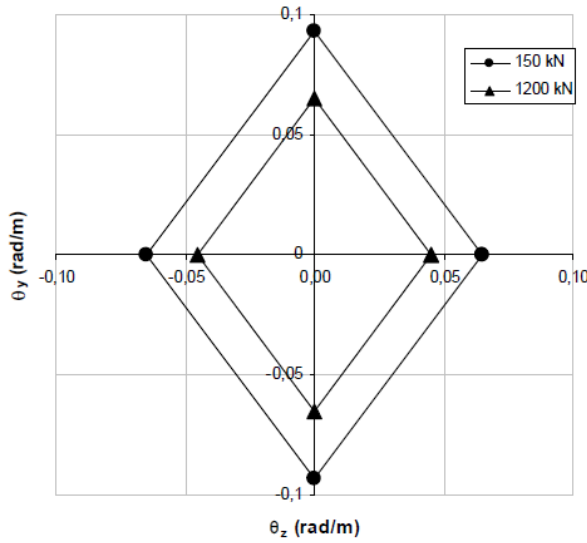


Figure 4.8 Example of collapse curvature domain for columns (Petti et al., 2007)

In Structure A, linear interpolation in the plane of the section is used to evaluate limit curvature for columns (rhomboidal domain). In addition, in the pushover analysis, the state at which the

first primary element goes beyond its limit is assumed to be global collapse. Under the above assumptions, the whole structure may not reach P- Δ instability at collapse. Since collapse is usually controlled by the failure of columns, the limit state of columns controls the limit domain of the whole structure. In the previous discussion, an elliptical column limit domain leads to a square structure limit domain. Similarly, a rhomboidal column limit domain leads to a circular structure limit domain.

In Structure B, two independent plastic hinges for bending about the two principal axes are used for columns. Since it is assumed the hysteretic behavior has no effect on the perpendicular direction, the limit domain of a column is a square domain with a constant value in X and Y. Therefore, the moment-frames in two principal directions are no longer coupled by the columns subjected to bi-axial bending. Based on this assumption, it could be easily concluded that the limit domain in terms of base shear for structure B should be close to a square.

The assumption in modeling Structure A tends to be conservative. Hence underestimate the limit domain is underestimated. While the assumption in modeling Structure B could over-estimate it. From the above discussion it could be concluded that the definition of collapse state is another factor that controls the shape of the limit domain.

4.3 Extending PFA Collapse Model to 3D Frame Buildings

The result of the study in the previous sections of this chapter could extend the use of the PFA collapse prediction model developed in Chapter 3 from 2D structures to 3D structures.

In Chapter 3 we proposed a collapse prediction model based on a new parameter: peak filtered acceleration (PFA). In order to predict whether a building will collapse in response to a given ground motion, we first estimated the maximum lateral capacity of the building. We then filtered the ground acceleration time history using a low-pass 2nd-order Butterworth filter (4th-order for ramp-like and pulse-like motions) and with a cutoff frequency that is typically lower than the first mode frequency. If the amplitude of the filtered acceleration record (given as a fraction of g) exceeds the building's pushover maximum strength (given as a fraction of the building weight) then P- Δ instability is expected. However, in Chapter 3, all the ten buildings are modeled in 2D space as planar frames. Thus, the developed prediction model is verified only for 2D buildings. The result of this chapter provides a tool to extend the result of Chapter 3 from 2D buildings to

3D buildings.

4.3.1 PFA Collapse Prediction Model for Regular 3D Buildings

For buildings that have regular distribution of moment-resisting frames (such as B1 and B2), the base shear limit domains are close to a square, with two principal axes identical to axes of moment frames in the structure. Therefore, it could be approximated that the ultimate strength of the structure is independent in two principal directions. Under this assumption, the original 3D structure could be decomposed into two independent 2D structures. In order to predict collapse of a 3D structure, we first decomposed the bi-directional ground motion into the two principal directions of the structure, then applied the PFA model to each of the decomposed 2D structure subjected to the ground motion in the corresponding direction. If one of the 2D structures collapsed, the corresponding 3D structure was predicted to collapse. The original 3D structure would survive the ground motion only if both decomposed 2D structures survived the corresponding ground motion.

4.3.2 Verification Using B1 Building

We verify the proposed PFA collapse prediction model for regular 3D buildings using building B1 and long-period ground motion set in this section. The long-period ground motion set has 50 records in total, and all of them are chosen from the 1999 Chi-Chi earthquake. However, all of the records are uni-directional. In order to simulate collapse of 3D structure in bi-directional ground motions, we grouped the 50 records into 25 bi-direction ground motion records.

In order to verify the PFA prediction model, we first predicted the threshold scale of each bi-direction record that could collapse the B1 building using the proposed method. We then compared the predicted collapse threshold scales to those computed by Frame3D simulations. If the scales obtained from the two methods agree with each other, then the proposed method is verified to be accurate.

In the PFA model, first we needed the fundamental period T_1 in each decomposed 2D structure. Since the first mode has 47.24% in X direction and 57.72% in Y direction, the first period of the 3D structure was used as the fundamental period for both decomposed 2D structures. Due to the fact that 40% live load was included in the dynamic analysis, T_1 was set to be 4.05s instead of

3.72s. From the pushover curve, the cutoff period coefficient c was calculated to be 1.3. The ultimate strength was 0.104g in X direction and 0.108g in Y direction. In order to compute the scale of each bi-direction record that could collapse B1 building, we first filtered the two ground acceleration components using a 2nd-order low-pass Butterworth filter with cutoff period $c*T_1$, and obtained the peak absolute values of the filtered records. We then divided the ultimate strength in X direction of the structure by the peak filtered acceleration (PFA) in the same direction to obtain the collapse threshold scale in this direction. We did the same calculation in the Y direction. Finally, we took a smaller collapse scale in the X and Y direction as the collapse scale for the entire 3D structure. The above calculation was repeated to all 25 bi-direction ground motion records. The results were compared with the collapse scales computed by Frame3D (see Table 4.2 and Figure 4.9), and they generally agree with each other very well.

Table 4.2 B1 building in long-period ground motion set

Record	PFA Collapse Scale	Frame3D Collapse Scale	PFA/Frame3D
1	6.9	6.0	1.14
2	5.6	5.4	1.04
3	6.6	5.6	1.17
4	8.7	12.5	0.69
5	6.9	7.4	0.93
6	8.2	8.4	0.98
7	6.2	5.4	1.15
8	12.6	17.0	0.74
9	5.8	6.4	0.91
10	5.4	4.6	1.17
11	5.5	4.6	1.20
12	6.2	5.0	1.23
13	5.3	6.2	0.86
14	3.5	2.8	1.26
15	2.3	2.1	1.09
16	3.6	3.2	1.11

17	3.4	3.8	0.89
18	2.7	2.8	0.97
19	3.2	4.0	0.80
20	2.0	2.1	0.97
21	2.7	2.8	0.95
22	2.7	2.8	0.96
23	3.0	2.4	1.25
24	15.6	17.0	0.92
25	9.6	9.0	1.07
Geometric mean			1.01

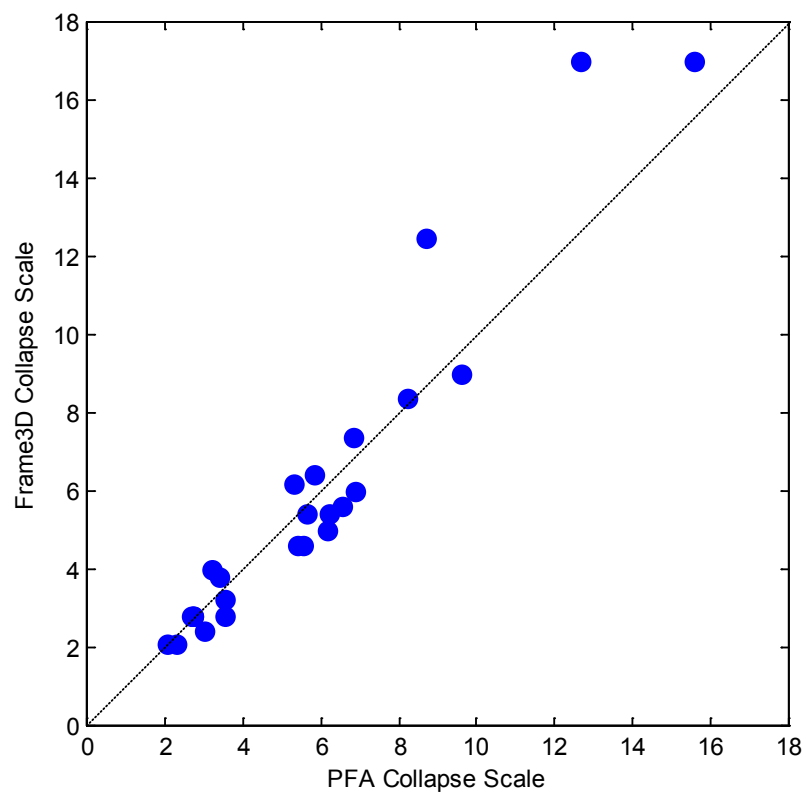


Figure 4.9 Comparison of PFA collapse scales and Frame3D collapse scales (building B1)

4.3.3 PFA Collapse Prediction Model for Irregular 3D Buildings

A 3D building with irregular stiffness distribution has a limit domain of square shape with round corners. Therefore, the strengths in two principal directions are not independent of each other. In this case the decomposition method we have proposed for 3D regular buildings would not apply. Hence we have no choice but to use filtered bi-directional ground motion as demand and 2D limit domain as building capacity. If the filtered bi-directional ground motion exceeds the limit domain in any direction, the building is expected to collapse. Otherwise, it will survive the ground motion. It should be noticed that the ground acceleration and the corresponding inertial force are in the opposite directions, and thus the limit domain in Figure 4.9 is reversed with respect to X and Y coordinates comparing to Figure 4.4.

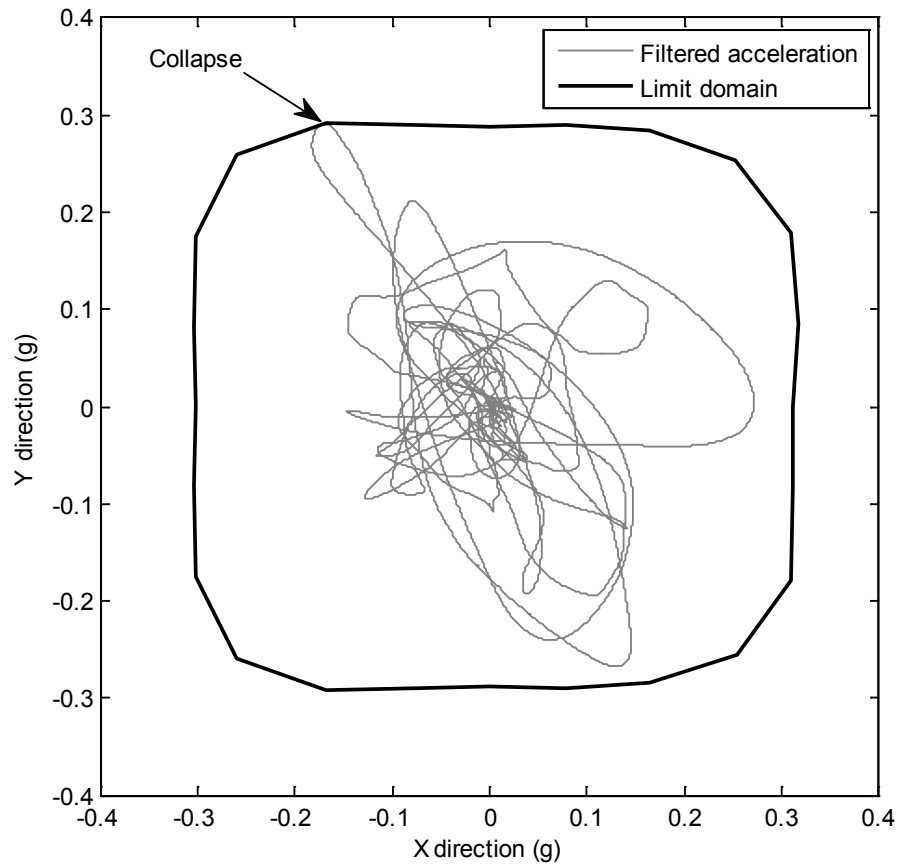


Figure 4.10 Collapse prediction for an irregular 3D frame building

4.3.4 Verification Using B3 Building

We verified the proposed PFA collapse prediction model for irregular 3D buildings using the B3 building and long-period ground motion set in this section. Similar to the previous section, the 50 long-period ground motion records are grouped into 25 bi-directional ground motion records.

The verification procedures are the same as used in section 4.3.2. We first calculated the scale of each bi-direction record that could collapse the B3 building using the PFA model; we then compared them to the collapse scales computed by Frame3D simulations. If the scales obtained from the two methods agreed with each other, then the proposed method was verified to be accurate.

The fundamental period T_1 is 2.03s in X direction and 3.21s in Y direction. The calculated cutoff period coefficient is 1.40 in X direction and 1.13 in Y direction. In order to predict whether building B3 will collapse when subjected to a bi-directional ground motion, we first filtered the bi-directional ground acceleration record in X and Y direction with the corresponding cutoff period (c^*T_1), and plotted the filtered acceleration in X-Y plane together with the 2D limit domain of building B3. The building was expected to collapse if the filtered ground motion exceeds the boundary of the limit domain in any direction. We compared the prediction with the FEM result in Table 4.3 and Figure 4.11. It could be concluded that, although not as good as the B1 building, the two results are still close to each other.

Table 4.3 B3 building in long-period ground motion set

Record	PFA Collapse Scale	Frame3D Collapse Scale	PFA/Frame3D
1	12.4	11.5	1.08
2	11.9	11.5	1.03
3	13.1	10.5	1.25
4	15.6	17	0.92
5	11.0	14	0.79
6	15.0	14	1.07
7	13.2	11.5	1.15
8	15.6	19	0.82
9	10.9	10.5	1.04

10	10.9	8.5	1.28
11	11.7	9.5	1.23
12	12.0	8.5	1.41
13	10.0	8.5	1.18
14	6.3	7	0.90
15	4.8	5.25	0.91
16	7.3	5.75	1.27
17	6.3	7.25	0.87
18	3.9	4.2	0.93
19	5.7	5.4	1.06
20	4.7	3.5	1.34
21	4.8	5.4	0.89
22	5.3	5.4	0.98
23	5.6	5.4	1.04
24	23.3	27	0.86
25	15.2	14	1.09
Geometric mean			1.04

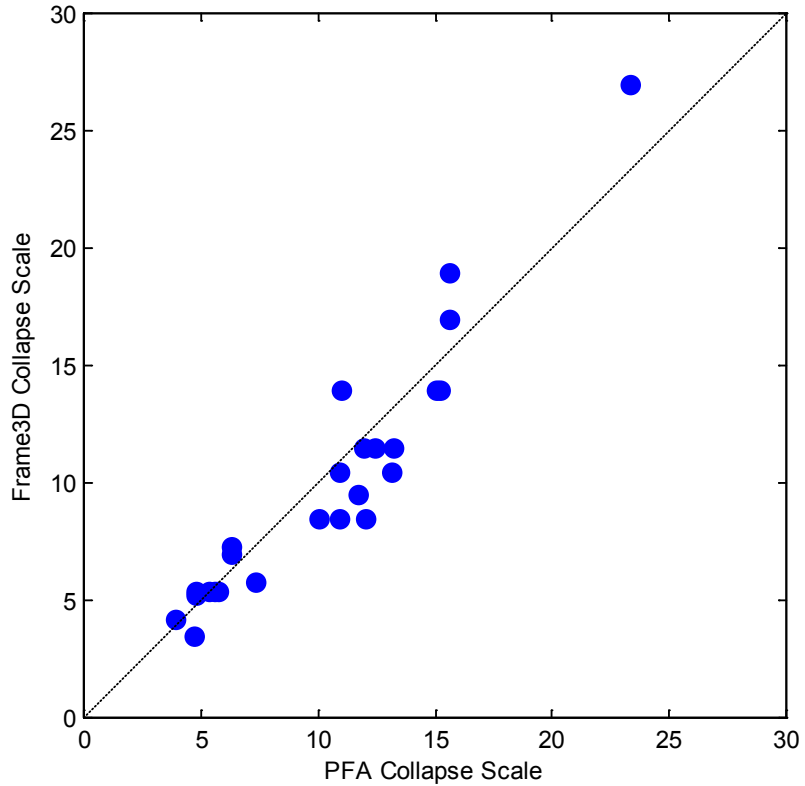


Figure 4.11 Comparison of PFA collapse scales and Frame3D collapse scales (building B3)

4.3.5 Summary of the PFA Collapse Prediction Model for 3D Frame Buildings

In this section, we summarize the PFA collapse prediction model for 3D moment-resisting frame buildings subjected to bi-directional ground motions. We first discuss how to identify the fundamental period in each principal direction, which determines the cutoff frequency of the low-pass Butterworth filter; we then summarize the procedures of PFA collapse prediction model for 3D frame buildings.

How to Identify the Fundamental Period in Each Principal Direction

For the 2D planer frames analyzed in Chapter 3, all the horizontal displacements are restricted in the principal direction. It is therefore guaranteed that all the mode shapes are in the principal direction. In this case, the fundamental period is just the period of the first mode. However, for

3D frames analyzed in this chapter, there is no restriction on horizontal displacements. In this case, there is no guarantee that the mode shapes are along the principal directions. Since the fundamental period used to determine the cutoff period is defined in the principal direction, it must be chosen carefully. We propose that for each principal direction, if a mode has a modal direction factor that is larger than 45% in this direction, it is considered as a mode in this direction. Then the fundamental period in this principal direction is the longest period of all the modes in this direction. We use this principle in Section 4.3.2 and 4.3.4, and they show good result.

Procedures of PFA Collapse Prediction Model for 3D Frame Buildings

Case 1: Regular 3D building without torsional effect

Step 1: Decompose the 3D building into two 2D buildings in the principal directions

Step 2: Apply the PFA model to each 2D building as it is done in Chapter 3, using the properties (fundamental period and ductility) and ground motion in the corresponding direction.

Step 3: If one of the 2D buildings collapses, then the 3D building is expected to collapse. The 3D building will survive the bi-directional ground motion only if each of the 2D buildings can resist the corresponding uni-directional ground motion.

Case 2: Irregular 3D building with torsional effect

Step 1: Obtain the limit domain of the building using multi-directional pushover analysis

Step 2: Filter the ground motion in each of the building's principal direction using the properties (fundamental period and ductility) in the same direction.

Step 3: If the filtered bi-directional acceleration exceeds the limit domain, then the building is expected to collapse under the ground motion. Otherwise, the building will survive the ground motion.

4.4 Discussion on the Effect of Torsion

In the previous sections of this chapter we obtained the limit domains in term of maximum base shear for three steel moment-resisting frame buildings. Based on the results, we extended the PFA (peak filtered acceleration) collapse prediction model from 2D buildings to 3D buildings. The limit

domains we obtained for the three steel moment-resisting frame buildings are different. For the two buildings without torsional irregularity the limit domains are close to squares, while for the building with torsional irregularity the limit domain is a square with round corners. We concluded that the torsional irregularity is an important factor which affects the buildings' limit domains and hence the buildings' collapse behavior.

Researchers have studied buildings' torsional effect in different ways. Stathopoulos (2005) has investigated the inelastic earthquake response of eccentric, multistory, frame-type, reinforced concrete buildings and shown the difference of ductility demands at the flexible and stiff side. Krishnan (2007) has studied the seismic response of three steel moment-frame buildings with torsional plan irregularity and shown that twisting in the torsionally sensitive buildings causes the plastic rotation on the moment frame on one face of the building to be as high as twice that on the opposite face.

In the second part of this chapter, as a first attempt we propose a new method, twistover analysis, to analyze the torsional capacity and behavior of buildings. We also discuss the effect of torsion on the shape of limit domains.

4.4.1 Twistover Analysis

Pushover analysis is a nonlinear static procedure which is widely used in structural analysis to determine the lateral capacity of a building. It is performed by applying lateral forces to each story based on specified distribution and increasing the forces until the building reaches its required limit state. The result is usually described by a pushover curve which plots base shear versus roof displacement. However, since pushover employs translational forces, it is not designed specifically for examining the torsional behavior and capacity of a building.

In order to break this limitation, we propose a modified nonlinear static procedure, twistover, to analyze buildings' torsional behavior and capacity. The general procedures are the same as pushover analysis except we use torsional displacement and force.

The steps of twistover analysis are listed as follows:

- 1) Apply torque in a vertical direction to each floor (see Figure 4.12). The torque has a specified distribution along the height.

- 2) Gradually increase the torques from zero until the building reaches its required limit state.
- 3) Plot roof torsional angle versus base torque.

We conducted the twistover analysis to building B1. The torque was applied using a force couple at the center of east and west sides of the building (Figure 4.12), and the distribution of torque along the building height was triangular. The result of the twistover analysis is plotted in Figure 4.13 and 4.14. In Figure 4.13, we plotted base torque against roof torsional angle. The shape is close to a pushover curve. The curve increases linearly at first, then goes into a plateau, and finally decreases at a negative slope. Three critical points are marked in the twistover curve. Point 1 is the start of global yielding. After Point 1 the twistover curve loses linearity and increases nonlinearly. Point 2 is the start of the plateau. After Point 2 the base torque approaches to a constant while the torsional angle still increases. Point 3 is the point of the maximum base torque. In Figure 4.14 we plotted the distribution of torsional angles along the building height at the three critical points. It could be noticed that before the building starts to yield, the torsional angles are approximately equally distributed along the height. After yielding the torsional angles increase faster at lower stories compared with upper stories. The building finally fails at the lower stories due to the larger deformations.

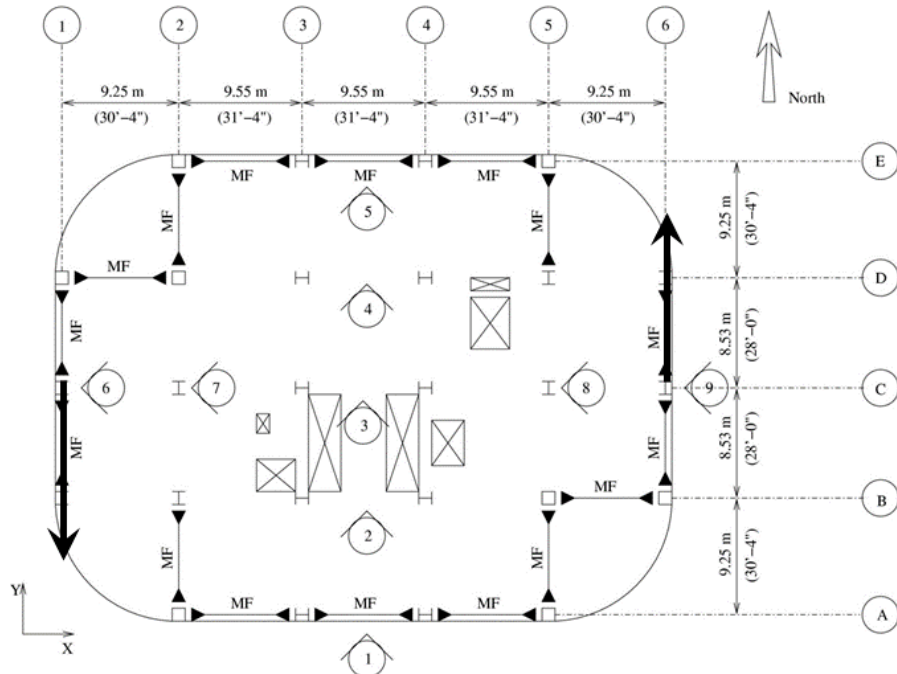


Figure 4.12 Force couple applied at each story of building B1

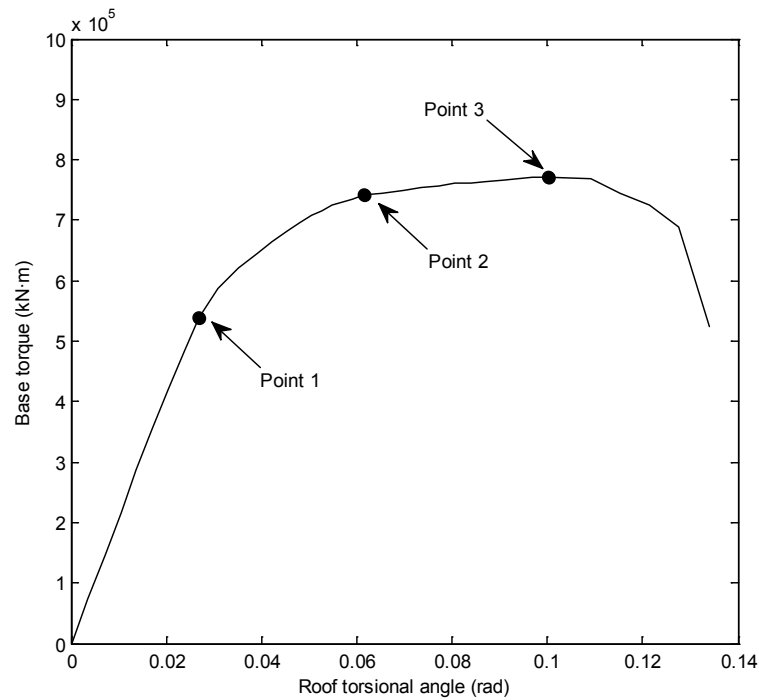


Figure 4.13 Twistor curve of building B1

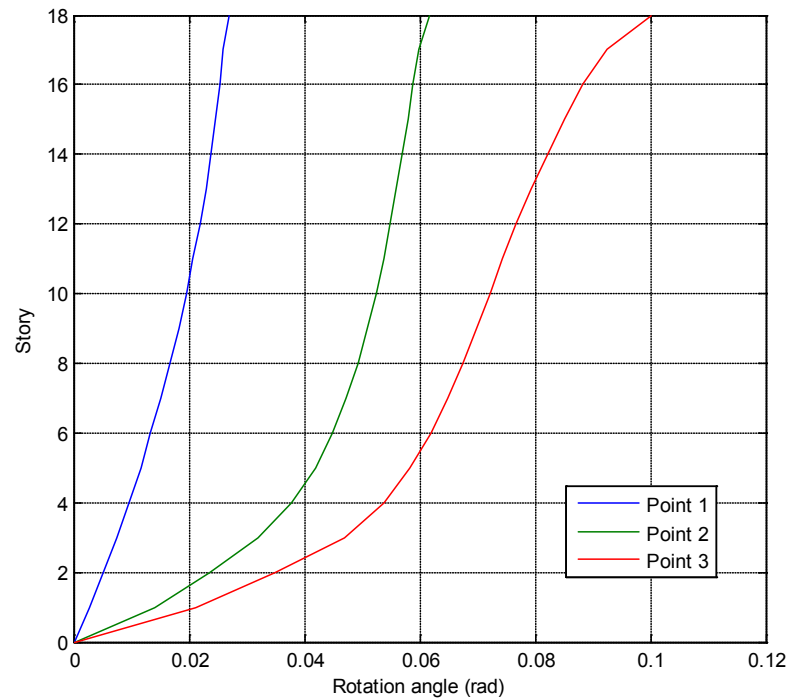


Figure 4.14 Rotational angles along the height of building B1 at different deformation stages

In the analysis we obtained the base torque through the forces at the ends of columns of the ground floor. If we used an equivalent force couple, located at the center of the east and west sides of the building (Figure 4.12), the maximum force would be 0.1238 times the seismic weight of the building. If we considered the forces to be generated by ground acceleration, the acceleration at the east and north sides of the building would be $0.1238g$, but in opposite directions. It is equivalent to saying the ground needs to rotate with an angular acceleration of 5.087 rad/s^2 .

4.4.2 Effect of Torsion on Limit Domain

In Section 4.2, we obtained the limit domain in term of base shear of the same building. The resultant limit domain is close to a square shape since the frames in two principal directions are not strongly coupled and will take the load in the frames' own direction. However this result is under the assumption that the frames will stay in their own directions while deformed. Usually, even if a building is symmetric in design, it is still possible to have accidental eccentricity during construction and operation. In this section we analyze the effect of torsion on the capacity (limit domain) of building B1. We conduct the analysis by applying three different initial torsions to the building and compute the limit domain with these initial torsions. The three initial deformations correspond to Point 1, 2, and 3 in Figure 4.13. The limit domains of building B1 with different initial torsions are plotted in Figure 4.15.

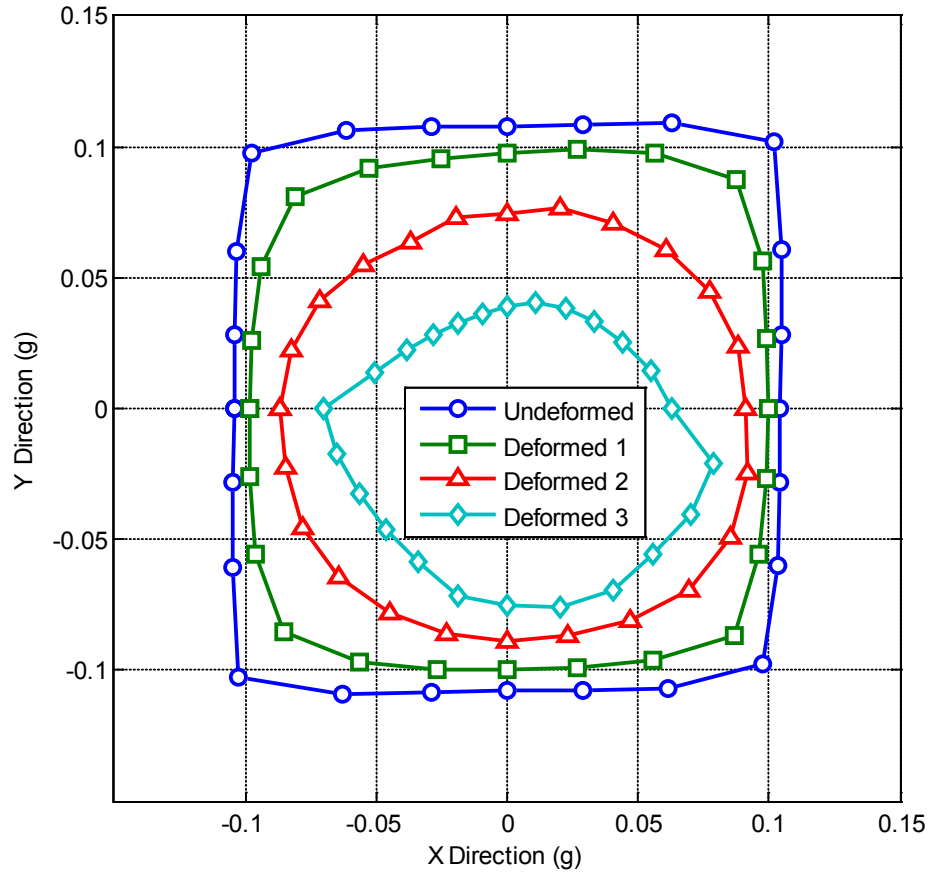


Figure 4.15 Effect of torsion on the limit domain of building B1

It could be concluded that when the initial torsion increases, the shape of the limit domain changes from a square with sharp corners to a square with round corners, then close to a circle and finally to an irregular asymmetric ellipse. From zero initial torsion to initial torsion 1, which is close to the end of elastic regime, the change of limit domain is relatively small. The scale is 0.93 on average at the principal direction and 0.85 on average at the diagonal directions. When the structure starts with the initial torsion 2, which is the beginning of the plateau in twistover curve, the limit domain is close to a circle, with the average scale 0.8 at the principal directions and 0.62 at the diagonal directions. It also could be noticed that the limit domain is no longer symmetric at this stage. The reason is that the analyzed building is not perfectly symmetrical throughout the building height. The floor plan is asymmetric at the second floor (see Figure 4.16). In the traditional pushover analysis this asymmetry does not show up, as the building does not have significantly large deformation at

the second floor. However, when we increase the torsion, the asymmetry starts to show up because the lower stories are weakened. Finally, when it comes to initial torsion 3, which is at the maximum strength point in the twistover curve, the limit domain loses symmetry completely and shows an irregular shape compared to the previous ones.

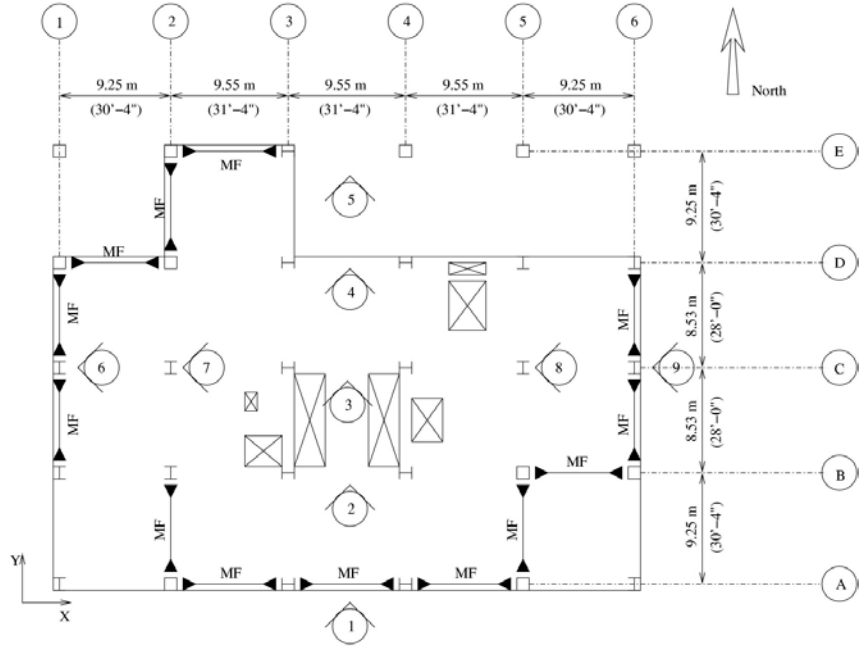


Figure 4.16 Second floor plan of building B1

From the above discussion, it could be concluded that torsion is a main factor that affects the shape of limit domains. When increasing the torsion, the limit domain could change from a sharp square to a round-cornered square and finally to a circle. Torsion could also expose the hidden asymmetry of a building, which does not show in pushover analysis.

PREDICTING THE COLLASPE OF A BUILDING TESTED BY E-DEFENSE USING THE PFA MODEL

In September 2007, a shaking table test of a full-scale 4-story steel moment frame building was conducted at the E-Defense 3-dimensional shaking table facility. The experiment was designed to evaluate the structural and functional performance of the building under design-level ground motions, as well as the safety margin against collapse under exceedingly large ground motions. The specimen building was shaken by five different levels of ground motions and finally collapsed in the experiment. In this chapter, we will use the PFA model to predict the response of the building under different levels of excitations, and compare the prediction with the result of the experiment.

5.1 Brief Description of the Experiment

The specimen building is a 4-story, two-bay by one-bay steel moment frame building (see Figure 5.1 and 5.2). The structure is 10m long in the longitudinal direction (Y) and 6m long in the transverse direction (X). It is designed following the most common design considerations exercised in Japan for post-Kobe steel moment frames. The columns are made of cold-formed square-tubes; the beams are made of hot-rolled wide-flanges and through diaphragm connection details are adopted in which short brackets are shop-welded to the columns. “Due to the recent adopted improvements, there is little likelihood that moment connections would fracture even under exceedingly large ground motions.” (Suita et al., 2008) External wall cladding panels of ALC are placed on three sides of the building, as shown in Figure 5.1.

The total weight of the building, including the safeguards inside, is 2113kN. The measured first period is 0.82s in the X direction and 0.76s in the Y direction.

The shaking tests are conducted at the E-Defense shaking table. The specimen is subjected to the ground motion recorded during 1995 Kobe earthquake at JR Takatori train station (see Figure 5.3). The tests consist of repeated applications of the same record with progressively increasing scale factors (0.05, 0.2, 0.4, 0.6, and 1.0).



Figure 5.1 Photos of the specimen building (reproduced from Yamada et al., 2008)

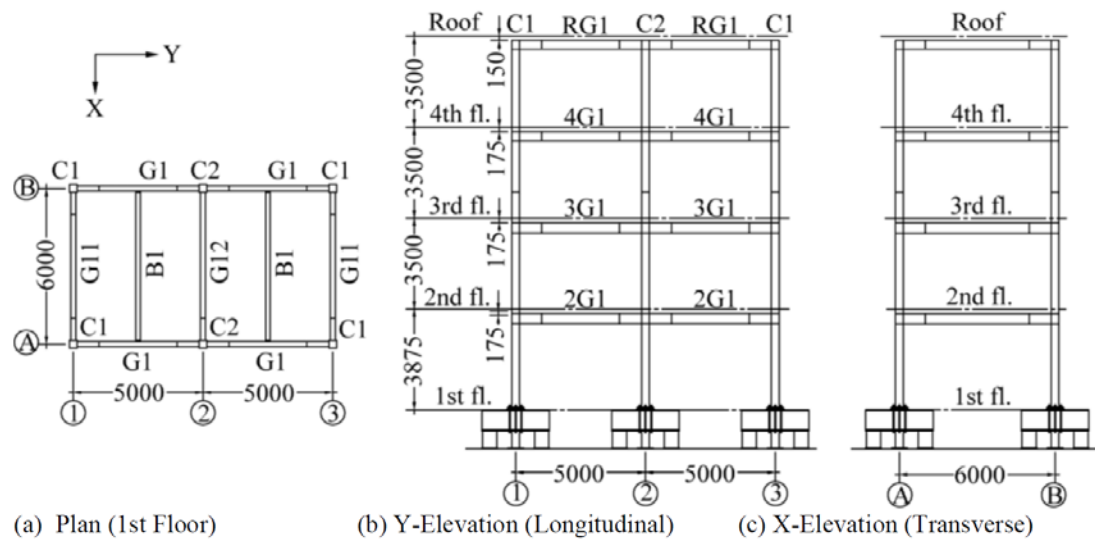


Figure 5.2 Plan and elevation views of the specimen building

(reproduced from Yamada et al., 2008)

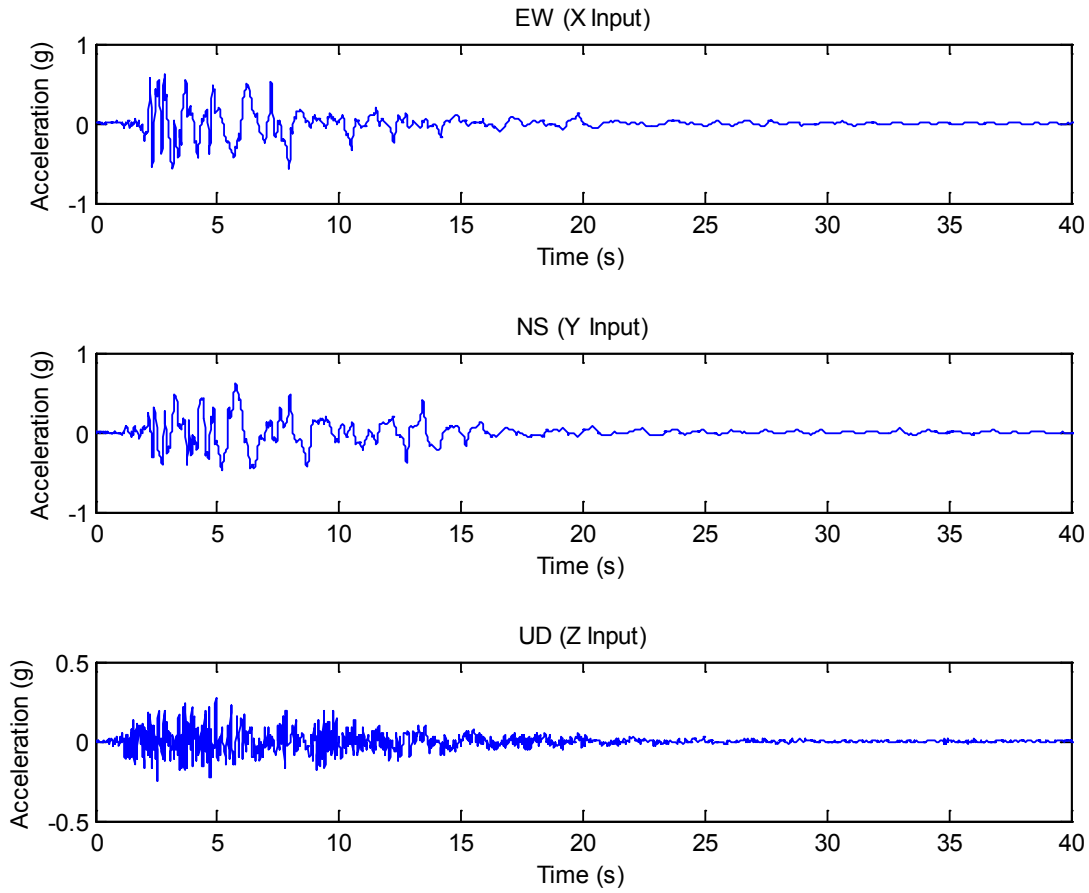


Figure 5.3 EW, NS, and UD components of Takatori record in 1995 Kobe earthquake

5.2 Collapse Prediction using the PFA Model

We use the PFA model developed in this thesis to predict the response of the specimen building under different levels of excitations. The prediction includes two parts: the pre-test prediction (blind prediction) and the post-test prediction. In the pre-test prediction, we only used the data that was available before the shaking table test. In the post-test prediction, we calibrated the pre-test prediction using the data measured from the experiment.

5.2.1 Pre-test Prediction

Three parameters, fundamental period, lateral capacity, and global ductility, are needed to predict the response of the specimen building using the PFA model. Before the experiment, the fundamental period was known through the free vibration test (Yamada et al., 2008). The estimation of the lateral capacity was provided by the pushover analyses in Figure 5.4 (Suita et al., 2008). The global ductility was the only unknown parameter. Hence, we needed to estimate the global ductility of the building. Unfortunately, the reference building system and the corresponding interpolation functions in this thesis were developed based on the US buildings, and could not properly represent the Japanese buildings. Hall (1997) designed a 6-story steel frame building according to Japanese building code, which is similar to the building tested in E-Defense. We used the 6-story building designed by Hall to estimate the global ductility of the 4-story frame building tested in E-Defense. Similar to the US steel frame building models used in Chapter 3, there are two numerical models of the 6-story Japanese building, one with perfect welds and the other with fracture-prone welds. Since post-Kobe specifications and practice ensure no weld fracture (Suita et al., 2008), we used the 6-story building model with perfect welds (J6P) in this analysis. From Figure 5.5, the global ductility of the building is 4.6667 and the cutoff period coefficient is 1.2722. We used these values for both the X and Y directions.

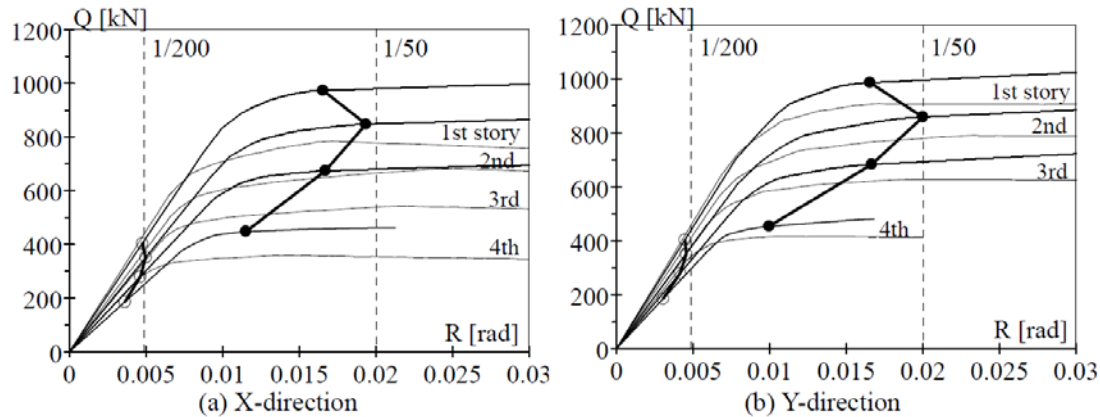
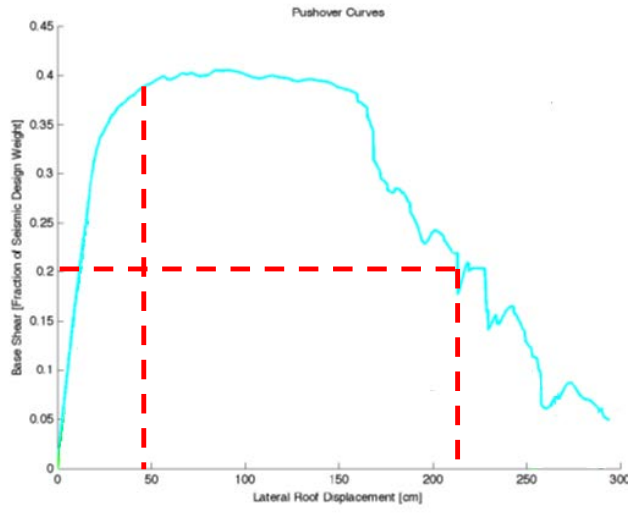


Figure 5.4 Story shear versus story drift relationships obtained from pushover analyses (reproduced from Suita et al., 2008)
(black lines – nominal material strength, gray lines – actual material strength)

As discussed in Chapter 4, since the building has a regular frame distribution, its limit domain is a square shape with 1000kN lateral capacity in both the X and Y directions (see Figure 5.4). However, it should be noted that the pushover analysis is applied to an undamaged numerical building model, while the actual specimen building is not guaranteed undamaged before each shaking test, as it experienced five ground motions in series. Thus, before the specimen building is shaken by the full scale Takatori ground motion, it probably already has some damage, since it has experienced the 0.6-scaled Takatori ground motion. The damage in the structure could decrease its seismic load resistance; as a result, the lateral capacity provided by the pushover analysis is actually the upper limit of the actual specimen building. We needed to find a lower limit of the lateral capacity for the structure. In order to make the estimation simple, we assumed that the first three ground motion inputs, 0.05-, 0.2-, and 0.4-scaled Takatori records did not damage the specimen building significantly, so we could neglect them. Therefore, we only needed to pay attention to the last two ground motion inputs, 0.6- and 1.0-scaled Takatori records. By neglecting the damage from the first three ground motion inputs, we assumed the structure was undamaged before being shaken by the 0.6-scaled record. We directly used the lateral capacity obtained from pushover analysis in the prediction for the 0.6-scaled record. For the 1.0-scaled record, since it was probably damaged by the previous 0.6-scaled record, we used an upper limit and a lower limit of the lateral capacity in the prediction.



$$c = 0.1241\mu + 0.6931 = 1.2722$$

Figure 5.5 Estimating the ductility ratio of the tested structure using the J6P building

In order to find the lower limit of lateral capacity for the specimen building subjected to the 1.0-scaled Takatori record, we first increased the last two ground motion inputs to two consequent 1.0-scaled Takatori records. Because the ground motion input is stronger, the collapse threshold should be smaller than the actual threshold in the test and could be used as the lower limit of the lateral capacity for the specimen building (see Figure 5.6).

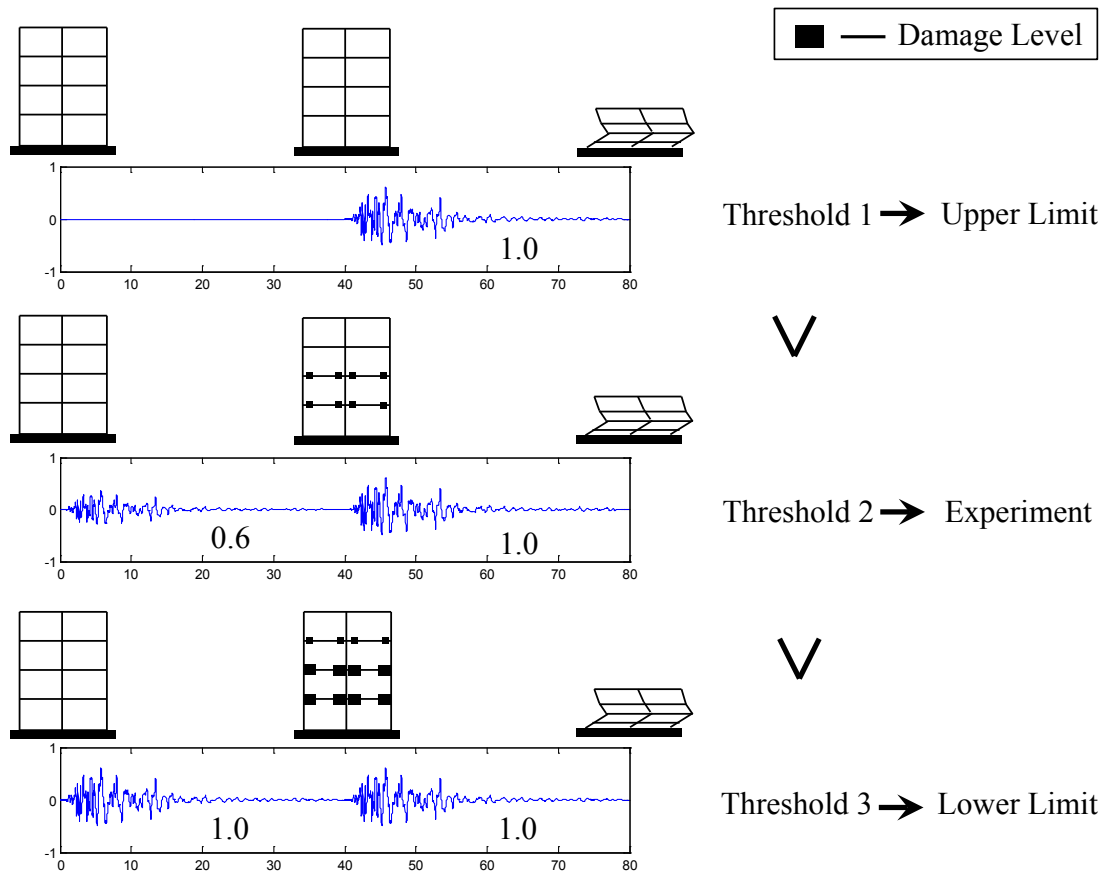


Figure 5.6 Estimating the upper limit and lower limit of lateral capacity for the specimen building under the 1.0-scaled Takatori record

From Figure 5.3, the duration of the record is 20s, and hence the duration of the two consequent records is about 40s. The problem then became how to find the collapse threshold of the specimen building subjected to the 40s-long ground motion. As discussed in Section 3.1.2, when we computed the minimum collapse PGA (MinCPGA) for building models, we used three ground

motion durations: 20s, 40s, and 100s. The results of 20s- and 40s-long ground motions could be directly used in this analysis. The MinCPGA curves of the U6P building, which is the closest to the test building, are shown in Figure 5.7.

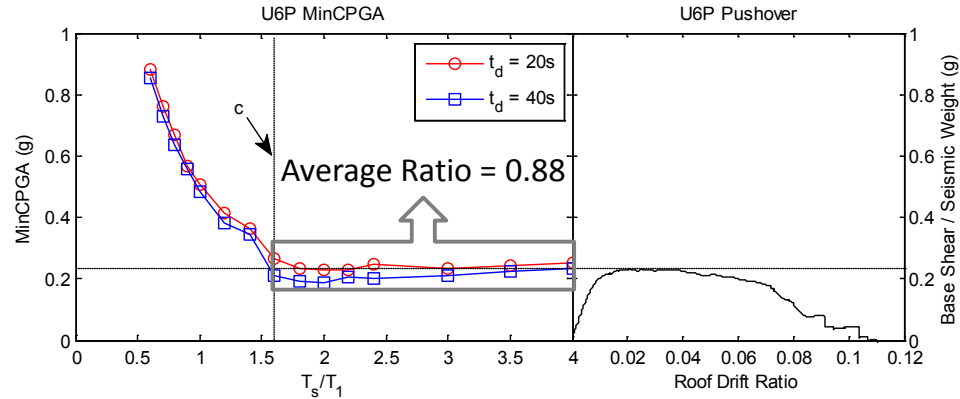


Figure 5.7 Estimating the lower limit of lateral capacity for the damaged building after being shaken by the 0.6-scaled Takatori record

From Figure 5.7, it could be concluded that when the period is longer than the cutoff period, the threshold in 20s ground motion is the closest to the lateral capacity of the building, while the threshold in 40s ground motion is smaller. The average ratio of the threshold in 40s ground motion over the threshold in 20s ground motion is 0.88. Hence, we used the lateral capacity obtained from pushover analysis as the upper limit of the limit domain and scaled it using the ratio 0.88 to obtain the lower limit.

We Butterworth low-pass filtered the ground motions with a cutoff period of $c^*T_{1,x}$ in the X direction and $c^*T_{1,y}$ in the Y direction. We then plotted the filtered bi-directional ground acceleration together with the limit domain of the specimen building. The results are shown in Figure 5.8 and Figure 5.9. In Figure 5.8, the filtered acceleration is well within the limit domain; thus the specimen building will not collapse in the 0.6-scaled record. In Figure 5.9, the filtered acceleration exceeds both the upper limit and the lower limit of the limit domain; therefore the specimen building will collapse in the 1.0-scaled record.

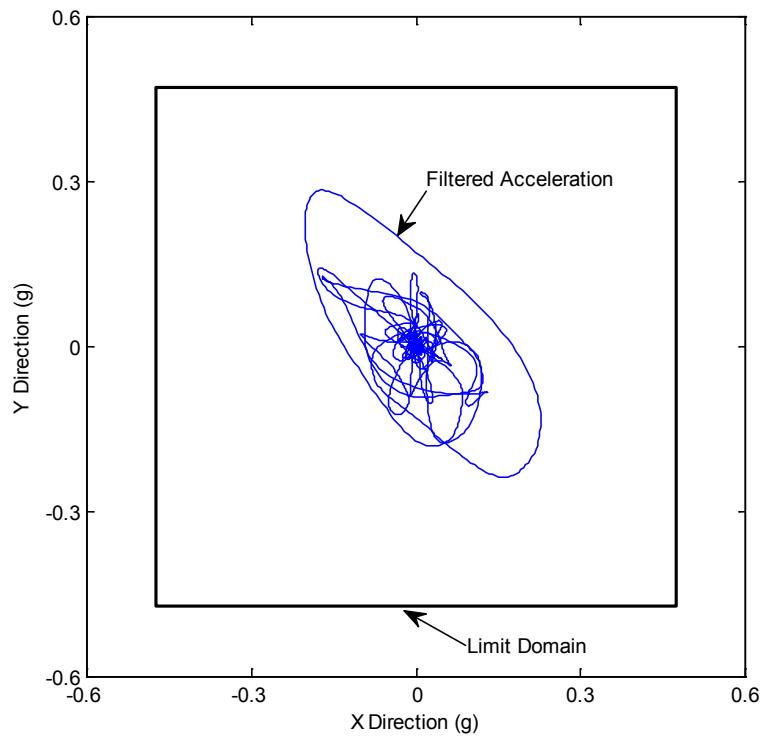


Figure 5.8 Pre-test collapse prediction for the structure subjected to the 0.6-scaled Takatori record

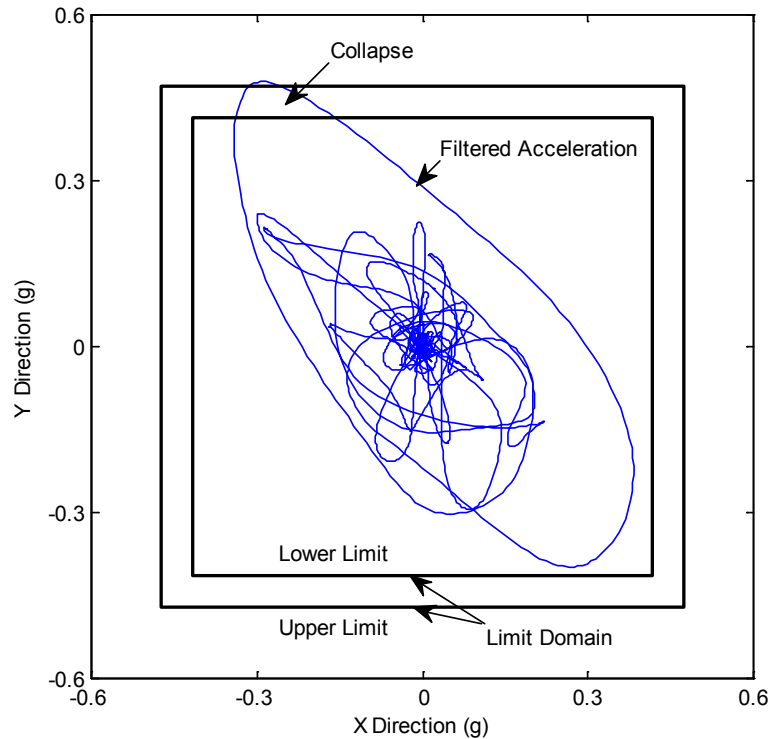


Figure 5.9 Pre-test collapse prediction for the structure subjected to the 1.0-scaled Takatori record

The result of the experiment is shown in Figure 5.10. The building experienced yielding under the 0.6-scaled excitation, but did not collapse. It collapsed in the Y direction under the 1.0-scaled excitation. The prediction provided by the PFA model agrees with the result of the experiment.



Figure 5.10 Collapse of the specimen building after being shaken by the 1.0-scaled Takatori record

5.2.2 Post-test Prediction

After the experiment, the measured base shear versus story drift relationship became available. It provides the actual lateral capacity and global ductility of the specimen building. In this section, we use the measured data to calibrate the pre-test prediction.

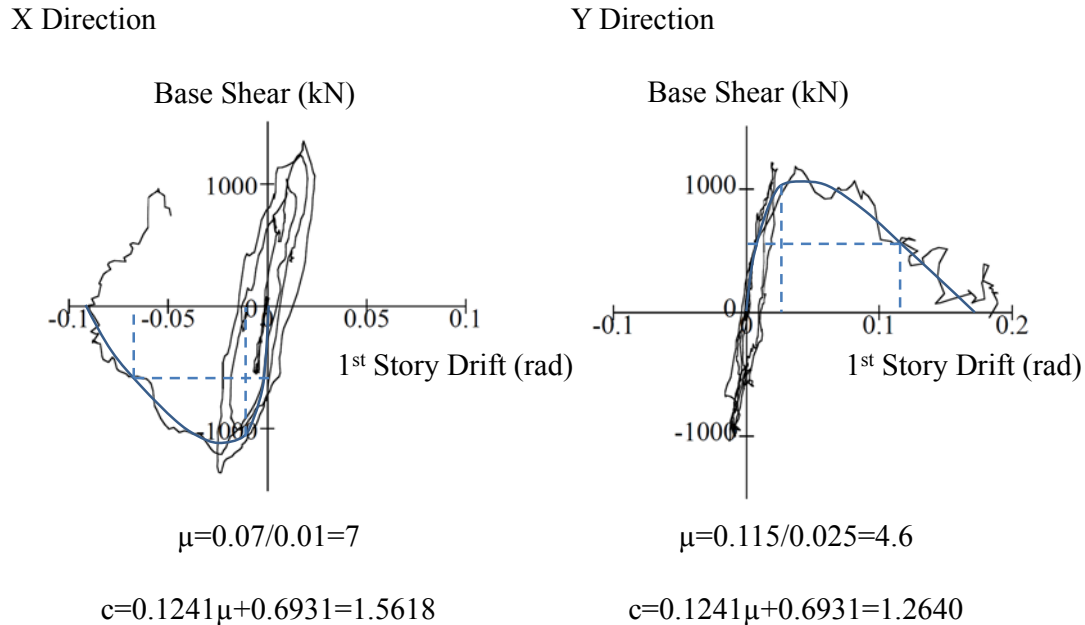


Figure 5.11 Calculating the cutoff period coefficient c using the measured data

We first calculated the cutoff period coefficient c for the X and Y direction. The relationship of base shear versus 1st story drift angle is provided in Saito et al. (2008). For the specimen building, collapse is caused by the large drift in the 1st story and the drifts of the upper stories almost stay in elastic range. Therefore, we used the data of the 1st story to calculate the global ductility of the building.

From Figure 5.11, the cutoff period coefficient c is 1.5618 in the X direction and 1.2640 in the Y direction. We Butterworth low-pass filtered the ground acceleration in the X direction with a cutoff period of $c_x * T_{1,x}$ and the ground acceleration in the Y direction with a cut off period of $c_y * T_{1,y}$. The bi-directional filtered ground acceleration was plotted in Figure 5.12, together with the actual limit domain of the building. The pre-test prediction has already shown that the 0.6-scaled record was far away from collapsing the specimen building, thus only the collapse prediction for the 1.0-scaled record was shown in the post-test prediction. The limit domain is a square with 1200kN in the X direction and 1000kN in the Y direction, since the moment frames are regularly distributed. In Figure 5.12, the filtered ground acceleration exceeds the limit domain in Y direction; hence the building will collapse in Y direction. The post-test prediction is the same as the pre-test prediction.

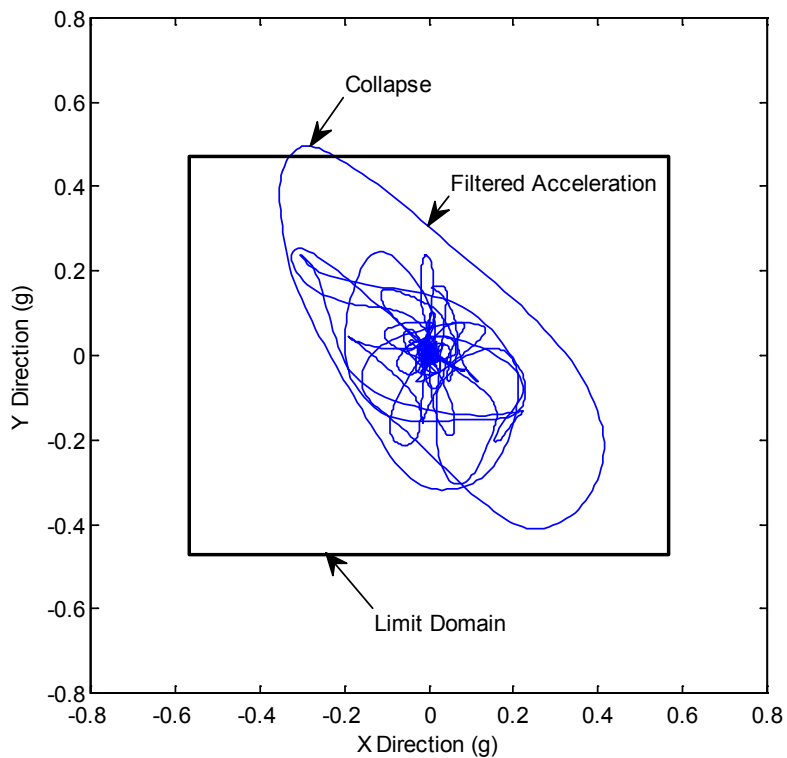


Figure 5.12 Post-test collapse prediction for the structure subjected to the 1.0-scaled Takatori record

DISCUSSION

6.1 Estimating the Fundamental Period, Global Ductility, and Lateral Capacity of an Actual Building

In the PFA collapse prediction model, three parameters are determined from a given building to predict whether or not it will collapse in response to loading by different ground motions. The parameters are fundamental period, lateral capacity, and global ductility. In the previous chapters, all three parameters were obtained by analyzing the finite element model of each building. The fundamental period was obtained by eigenvalue analysis; the lateral capacity and global ductility were obtained by pushover analysis. Hence, up until now, it could only be concluded that the PFA model can predict collapse for buildings simulated using fully nonlinear simulation.

The PFA collapse prediction model can be applied to an actual building, if it is possible to obtain all three parameters to accurately represent the building. Constructing a finite element model of the studied building and obtaining the parameters through numerical analysis is one solution to this problem. However, in this chapter we will discuss another possible solution to the problem of how to obtain fundamental period, lateral capacity, and global ductility from the fundamental information of a real-world building directly, and without constructing a numerical model.

6.1.1 Fundamental Period

Generally, there are two ways to obtain the fundamental period of a building. The first one is to measure the period directly using instruments, while the second one is to estimate the period using an empirical equation.

Measurement of Fundamental Period

In practice there are two kinds of tests designed to measure the periods of buildings: they are ambient vibration tests and forced vibration tests.

The ambient vibration tests use wind, micro tremors, microseisms, and various local random and periodic sources as the sources of excitation (Ivanovic et al., 2000), and measure the response of buildings when subjected to the excitation.

The forced vibration tests generally require larger forces to produce a larger response. Usually this is done by a vibration generator (a shaker) located on top of a building.

The ambient vibration test is usually the easier one of the two methods, since it requires light equipment and a smaller number of operators (Ivanovic et al., 2000).

Estimation of Fundamental Period

If measurement of the fundamental period is not available, there are still empirical equations which can be used to estimate the fundamental period of a building.

Since the fundamental period is usually related to the structural system and building height, empirical equations usually take structural system and building height as input parameters. For example, in UBC 97 (ICBO, 1997), the fundamental period T of a building may be approximated from the following formula:

$$T = C_t(h_n)^{3/4} \quad (6.1)$$

where: $C_t=0.0853$ (SI) for steel moment-resisting frames, 0.0731 (SI) for reinforced concrete moment-resisting frames and eccentrically braced frames, and 0.0488 (SI) for all other buildings

6.1.2 Lateral Capacity

Lateral capacity is the maximum lateral force a structure can resist. This is a parameter that is impossible to measure since it needs a destructive experiment to make the structure yield globally. Hence, we can only estimate the lateral capacity of an actual building. For convenience, we broke lateral capacity into two parts: design strength and over-strength factor. Design strength is the base shear required in building code that a building needs to resist. Design strength is usually the lower limit of actual strength. However, due to different reasons, an actual building usually shows a significant reserve strength which makes actual strength larger than design strength. This reserve

strength is characterized by the over-strength factor, which is the ratio between actual strength and design strength.

Thus, the relationship of lateral capacity, design strength, and over-strength factor is

$$\text{Lateral capacity} = \text{Design strength} \times \text{Over-strength factor} \quad (6.2)$$

The reason for breaking lateral capacity into design strength and over-strength is that design strengths could be obtained directly from building codes and over-strength factors could be obtained through numerical analysis of reference buildings and documented into the reference building system.

Design Strength

Calculating design strength is straightforward. For a specific building, it is only needed to follow the standard procedures in the building code upon which the building is designed.

For example, in UBC 97 (ICBO, 1997), section 1630.2.1, the design base shear shall be determined from the following formula:

$$V = \frac{C_v I}{R T} W \quad (6.3)$$

where C_v is the seismic coefficient, I is the seismic importance factor, R is the strength reduction factor, and T is the fundamental period.

Over-strength Factor (Ω)

Over-strength factors are obtained from the regression model based on the reference buildings. In this section we only illustrate the regression model of over-strength factors for RC frame buildings as an example. Over-strength factors for other structural systems could be obtained using the same method. For all the RC frame buildings designed by Haselton, we plot over-strength factors versus fundamental period in Figure 6.1.

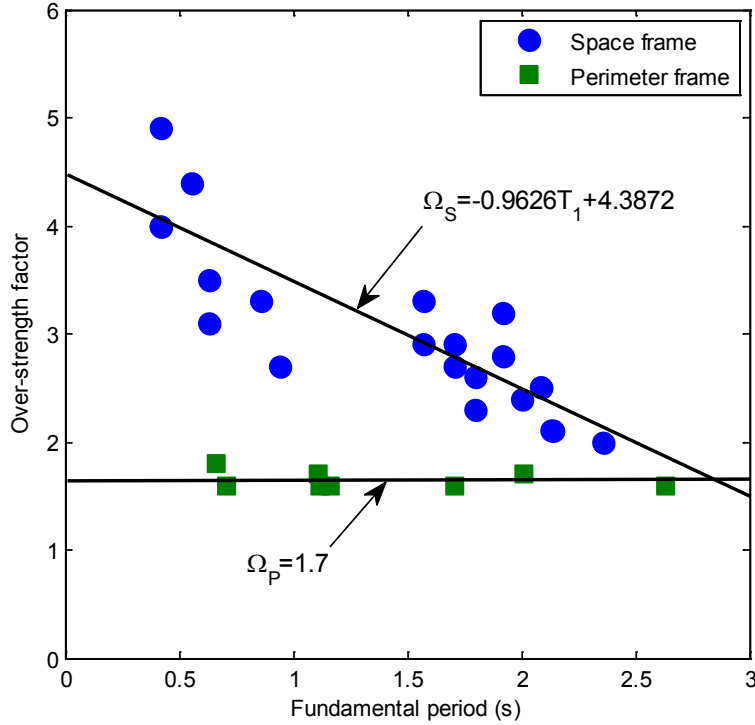


Figure 6.1 Over-strength factors versus fundamental periods for space and perimeter RC frame buildings in Haselton's study (Haselton, 2006)

From Figure 6.1 it could be noticed that the over-strength factor for perimeter frame buildings is close to a constant.

$$\Omega_p = 1.7 \quad (6.4)$$

For space frame buildings, the over-strength factor decreases with fundamental period increasing. The corresponding regression equation is

$$\Omega_s = -0.9626T_1 + 4.3872 \quad (6.5)$$

The difference between perimeter frame buildings and space frame buildings is that every bay of frames is designed as a moment-resisting frame in space frame buildings, while only perimeter frames are designed as a moment-resisting frame in perimeter frame buildings.

For space frame buildings, since every bay of frame is designed as a moment-resisting frame, seismic load is distributed into each frame when calculating the design requirements. For shorter space frame buildings with smaller seismic load, the resultant seismic design requirement is usually weaker than other requirements such as minimum beam and column section. For shorter space frame buildings, this will contribute to a reserve strength which leads to larger over-strength factors. The shorter a building is, the smaller the seismic load is and hence the larger the reserve strength is. This explains why the over-strength factor for space frame buildings decreases when the number of stories (fundamental period) increases.

For perimeter frame buildings, seismic load is only distributed to perimeter frames. This usually results in a design requirement which is stronger than other design requirements. The designs of perimeter frame buildings differ from space frame buildings in that seismic loads usually control them, and less reserve strength is introduced by other design requirements. As a result, the over-strength factors for perimeter frame buildings are smaller than those of space frame buildings and are unaffected by number of stories (fundamental period).

6.1.3 Global Ductility

Global ductility is another parameter that is impossible to measure from an actual building, since a destructive experiment is also needed. Hence, we can only obtain ductility through a reference building system. Toward this end, we need to do numerical analysis to every reference building and document the resultant ductility into a reference building system.

The global ductility ratios of all ductile frame buildings analyzed in Chapter 3 are plotted in Figure 6.2. The regression equation for the global ductility ratio is

$$\mu = -1.3081T_1 + 9.7975 \quad (6.6)$$

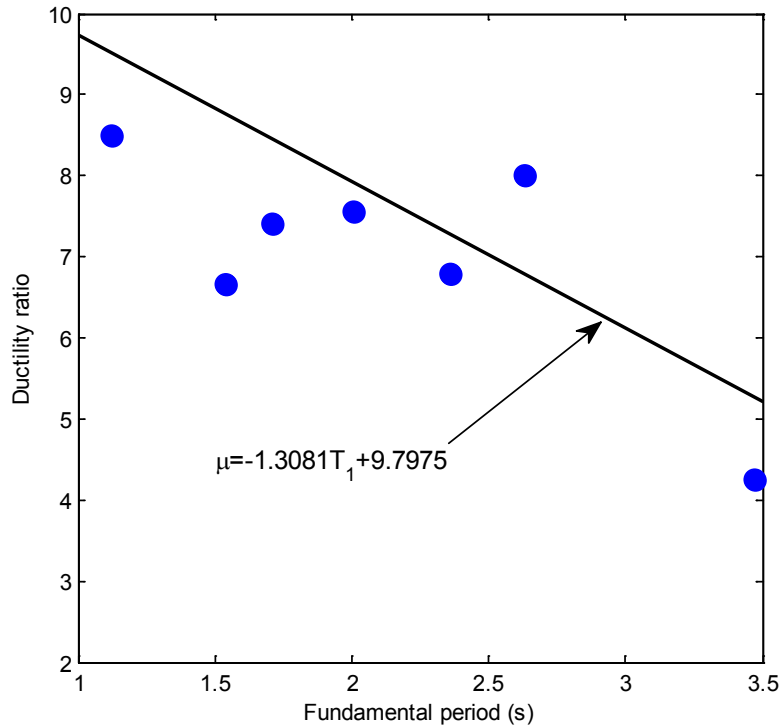


Figure 6.2 Ductility ratios versus fundamental periods for frame buildings analyzed in Chapter 3

6.1.4 Transfer Functions between Direct Parameter and Indirect Parameters

As discussed in Chapter 2, there are two kinds of parameters in building representation, direct parameters and indirect parameters. The parameters that could be obtained directly from a building, such as structural system, number of stories, and year of built, are direct parameters, while the parameters that must be obtained through analysis are indirect parameters. The three parameters used in the PFA collapse prediction model (fundamental period, lateral capacity, and global ductility) are all indirect parameter.

From Section 6.1.1 to 6.1.3, we discussed the procedures to obtain indirect parameters from direct parameters. Fundamental period is selected as a primary indirect parameter and other two indirect parameter, lateral capacity and global ductility, are evaluated using fundamental period (see Figure 6.3). This means if the fundamental period could be evaluated from the direct parameters, lateral

capacity and global ductility could be easily obtained using a regression model such as Equation 6.4, 6.5, and 6.6.

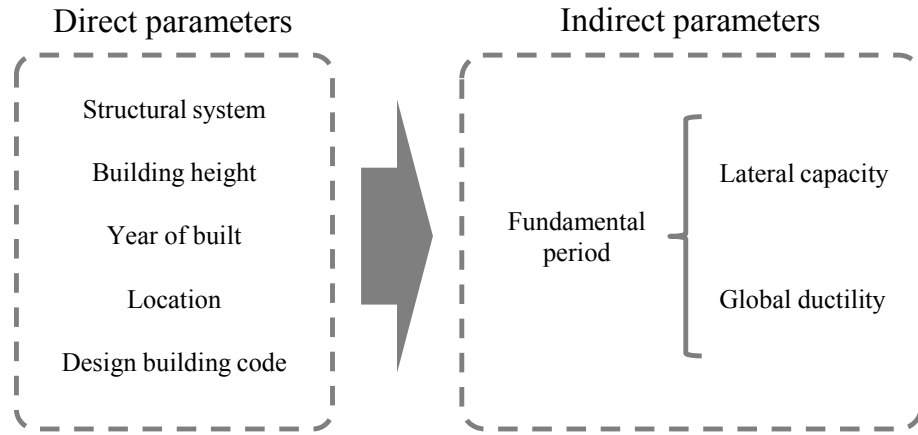


Figure 6.3 Procedures to obtain indirect parameters from direct parameters

Again, this thesis aims to develop the framework for a new collapse prediction model. Therefore, only the regression equations of indirect parameters for a selected building inventory are provided. If the reader would like to predict the collapse of types of buildings which are not discussed in this thesis, they will need to develop their own regression models using the framework provided in this thesis.

6.2 Comparison of PFA with other Intensity Measures in Collapse Prediction

In this section, we compare the PFA with the traditional and modified ground motion intensity measures reviewed in Chapter 1, Section 1.2.2.

6.2.1 Comparison with Traditional Ground Motion Intensity Measures

We first compared the performance of PFA with traditional ground motion intensity measures in collapse prediction. We chose four traditional ground motion intensity measures: PGA (peak ground acceleration), PGV (peak ground velocity), PGD (peak ground displacement), and S_a (spectral acceleration). In Chapter 3, we have already done the IDA analysis for ten building models and three ground motion sets. For each pair of building model and ground motion record, IDA analysis gives one data point of the threshold scale at which the ground motion collapses the

building. A total of 1500 collapse data points were used. We then multiplied the scales by different intensity measures to obtain the intensity measures at collapse thresholds

Plotted in Figure 6.4 to Figure 6.6 are the histograms of all five ground motion intensity measures at collapse thresholds. The three plots correspond to three ground motion sets, ramp-pulse-like ground motions, long-period ground motions, and short-period ground motions. In order to better compare the performances of different intensity measures, each intensity measure is normalized by its geometric mean value and plotted in log scale. The intensity measures are ordered according to their performances in each plot, with the best on top and the worst at the bottom. We used standard deviation to evaluate the performance of each intensity measure in collapse prediction. The smaller the standard deviation is, the better the performance is.

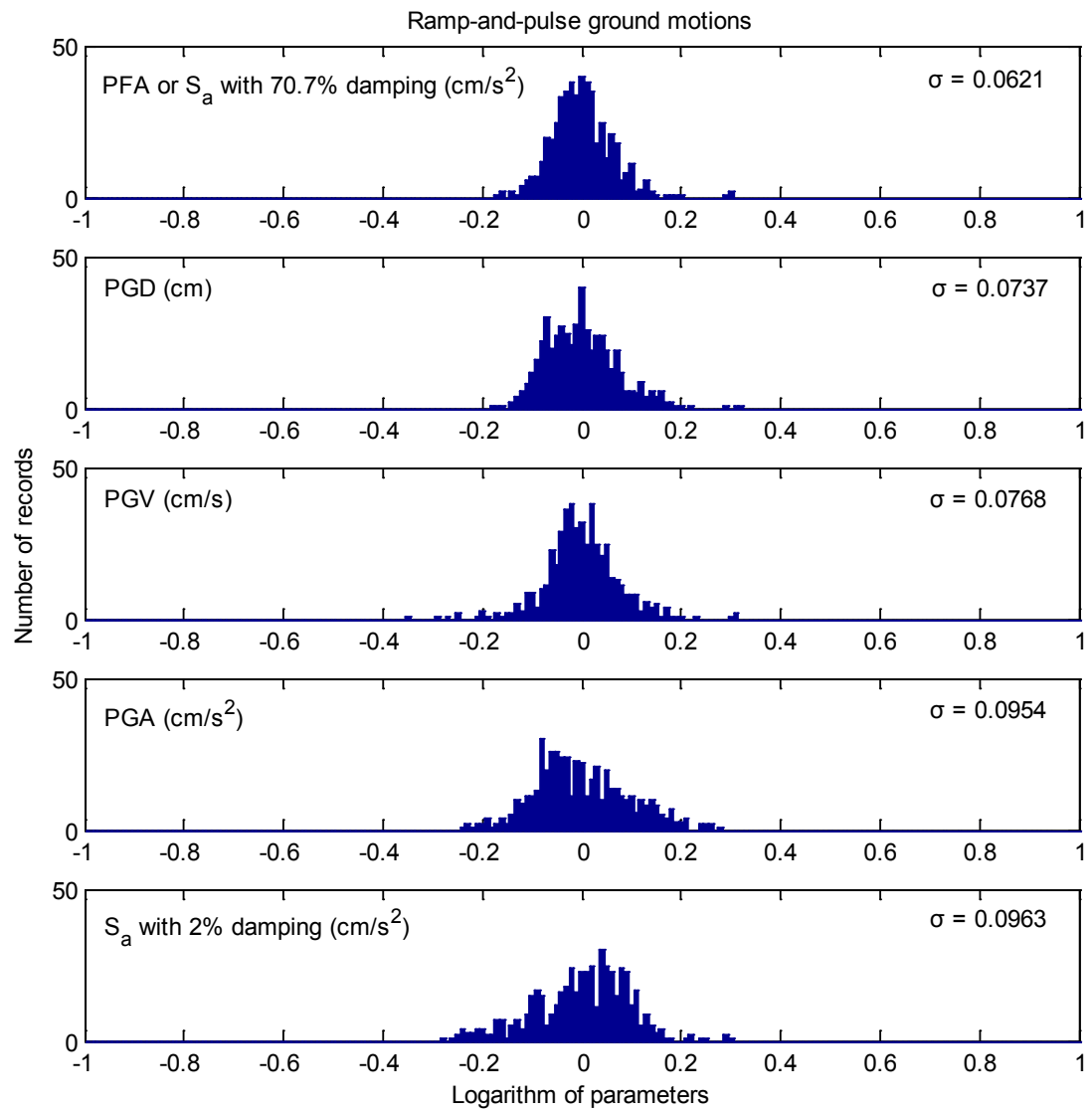


Figure 6.4 Comparison of performance of PFA, PGA, PGV, PGD, and S_a in collapse prediction of buildings subjected to ramp-and-pulse ground motions

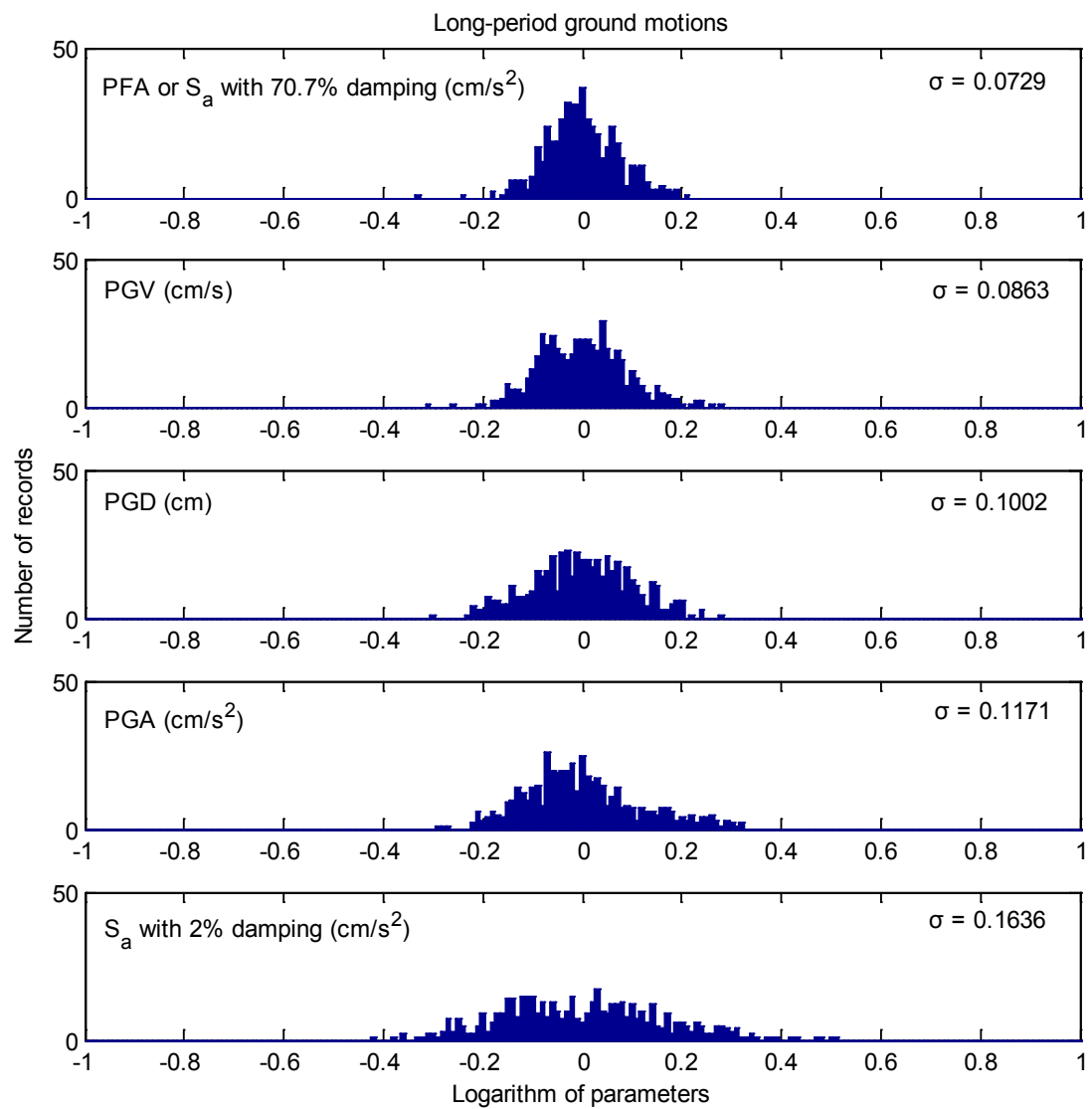


Figure 6.5 Comparison of performance of PFA, PGA, PGV, PGD, and S_a in collapse prediction of buildings subjected to long-period ground motions

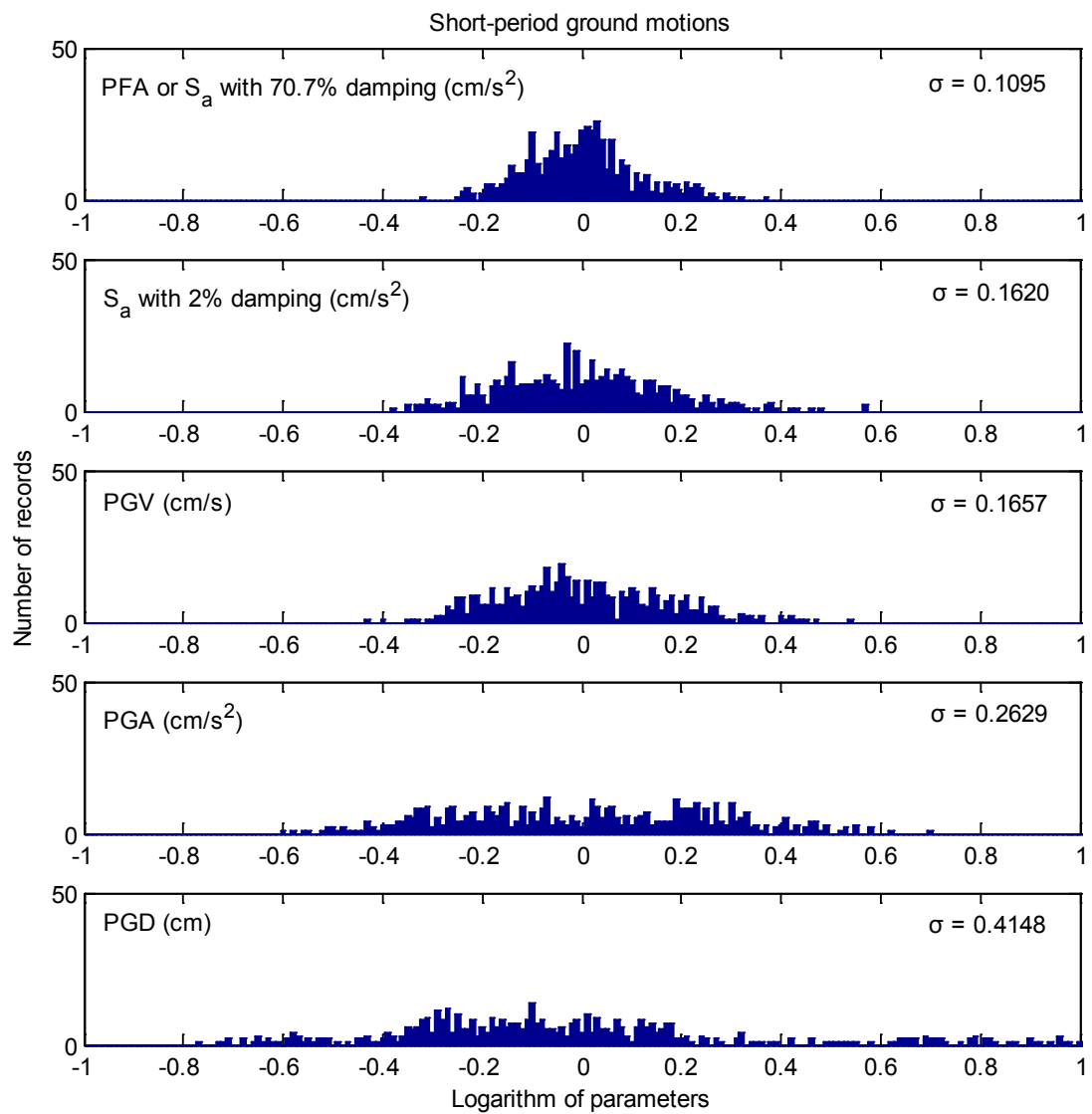


Figure 6.6 Comparison of performance of PFA, PGA, PGV, PGD, and S_a in collapse prediction of buildings subjected to short-period ground motions

Table 6.1 Performance of different ground motion intensity measures

Rank	Ramp-and-pulse	Long-period	Short-period
No.1	PFA	PFA	PFA
No.2	PGD	PGV	S _a
No.3	PGV	PGD	PGV
No.4	PGA	PGA	PGA
No.5	S _a	S _a	PGD

It could be concluded that PFA has the best performance in all of the three ground motion sets. However, the other four intensity measures have different performance orders in each ground motion set (see Table 6.1). It could be noticed that in ramp-pulse-like ground motions and long-period ground motions, PGV and PGD have the best performance among the traditional intensity measures, while S_a was the worst one. In short-period ground motions, S_a is the best one while PGD falls into the last place. If all three ground motion sets are considered, PGV has the best performance among the traditional intensity measures (1st or 2nd), while PGA always has a bad performance. The reason why PGA is not a good intensity measure for collapse prediction is that PGA usually corresponds to the high-frequency component of a ground motion record, but the buildings we used in developing the PFA model have a relatively long period, with 1.12s being the shortest. According to the PFA model, the high-frequency component of ground motion is irrelevant in collapse prediction. Hence PGA is obviously not a good intensity measure in this case.

The result in this section also explains why in Olsen's study (Olsen and Heaton, 2013) (PGV, PGD) is a good intensity measure in collapse prediction. In Olsen's study, all the ground motion records are not scaled. In this case, the ground motions that are strong enough to collapse the buildings very likely belong to either the ramp-pulse-like ground motion set or the long-period ground motion set, which are typically extremely strong and destructive, while the short-period ground motions are usually less strong since most of them are far-field ground motions that are already subjected to significant decay. In ramp-pulse-like and long-period ground motions, either PGV or PGD is the best traditional intensity measure in collapse prediction. If PGV and PGD are combined into one vector intensity measure, the performance is further improved by the guarantee of including the best intensity measure. Hence, (PGV, PGD) is found to be a good intensity measure for collapse prediction in Olsen's study.

6.2.2 Comparison with Modified Ground Motion Intensity Measures

In this section we compare PFA with typical modified ground motion intensity measures, Epsilon (ε), $R_{T1,T2}$, and Eta (η), by discussing the similarities and differences between PFA and each modified ground motion intensity measure.

Epsilon (ε)

Baker and Cornell (2005) have shown that the spectral shape factor has an important effect on the non-linear response of structures. One of the spectral shape indicators they introduce is Epsilon (ε), which measures the deviation of a given intensity measure (IM) of a ground motion from the geometric mean IM computed from a ground motion prediction model. In other words, Epsilon is defined as the difference between the natural logarithms of two IMs normalized by the standard deviation of the IM obtained from the attenuation model:

$$\varepsilon_{IM} = \frac{\ln IM_{Observed} - \ln IM_{Mean}}{\sigma_{\ln IM}} \quad (6.7)$$

By definition, Epsilon is a standard random variable. In practice, Epsilon corresponds to the spectral acceleration at the fundamental period of the structure with a specific damping ratio, e.g. $S_a(T_1, 5\%)$. From Equation 6.7, it could be concluded that if the observed IM is larger than the mean IM, Epsilon has a positive value and the response spectrum shows a peak at the corresponding period (see Figure 6.7). Similarly, if the observed IM is smaller than the mean value, Epsilon has a negative value and the response spectrum shows a valley at the corresponding period (see Figure 6.7). It is concluded by Baker and Cornell (2005) that for a fixed $S_a(T_1)$, records with positive ε values cause systematically smaller demands in structures than records with negative ε values.

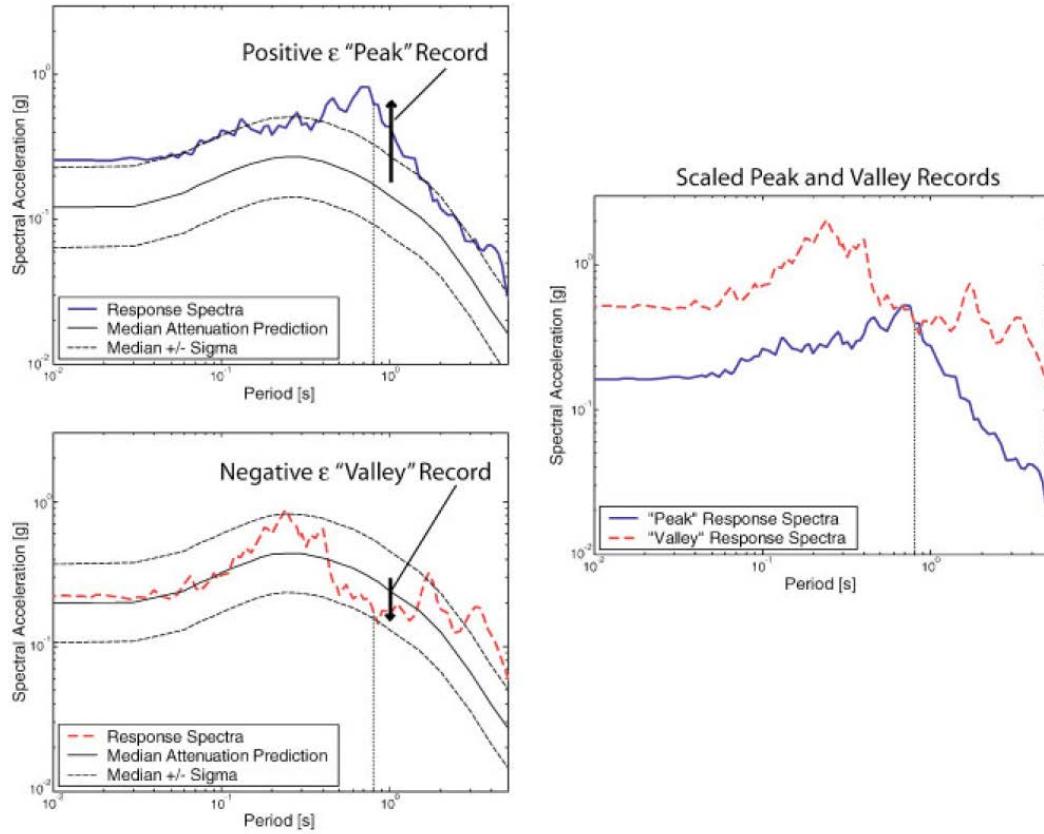


Figure 6.7 Examples of a record with a positive ϵ and a record with a negative ϵ scaled to the same $S_a(T_1)$ (Baker and Cornell, 2005)

If we interpret the above result using the framework of the PFA model, the result becomes obvious. When Epsilon has a positive value, the corresponding response spectrum has a peak near the period T_1 . Usually, this means that when $S_a(T_1)$ is scaled to a specific value, $S_a(cT_1)$ (c is the cutoff period coefficient in the PFA model and usually larger than 1) will be below average since $S_a(T_1)$ is a local peak. This will give a smaller PFA because the only difference between $S_a(cT_1)$ and PFA is the corresponding damping ratio. The PFA model indicates that ground motions with smaller PFA are less destructive, which agrees with Baker and Cornell's conclusion. The above discussion works the same for records with negative ϵ values.

R_{T1,T2}

Cordova et al. (2000), Vamvatsikos (2002), and Baker and Cornell (2008) introduce another spectral shape indicator, R_{T1,T2}. They define R_{T1,T2} as the ratio two spectral accelerations:

$$R_{T_1, T_2} = \frac{S_a(T_2)}{S_a(T_1)} \quad (6.8)$$

T₁ is chosen as the fundamental period of the structure. As for T₂, the recommended value is 1.65 by Cordova et al. (2000), 1.5 by Vamvatsikos (2002), and 2 by Baker and Cornell (2008).

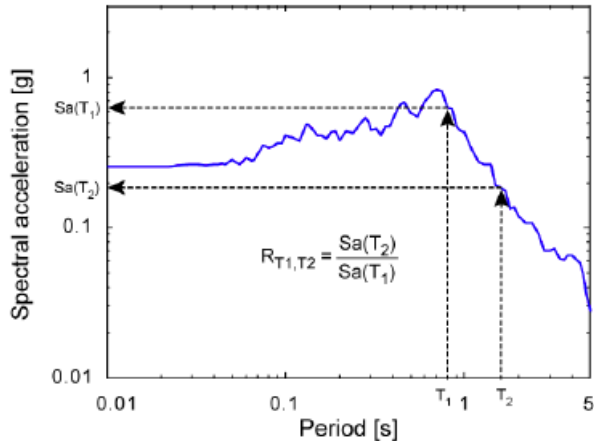


Figure 6.8 Calculation of R_{T1,T2} for a given response spectrum (Baker and Cornell, 2008)

Compared with Epsilon, the R_{T1,T2} indicator is even more straightforward, since it explicitly considers the effect of the long-period component of a ground motion. For the fixed S_a(T₁), if R_{T1,T2} is small, the ground motion has less long-period component compared with the average level, and hence is less destructive. Similarly, if R_{T1,T2} is large, the ground motion has more long-period component compared to the average level, and hence is more destructive.

Eta (η)

In order to improve the performance of the spectral shape indicator in predicting linear and non-linear structural response, Mousavi et al. (2011) have introduced an alternative spectral shaper indicator, Eta (η). The Eta indicator is defined as

$$\eta = \varepsilon_{S_a} + c_1 \varepsilon_{PGA} + c_2 \varepsilon_{PGV} + c_3 \varepsilon_{PGD} \quad (6.9)$$

By definition, the concept of this new spectral shape indicator is just employing more IM's associated with S_a by a linear combination of them. The coefficients of IM Epsilons are determined through an optimization problem in such a way that the average correlation between the indicator and the non-linear response of 84 SDOF with different periods and ductility becomes maximized. As a result, the combination of ε_{S_a} and ε_{PGV} works approximately equivalently to the full combination. Hence, the Eta indicator is simplified to

$$\eta = \varepsilon_{S_a} - b \varepsilon_{PGV} \quad (6.10)$$

If we interpret this result using the PFA framework, it does nothing but includes more long-period component. As we discussed in Chapter 3, integration is a low-pass filter, hence PGV represents the amplitude of long-period component of ground motion. Since collapse is controlled by long-period component, including more long-period component usually leads to a better prediction model.

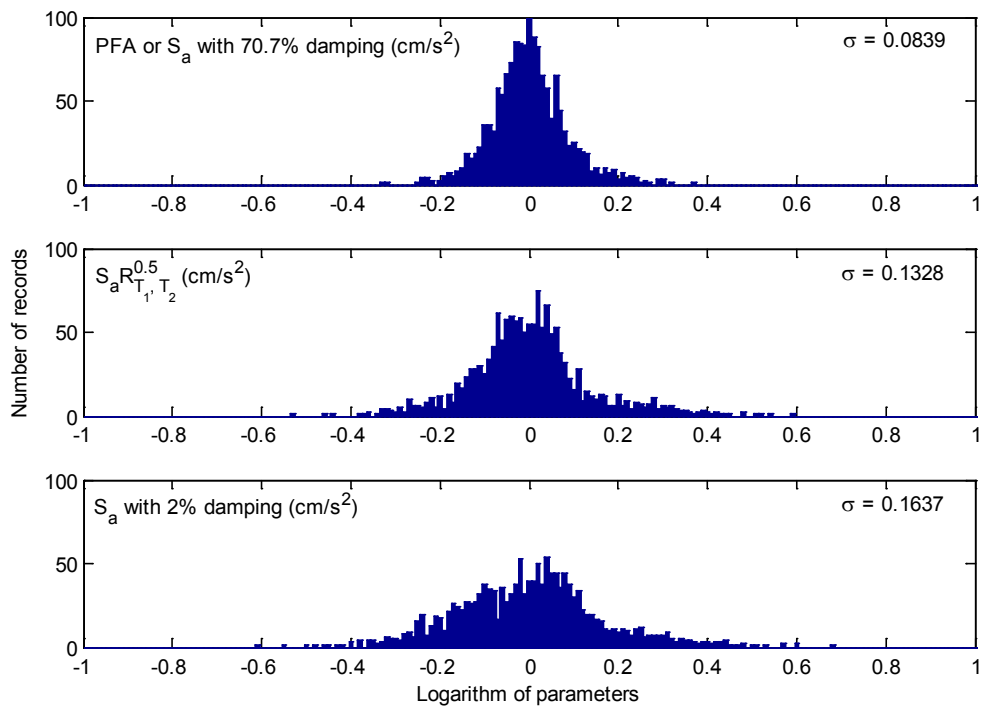


Figure 6.9 Comparison of PFA, $S_a R_{T_1, T_2}^{0.5}$, and S_a in collapse prediction

Since most modified intensity measures are vectors not comparable with the scalar intensity measure PFA, we only compare the performance of $S_a R_{T_1, T_2}^{0.5}$ proposed by Cordova et al. (2000) with PFA in collapse prediction. From Figure 6.9, it could be noticed that compared with S_a itself, the performance of $S_a R_{T_1, T_2}^{0.5}$ is improved by considering the spectral shape effect. However, it is still not as good as PFA.

From the above discussion, it could be concluded that all the modified ground motion intensity measures improve their performance in collapse prediction by explicitly or implicitly considering the effect of long-period components of ground motions (including (PGV, PGD) discussed in Chapter 3), which has the same physics as the PFA model. However, it should be noted that all of the above modified intensity measures are developed by maximizing the correlation between predictions and measured data using statistical methods. These studies do not reveal the fundamental physics in collapse, and hence the results strongly depend on the characteristics of the ground motion records and the building models used in the studies. This explains why for the same intensity measure R_{T_1, T_2} , three research groups end up with three different recommended values. In contrast, the PFA model is developed based on the understanding of the fundamental physics of collapse by constructing the equivalency among structural collapse, highly damped response spectrum, and Butterworth low-pass filter. We also identify the most important parameters that control the performance of collapse prediction and give the regression equation for each of them. Hence, the PFA model is a collapse prediction framework that could be easily extended to other buildings not considered in this study.

From the discussion in this section, we conclude that PFA is a more advanced ground motion intensity measure in collapse prediction compared with all the traditional and modified ground motion intensity measures. Based on the result, we propose to use PFA as a ground motion intensity measure in practicing collapse prediction.

6.3 Potential Application of the PFA Collapse Prediction Model to other Structural Systems

In Chapter 3 and Chapter 4, we develop the peak filtered acceleration (PFA) collapse prediction model and verify the model using steel and reinforced concrete moment-resisting frame buildings. The results demonstrate that the PFA model has a good performance in collapse prediction for these buildings.

However, besides steel and reinforced concrete moment-resisting frames, there are still other structural systems that are commonly used in seismic design, such as concrete shear wall buildings, brace frame buildings, wooden buildings, and base-isolated buildings.

In this section we discuss the possibility of applying the PFA collapse prediction model to other structural systems, using RC shear wall building as an example. Again, the goal of this thesis is to provide the methodology and framework of the PFA collapse prediction model, not to demonstrate the possibility of applying it to different structural systems. Towards this end, we only provide some support for extending the PFA collapse prediction model to other structural systems, using some simple numerical models. Those who are interested in applying the PFA model to a specific structural system can develop their own version of the PFA model based on the framework we provide in addition to their knowledge and experience.

In order to examine the possibility of applying the PFA collapse prediction model to RC shear wall buildings, we designed a simple 6-story RC shear wall building. The elevation and floor plan were identical to the U6 building. It should be noted that this building model was only designed for demonstrating the possibility of applying the PFA collapse prediction model to RC shear wall buildings, not for studying the behaviors of RC shear wall buildings. Under this assumption, the details of the building were highly simplified, only ensuring that the model could represent the most important behaviors of RC shear wall buildings. The placement of shear walls is shown in Figure 6.10 and 6.11. The building was designed according to UBC 97 (ICBO, 1997); the details of the design can be found in Appendix A.3.

The reinforced concrete shear wall was modeled using multi-layer shell elements. The same analysis was conducted on the shear wall building model as was done with the building models in Chapter 3. The shear wall building model was subjected to a series of sinusoidal ground motions of different periods, and incremental dynamic analysis (IDA) was applied to determine the threshold of collapse. The result is shown in Figure 6.12; minimum collapse peak ground acceleration (MinCPGA) is plotted versus T_s/T_1 , and compared with the pushover curve. A similar conclusion is made for the U6 shear wall building. Much smaller amplitudes are needed at long-period ground motions ($T_s/T_1 > c$) to cause collapse, and these long-period amplitudes are close to the maximum lateral strength calculated in the pushover analysis. Hence, a low-pass Butterworth filter could be

used to extract the long-period components from a ground motion to predict collapse, which means the PFA collapse prediction model could be extended to shear wall buildings.

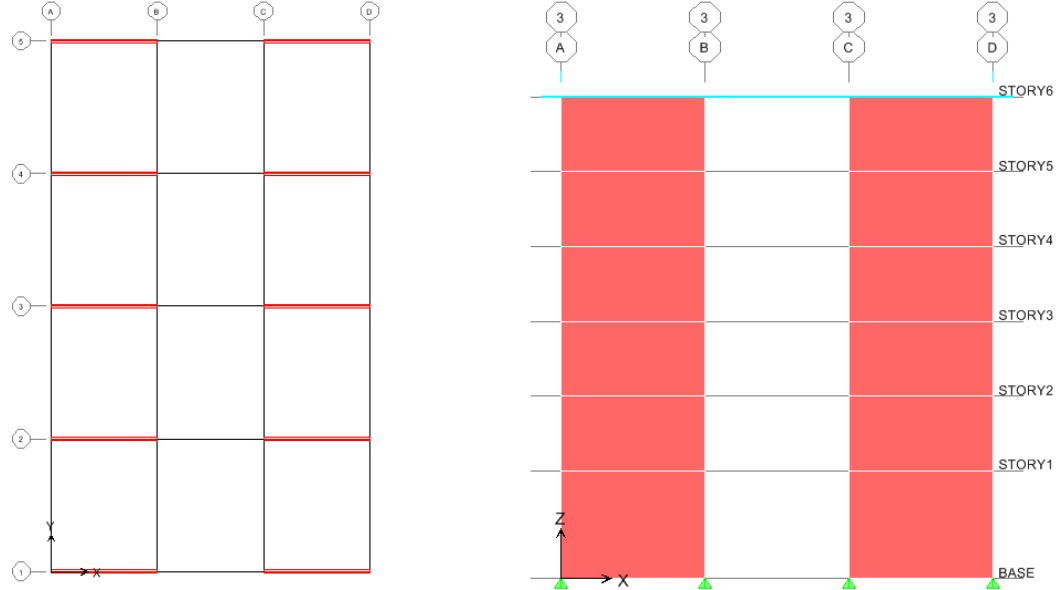


Figure 6.10 Floor plan of building U6SW

Figure 6.11 Elevation view of building U6SW

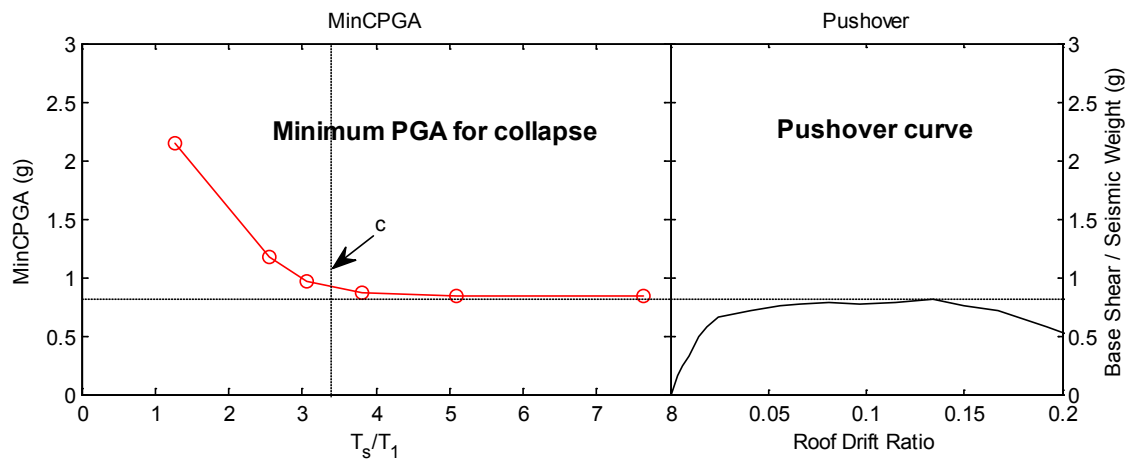


Figure 6.12 Minimum Collapse PGA (left) and pushover curve (right) for U6 shear wall building. A common vertical axis is used for both panels.

However, when we calculated the cutoff period using the regression equation developed in Chapter 3 (Equation 3.1), c is equal to 1.73, which is quite different from the c in Figure 6.12

(approximately 3.3). Therefore, it could be concluded that the cutoff period regression equation developed using frame buildings does not apply to shear wall buildings. A new cutoff period regression model is needed for the PFA shear wall building collapse prediction model.

CONCLUSIONS AND FUTURE WORK

7.1 Summary of PFA Collapse Prediction Model

In this section, we summarize the PFA collapse prediction model developed in this thesis.

Given a building and a ground motion, whether the building will collapse in the ground motion could be predicted by the PFA model, and the prediction could be divided into three cases.

Case 1: 2D building subjected to uni-directional ground motions

Step 1: Obtain the fundamental period T_1 , the maximum base shear force V_{\max} , the seismic weight W , and the ductility μ of the building. Ductility is defined as

$$\mu = \frac{d_{0.5}}{d_y} \quad (7.1)$$

where d_y denotes the roof displacement at which the building starts to yield globally, and $d_{0.5}$ denotes the roof displacement at which the building loses 50% of the maximum strength. If numerical model is not available, measurement or estimation of the three parameters could be used instead (see Chapter 6, section 6.1).

Step 2: Compute the cutoff period coefficient c for the building with Equation 7.2.

$$c = 0.1241\mu + 0.6931 \quad (7.2)$$

Step 3: Identify the type of the ground motion as one of the following:

- a. Ramp-pulse-like ground motion (RP).
- b. Long-period ground motion (LP).
- c. Short-period ground motion (SP).

Step 4: Filter the acceleration time history using low-pass Butterworth filter with the order and the cutoff frequency given in Table 7.1.

Table 7.1 Parameters of Butterworth filter

Type of ground motion	Order	Cutoff frequency
RP	4	$1/cT_1$
LP & SP	2	$1/cT_1$

Step 7: Predict the building behavior with Table 7.2.

Table 7.2 Chart of collapse prediction (g is gravity acceleration)

Type of ground motion	Intensity measure	Condition	Prediction
RP	Half of peak-to-peak acceleration	$>V_{max}/W \cdot g$	Collapse
		$<V_{max}/W \cdot g$	Standing
LP	Peak ground acceleration	$>V_{max}/W \cdot g$	Collapse
		$<V_{max}/W \cdot g$	Standing
SP	Half of peak-to-peak acceleration	$>V_{max}/W \cdot g$	Collapse
		$<V_{max}/W \cdot g$	Standing

Case 2: 3D regular building without torsional effect subjected to bi-directional ground motion

Step 1: Decompose the 3D building into two 2D buildings in the principal directions.

Step 2: Apply the PFA model to each 2D building as it is done in Case 1, using the properties (fundamental period and ductility) and ground motion in the corresponding direction.

Step 3: If one of the 2D buildings collapses, the 3D building is expected to collapse. The 3D building will survive the bi-directional ground motion only if each of the 2D buildings can resist the corresponding uni-directional ground motion.

Case 3: 3D irregular building with torsional effect subjected to bi-directional ground motion

Step 1: Obtain the limit domain of the building using multi-directional pushover analysis.

Step 2: Filter the ground motion in each of the building's principal directions using the properties (fundamental period and ductility) in the same direction as it is done in Case 1.

Step 3: If the filtered bi-directional acceleration exceeds the limit domain, the building is expected to collapse under the ground motion. Otherwise, the building will survive the ground motion.

For Case 2 and Case 3, the fundamental period in each principal direction is the longest period of all the modes that have a modal direction factor larger than 45% in this direction.

7.2 Conclusions

In this thesis, we develop a new collapse prediction model, the PFA (Peak Filtered Acceleration) model, for buildings subjected to different types of ground motions.

For the structural system, this model covers modern steel and reinforced concrete moment-resisting frame buildings (potentially reinforced concrete shear wall buildings). For ground motions, this model covers ramp-pulse-like, long-period, and short-period ground motions.

To predict whether a building will collapse in a given ground motion, we first extract long-period components from the ground motion using a low-pass Butterworth filter with suggested order (related to ground motion type) and cutoff frequency (related to fundamental period and global ductility). We then compare the filtered acceleration time history with the capacity of the building (constant for 2D building and limit domain for 3D building). If the filtered acceleration exceeds the building's capacity, the building is predicted to collapse. Otherwise, it is expected to survive the ground motion.

The parameters used in the PFA model (fundamental period, global ductility, and lateral capacity) could be obtained from either numerical analysis, measurement, or interpolation based on the reference building system proposed in this thesis.

The PFA collapse prediction model is simple in concept, easy to use, and real-time fast while archiving computational accuracy. It is verified by FEM simulations of 13 frame building models and 150 ground motion records.

Based on the developed collapse prediction model, we propose to use PFA (Peak Filtered Acceleration) as a new ground motion intensity measure for collapse prediction. We compare PFA with traditional intensity measures PGA, PGV, PGD, and S_a in collapse prediction and find that PFA has the best performance among all the intensity measures.

We also provide a close form in term of a vector intensity measure (PGV, PGD) of the PFA collapse prediction model for practical collapse risk assessment.

7.3 Future Work

7.3.1 Full-range Intensity Measure

The PFA model developed in this thesis only works for one damage level: collapse. However, in seismic risk assessment, there are still other damage levels, such as slight damage, moderate damage, and heavy damage.

Researchers have shown that spectral acceleration at T_1 , $S_a(T_1)$, is an effective IM in structure response prediction, especially within their elastic range (Shome et al, 1998). Hence, $S_a(T_1)$ has good performance in assessment of a building with no damage or slight damage.

Since $S_a(T_1)$ works well for no damage or slight damage and PFA works well for collapse, if we make a linear combination of the two intensity measures (Equation 7.3), we could end up with a new parameter that potentially works for all damage levels.

$$IM = a \cdot S_a(T_1) + b \cdot PFA \quad (7.3)$$

In Equation 7.3, a and b are coefficients of $S_a(T_1)$ and PFA. If the ground motion intensity is small enough that the building response is within its elastic range, IM should be equal to $S_a(T_1)$. In this case, coefficient ‘ a ’ should be equal to 1 and coefficient ‘ b ’ should be equal to 0. If the ground motion intensity is large enough that the building response is close to collapse, IM should be equal to PFA. In this case, coefficient ‘ a ’ should be equal to 0 and coefficient ‘ b ’ should be equal to 1. If ground motion intensity is increased from zero to collapse level, coefficient ‘ a ’ is a decreasing function from 1 to 0 and coefficient ‘ b ’ is an increasing function from 0 to 1. The forms of these functions are to be determined.

7.3.2 Updating Scheme Using Measured Data

In the PFA collapse prediction model developed in this thesis, three key parameters are needed in collapse prediction of a building: fundamental period, lateral capacity, and global ductility. Among these parameters, only fundamental parameter could be measured from a real building, while the other two parameters could be estimated using the reference building system. The building reference system is designed to represent the real-world building inventory. However, the actual

property of a specific building could be very different from the estimation due to unpredictable reasons. In this case, the PFA model could result in a wrong prediction. This proposes a challenge that if we could use the measured data from the building to update the PFA model, the prediction will get closer and closer to the situation in the real world. The most challenging part in this problem is that the collapse is an extreme nonlinear behavior, while the response data obtained from the building is most likely within the elastic range. Once the nonlinear response was measured, the model could receive a better update. However, if nonlinear deformation happens, the building must be damaged and either be retrofitted (repairable) or abandoned (not repairable). In this case, the updated model could not be applied to the building anymore since the property of the building is changed. Hence, we can only use linear response data to update a prediction model for nonlinear response. This will be a challenging research project.

7.3.3 3D Limit Domain and the Corresponding Collapse Prediction

It could be noticed that, in this thesis, all the ground motions used are in horizontal directions. For 2D buildings, we use uni-directional ground motion in horizontal direction. For 3D buildings, we use bi-directional ground motion in horizontal direction. We have not discussed vertical ground motion, since most of time it has little contribution to collapse. However, strong vertical ground motions are recorded in some earthquakes, and field evidence shows that these strong vertical ground motions have caused significant damage in buildings (Papazoglou and Elnashai, 1996). So, in order to predict building collapse under strong vertical ground motions, the PFA model needs the inclusion of 3D ground motions. We obtained 3D limit domain of building B1 (see Figure 7.1) by applying forces in various directions, similar to in Chapter 4. It could be noticed that the 3D limit domain has an obelisk shape. The challenge of predicting collapse using this 3D limit domain is that the building has different behaviors in the horizontal and vertical direction. In the horizontal direction, the building deforms in frame mechanism, while in the vertical direction, the building deforms mainly in axial deformation of columns. How to combine different mechanisms into one collapse prediction model is a challenging research project.

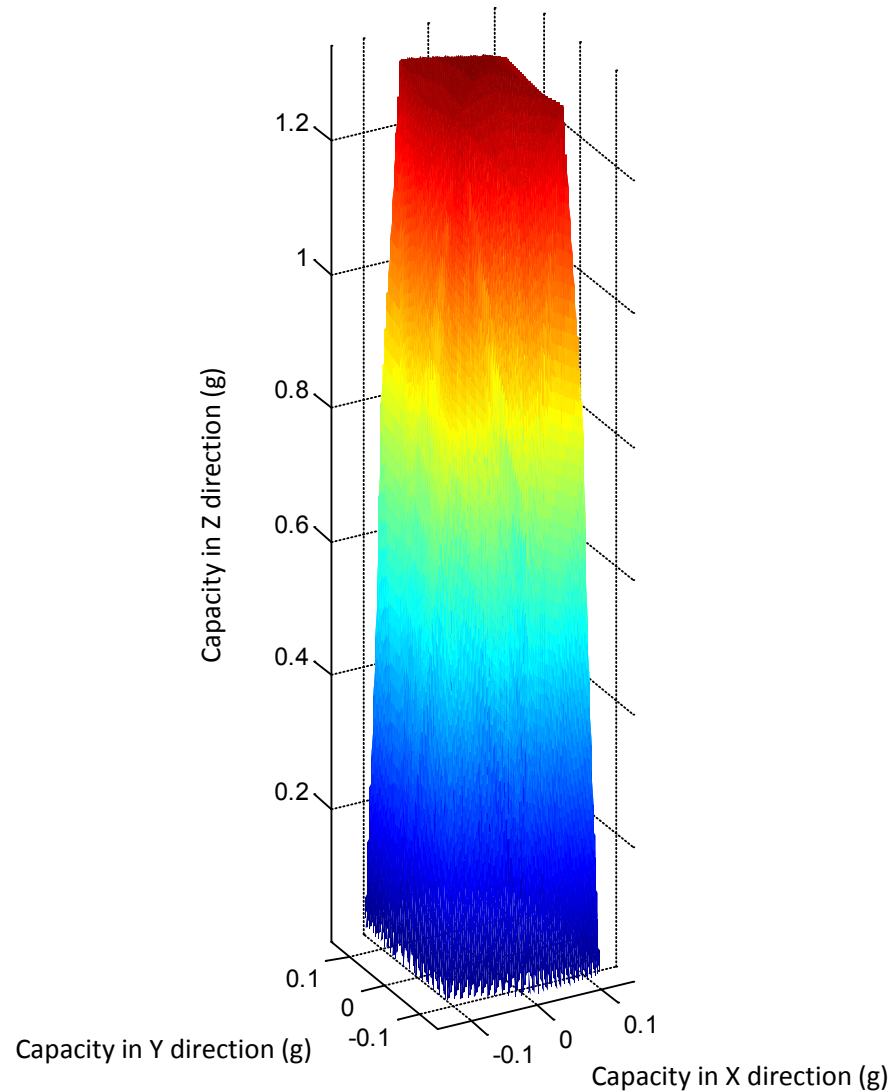


Figure 7.1 3D limit domain of building B1

BIBLIOGRAPHY

- American Concrete Institute. (2002). *Building Code Requirements for Structural Concrete (ACI 318-02) and Commentary (ACI 318R-02)*, Farmington Hills, MI.
- American Society of Civil Engineers. (2002). ASCE7-02: Minimum Design Loads for Buildings and Other Structures, Reston, VA.
- ATC. (1985). *Earthquake Damage Evaluation Data for California ATC-13*. Redwood City, California: Applied Technology Council.
- ATC. (2000). Database on the Performance of Structures near Strong-Motion Recordings: 1994 Northridge, California, Earthquake. ATC 38 (pp. 260). Redwood City, California: Applied Technology Council.
- Baker, J. W., & Cornell, C. A. (2005). A Vector-Valued Ground Motion Intensity Measure Consisting of Spectral Acceleration and Epsilon. *Earthquake Engineering and Structural Dynamics*, 34(10), 1193-1217.
- Baker, J. W., & Cornell, C. A. (2006). Spectral Shape, Epsilon and Record Selection. *Earthquake Engineering and Structural Dynamics*, 35(9), 1077-1095.
- Baker, J. W., & Cornell, C. A. (2008). Vector-valued Intensity Measures Incorporating Spectral Shape for Prediction of Structural Response. *Journal of Earthquake Engineering*, 12(4), 534-554.
- Bernal, D. (1987). Amplification Factors for Inelastic Dynamic P-Δ Effects in Earthquake Analysis. *Earthquake Engineering and Structural Dynamics*, 15(5), 635-651.
- Challa, V. R. M., & Hall, J. F. (1994). Earthquake Collapse Analysis of Steel Frames. *Earthquake Engineering and Structural Dynamics*, 23(11), 1199-1218.
- Champion, C., & Liel, A. (2012). The Effect of Near-Fault Directivity on Building Seismic Collapse Risk. *Earthquake Engineering and Structural Dynamics*, 41(10), 1391-1409.
- Chi, W.-M., El-Tawil, S., Deierlein, G. G., & Abel, J. F. (1998). Inelastic Analyses of a 17-Story Steel Framed Building Damaged During Northridge. *Engineering Structures*, 20(4-6), 481-495.

- Chopra, A. K., & Goel, R. K. (2002). A Modal Pushover Analysis Procedure for Estimating Seismic Demands for Buildings. *Earthquake Engineering and Structural Dynamics*, 31(3), 561-582.
- Chopra, A. K., & Goel, R. K. (2004). Evaluation of Model and FEMA Pushover Analyses: Vertically 'Regular' and Irregular Generic Frames. *Earthquake Spectra*, 20(1), 255-271.
- Cordova, P. P., Deierlein, G. G., Mehanny, S. S. F., & Cornell, C. A. (2000, 11-13 September). Development of a two Parameter Seismic Intensity Measure and Probabilistic Assessment Procedure. Paper presented at the Second U.S. - Japan Workshop on Performance-Based Earthquake Engineering for Reinforced Concrete Building Structures, Sapporo, Hokkaido, Japan.
- Fajfar, P., & Gaspersic, P. (1996). The N2 Method for the Seismic Damage Analysis of RC Buildings. *Earthquake Engineering and Structural Dynamics*, 25(1), 31-46.
- FEMA. (1997). NEHRP Guidelines for the Seismic Rehabilitation of Buildings (FEMA Publication 273).
- FEMA. (2000). Prestandard and Commentary for the Seismic Rehabilitation of Buildings (FEMA Publication 356).
- Graves, R. W., & Somerville, P. G. (2006). Broadband Ground Motion Simulations for Scenario Ruptures of the Puente Hills Fault. Paper presented at the 8th Nat. Conf. Earthquake Engineering, San Francisco, CA.
- Gupta, B., & Kunnath, S. K. (2000). Adaptive Spectra-Based Pushover Procedure for Seismic Evaluation of Structures. *Earthquake Spectra*, 16(2), 367-391.
- Hall, J. F. (1995). *Parameter Study of the Response of Moment-Resisting Steel Frame Buildings to Near-Source Ground Motions*. Pasadena: California Institute of Technology.
- Hall, J. F. (1997). *Seismic Response of Steel Frame Buildings to Near-Source Ground Motions (Vol. 97)*. Pasadena: California Institute of Technology.
- Hall, J. F. (1998). Seismic Response of Steel Frame Buildings to Near-Source Ground Motions. *Earthquake Engineering and Structural Dynamics*, 27(12), 1445-1464.
- Hall, J. F., & Challa, V. R. M. (1995). Beam-Column Modeling. *Journal of Engineering Mechanics*, 121(12), 1284-1291.

- Haselton, C. B. (2006). *Assessing Seismic Collapse Safety of Modern Reinforced Concrete Moment Frame Buildings*. Doctor of Philosophy, Stanford.
- Haselton, C. B., & Baker, J. W. (2006). Ground Motion Intensity Measures for Collapse Capacity Prediction: Choice of Optimal Spectral Period and Effect of Spectral Shape. Paper presented at the 8NCEE, San Francisco, California.
- Haselton, C. B., Baker, J. W., Liel, A. B., & Deierlein, G. G. (2011). Accounting for Ground-Motion Spectral Shape Characteristics in Structural Collapse Assessment through an Adjustment for Epsilon. *Journal of Structural Engineering*, 137(3), 332-344.
- Ibarra, L. F., Medina, R. A., & Krawinkler, H. (2005). Hysteretic Models That Incorporate Strength and Stiffness Deterioration. *Earthquake Engineering and Structural Dynamics*, 34(12), 1489-1511.
- ICBO. (1982). *1982 Uniform Building Code Structural Engineering Design Provisions*, Whittier, California, USA.
- ICBO. (1994). *1994 Uniform Building Code Structural Engineering Design Provisions*, Whittier, California, USA.
- ICBO. (1997). *1997 Uniform Building Code Structural Engineering Design Provisions*, Whittier, California, USA.
- Ivanovic, S. S., Trifunac, M. D., & Todorovska, M. I. (2000). Ambient Vibration Tests of Structures- A Review. *ISET Journal of Earthquake Technology*, 37(4), 165-197.
- Jeong, S.-H., & Elnashai, A. S. (2007). Probabilistic Fragility Analysis Parameterized by Fundamental Response Quantities. *Engineering Structures*, 29, 1238-1251.
- Kalkan, E., & Kunzath, S. K. (2006). Effects of Fling Step and Forward Directivity on Seismic Response of Buildings. *Earthquake Spectra*, 22(2), 367-390.
- Kirçil, M. S., & Polat, Z. (2006). Fragility Analysis of Mid-Rise R/C Frame Buildings. *Engineering Structures*, 28(9), 1335-1345.
- Krawinkler, H., & Seneviratna, G. D. P. K. (1998). Pros and Cons of a Pushover Analysis of Seismic Performance Evaluation. *Engineering Structures*, 20(4-6), 452-464.
- Krawinkler, H., Zareian, F., Lignos, D. G., & Ibarra, L. F. (2009). Prediction of Collapse of Structures under Earthquake Excitations. Paper presented at the ECCOMAS Thematic

Conference on Computational Methods in Structural Dynamics and Earthquake Engineering, Rhodes, Greece.

Krishnan, S. (2003). *Three-Dimensional Nonlinear Analysis of Tall Irregular Steel Buildings Subject to Strong Ground Motion*. Doctor of Philosophy, California Institute of Technology, Pasadena.

Krishnan, S., Ji, C., Komatitisch, D., & Tromp, J. (2006). Performance of Two 18-Story Steel Moment-Frame Buildings in Southern California during Two Large Simulated San Andreas Earthquakes. *Earthquake Spectra*, 22(4), 1035-1061.

Krishnan, S. (2007). Case Studies of Damage to 19-Storey Irregular Steel Moment-Frame Buildings under Near-Source Ground Motion. *Earthquake Engineering and Structural Dynamics*, 36(7), 861-885

Lang, K. (2002). *Seismic vulnerability of existing buildings*. Doctor of Technical Sciences, Swiss Federal Institute of Technology Zurich.

Lee, B. J., Chou, T. Y., Hsiao, C. P., Chung, L. K., Huang, P. H., & Wu, Y. B. (2002). The Statistics and Analysis of Building Damage on Chi-Chi Earthquake. Paper presented at the International Training Programs for Seismic Design of Building Structures, Taipei, Taiwan.

Liel, A. B., Haselton, C. B., & Deierlein, G. G. (2011). Seismic Collapse Safety of Reinforced Concrete Buildings. II: Comparative Assessment of Nonductile and Ductile Moment Frames. *Journal of Structural Engineering*, 137(4), 492-502.

Lu, X., Lu, X., Guan, H., & Ye, L. (2013). Collapse Simulation of RC High-Rise Building Induced by Extreme Earthquakes. *Earthquake Engineering and Structural Dynamics*, 42(5), 705-723.

Lynch, K. P., Rowe, K. L., & Liel, A. B. (2011). Seismic Performance of Reinforced Concrete Frame Buildings in Southern California. *Earthquake Spectra*, 27(2), 399-418.

Mousavi, M., Ghafory-Ashtiani, M., & Azarbakht, A. (2011). A New Indicator of Elastic Spectral Shape for the Reliable Selection of Ground Motion Records. *Earthquake Engineering and Structural Dynamics*, 40(12), 1403-1416.

Muto, M., & Krishnan, S. (2011). Hope for the Best, Prepare for the Worst: Response of Tall Steel Buildings to the ShakeOut Scenario Earthquake. *Shake Out Special Issue, Earthquake Spectra*, 27(2), 375-398.

- Olsen, A. H., & Heaton, T. H. (2013). Characterizing Ground Motions that Collapse Steel, Moment-Resisting Frames or Make Them Unrepairable. *Earthquake Spectra (in press)*.
- Papazoglou, A. J., & Elnashai, A. S. (1996). Analytical and Field Evidence of the Damaging Effect of Vertical Earthquake Ground Motion. *Earthquake Engineering and Structural Dynamics*, 25(10), 1109-1137.
- Petti, L., Marino, I., Cuoco, L., & B., P. (2007). Assessment of Seismic Response of Plan-Asymmetric Structures through simplified Static Nonlinear Analyses. *Proc. 3rd Structural Engineering World Congress*. Bangalore, India.
- Petti, L., Marino, I., & Cuoco, L. (2008). Seismic Response Analysis of 3D Structures through Simplified Non-Linear Procedures. Paper presented at the 14th World Conference on Earthquake Engineering, Beijing, China.
- Porter, K. A., Jaiswal, K. S., Wald, D. J., Greene, M., & Comartin, C. (2008). Whe-Pager Project: A New Initiative in Estimating Global Building Inventory and its Seismic Vulnerability. Paper presented at the The 14th World Conference on Earthquake Engineering, Beijing, China.
- Saiidi, M., & Sozen, M. A. (1981). Simple Nonlinear Seismic Analysis of R/C Structures. *Journal of the Structural Division*, 107(5), 937-953.
- Shome, N., Cornell, C. A., Bazzurro, P., & Carballo, J. E. (1998). Earthquakes, Records, and Nonlinear Responses. *Earthquake Spectra*, 14(3), 469-500.
- Somerville, P. G. (1998, Sept. 15). Development of an Improved Representation of Near-Fault Ground Motions. Paper presented at the SMIP98 Proceedings, Seminar on Utilization of Strong-Motion Data, Oakland, CA.
- Stathopoulos, K. G., & Anagnostopoulos, S. A. (2005). Inelastic Torsion of Multistorey Buildings Under Earthquake Excitations. *Earthquake Engineering and Structural Dynamics*, 34(12), 1449-1465.
- Suita, K., Yamada, S., Tada, M., Kasai, K., Matsuoka, Y., & Shimada, Y. (2008). Collapse Experiment on 4-Story Steel Moment Frame Part 2 Detail of Collapse Behavior. Paper presented at the 14th World Conference on Earthquake Engineering, Beijing, China.

- Tan, A., & Irfanoglu, A. (2012). Correlation between Ground Motion Based Shaking Intensity Estimates and Actual Building Damage. Paper presented at the 15th World Conference on Earthquake Engineering, Lisbon, Portugal.
- Takizawa, H., & Jennings, P. C. (1980). Collapse of a Model for Ductile Reinforced Concrete Frames under Extreme Earthquake Motions. *Earthquake Engineering and Structural Dynamics*, 8(2), 117-144.
- Vamvatsikos, D. (2002). *Seismic Performance, Capacity and Reliability of Structures as Seen through Incremental Dynamic Analysis*. Doctor of Philosophy, Stanford University.
- Villaverde, R. (2007). Methods to Assess the Seismic Collapse Capacity of Building Structures: State of the Art. *Journal of Structural Engineering*, 133(1), 57-66.
- Williamson, E. B. (2003). Evaluation of Damage and P-Δ Effects for Systems under Earthquake Excitation. *Journal of Structural Engineering*, 129(8), 1036-1046.
- Yakut, A., Ozcebe, G., & Yucemen, M. S. (2006). Seismic Vulnerability Assessment Using Regional Empirical Data. *Earthquake Engineering and Structural Dynamics*, 35(10), 1187-1202.
- Yamada, S., Suita, K., Tada, M., Kasai, K., Matsuoka, Y., & Shimada, Y. (2008). Collapse Experiment on 4-Story Steel Moment Frame: Part 1 Outline Of Test Results. Paper presented at the 14th World Conference on Earthquake Engineering, Beijing, China.
- Yang, J. (2009). *Nonlinear Response of High-Rise Buildings in Giant Subduction Earthquakes*. Doctor of Philosophy, California Institute of Technology, Pasadena.

APPENDIX A: BUILDING MODELS USED IN THIS THESIS

Appendix A describes all the building models used in this thesis. They are grouped into four categories: (1) 2D steel moment-resisting frame buildings; (2) 2D RC moment-resisting frame buildings; (3) 2D RC shear wall buildings; (4) 3D steel moment-resisting frame buildings.

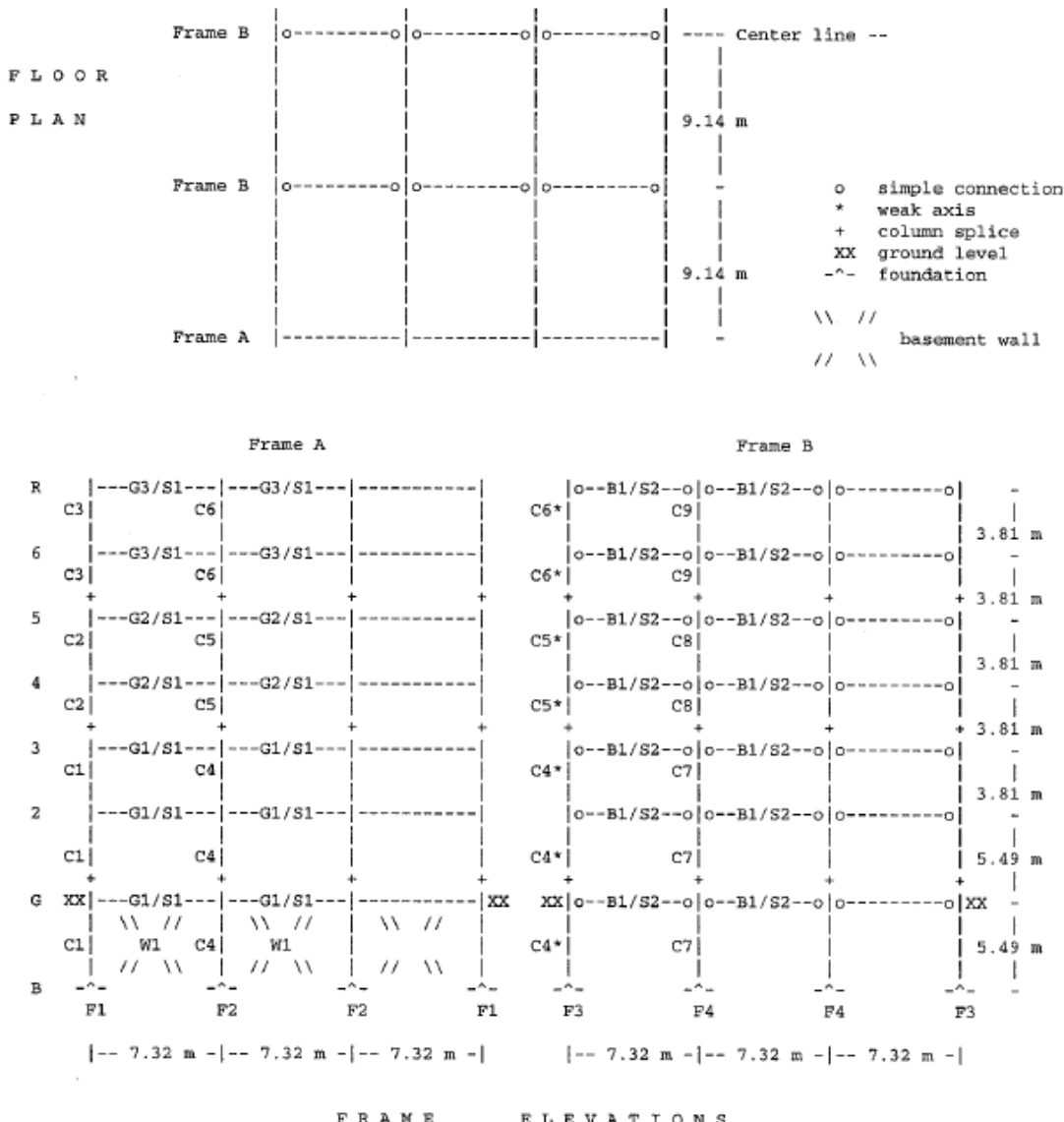
A.1 2D Steel Moment-resisting Frame Buildings

A.1.1 Building Designs

Three designs for steel moment-resisting frame buildings are used in this thesis. They are denoted with U6, U13, and U20, respectively. U represents that the design of the lateral force-resisting system conforms to 1994 Uniform Building Code (UBC) and the following number is the number of stories above ground for each building. U6 and U20 are designed by Hall (1997) and U13 is designed by the author. Figures A.1 to A.3 list the floor plan, frame elevation, and beam and column schedule of U6, U13, and U20. All three designs have five frames. The perimeter frames have moment-resisting joints, while the interior frames mostly have simply-supported joints.

For all buildings, the first floor height is 5.49m, and the height of each upper story is 3.81m. All three designs contain one story of basement, of the height 5.49m. Hence, the ground-to-roof height is 24.54m for U6 building, 51.21m for U13, and 77.88m for U20.

Designs are carried out for gravity plus wind (basic wind speed=113kph, urban exposure B) and gravity plus seismic loads (Zone 4, deep stiff soil, Type S₂).



(a) Floor plan and frame elevations

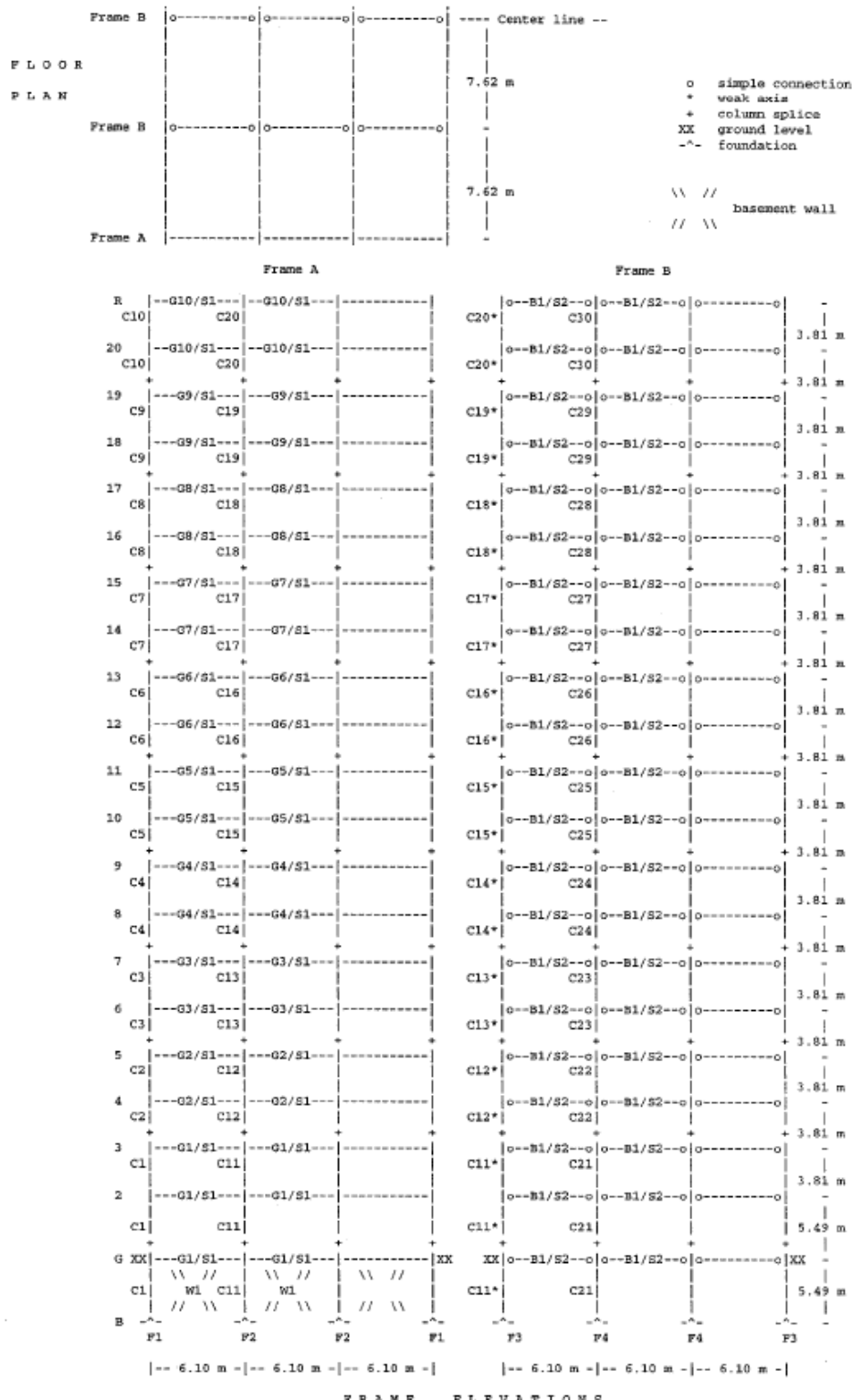
Columns													
C3	W14X99	C6	W24X84	C9	W14X74	C8	W14X74	C7	W14X132	.			
C2	W14X132	C5	W27X114	C8	W14X74	C7	W14X132	C7	W14X132	.			
C1	W14X159	C4	W27X161	C7	W14X132	C7	W14X132	C7	W14X132	.			
Girders													
G3	W24X55	B1	W24X55	F1	150-2.5	S1	1160-7.6	.					
G2	W24X76			F2	153-2.5	S2	2090-7.6	.					
G1	W24X94			F3	161-2.5			.					
			Walls	F4	247-2.5			.					
W1 61 cm thk													

foundations: $K_H - D_{YH}$ where K_H = horizontal stiffness (tons/cm)
 and D_{YH} = yield displacement for horizontal (cm).
 For vertical: $K_V = K_H$, $D_{VD} = D_{YH}$ (down) and
 $D_{VU} = D_{YH}/2$ (up).
 slabs: $A_{10} - h_{10}$ where A_{10} = effective area (cm^2) and h_{10} = dis-
 tance from top of girder/beam to centroid of slab (cm).

(b) Beam and column schedule

Figure A.1 6-story building (U6), designed according to the 1994 UBC seismic provisions.

Reproduced from Hall (1997).



(a) Floor plan and frame elevations

Columns							
C10	W14X109	C20	W21X122	C30	W14X74		
C9	W14X132	C19	W24X146	C29	W14X74		
C8	W14X159	C18	W24X146	C28	W14X82		
C7	W14X176	C17	W24X162	C27	W14X109		
C6	W14X211	C16	W24X176	C26	W14X132		
C5	W14X257	C15	W24X176	C25	W14X159		
C4	W14X283	C14	W27X178	C24	W14X193		
C3	W14X311	C13	W27X178	C23	W14X211		
C2	W14X342	C12	W27X178	C22	W14X233		
C1	W14X370	C11	W30X191	C21	W14X283		

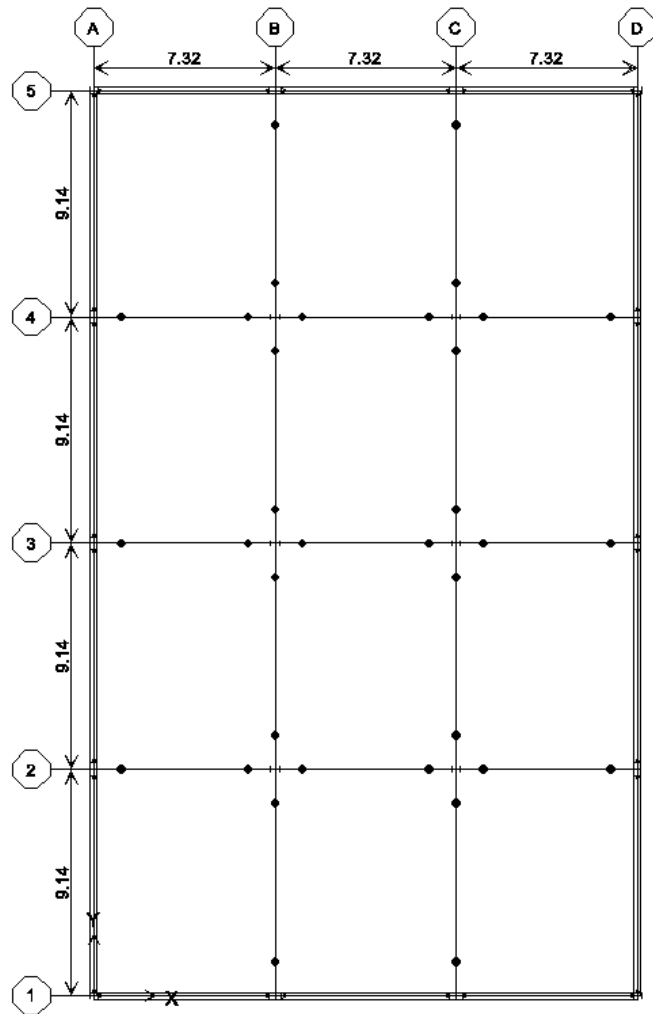
Girders	Beams	Foundations	Slabs
G10 W27X84	B1 W21X50	F1 468-2.5	S1 1160-7.6
G9 W27X94		F2 336-2.5	S2 2090-7.6
G8 W30X99		F3 353-2.5	
G7 W30X108	Walls	F4 534-2.5	
G6 W30X116			
G5 W30X116	W1 61 cm thk		
G4 W30X116			
G3 W30X116			
G2 W30X116			
G1 W30X116			

foundations: $K_H \cdot D_{YH}$ where K_H = horizontal stiffness (tons/cm)
 and D_{YH} = yield displacement for horizontal (cm).
 For vertical: $K_V = K_H$, $D_{VD} = D_{YH}$ (down) and
 $D_{VU} = D_{YH}/2$ (up).
 slabs: $A_{10} \cdot h_{10}$ where A_{10} = effective area (cm^2) and h_{10} = dis-
 tance from top of girder/beam to centroid of slab (cm).

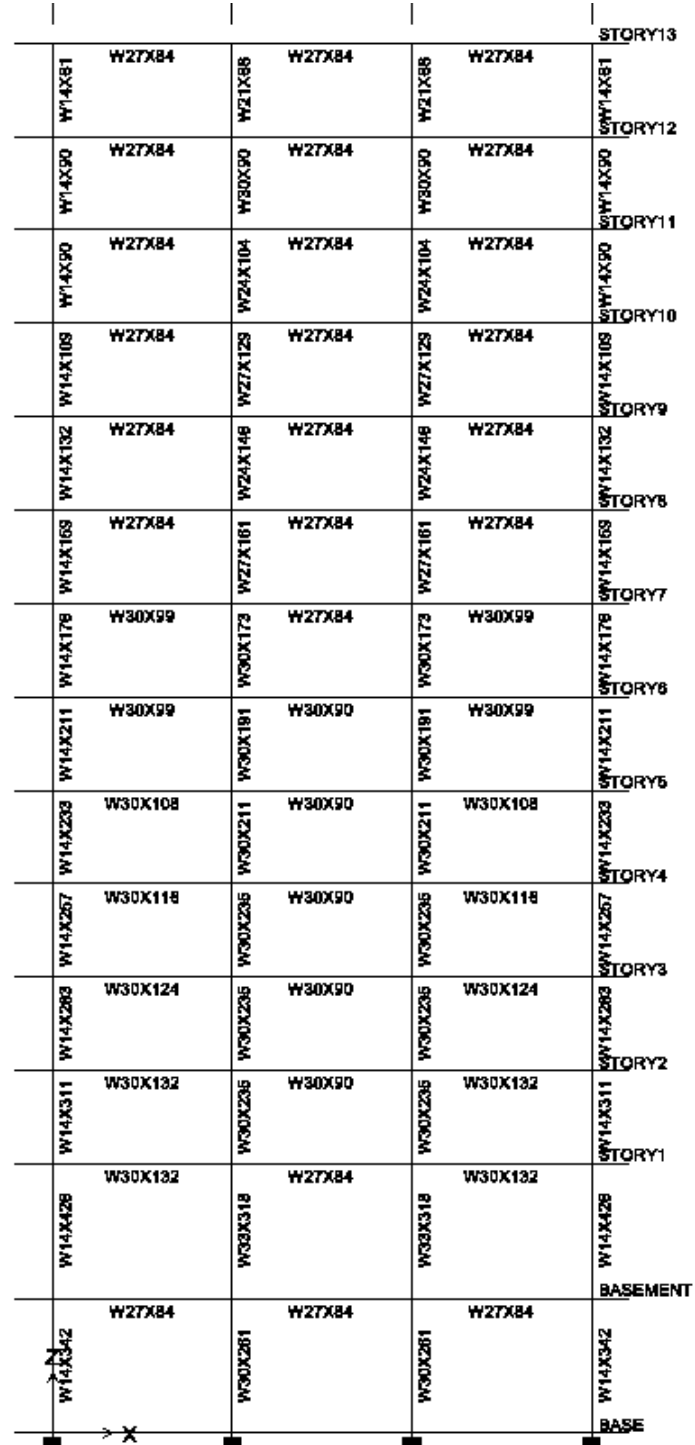
(b) Beam and column schedule

Figure A.2 20-story building (U20), designed according to the 1994 UBC seismic provisions.

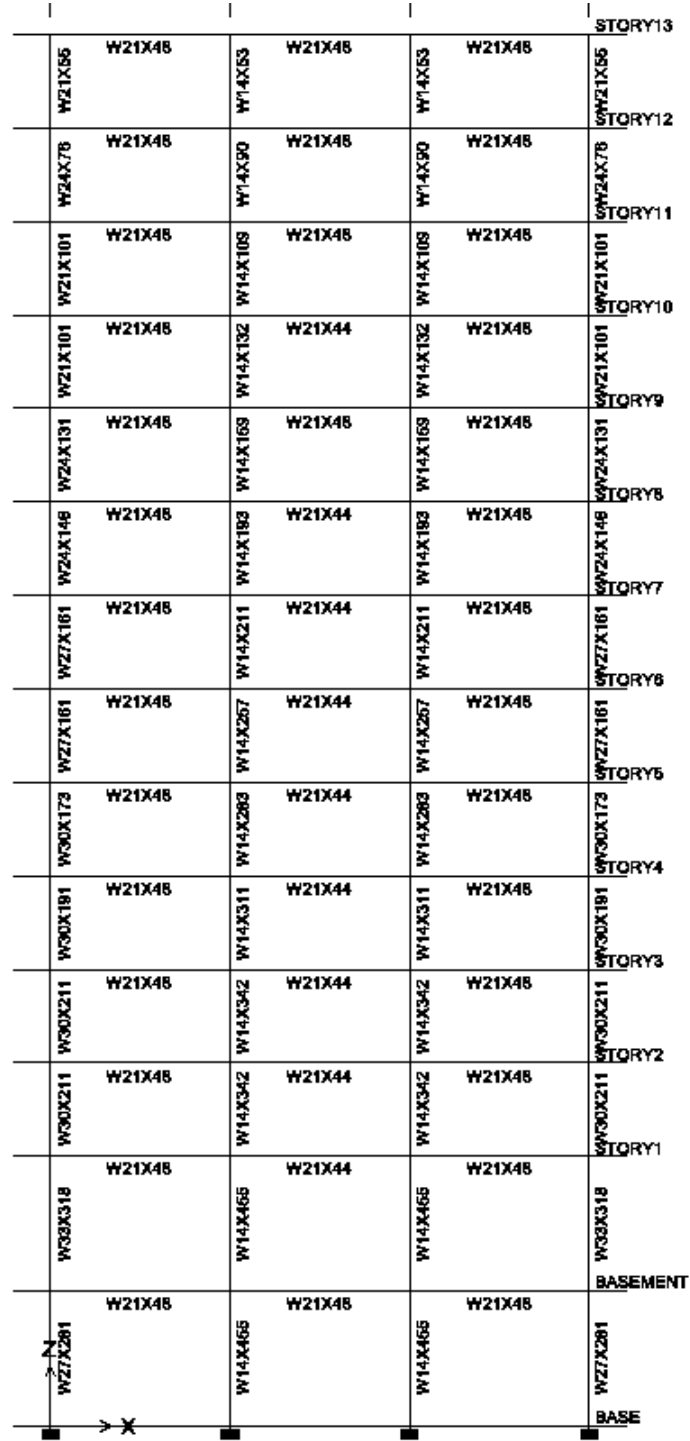
Reproduced from Hall (1997).



(a) Floor plan.



(b) Frame elevation, Grid 1.



(c) Frame elevation, Grid 2.

Figure A.3 13-story building (U13), designed according to the 1994 UBC seismic provisions.

A.1.2 Finite Element Models

We used finite element models of each building design, detailed in Hall (1997), as well as the computer program Frame-2d, which is specifically designed to calculate the response of steel, moment-frame, and braced-frame buildings to large ground motions. Challa and Hall (1994), Hall and Challa (1995), and Hall (1998) validate the special features of Frame-2d, such as joint modeling, nodal updating, and weld fracture, by extensive numerical testing and comparison with experimental data.

Although Hall takes advantage of the buildings' symmetry by modeling only half of each building, all three-bay, moment-resisting, or gravity frames are explicitly modeled to the same level of detail. Interior gravity frames contribute realistically to each building's stiffness and strength. The bending strength at a simple beam-to-column connection is modeled by connecting only the web fibers to the joint. The models also fully account for geometric non-linearities (that is, moment amplification and P- Δ): each member has geometric stiffness, and the Frame-2d program updates the positions of end-member nodes. Structure-foundation interaction is modeled with horizontal and vertical springs at the base of each column. The stress-strain relationship of the springs is bilinear and hysteretic; see Hall (1997) for specifications of the springs. We do not, however, expect that this interaction contributes significantly to the behavior of the frame models (Tall Buildings Initiative Guidelines Working Group, 2010, Section 5.3).

Figure A.4 shows pushover curves for modified finite element models of the six buildings following the procedure described in Hall (1997). We modified the masses assigned to the horizontal degrees of freedom such that the total mass is the seismic design mass and is distributed in proportion to the seismic design loads. Then we applied a horizontal ground acceleration that increases linearly at a rate of 0.3 g per minute and calculated the frame model's response dynamically. Since the ground acceleration increases slowly, we could use a dynamic analysis procedure to replicate a series of static calculations, with the applied lateral forces at each time step proportional to the seismic design forces. As seen in Figure A.4, this approach introduces dynamic vibrations in the frame models when the stiffness changes at yielding and especially at weld fracture. This method of pushover analysis allows us to model the strength-degrading part of the curve.

The finite element models use the fiber method to capture the behavior of beams and columns. The length of each beam or column is subdivided into eight segments, and the cross-section of each

segment is divided into eight fibers representing the steel, wide-flange beam or column and, for each beam, two additional fibers representing the concrete slab and metal deck. Each fiber has a hysteretic, axial stress-strain relationship, including a yield plateau and strain hardening, and each segment has a linear shear stress-strain relation. The end segments of the beams and columns are short to capture the spread of yielding at plastic hinge zones. The yield strength of steel is higher than the nominal value. Hall and Challa (1995) compared models of steel members using the plastic hinge method or the fiber method to experimental test data. The model using the fiber method (also employed in this study) showed excellent agreement with the experimental results.

The weld fracture model is based on the failures observed after the 1994 Northridge Earthquake. In general, these welds proved to be brittle, fracturing prior to local flange buckling. Beam-to-column, column splice, and column baseplate welds are represented by sets of fibers at each weld location. The model randomly assigns an axial fracture strain to each weld according to a user-defined distribution. If the developed tensile strain of a weld fiber exceeds the fracture strain, then the fiber no longer resists tension. For frame models with fracture-prone welds, the distribution of axial fracture strain, ε_f , normalized by the yield strain, ε_y , throughout all welds in the building is as follows: for beam top-flange welds, column splices, and welds at column baseplates, 40% have $\varepsilon_f / \varepsilon_y = 1$, 30% have $\varepsilon_f / \varepsilon_y = 10$, and 30% have $\varepsilon_f / \varepsilon_y = 100$; and for beam bottom-flange welds, 20% have $\varepsilon_f / \varepsilon_y = 0.7$, 40% have $\varepsilon_f / \varepsilon_y = 1$, 20% have $\varepsilon_f / \varepsilon_y = 10$, 10% have $\varepsilon_f / \varepsilon_y = 50$, and 10% have $\varepsilon_f / \varepsilon_y = 100$. (Again, these distributions are denoted B.) Hall (1998, Sections 2.4-2.5) defined a different set of fracture strains (denoted F) and found agreement between the model simulations and observations of weld fractures in the Northridge Earthquake. Olsen (2008, Section 2.7.3) compared frame model responses assuming the B and F distributions. For the same ground motion, the B distribution resulted in frame models less likely to “collapse” than models with the F distribution, and when the frames did not “collapse,” frames with the B distribution tended to have smaller IDRs than those with the F distribution. Thus, the fracture strain distributions used in this paper are less “bad” than those Hall (1998) used to compare with observations of weld fracture in the Northridge Earthquake.

Although weld fibers are allowed to fail in tension, welded connections maintain residual bending strength through several mechanisms. First, our distribution of axial fracture strains assumes that beam bottom-flange welds are more susceptible to fracture, consistent with observations after the Northridge Earthquake. Thus, in many simulations with weld fractures, only the fibers representing

the bottom-flange weld fail, leaving the other fibers intact. Second, a fractured fiber is allowed to resist compression if the fracture gap closes. Third, the nodal positions of the beam segments are updated during the simulation, which accounts for axial compression in the beam resulting from flange fracture. This prevents some drop in the bending moment due to the higher force in the flange carrying compression. Finally, fibers representing the shear tab cannot fracture.

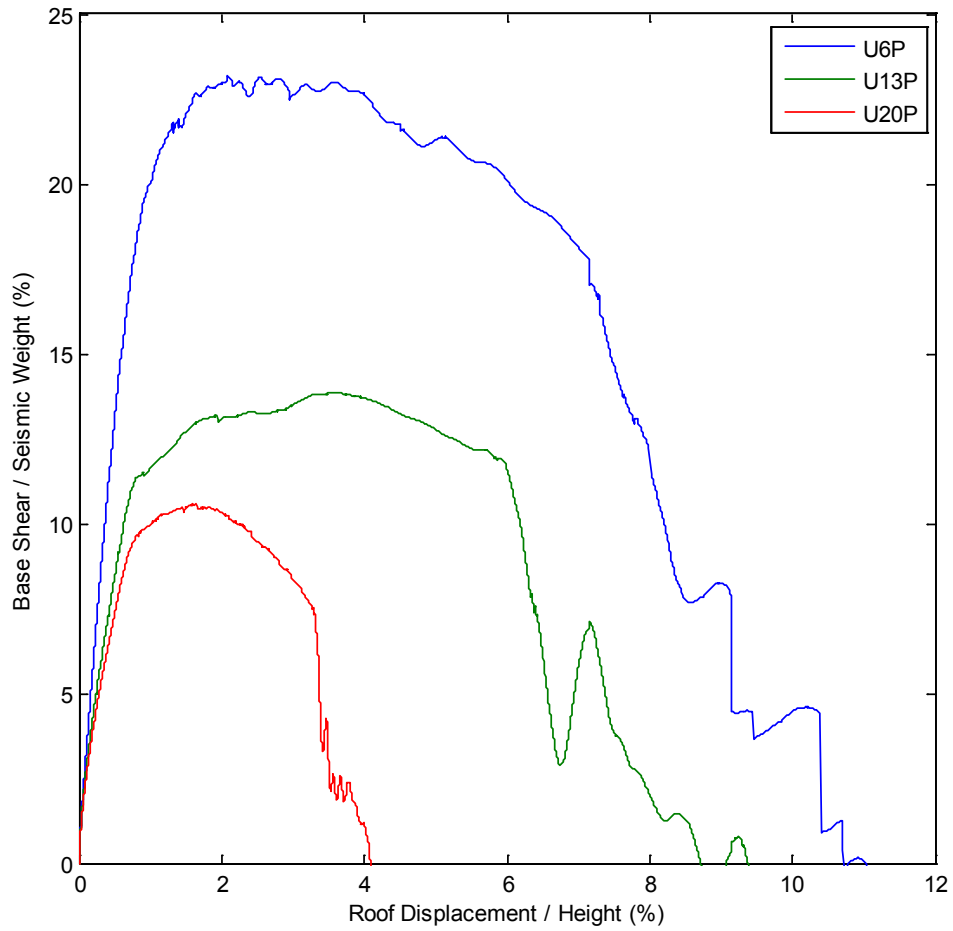
Special elements model the behaviors of panel zones and basement concrete walls. A panel zone is represented by an element with a nonlinear and hysteretic relationship between moment and shear strain, calibrated with test data (Challa, 1992). Also, the panel-zone element has the capability to model doubler plates by increasing the thickness of the panel zone. The panel zone element occupies a properly dimensioned finite space within the column and connects to beam elements on their edges. Thus, the beams have clear-span dimensions. For basement stories, a plane stress element represents the stiffness of concrete walls.

Table A.1 Information of the building models

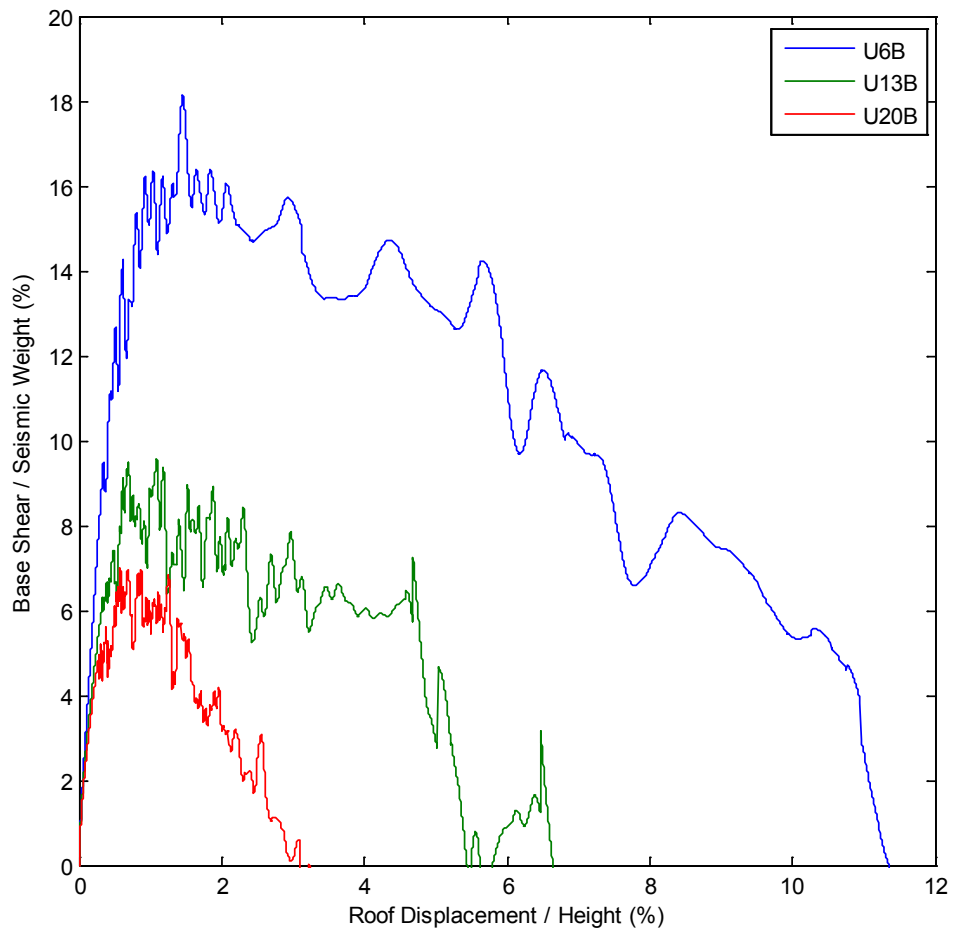
Building	No. of Stories	Material	T ₁ (s)*	Max Strength **	ductility	Welds
U6P	6	Steel	1.54	0.2319	6.67	Perfect
U6B	6	Steel	1.54	0.1629	7.50	Brittle
U13P	13	Steel	2.63	0.1387	8.00	Perfect
U13B	13	Steel	2.63	0.0844	6.86	Brittle
U20P	20	Steel	3.47	0.1060	4.25	Perfect
U20B	20	Steel	3.47	0.0630	4.50	Brittle

*- Fundamental period

** - The maximum base shear in pushover analysis, normalized by seismic weight of the building



(a) Buildings with sound welds



(b) Buildings with brittle welds

Figure A.4 Pushover curves of steel moment-resisting frame buildings

A.2 2D RC Moment-resisting Frame Buildings

A.2.1 Structural Designs

All of the 2D RC moment-resisting frame buildings are designed by Haselton et al. (2006, 2011). They designed 30 building archetypes which encompass key structural design parameters, including building heights from 1 to 20 stories, space and parameter frame systems, and bay widths of 20 and 30 ft (6.1 and 9.1m). Each archetype is designed according to the provisions of the International Building code [International Code Council (ICC) 2003], ASCE 7-02 (ASCE 2002), and ACI 318 (ACI 2002), including requirements for strength, stiffness, capacity design, and detailing. The designs were reviewed by a practicing engineering (J. Hooper, June 15, 2006) to ensure they conform to typical design practice.

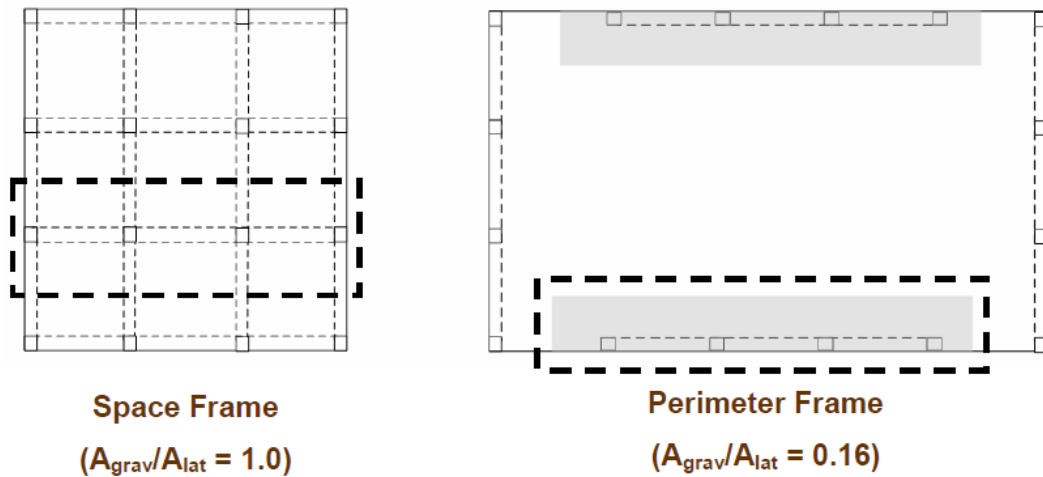


Figure A.5 Illustration of the gravity/lateral tributary areas for a space frame and a perimeter frame building. Reproduced from Haselton (2006).

Table A.2 Summary of design information of 30 RC MRF buildings. Reproduced from Haselton (2011).

A.2.2 Finite element models

The analysis model for each building is a two-dimensional three-nay nonlinear frame model in OpenSEES (OpenSEES 2009), as illustrated in Figure A.6.

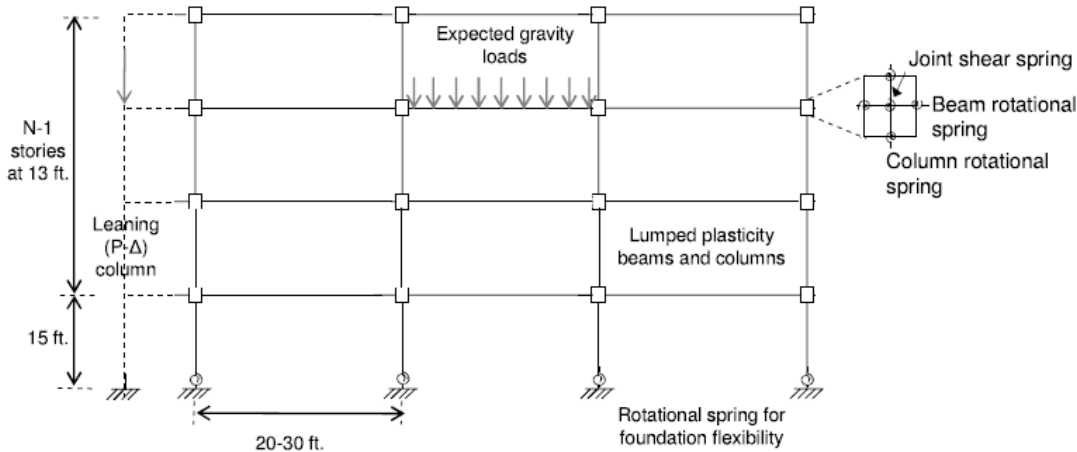
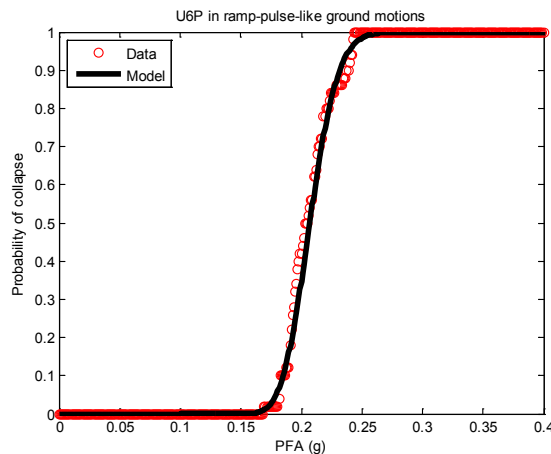


Figure A.6 Schematic of RC frame structural analysis model. Reproduced from Haselton (2006).

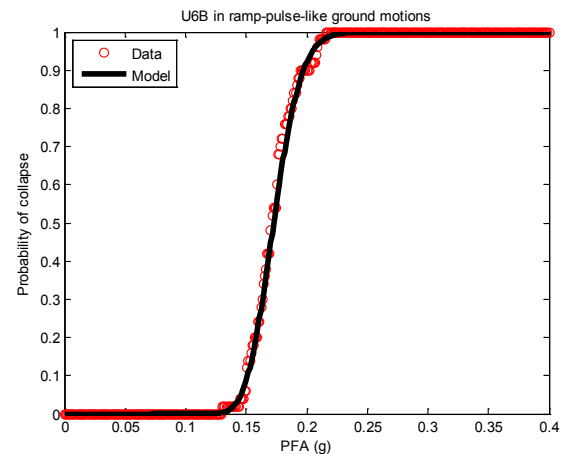
$P-\Delta$ effects are accounted for by applying gravity loads on a leaning column in the analysis model. Rayleigh damping corresponding to 5% of critical damping in the first and third modes is applied. Element modeling consists of lumped plasticity beam-column elements and finite joint shear panel springs. The nonlinear hinge model with degrading strength and stiffness is developed by Ibarra et al. (2005). All the designs and analysis models are downloadable from Haselton's website <http://myweb.csuchico.edu/~chaselton/>.

A.3 Fragility Curves of Steel and RC Frame Buildings

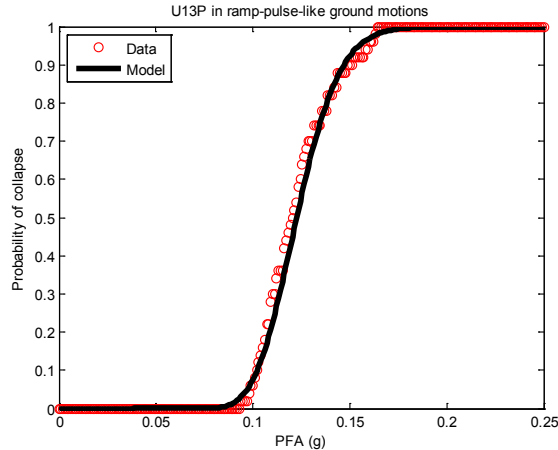
The collapse fragility curves of all 10 buildings described in Chapter 3 are shown in Figure A.7



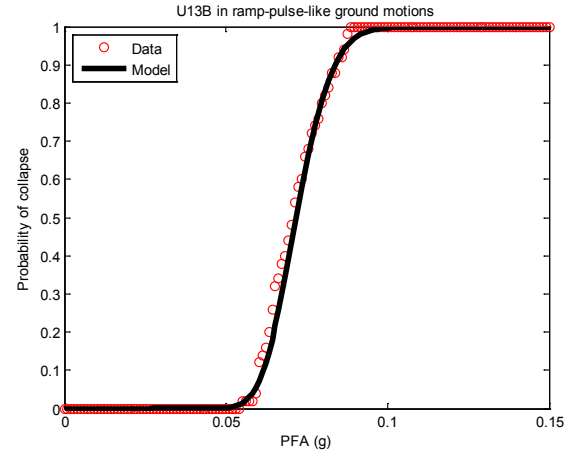
(1) U6P in ramp-pulse-like ground motions



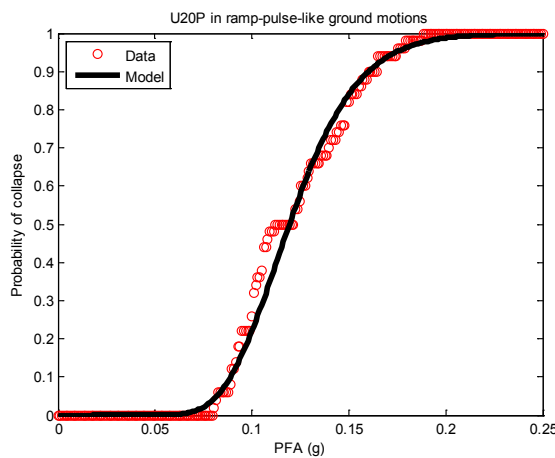
(2) U6B in ramp-pulse-like ground motions



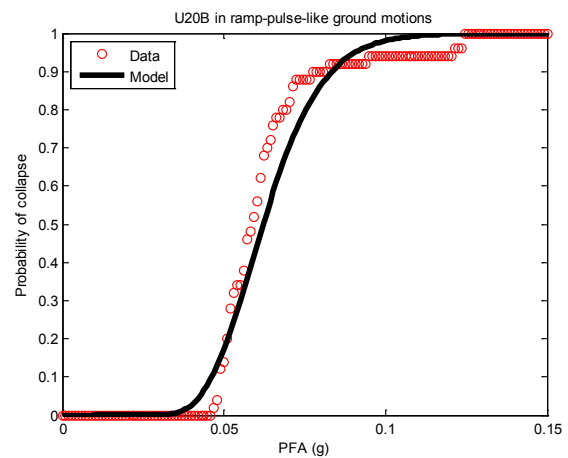
(3) U13P in ramp-pulse-like ground motions



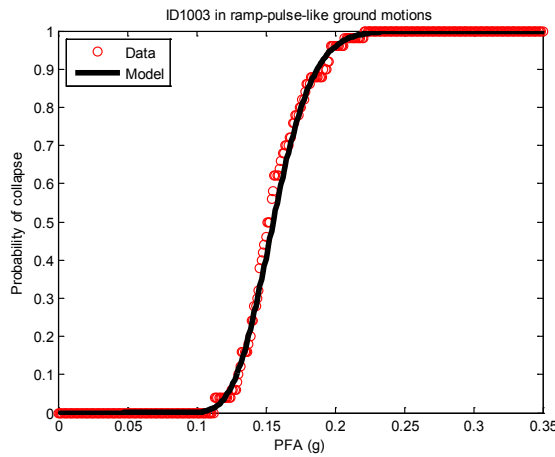
(4) U13B in ramp-pulse-like ground motions



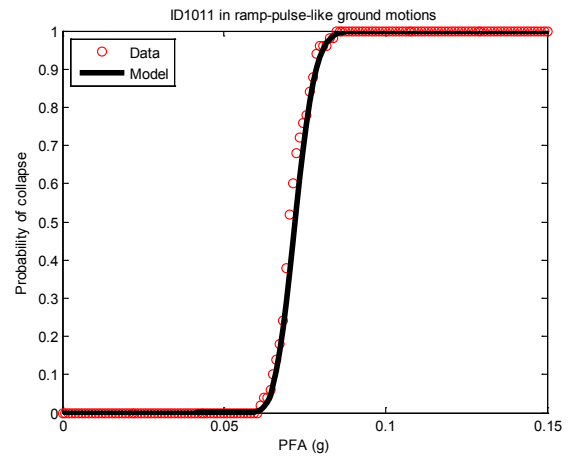
(5) U20P in ramp-pulse-like ground motions



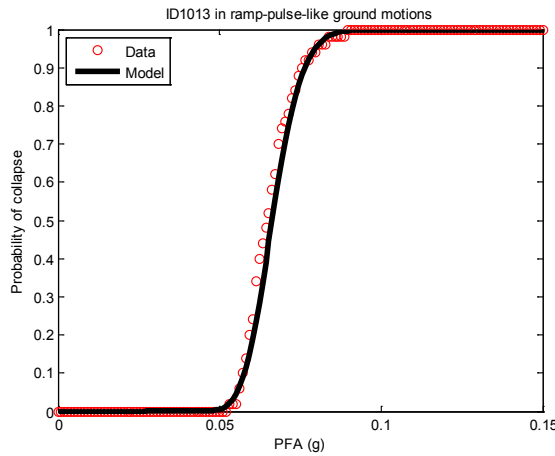
(6) U20B in ramp-pulse-like ground motions



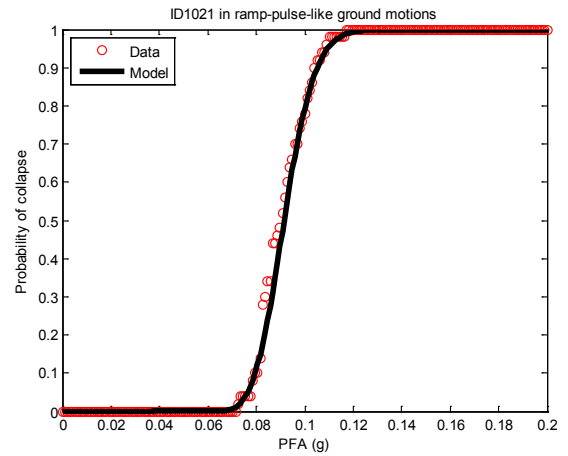
(7) ID1003 in ramp-pulse-like ground motions



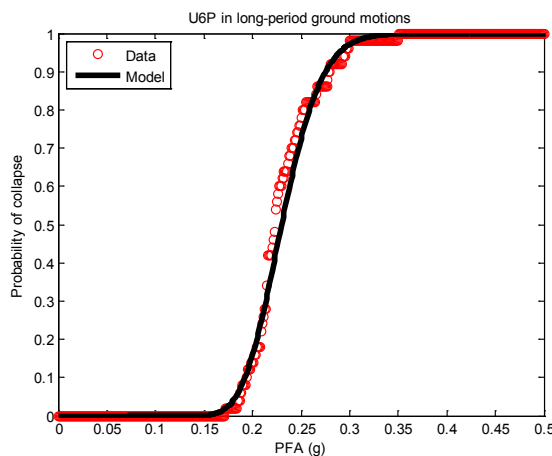
(8) ID1011 in ramp-pulse-like ground motions



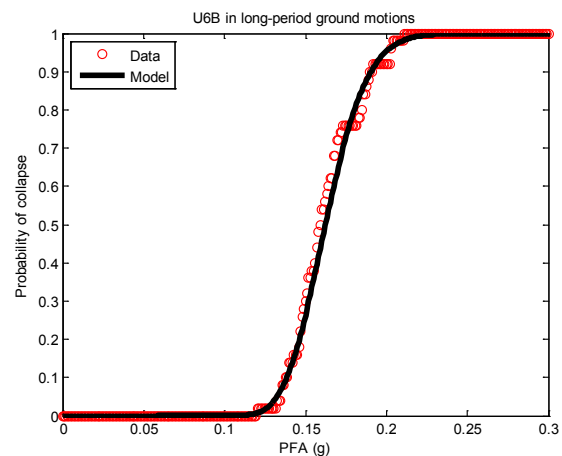
(9) ID1013 in ramp-pulse-like ground motions



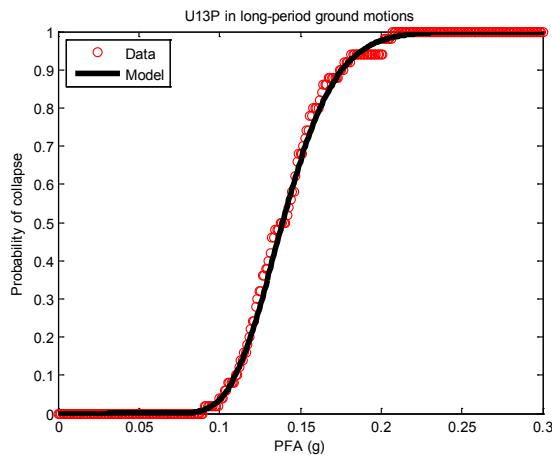
(10) ID1021 in ramp-pulse-like ground motions



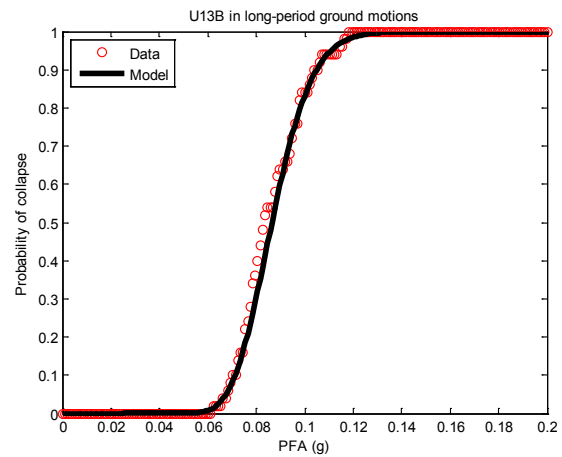
(11) U6P in long-period ground motions



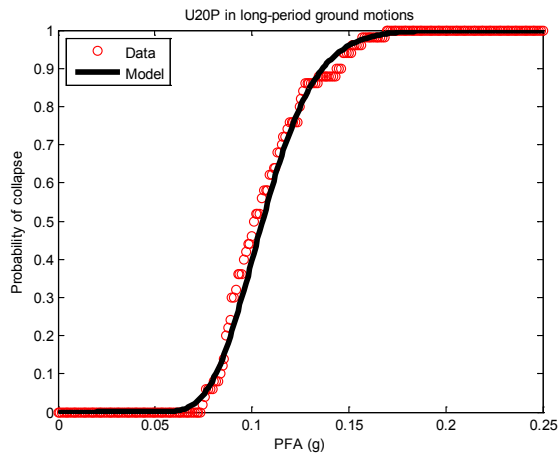
(12) U6B in long-period ground motions



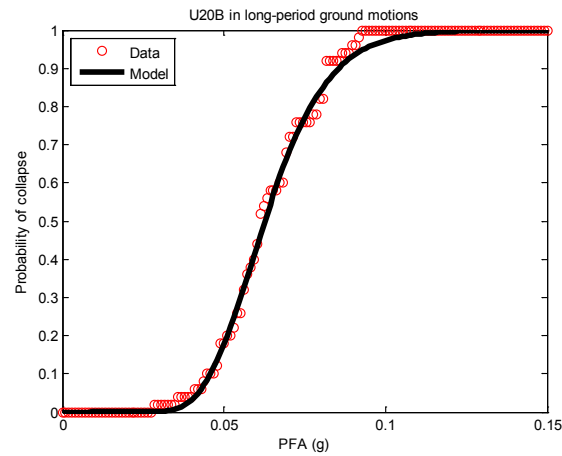
(13) U13P in long-period ground motions



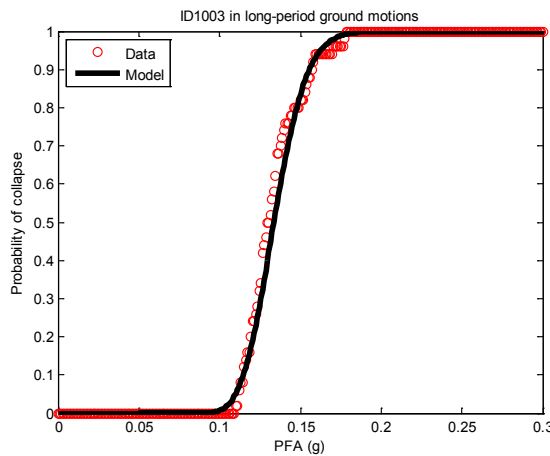
(14) U13B in long-period ground motions



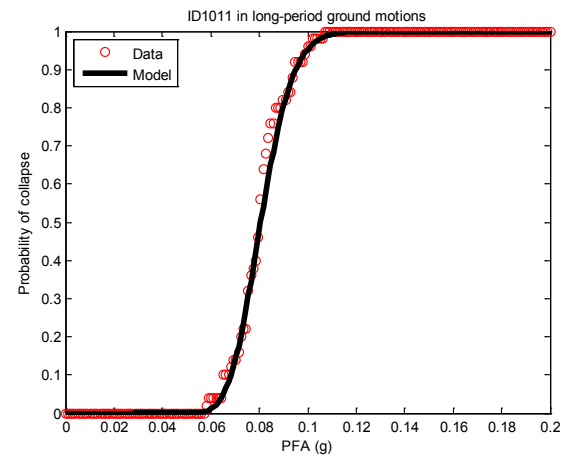
(15) U20P in long-period ground motions



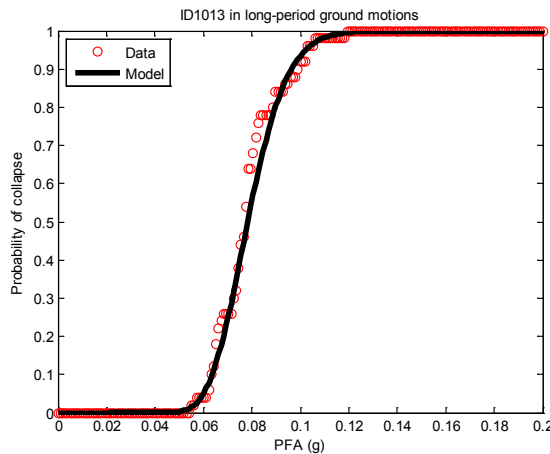
(16) U20B in long-period ground motions



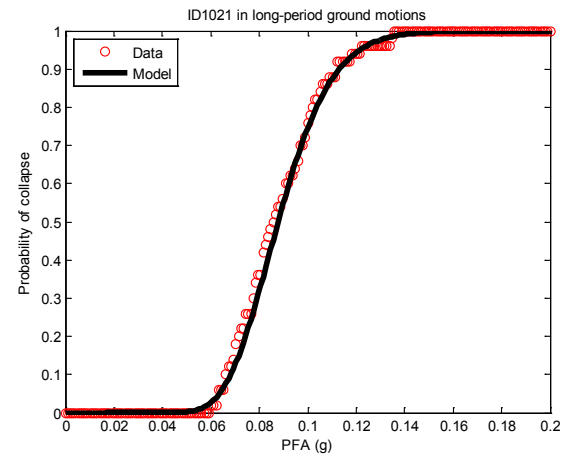
(17) ID1003 in long-period ground motions



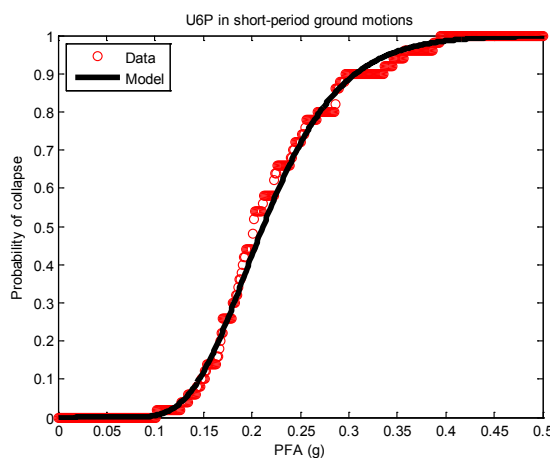
(18) ID1011 in long-period ground motions



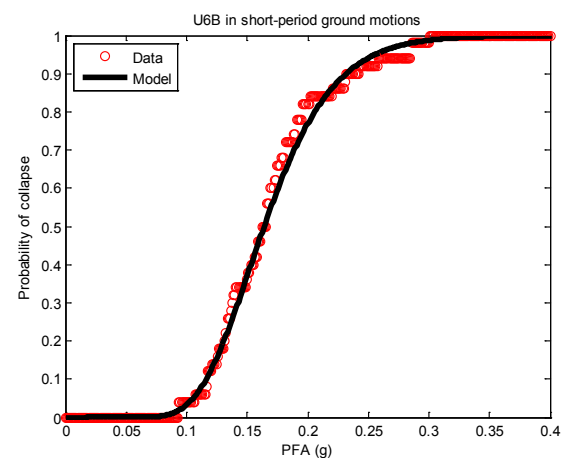
(19) ID1013 in long-period ground motions



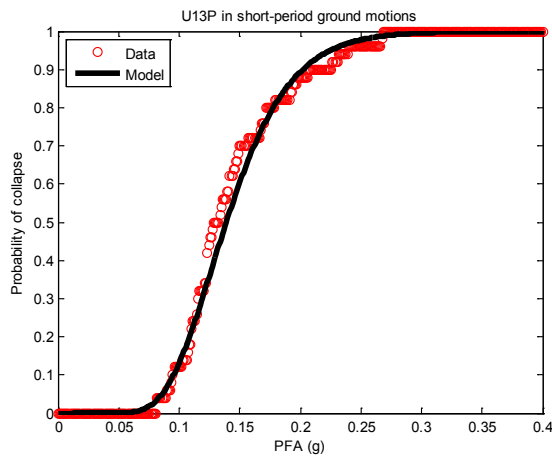
(20) ID1021 in long-period ground motions



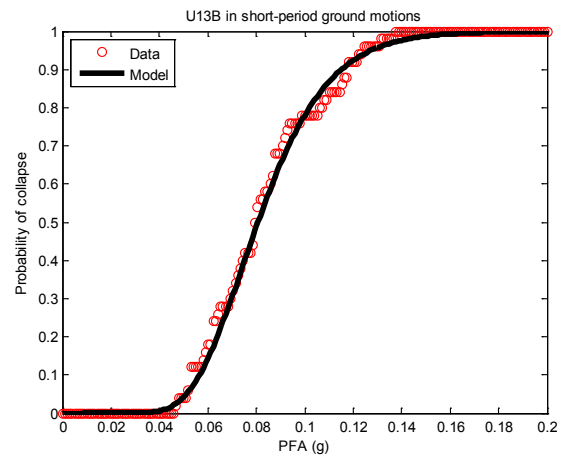
(21) U6P in short-period ground motions



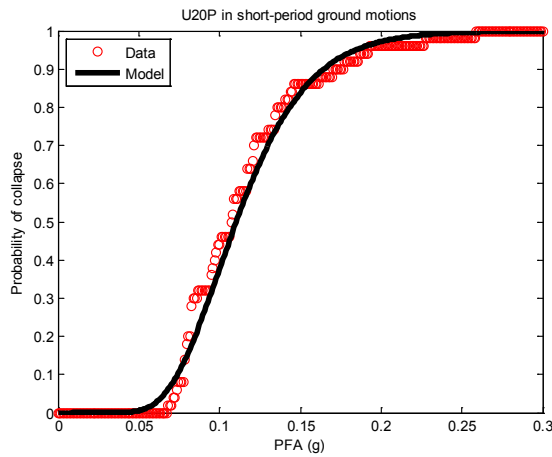
(22) U6P in short-period ground motions



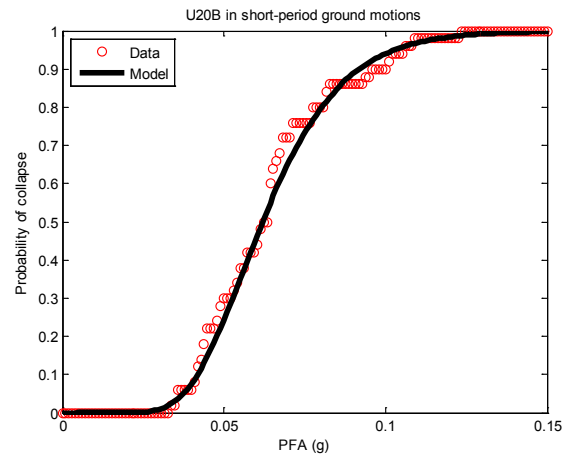
(23) U13P in short-period ground motions



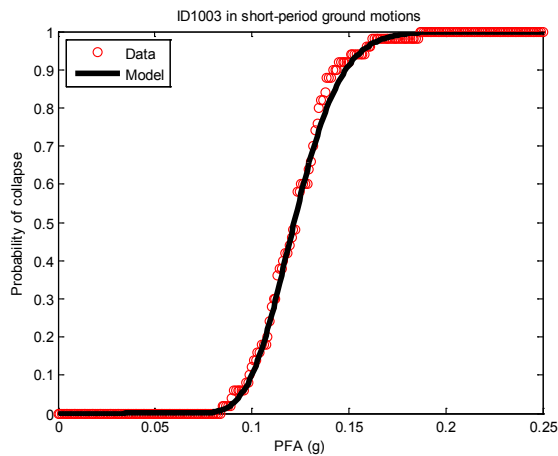
(24) U13B in short-period ground motions



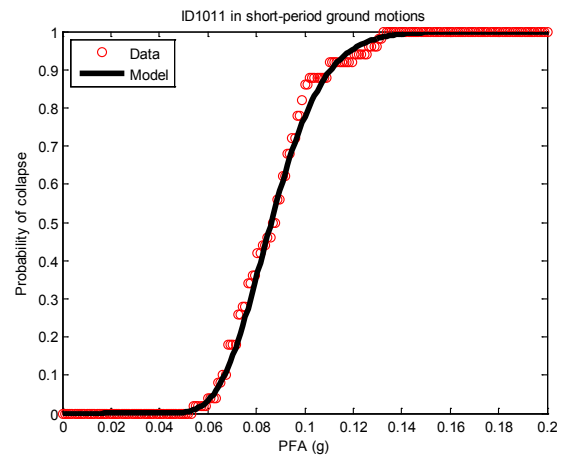
(25) U20P in short-period ground motions



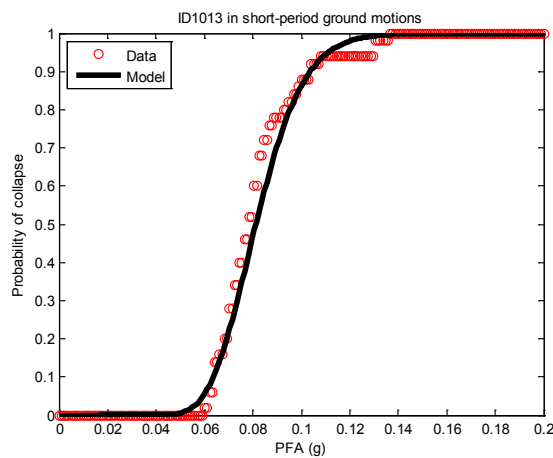
(26) U20B in short-period ground motions



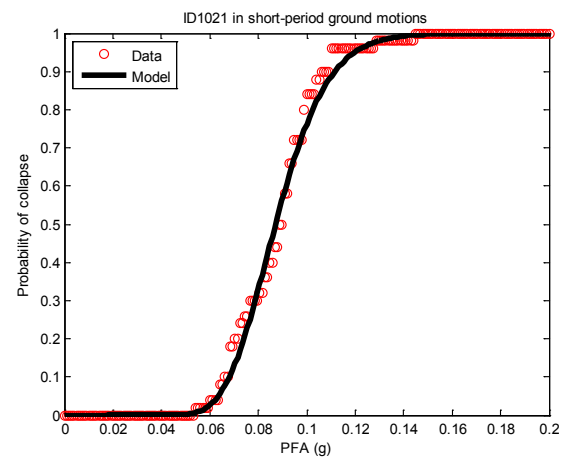
(27) ID1003 in short-period ground motions



(28) ID1011 in short-period ground motions



(29) ID1013 in short-period ground motions



(30) ID1021 in short-period ground motions

Figure A.7 Fragility curves of steel and RC frame buildings

A.3 2D RC Shear Wall Buildings

A.3.1 Design Parameters

To make a better comparison between moment-resisting frame buildings and shear wall buildings, for shear wall building design, we use exactly the same floor plan as used in frame building design (see Figure A.8). The designed shear wall building is denoted with U6SW. The load and material used in the design are listed in Table A.3 and A.4.

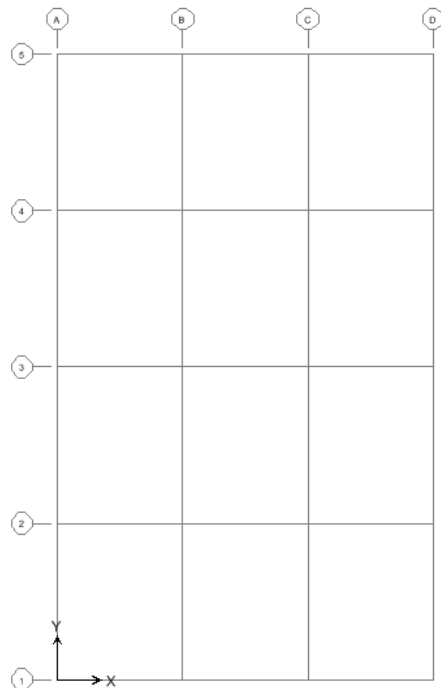


Figure A.8 Floor plan of building U6SW

Table A.3 Design load for building U6SW

Dead load	Roof	0.391 tons/m ²
	Floor	0.464 tons/m ²
Live load	Floor	0.244 tons/m ²

Table A.4 Material properties for building U6SW

Concrete	4 ksi
Steel	Grade 60

A.3.2 Design Result

In order to study the behavior of shear wall buildings and avoid including the interaction between shear walls and moment-resisting frames, we use only shear walls to resist seismic load. The shear walls are placed between axis A and B, C and D at each bay (see Figure A.9 and A.10). The thickness of the shear wall is set to be 15cm from the second to sixth floor and 25 cm for the first floor. The design is carried out according to the 1997 Uniform Building Code for gravity and seismic load using ETABS. The resultant building has a fundamental period of 0.3930s.

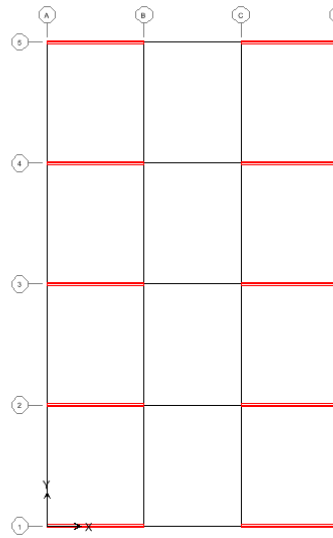


Figure A.9 Floor plan of building U6SW

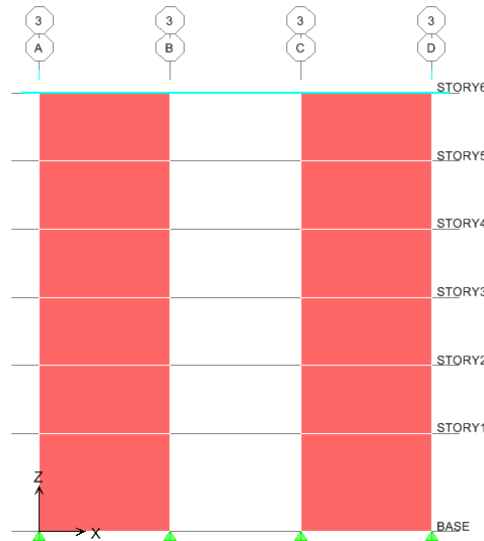


Figure A.10 Elevation View of building U6SW

The result of reinforcement is listed in Table A.5. The result is identical for every shear wall in the same story.

Table A.5 Design reinforcement ratio (%) and placement of rebars

Story		Reinforcement ratio (%)	Rebar placement
6	Top	0.25	#3@0.4
	Bottom	0.25	
5	Top	0.25	#3@0.4
	Bottom	0.25	
4	Top	0.25	#3@0.4
	Bottom	0.25	
3	Top	0.25	#4@0.4
	Bottom	0.47	
2	Top	0.39	#5@0.3
	Bottom	0.90	
1	Top	0.36	#5@0.2
	Bottom	0.77	

A.3.3 Finite Element Model

The building was modeled in SAP2000. For simplicity, only the walls in Grid-③ are modeled, and the deformation of the model is restricted in 2D space.

Shear walls are modeled with multi-layered shell element. This type of element is based on the principles of composite material mechanics and is capable of simulating coupled in-plane/out-of-plane bending, as well as in-plane direct shear and coupled bending-shear behavior of RC shear walls. For this building model, the multi-layer shell element is divided into five layers with different material properties. The rebars are smeared into the second and fourth layer, as shown in Figure A.11. The multi-layer shell elements are constructed using the build-in shear wall modeling toolbox in SAP2000 V14.

Since it was found that the shear walls of U6SW building fail mainly at the bottom part, only the shear walls at the first floor are meshed into small elements to reduce computational effort (see Figure A.12).

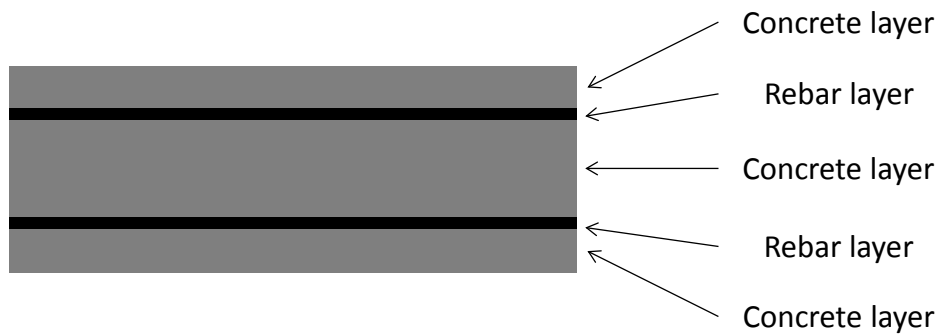


Figure A.11 Layers of shell element in building U6SW

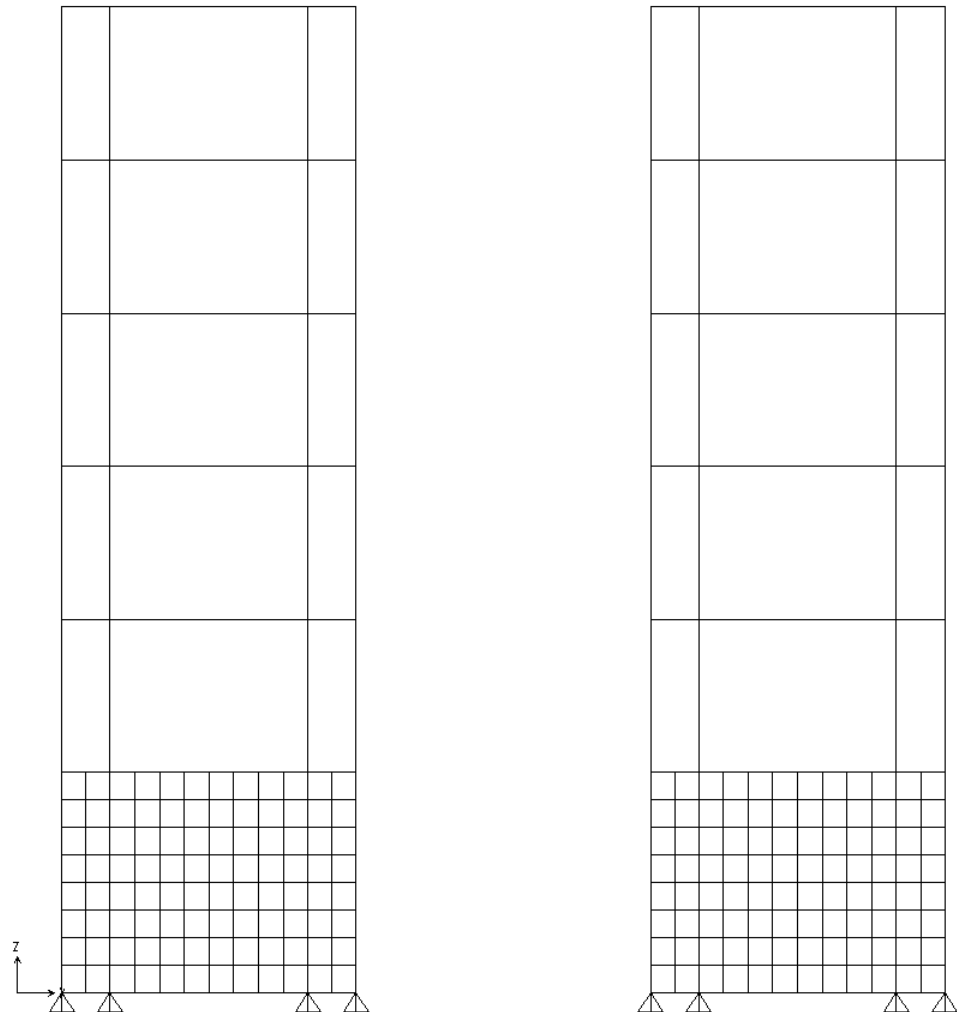


Figure A.12 Mesh of building U6SW

A.3.4 Pushover Result

The pushover curve is plotted in Figure A.13. Triangular lateral force distribution is used in the pushover analysis.

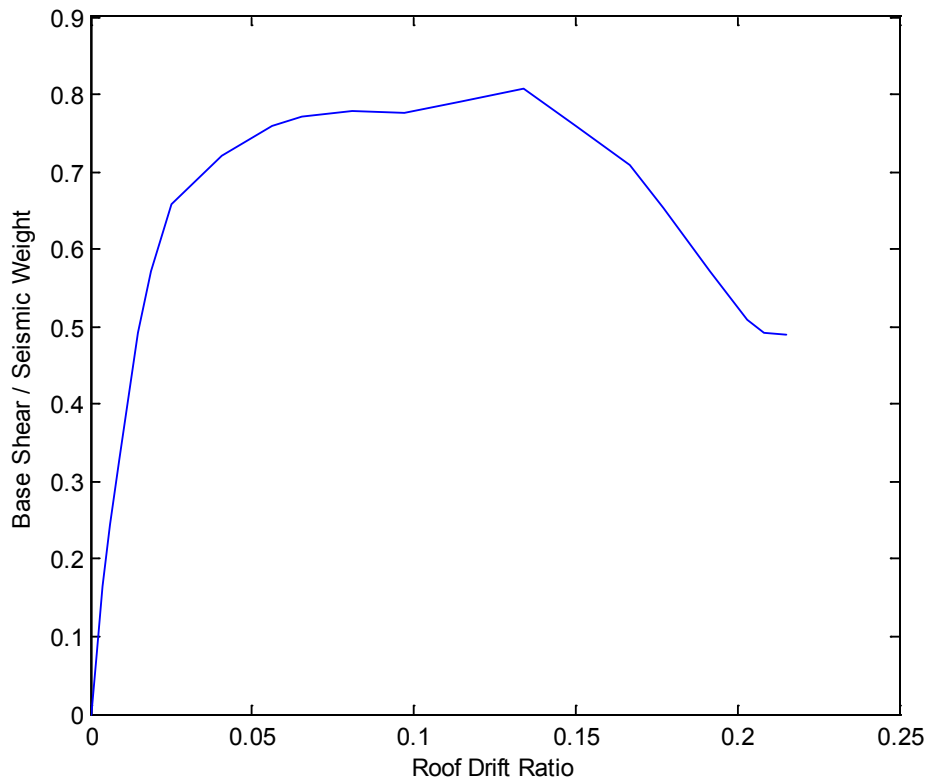


Figure A.13 Pushover curve of building U6SW

A.4 3D Steel Moment-resisting Frame Buildings

Three steel moment-resisting frame buildings are studied using 3D finite-element models in this thesis. They are denoted with B1, B2, and B3, respectively. All three buildings are designed by Krishnan (2006; 2007) according to UBC 97 (1997), assumed to be located in Seismic Zone 4 at a distance of 5km from a Type A fault. The soil at the site is assumed to be of Type S_b per the UBC97 soil classification. ASTM-A572, Grade 50 is used for the beams and columns in all the three buildings. It is assumed that the nominal yield stress is 344.85 MPa (50ksi) and the nominal ultimate stress is 448.31 MPa (65ksi).

All three buildings are modeled as 3D finite-element models using Frame3D (Krishnan, 2003) and analyzed in the Virtual Shaker platform (virtualshaker.caltech.edu). Frame3D is the extended version of Frame2D and Krishnan (2003) showed that both versions give the same results for a specialized two-dimensional problem. Similar to Frame2D models, in Frame3D, moment-frames beams and columns are modeled using fiber elements, beam-column joints using panel zone elements, and floor slabs using elastic plane stress elements.

A.4.1 Building B1

Building B1 is a redesigned version of an existing 18-story building. The building is a modern 18-story welded steel moment-frame building located within five miles of the epicenter of the 1994 Northridge earthquake. It was designed in 1984 according to the lateral force requirements of the 1982 Uniform Building Code (ICBO, 1982). It has 17 office stories above ground and a mechanical penthouse on top (see Figure A.14). The height of the building above ground is 75.7m, with a typical story height of 3.96m and taller 1st, 17th, and penthouse stories. The redesigned version has a greater number of bays of moment frames in each direction due to the higher requirements of UBC 97 (ICBO, 1997).

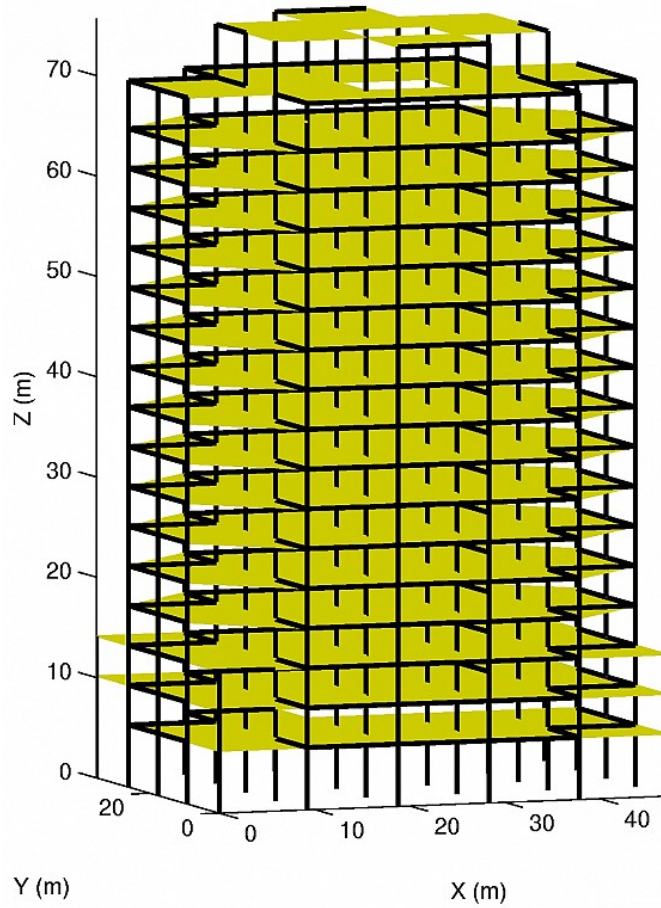


Figure A.14 Isometric view of building B1

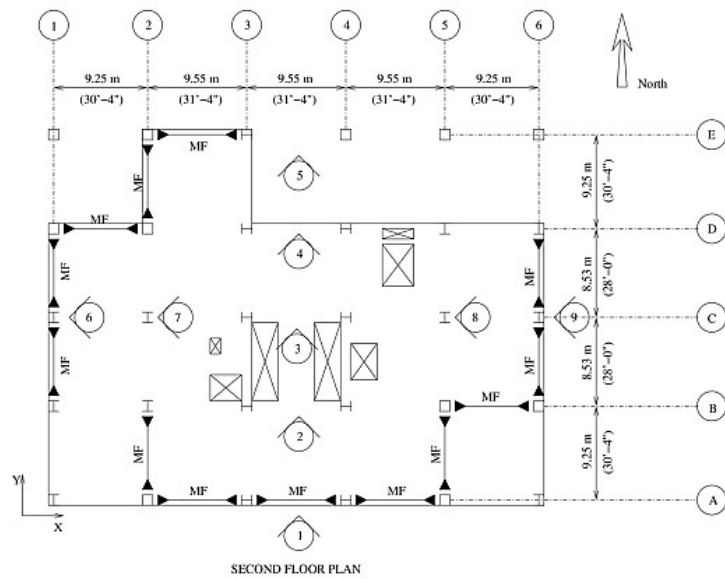


Figure A.15 Second floor plan of building B1

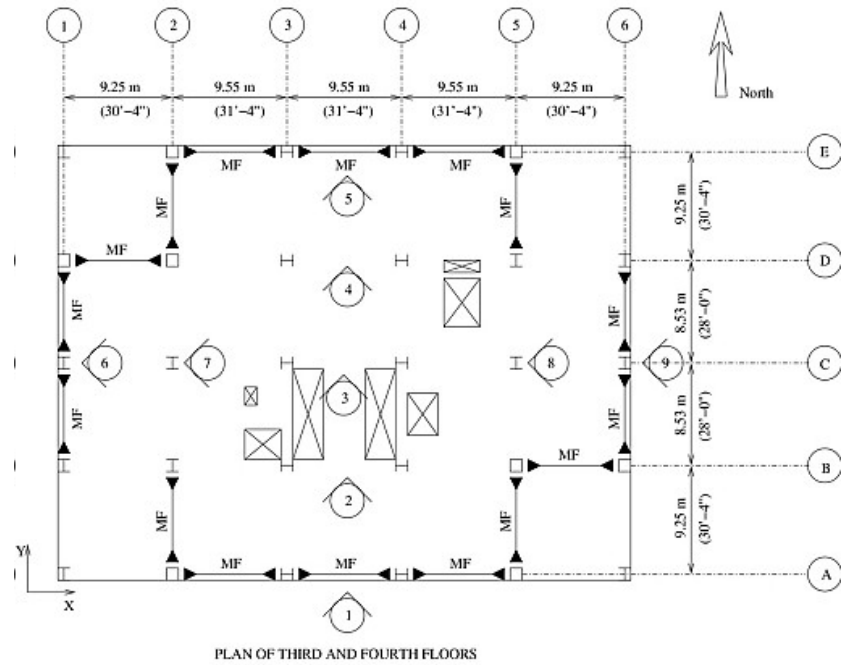


Figure A.16 Plan of third and fourth floors of building B1

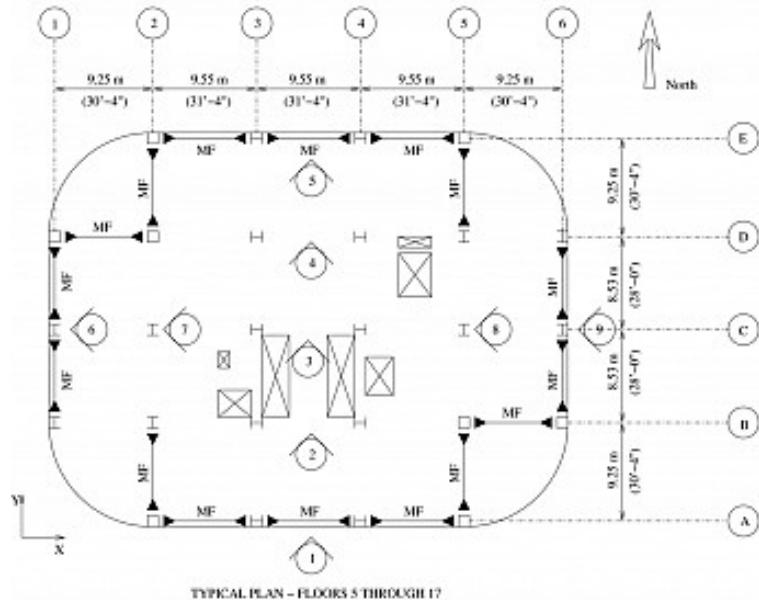


Figure A.17 Typical floor plan – floor 5 through 17 of building B1

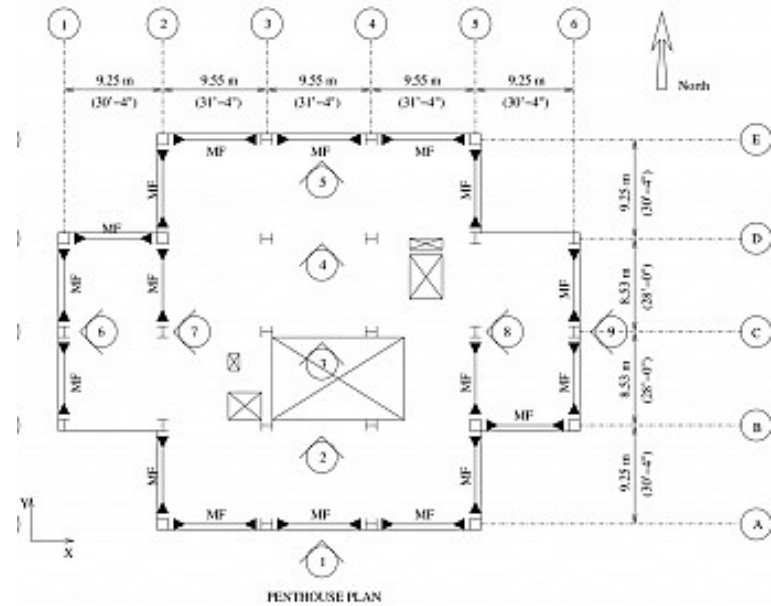


Figure A.18 Penthouse plan of building B1

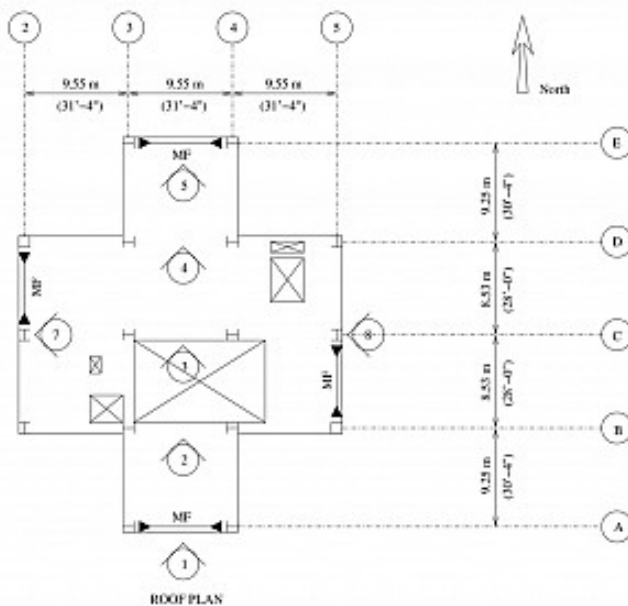


Figure A.19 Roof plan of building B1

A.4.2 Building B2

Building B2 is L-shaped in plan (Figure A.20) with one elevator core serving both wings of the building. The height of the building above ground is 78.3m with a typical story height of 4m.

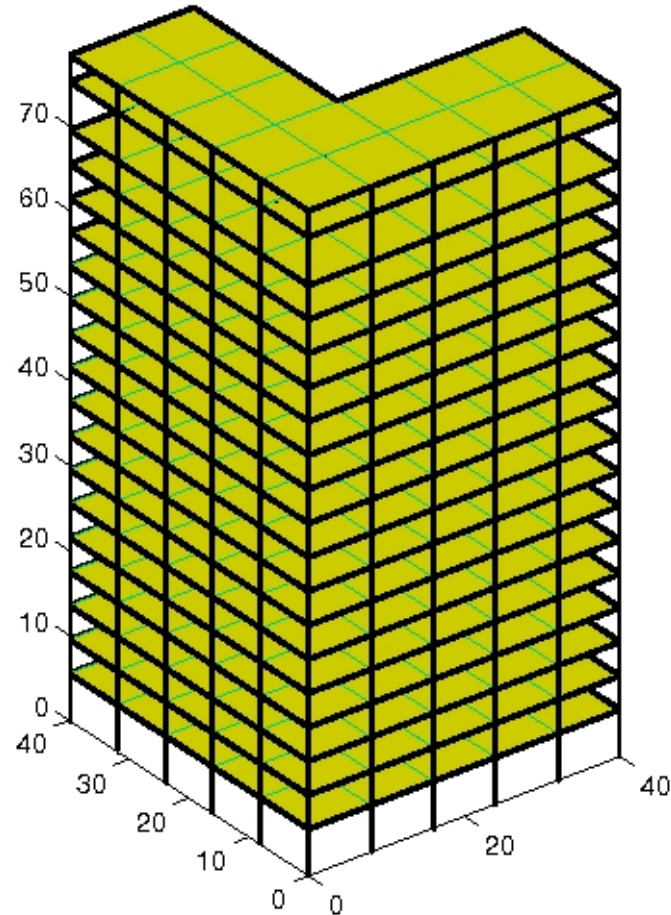


Figure A.20 Isometric view of building B2

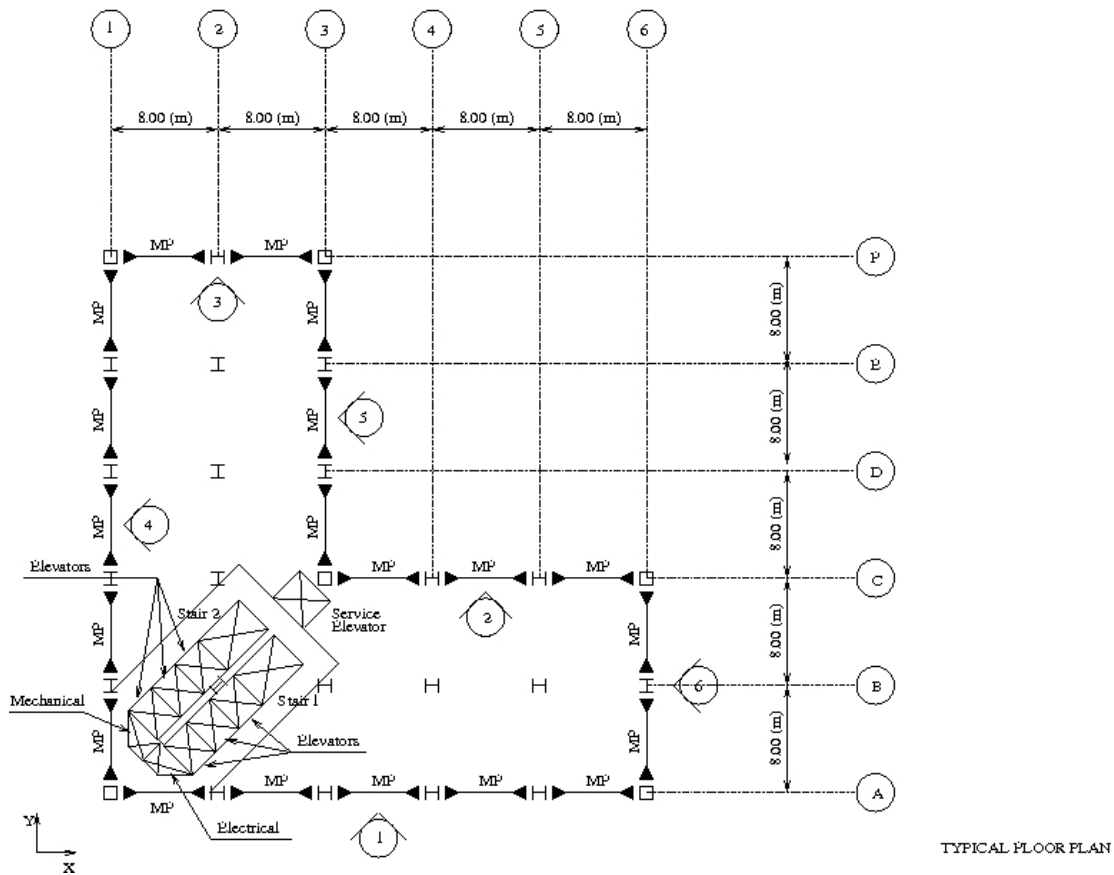


Figure A.21 Typical floor plan of building B2

A.4.3 Building B3

Building B3 is rectangular-shaped in plan (Figure A.22) with the elevators and stairs located along one face of the building in order to achieve a better ocean view. The height of the building above ground is 78.3m with a typical story height of 4m.

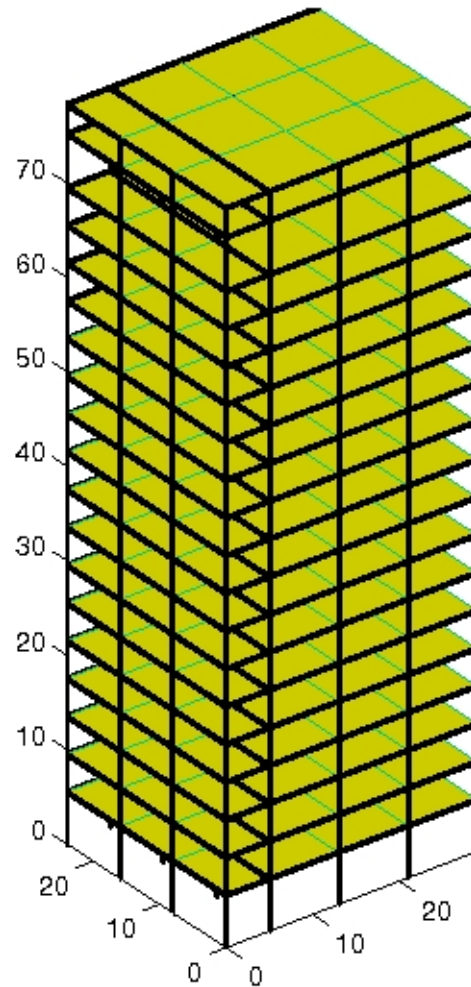


Figure A.22 Isometric view of building B3

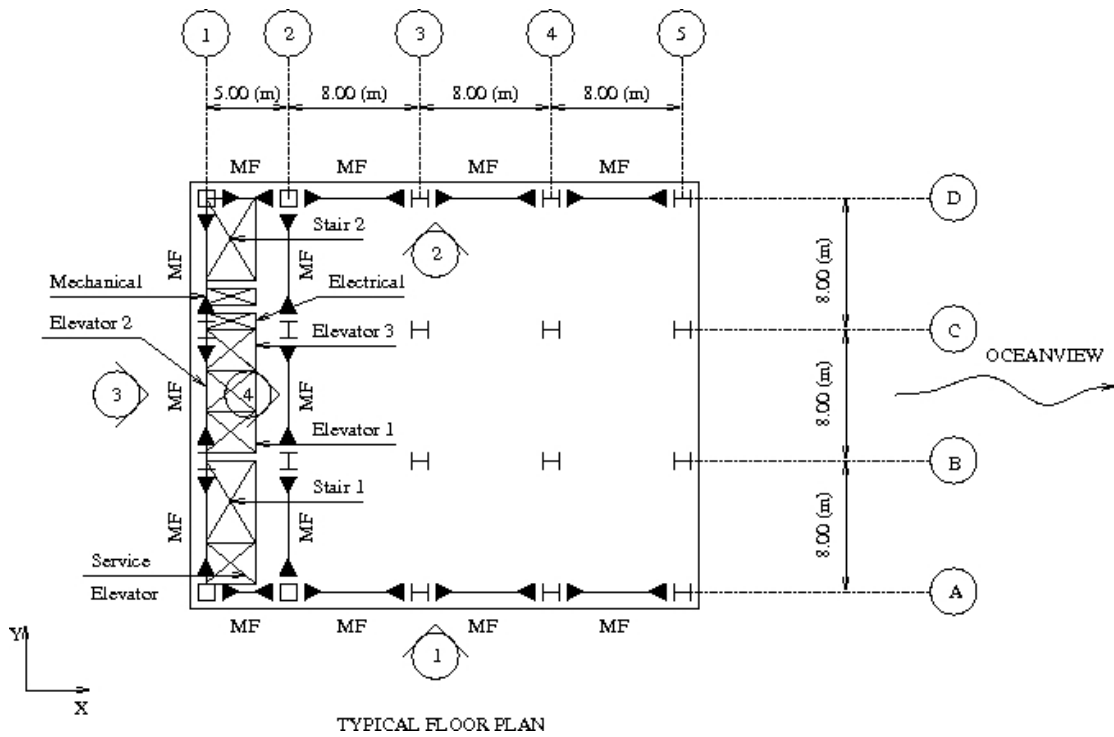


Figure A.23 Typical floor plan of building B3

APPENDIX B: GROUND MOTIONS USED IN THIS THESIS

There are 150 ground motion records used in this thesis. They are divided into three groups: ramp-pulse-like ground motions, long-period ground motions, and short-period ground motions. Ramp-pulse-like ground motions are selected from a study by Graves and Somerville (2006). Long-period and short-period ground motions are selected from the 1999 M7.6 Chi-Chi earthquake. The detail information of all the ground motion records is listed in Table B.1, Table B.2, and Table B.3

Table B.1 Information of ramp-and-pulse-like ground motion set

No.	Scenario	Station	Direction	PGA (cm/s ²)	PGV (cm/s)	PGD (cm)	S _a (1s) (cm/s ²)	S _a (2s) (cm/s ²)	S _a (3s) (cm/s ²)
1	1	s0081	NS	833.64	124.28	154.65	1009.07	561.05	503.46
2	1	s0082	NS	887.26	130.17	147.83	1787.42	756.27	508.19
3	1	s0083	NS	591.50	113.56	118.77	1517.06	479.83	385.56
4	1	s0084	NS	630.36	102.18	94.48	1279.69	442.92	288.79
5	1	s0093	NS	698.54	129.19	146.73	722.91	760.08	532.41
6	1	s0094	NS	751.96	200.35	163.36	1943.13	1240.19	713.10
7	1	s0095	NS	873.85	192.75	139.67	2204.12	962.48	613.29
8	1	s0096	NS	883.10	112.83	106.26	1648.18	499.92	439.33
9	1	s0097	NS	766.54	98.85	99.48	1282.60	574.21	419.89
10	1	s0098	NS	910.95	105.46	90.23	1029.07	609.92	394.32

11	1	s0106	NS	765.52	228.43	177.13	1584.89	1496.63	851.07
12	1	s0107	NS	705.96	183.23	143.05	1355.37	1083.98	691.97
13	1	s0225	EW	1438.45	349.95	255.40	3180.39	2718.99	1313.33
14	1	s0239	EW	1295.80	308.08	234.81	2642.23	2154.52	1213.43
15	2	s0081	NS	994.28	177.41	171.22	906.22	945.95	622.45
16	2	s0082	NS	846.35	171.66	157.17	1606.00	1036.56	636.21
17	2	s0083	NS	879.40	165.62	136.02	1948.48	1136.14	610.45
18	2	s0084	NS	968.96	189.69	126.05	2445.91	1248.32	641.77
19	2	s0094	NS	812.92	187.50	170.92	1157.56	1242.92	792.62
20	2	s0095	NS	1070.72	256.55	157.14	2221.77	1674.17	829.44
21	2	s0096	NS	1369.32	231.17	133.99	2808.33	1438.72	785.09
22	2	s0106	NS	1107.47	247.97	188.20	1740.70	1696.12	947.96
23	2	s0107	NS	1011.22	228.20	141.39	1217.82	1443.96	851.30
24	3	s0083	NS	818.24	175.81	159.56	1494.43	1277.99	679.16
25	3	s0084	NS	622.48	155.47	137.60	1168.77	1068.16	586.07
26	3	s0094	NS	928.95	212.12	183.49	1764.77	1497.73	794.05
27	3	s0095	NS	954.53	204.02	175.72	1859.40	1523.03	789.67
28	3	s0096	NS	697.32	158.89	137.94	1045.33	1115.95	618.90
29	3	s0097	NS	488.47	92.04	93.73	610.32	677.29	403.56
30	4	s0081	NS	684.04	152.00	155.82	771.88	732.92	534.51

31	4	s0082	NS	823.64	153.39	149.65	1179.26	1010.34	594.75
32	4	s0083	NS	483.03	109.83	103.67	816.14	714.34	381.67
33	4	s0093	NS	579.60	122.26	134.06	819.67	616.76	450.14
34	4	s0094	NS	627.40	149.94	143.01	894.94	1048.05	639.35
35	4	s0095	NS	581.49	138.93	111.16	1053.18	764.90	527.95
36	4	s0106	NS	813.84	140.36	138.08	896.60	907.94	606.81
37	4	s0107	NS	584.88	102.41	104.83	723.39	617.58	453.89
38	5	s0068	NS	1095.73	251.81	208.38	2050.68	1982.91	973.30
39	5	s0070	NS	838.75	217.75	155.33	1943.21	1641.06	734.29
40	5	s0071	NS	650.67	153.61	114.93	1164.03	999.35	522.57
41	5	s0081	NS	1016.09	245.51	209.38	1617.37	1796.87	939.70
42	5	s0082	NS	1220.03	235.12	196.13	1730.09	2023.30	965.49
43	5	s0083	NS	912.48	194.50	152.02	1571.70	1563.84	730.06
44	5	s0084	NS	896.51	154.07	114.06	1005.67	1192.13	570.62
45	5	s0093	NS	962.20	242.08	202.33	1239.62	1725.87	909.38
46	5	s0094	NS	1229.04	242.53	207.08	1554.58	2110.18	1028.36
47	5	s0095	NS	1099.86	257.77	179.14	2185.74	1978.07	952.01
48	5	s0096	NS	789.04	204.23	142.01	1606.90	1458.84	804.46
49	5	s0106	NS	1452.22	279.26	220.84	2097.64	2223.81	1082.35
50	5	s0107	NS	1263.68	312.11	202.45	2652.63	2147.65	1073.86

Table B.2 Information of long-period ground motion set

No.	Sequence No.	Station	Direction	PGA (cm/s ²)	PGV (cm/s)	PGD (cm)	S _a (1s) (cm/s ²)	S _a (2s) (cm/s ²)	S _a (3s) (cm/s ²)
1	1180	CHY002	EW	114.90	45.74	45.39	286.41	267.37	259.85
2	1180	CHY002	NS	143.95	52.83	59.78	330.77	178.28	133.93
3	1189	CHY017	EW	51.60	14.86	13.00	138.46	99.32	89.29
4	1189	CHY017	NS	54.83	18.60	15.48	165.08	138.92	103.38
5	1195	CHY026	EW	74.61	46.18	35.21	219.14	224.04	296.49
6	1195	CHY026	NS	64.22	32.61	26.96	188.68	179.16	163.41
7	1199	CHY032	EW	86.71	26.38	17.73	251.47	356.17	182.52
8	1199	CHY032	NS	76.52	19.34	18.99	250.04	156.10	94.99
9	1216	CHY059	EW	48.29	11.94	12.92	116.30	144.41	128.99
10	1216	CHY059	NS	48.44	19.08	14.26	154.86	139.60	104.03
11	1228	CHY076	EW	70.60	23.99	20.36	187.07	103.32	98.37
12	1228	CHY076	NS	71.33	15.74	16.96	192.77	84.66	106.90
13	1233	CHY082	EW	65.77	20.92	20.69	120.82	95.59	119.53
14	1233	CHY082	NS	61.37	24.65	25.77	94.48	74.84	86.97
15	1238	CHY092	EW	109.06	54.73	37.24	329.51	278.39	335.10
16	1238	CHY092	NS	80.64	34.39	30.52	294.62	235.29	211.76
17	1239	CHY093	EW	52.73	17.61	13.73	96.89	65.12	85.69

18	1239	CHY093	NS	68.85	14.11	12.78	180.92	54.26	48.44
19	1240	CHY094	EW	66.78	24.30	19.52	134.99	115.90	109.42
20	1240	CHY094	NS	53.00	18.90	19.75	110.81	164.44	114.46
21	1246	CHY104	EW	158.63	52.54	36.12	368.22	441.56	251.21
22	1246	CHY104	NS	182.95	55.17	47.20	377.43	476.28	297.11
23	1356	KAU010	EW	32.92	11.26	9.14	84.85	127.04	35.88
24	1356	KAU010	NS	33.80	16.60	14.68	130.39	62.46	109.08
25	1390	KAU075	EW	27.90	9.43	6.55	94.97	71.31	47.22
26	1390	KAU075	NS	38.92	11.64	8.03	138.28	114.41	70.38
27	1397	KAU086	EW	40.64	9.88	11.33	108.24	127.05	47.62
28	1397	KAU086	NS	44.32	16.39	17.99	152.19	102.73	148.41
29	1398	KAU087	EW	26.07	10.02	11.96	124.37	96.57	88.93
30	1398	KAU087	NS	31.10	13.02	8.43	162.14	92.47	85.82
31	1537	TCU111	EW	132.83	57.79	55.20	515.21	261.91	309.48
32	1537	TCU111	NS	97.29	35.54	31.28	235.54	139.09	250.43
33	1538	TCU112	EW	81.12	41.32	30.04	289.30	207.14	211.24
34	1538	TCU112	NS	71.59	33.39	37.41	195.31	228.10	194.18
35	1539	TCU113	EW	68.16	27.84	22.20	116.04	185.08	103.62
36	1539	TCU113	NS	73.04	23.41	27.11	163.88	162.72	78.04
37	1540	TCU115	EW	93.73	53.94	37.80	270.90	232.15	283.73

38	1540	TCU115	NS	114.58	38.69	33.01	130.35	314.15	258.36
39	1542	TCU117	EW	116.72	57.77	48.98	330.09	311.39	204.51
40	1542	TCU117	NS	117.91	54.34	45.51	483.36	355.57	304.36
41	1543	TCU118	EW	112.00	30.45	23.86	239.22	189.67	175.69
42	1543	TCU118	NS	90.55	33.46	36.46	162.72	183.60	144.77
43	1544	TCU119	EW	70.18	26.50	22.51	159.41	113.97	109.76
44	1544	TCU119	NS	57.28	16.75	19.74	102.79	165.42	122.42
45	1552	TCU140	EW	68.84	23.99	21.43	194.14	249.02	138.43
46	1552	TCU140	NS	55.37	20.51	17.52	114.45	124.77	140.51
47	1553	TCU141	EW	103.25	43.28	34.97	257.23	185.69	141.66
48	1553	TCU141	NS	83.12	28.07	23.10	176.09	256.51	156.84
49	1554	TCU145	EW	75.71	28.06	27.55	227.28	258.28	136.39
50	1554	TCU145	NS	63.38	19.20	18.60	148.82	122.12	109.62

Table B.3 Information of short-period ground motion set

No.	Sequence No.	Station	Direction	PGA (cm/s ²)	PGV (cm/s)	PGD (cm)	S _a (1s) (cm/s ²)	S _a (2s) (cm/s ²)	S _a (3s) (cm/s ²)
1	1190	CHY019	EW	62.39	6.41	14.68	53.73	43.27	37.21
2	1190	CHY019	NS	49.00	6.31	16.60	44.48	23.20	13.53
3	1191	CHY022	EW	42.62	5.02	7.83	48.45	21.45	19.05
4	1191	CHY022	NS	63.75	6.83	7.70	60.13	38.44	35.93
5	1192	CHY023	EW	57.24	10.10	9.94	88.45	59.15	30.93
6	1192	CHY023	NS	45.71	8.16	8.20	90.08	46.79	43.18
7	1210	CHY050	EW	58.35	10.78	10.25	78.06	34.20	34.65
8	1210	CHY050	NS	57.79	8.76	10.86	42.32	58.23	42.12
9	1214	CHY057	EW	66.51	7.98	60.59	57.63	32.17	13.30
10	1214	CHY057	NS	104.07	8.75	232.19	73.04	27.68	24.70
11	1215	CHY058	EW	38.04	10.26	8.36	168.15	113.63	92.92
12	1215	CHY058	NS	44.84	10.84	9.11	101.50	45.35	53.79
13	1219	CHY062	EW	54.27	6.15	8.02	52.14	26.59	38.99
14	1219	CHY062	NS	37.55	7.21	31.52	30.37	31.26	33.57
15	1220	CHY063	EW	55.22	14.43	10.89	86.31	46.94	52.94
16	1220	CHY063	NS	48.68	9.36	32.42	41.63	40.48	18.05
17	1221	CHY065	EW	44.38	9.84	7.71	220.38	83.22	71.36

18	1221	CHY065	NS	51.13	11.04	7.82	116.44	48.53	64.77
19	1222	CHY066	EW	43.54	10.85	9.04	115.47	80.84	71.88
20	1222	CHY066	NS	31.50	7.38	7.52	111.60	75.31	74.20
21	1223	CHY067	EW	45.70	9.77	10.45	96.31	79.26	51.33
22	1223	CHY067	NS	84.07	9.96	6.92	153.87	52.48	69.26
23	1224	CHY069	EW	29.29	10.64	9.63	99.38	83.07	48.96
24	1224	CHY069	NS	25.46	6.87	8.90	139.06	41.45	53.81
25	1232	CHY081	EW	29.42	5.98	5.49	138.18	45.98	47.24
26	1232	CHY081	NS	31.16	6.40	6.37	128.45	66.87	61.17
27	1241	CHY096	EW	23.30	9.11	6.87	103.16	93.59	52.52
28	1241	CHY096	NS	22.52	6.13	8.22	73.56	49.08	56.81
29	1358	KAU012	EW	32.44	7.97	8.33	58.78	48.96	18.96
30	1358	KAU012	NS	26.82	6.63	10.34	67.33	62.07	78.60
31	1359	KAU015	EW	40.47	10.36	11.23	119.68	95.38	48.17
32	1359	KAU015	NS	38.59	12.51	11.57	54.37	38.45	31.92
33	1362	KAU022	EW	51.92	4.80	35.17	90.29	46.47	23.57
34	1362	KAU022	NS	51.74	4.46	1.60	105.60	45.22	15.37
35	1382	KAU058	EW	67.03	9.34	7.22	88.72	39.58	36.97
36	1382	KAU058	NS	58.41	7.90	8.68	60.23	43.98	21.38
37	1383	KAU062	EW	30.68	8.40	8.51	55.82	52.80	31.05

38	1383	KAU062	NS	39.47	7.81	7.00	104.30	56.48	30.87
39	1384	KAU063	EW	42.09	7.66	6.93	119.37	62.02	67.57
40	1384	KAU063	NS	32.89	8.36	8.14	97.72	124.63	62.78
41	1385	KAU064	EW	30.00	8.75	6.54	129.22	55.34	33.12
42	1385	KAU064	NS	23.55	8.88	9.79	134.75	60.01	33.92
43	1386	KAU066	EW	28.41	5.99	2.37	103.23	39.50	25.16
44	1386	KAU066	NS	37.28	7.70	3.69	87.93	38.47	50.74
45	1399	KAU088	EW	44.76	7.07	3.42	61.60	59.89	36.20
46	1399	KAU088	NS	92.21	8.92	2.90	89.84	55.53	68.20
47	1405	SGL	EW	95.52	12.50	8.64	80.46	35.96	20.30
48	1405	SGL	NS	115.58	15.87	43.20	96.34	37.80	13.35
49	1408	TAI1	EW	40.35	10.72	9.77	110.12	45.49	27.43
50	1408	TAI1	NS	54.42	10.33	10.02	108.70	61.62	41.86

APPENDIX C: EQUIVALENCY BETWEEN BUTTERWORTH FILTER AND DAMPED
OSCILLATOR

C.1 Equivalency between 2nd-order Butterworth Filter and 70.7% Damped Oscillator

The following is proof of the equivalency of the 2nd-order Butterworth filter and 70.7% damped oscillator. Starting from the governing equation of a damped oscillator with 70.7% damping, we have

$$\ddot{x}(t) + \sqrt{2}\omega_n\dot{x}(t) + \omega_n^2x(t) = -a(t) \quad (\text{C.1})$$

Apply Laplace transform and notice the oscillator is initially at rest, $x(0) = 0$ and $\dot{x}(0) = 0$

$$s^2X(s) + \sqrt{2}\omega_n sX(s) + \omega_n^2X(s) = -A(s) \quad (\text{C.2})$$

Then the pseudo spectral acceleration is

$$S_a = \omega_n^2X(s) = \frac{-A(s)}{1 + \sqrt{2}\frac{s}{\omega_n} + (\frac{s}{\omega_n})^2} \quad (\text{C.3})$$

Notice this is just the governing equation of a 2nd-order Butterworth filter.

C.2 Equivalency between 4th-order Butterworth Filter and Highly Damped Oscillators

The governing equation of a 4th-order Butterworth filter could be written as

$$S_a = \frac{-A(s)}{\left[1 + 0.7654\frac{s}{\omega_n} + \left(\frac{s}{\omega_n}\right)^2\right] \cdot \left[1 + 1.8478\frac{s}{\omega_n} + \left(\frac{s}{\omega_n}\right)^2\right]} \quad (\text{C.4})$$

It could be noticed that this is equivalent to the combination of two damped oscillators, one with 38.27% damping and the other with 92.39% damping.